EXPERIMENTAL STUDIES OF THE HYDRO-THERMO-MECHANICAL BEHAVIOUR OF JOINTS IN GRANITE

by

JIAN ZHAO B.Sc.

June 1987

A thesis submitted to the University of London for the degree of Doctor of Philosophy in the Faculty of Engineering, and to Imperial College of Science and Technology for the D.I.C.

Rock Mechanics Section,

Royal School of Mines, Imperial College,

London SW7

花岗岩裂隙之水文-热学-力学性能

及其在干热性地热能开发上的应用

赵坚

一九八七年六月

英国伦敦大学帝国理工学院

皇家矿业学院岩石力学组

ABSTRACT

The recent development of research on Hot Dry Rock geothermal energy extraction (and on radioactive waste repository design) requires studies of rock mass assessment methodology, fluid flow in discontinuous rock and stress measurement techniques. The research presented in this thesis is a laboratory study of rock joint fluid flow under simulated stress and thermal conditions.

Tests on joints in the Carnmenellis granite from Cornwall, U.K., were carried out on the Geothermal Rock Mechanics Test System at Imperial College. Both natural joints and artificially induced extension fractures were tested at effective normal stresses of up to 40 MPa, differential pore pressures to 6 MPa and temperatures to 200°C.

The results suggest that present methods of describing rock joint characteristics do not provide a suitable basis on which to interpret hydromechanical property measurements. A Joint Matching Coefficient (JMC) is introduced and coupled with the Joint Roughness Coefficient (JRC) to provide a suitable parameter for correlating joint properties.

The results suggest a linear relationship between the changes in mechanical aperture and of hydraulic aperture. The initial aperture can be related

to the JRC and JMC. The initial aperture increases with test temperature according to a logarithmic relation.

The Joint Condition Factor (JCF) which represents the deviation from smooth parallel plate theory varies with temperature according to a logarithmic relation; the initial JCF is a function of initial aperture and JRC.

A concept of joint thermal expansion is proposed and expressed as a function of initial joint aperture and temperature increment.

Methods and experimental results of studies of heat transfer between rock and fluid are presented. The rate of heat exchange increases with the flow velocity.

Comparison with field test results and applications to the geothermal energy extraction are proposed and recommendations made for further research.

ACKNOWLEDGEMENTS

The author would like to express his sincere thanks to the following who assisted in the completion of this work.

Professor E.T. Brown, the author's supervisor, for his guidance and encouragement throughout the investigation, and for his immense and meticulous help, particularly with the English expression, during the writing of this thesis;

Dr. G.M. Elliott, for his help and advice in the early stages of this work;

Mr. J.W. Dennis, for his masterful technical skill and co-operation on the experimental work;

Dr. J.A. Hudson, for his helpful remarks and criticisms of the research;

Professor M.S. King, for his useful comments and suggestions;

Messrs. L.D. Wilson, B. Lyddall, W. Harman and A.R. Jones for their help in various aspects of this work;

Dr. Y. Wang, for his help and useful discussions on Scanning Electron Microscopy;

Drs. H.Q. Qin and Z.Y. Wu for their suggestions and discussions related to the problem of heat transfer;

Dr. J. Zhang, for her support during the final stages of preparation of this thesis;

colleagues in Rock Mechanics Section, for their stimulating discussions and help in various ways;

the Science and Engineering Research Council for their financial support for the research work;

the Committee of Vice Chancellors and Principals through an Overseas Research Studentship Award and the Department of Mineral Resources Engineering, Imperial College, for their major financial support for overseas student tuition fees;

the State Education Commission of the People's Republic of China, the Henry Lester Trust and the Universities' China Committee in London, for their financial assistance during the final stages of the work.

献给

我的双亲

CONTENTS

		Page
	Title	i
	Abstract	iii
	Acknowledgement	v
	Dedication	vii
	Contents	viii
	List of Figures	xv
	List of Tables	xix
	Notation and Conventions (Chapter 1 - 6)	xx
	Notation and Conventions (Chapter 7)	xxiii
	Chapter 1 INTRODUCTION	
1.1	Introduction to Hot Dry Rock (HDR) Geothermal Energy Extraction	1
1.2	Analysis of the Problems Involved Requiring Laboratory Investigations	6
1.3	Laboratory Determinations of Hydro-mechanical Properties of Rock Discontinuities	9
1.4	Structure of the Thesis	12
	Chapter 2 FRACTURE PERMEABILITY AND DEFORMATION	
2.1	Permeability Determination	14
	2.1.1 Equations of permeability	14

2.1.2 Laboratory tests on single joint 17

2.2 Joint Surface Properties 22

2.2.1 Joint roughness 22

2.2.2 Joint wall compression strength 28

2.2.3 Fracture aperture 29

2.2.4 Joint matching 30

2.3 Hydro-mechanical Properties of Single Joints 39

2.3.1 Modification of parallel plate theory 39

2.3.2 Elastic and non-elastic behaviour 40

2.3.3 High temperature mechanical, physical and thermal properties of granitic rock 42

2.3.4 Stress, joint surface properties and temperature coupled effects on joint hydro-mechanical behaviour 49

2.3.5 Joint Condition Factor, JCF 51

2.4 Review of Previous Work and Models of Joint Hydraulic Behaviour 53

2.4.1 Review of previous work 53

2.4.2 Gangi's "Bed of nails" model 61

2.4.3 "Asperity or void" model proposed by Tsang and Witherspoon 64

2.4.4 Other models 67

2.5 Summary and Topics for Investigation 71

Chapter 3
JOINT HYDRO-THERMO-MECHANICAL PROPERTIES TESTING SYSTEM

3.1 Testing Requirements and Introduction to the Facility 74

3.1.1 Test requirements 74

3.1.2 Features of the testing facility 75

3.2 Arrangement of the Testing System at Room Temperature 83

3.2.1 Arrangement of the testing cell 83

3.2.2 Confining pressure system 84

3.2.3 Permeating fluid pressure and pore pressure system 86

3.3 Tests at Elevated Temperatures 89

3.3.1 Heating system 89

3.3.2 Rock-fluid heat transfer measurement 91

3.4 Measurements and Calibration 93

3.4.1 Measurements and calibration at room temperature 93

3.4.2 Temperature measurements 97

3.4.3 Errors introduced in the tests 98

3.5 Electrical Output and Data Acquisition 101

Chapter 4
EXPERIMENTAL PROGRAMME AND TECHNIQUES

4.1 Outline Plan 103

4.2 Description of the Rock 106

4.3 Sample Preparation and Description 110

4.3.1 Natural joints 110

4.3.2 Artificial extension fractures 111

4.4 Measurement of Joint Surface Properties 112

4.5 Setting Up of Samples 130

4.6 Testing Procedure 134

4.6.1 Testing at room temperature 134

4.6.2 Tests at elevated temperatures 137

Chapter 5
RESULTS AND DISCUSSION
--JOINT MECHANICAL AND HYDRAULIC PROPERTIES

5.1 Joint Surface Properties 140

5.1.1 Observations on joint roughness 140

5.1.2 Observations on joint matching 142

5.1.3 Discussion on joint surface geometrical properties 144

5.2 Initial Apertures of the Joints 147

5.2.1 Calculation of joint initial apertures 147

5.2.2 Joint initial aperture and relations with joint surface properties 150

5.2.3 In-situ joint aperture 154

5.2.4 The differences in hydraulic aperture, mechanical aperture and maximum closure 157

5.3 Joint Mechanical Behaviour Under Normal Stresses 160

5.3.1 Effective normal stress - joint closure relations 160

5.3.2 Joint mechanical closure behaviour and comparison with Goodman's model 164

5.3.3 Joint mechanical behaviour --a logarithmic relation 168

5.4 Flow Rate and Hydraulic Aperture 170

5.4.1 Flow rate -hydraulic gradient relations 170

5.4.2 Calculation of hydraulic aperture 174

5.5 Joint Hydraulic Behaviour Under Normal Stress 175

5.5.1 Flow rate - effective normal stress relations 175

5.5.2 Joint hydraulic properties and comparison with other models 179

5.6 Joint Condition Factor, JCF 188

5.6.1 Calculation of JCF 188

5.6.2 Influences of joint surface properties and of initial aperture 189

5.6.3 Influence of cyclic loading 193

Chapter 6
RESULTS AND DISCUSSION -- EFFECTS OF TEMPERATURE, JOINT HYDRO-THERMO-MECHANICAL RELATIONS AND JOINT THERMAL EXPANSION

6.1 Influence of Temperature on Initial Aperture 195

6.2 Influence of Temperature on Joint Hydro-mechanical Behaviour 200

6.2.1 Change in mechanical behaviour 200

6.2.2 Change in hydraulic behaviour 201

6.2.3 Change in Joint Condition Factor, JCF 202

6.3 Joint Hydro-thermo-mechanical Properties and a New JCF Approach 206

6.4 Effects of Thermal Cracking on the Hydro-thermo-mechanical Behaviour of Rock Joints 210

6.4.1 Scanning Electron Microscopy (SEM) 210

6.4.2 Observations 211

6.4.3 Effects of cracks on the hydro-thermo-mechanical behaviour of joints 217

6.5 Thermal Expansion of Rock Joints 219

6.5.1 Joint thermal expansion 219

6.5.2 Joint thermal expansion mechanism and joint healing mechanism 223

Chapter 7
THERMAL ENERGY TRANSFER ANALYSIS AND EXPERIMENTAL STUDIES

7.1 Introduction 229

7.2 Fundamentals of Heat Transfer 232

7.2.1 Thermal conduction 232

7.2.2 Fluid motion and heat convection 235

7.3 Experimental Results for Thermal Conductivity of Granite 237

7.3.1 Testing theory 237

7.3.2 Testing methods and results 240

7.4 Analytical Solutions for Forced Convection Between Parallel Plates 246

7.4.1 General considerations 246

7.4.2 Working formulae 249

7.5 Total Heat Transfer Coefficient 255

7.6 Analysis and Results of Heat Transfer Measurements 256

7.7 Discussion 263

7.7.1 Flow velocity - heat transfer coefficient relation 263

7.7.2 Temperature - heat transfer coefficient relation 269

7.7.3 Joint aperture - energy transportation relation 269

7.8 Methods of Numerical Analysis of Heat Energy Transfer 270

Chapter 8
CONCLUSIONS AND APPLICATIONS

8.1 Summary and Conclusions 273

8.2 Applications to Hot Dry Rock Geothermal Energy Extraction 277

8.3 Aspects Requiring Further Research 281

REFERENCES 284

LIST OF FIGURES

Figure	Titles	Page
Chapter 1		
1.1	Hot Dry Rock reservoir formed by hydro-fracturing.	4
1.2	Hot Dry Rock reservoir formed by stimulation of natural joints.	5
Chapter 2		
2.1	Darcy's experiment.	15
2.2	Direct injection method of joint permeability determination.	19
2.3	Radial flow method of joint permeability determination.	20
2.4	Typical roughness profiles and corresponding range of Joint Roughness Coefficient (JRC).	23
2.5	Tilt test.	24
2.6	Typical roughness profiles and ISRM suggested nomenclatures.	27
2.7	Joint Matching Coefficient.	33
2.8	Typical joint profiles with JMC ranges.	34
2.9	Typical joint closure - effective normal stress behaviour.	41
2.10	Cornish granite failure envelopes at test temperatures of 20°C and 200°C.	44
2.11	Gangi's "bed of nails" model.	62
2.12	Tsang and Witherspoon's "asperity and voids" model.	65

Chapter 3

3.1	Geothermal Rock Testing Facility - Terra Tek Systems.	76
3.2	Test configuration inside load frame and cell.	78
3.3	Confining pressure cart and pressure intensifier.	79
3.4	Hydro-thermo-mechanical test stack assembly.	80
3.5	Permeating pressure and joint fluid pressure cart.	81
3.6	Data aquisition and display systems.	82
3.7	Schematic of confining pressure system.	85
3.8	Schematic of permeating pressure and pore pressure system.	88
3.9	Schematic of heating system.	90
3.10	Rock-fluid heat transfer measurement assembly.	92
3.11	Stack assembly for triaxial compression test.	95

Chapter 4

4.1	The in-situ experimental site at Cornwall, SW England.	108
4.2	A typical surface profile of natural joint.	111
4.3	A typical surface profile of extension fracture.	112
4.4	Tested natural joint surfaces.	113
4.5	Tested extension fracture surfaces.	116
4.6	Surface profiles of natural joints.	120
4.7	Surface profiles of extension fractures.	125
4.8	Details of sample set up.	131
4.9	Stack assembly for hydro-thermo-mechanical tests.	132
4.10	Schematic of the arrangement for hydro-thermo-mechanical tests.	133

4.11 Schematic representations of test procedures. 136

Chapter 5

5.1 Plot of JMC with JRC for natural joints and extension fractures. 143

5.2 Typical relation between hydraulic apertures and mechanical apertures for a rock fracture. 149

5.3 Plots of initial apertures with JRC and JMC. 153

5.4 Chart for relating initial aperture to JRC and JMC. 154

5.5 Differences between mechanical aperture, hydraulic aperture and maximum closure. 159

5.6 Test data of effective normal stress - joint mechanical closure relation. 161

5.7 Experimental results compared with Goodman's model and the logarithmic relation. 165

5.8 Typical plots of flow rate against differential pressure. 171

5.9 Verification of the cubic flow law. 172

5.10 Effective Normal stress - flow rate relation. 176

5.11 Joint permeability - effective normal stress data compared with various models. 180

5.12 Schematics of Walsh's model with upper and lower boundaries. 183

5.13 Flow data compared with Tsang and Witherspoon's model. 185

5.14 Variation of Joint Condition Factor with joint initial aperture and JRC. 191

5.15 Relations between JCF, initial aperture and JRC. 192

Chapter 6

6.1 Variation of initial aperture with temperature and JRC. 198

6.2 Proposed relation of joint initial aperture, 199

temperature and JRC.

6.3 Values of parameters A and B. 199

6.4 Variation of Joint Condition Factor with temperature. 205

6.5 Fresh fractured granite sample under SEM. 213

6.6 Tested fractured granite sample (up to 100°C) under SEM. 214

6.7 Tested fractured granite sample (up to 180 °C) under SEM. 215

6.8 Experimental results for joint thermal expansion. 222

6.9 Variation of joint thermal expansion coefficient with joint initial aperture. 223

6.10 Mechanism of joint thermal expansion. 225

6.8 Schematics of flow through different joints. 227

Chapter 7

7.1 Thermal conduction. 233

7.2 Stack assembly for thermal conductivity test. 241

7.3 Typical temperature - time plot for a thermal conductivity measurement. 243

7.4 Thermal conductivity of Carnmenellis granite. 245

7.5 Temperature distribution of flow between parallel plates. 248

7.6 Combined effect of conduction and convection. 255

7.7 2-dimensional representation of heat transfer system. 258

7.8 Variations of heat transfer coefficient with flow velocity. 265

LIST OF TABLES

Table	Titles	Page
2.1	ISRM descriptive terms for joint roughness.	26
2.2	Joint Matching Coefficient (JMC).	33
2.3	Mechanical properties of Cornish granite.	43
4.1	Tests conducted on natural joints and extension fractures in Carnmenellis granite.	105
5.1	Values of joint initial mechanical aperture, initial hydraulic aperture, JRC and JMC.	151
5.2	In-situ joint hydraulic apertures.	156
5.3	Joint stiffness and parameters in Goodman's model and logarithmic relation.	167
5.4	Flow properties comparison with different hydraulic models.	182
5.5	Results of initial mechanical aperture, Joint Condition Factor (JCF), JRC and JMC.	190
5.6	Influence of cyclic loading on JCF.	194
6.1a	Effect of sample temperature on joint initial aperture.	196
6.1b	Effect of sample temperature on joint initial aperture.	197
6.2a	Effect of sample temperature on JCF.	203
6.2b	Effect of sample temperature on JCF.	204
6.3	Summary of the results of joint thermal expansion.	221
7.1	Variation of water boiling temperature at different pressures.	231
7.2	Results of heat transfer coefficient calculations.	259

NOTATION AND CONVENTIONS

The following notation is used unless defined otherwise (except in Chapter 7)

A : Area

a : A parameter in Gale's model

B : A fracture parameter, depending on the joint surface geometry

b : Spacing between openings in a rock mass

C : A parameter in flow law, = $wg/12\nu$

c : A parameter in Swan's model

c_p : Specific heat

D : Material constant, being the effective modulus of the asperities

d : Thickness of the fluid lamina, for laminar flow, also the aperture of the parallel plates

E : Joint mechanical aperture

E_o : Joint initial mechanical aperture

E_o^* : Joint initial mechanical aperture at room temperature

E_1 : Joint mechanical aperture at a reference effective normal stress

ΔE : Change of joint mechanical aperture, i.e., joint mechanical closure

e : Joint theoretical hydraulic aperture

e_o : Joint initial hydraulic aperture

e_1 : Joint hydraulic aperture at a reference effective normal stress

Δe : Change of joint hydraulic aperture, i.e., joint hydraulic aperture closure

F : A factor in the flow law, =JCF

g : Gravitational acceleration

h : r.m.s. of the fracture asperity height dis-

tribution

h_1 : Water pressure head at inlet

h_2 : Water pressure head at outlet

Δh : Differential head pressure

i : Hydraulic gradient = h/L

JCF : Joint Condition Factor

JCF^* : Joint Condition Factor at room temperature

JCS : Joint wall compressive strength

JMC : Joint Matching Coefficient

JRC : Joint Roughness Coefficient

Δj : Joint thermal expansion

K : Permeability, intrinsic permeability

K_f : Permeability of joints and fractures

K_o : Initial permeability of joints and fractures

K_1 : Permeability of joints and fractures at a reference effective normal stress

k : Coefficient of permeability, hydraulic conductivity

L : Length

M : A parameter in initial aperture, JRC and temperature relation

m : A parameter in Swan's model

N : A parameter in initial aperture, JRC and temperature relation

n : A parameter in Gangi's model

P : Thermal energy extraction rate, i.e., thermal power

Q : Fluid flow rate

Q_1 : Fluid flow rate at a reference effective normal stress

R : Radius of fractured sample

r : Radius of the injection hole

Re : The Reynolds number

S : A parameter in Goodman's model

s : Value of joint permeability at an effective normal stress of 1.0 MPa in Gale's model

T_1 : Test temperature

T_2 : Test temperature

ΔT : Change of temperature

t : A parameter in Goodman's model

V_{mc} : Joint maximum closure

ΔV : Joint normal closure

ΔV_1 : Joint normal closure at a reference effective normal stress

V_t : Joint thickness

w : Width

α : Linear thermal expansion coefficient

α_j : Thermal expansion coefficient of joint

β : A parameter in Tsang and Witherspoon's model

ε_j : Joint thermal strain

σ : Normal stress

σ' : Effective normal stress

σ_1' : Reference effective normal stress

σ_c : Uniaxial compressive strength of the rock

ζ : Seating pressure, i.e., a small reference effective normal stress

μ : Fluid dynamic viscosity

ν : Poisson's ratio

ν : Fluid kinematic viscosity

ω : Percentage of contacting area to total joint surface area

NOTATION AND CONVENTIONS

(used in Chapter 7)

A	:	Area
C	:	Euler's constant, 0.5772
c_p	:	Specific heat
Ec	:	The Eckert number
e	:	Joint aperture
Gr	:	The Grashof number
g	:	Acceleration due to gravity
H	:	Thickness of the solid
h	:	Heat transfer coefficient, heat convection coefficient
k	:	Thermal conductivity
k_f	:	Thermal conductivity of the fluid
k_s	:	Thermal conductivity of the solid
L	:	Length of the flow path, i.e., the joint
l	:	Length
M	:	Total heat transfer coefficient
Nu	:	The Nusselt number
Nu_x	:	The local Nusselt number
Nu_l	:	The average Nusselt number over the plate length
Pr	:	The Prandtl number
P	:	Static flow pressure
p	:	Power input per unit length
Q	:	Heat energy input from other source
q	:	Heat flow
q'	:	Internal heat generation rate per unit volume
Re	:	The Reynolds number

r : Radius, radial distance

T : Temperature; temperature of the solid far from the fluid surface

t : Temperature

t_f : Temperature of fluid far removed from the solid surface

t_m : Mean film temperature for heat convection

t_s : Temperature of solid surface

ΔT : Change in temperature

Δt : Characteristic temperature difference

v : Flow velocity

W : Width of the solid plate i.e., the joint

Δx : Thickness

α : Thermal diffusivity

ξ : Dimensionless coordinate = x/l

η : Dimensionless coordinate = y/l

ρ : Density

τ : Time

μ : Kinematic viscosity

ν : Dynamic viscosity

Chapter 1

INTRODUCTION

1.1 Introduction to Hot Dry Rock Geothermal Energy Extraction

Geothermal energy is one of the alternative energy sources whose use does not yet rival that of the main energy sources (oil, natural gas, coal, nuclear, or even hydropower). There is however abundant geothermal energy in the Earth's crust, and geothermal energy has the potential to alter the energy economies of many countries throughout the world, particularly as fossil fuels grow more expensive and scarce. But geothermal energy is not an exotic twenty-first century hope, demanding expensive and uncertain breakthroughs in physics or high technology. Instead, the use of geothermal energy has already been demonstrated in many different settings throughout the world [Rybach 1981]. The first large geothermal power plant was built at Larderello, Italy in 1904, and is still in operation. Geothermal power plants are in productive operation in Mexico, Japan, USA, USSR and other countries over the world.

Geothermal fields may be classified into three

types [Rybach 1981] - dry steam, hot water and hot dry rock reservoirs. The hot water fields may be further subdivided into those containing superheated water (wet steam) and reservoirs of low temperatures. Larderello and the Geysers, USA, are examples of dry steam fields; the Wairakei, New Zealand, fields are of the wet steam type. Dry hot rock reservoirs have started to be exploited commercially, and extensive research has been undertaken with mainly conventional methods of hydraulic stimulation [Smith 1983]. Field tests have been under development in the Jemez Mountains, New Mexico, USA [Heiken and Goff 1983, Dash et al 1983] and the Rosemanoes Quarry, Cornwall, UK [Batchlor 1982].

The out flow of heat from the Earth's interior is a fundamental quantity in its energy balance; it arises from heat liberated during the decay of radioactive nuclei in crustal rock. A natural geothermal system (dry steam, hot water type) requires the combination of elevated temperature due to high level igneous intrusion and naturally occurring groudwater in an area of well developed vertical and horizontal permeability. The geological concept of plate tectonics suggests us that such conditions are restricted to the worldwide distribution of tectonically active regions close to the plate boundaries. Thus geothermal resources of this kind are only expected to occur mainly along spreading ridges, convergent margins (subduction zones) and intraplate melting anomalies.

In most "normal" continental areas, geothermal heat is present in great quantities at depths which are accessible with today's drilling technology. Since working fluids are absent due to the low natural permeability of the deep strata, heat can be extracted from such Hot Dry Rock (HDR) sources only by establishing artificial fluid circulation. For electrical power production the main conditions for the HDR sources are [Rybach 1981]: (a) temperature >200°C and (b) a very low permeability to fluid flow (<10 darcy, 1 darcy = 10^{-12} m). Thus a HDR reservoir can mainly be characterized by its natural permeability and heat content.

The original concept proposed by Robinson et al [1971] (see Berman [1975]) involved the creation of a single vertical disc shaped fracture within a suitable HDR zone by hydrofracturing from a vertical well-bore. This fracture is then intersected by the upper well. Heat exchange facilities at the surface withdraw the accessible heat and cooled fluid is then reinjected, forming a closed loop circulation system. This method has been tested by Los Almos Scientific Laboratory (LASL) at the depth down to 800 meters in New Mexico [Dash et al 1983] (Figure 1.1).

The approach of the Camborne School of Mines (CSM)/Department of Energy (U.K.) project [Batchlor 1982] in Cornwall, SW England, is radically different and actually a logical extension of that of the LASL program. The CSM/DoE program has conducted field research into stimulating the reservoir rock by opening pre-

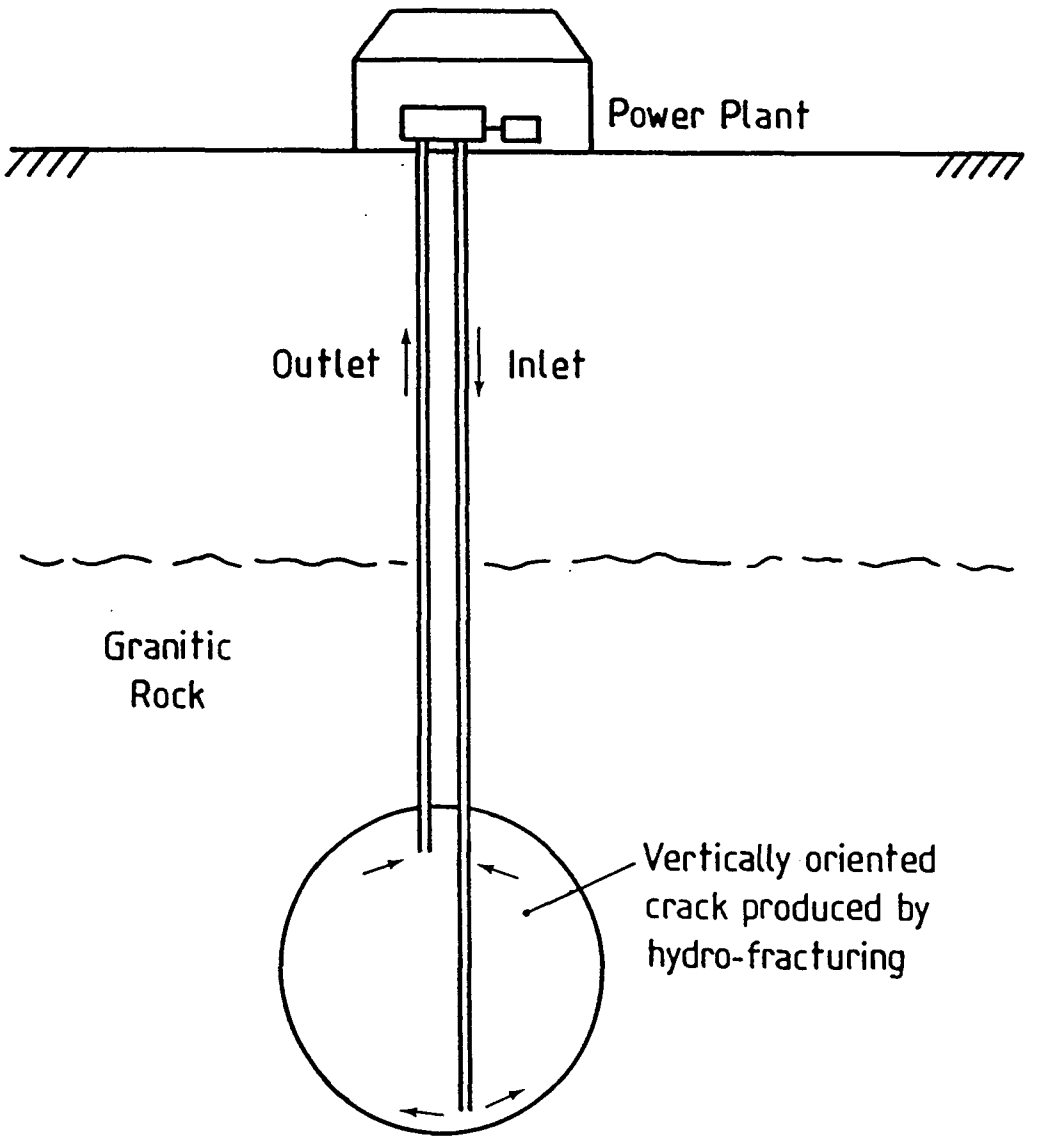


Figure 1.1 Hot Dry Rock Reservoir Formed by Hydro-fracturing.

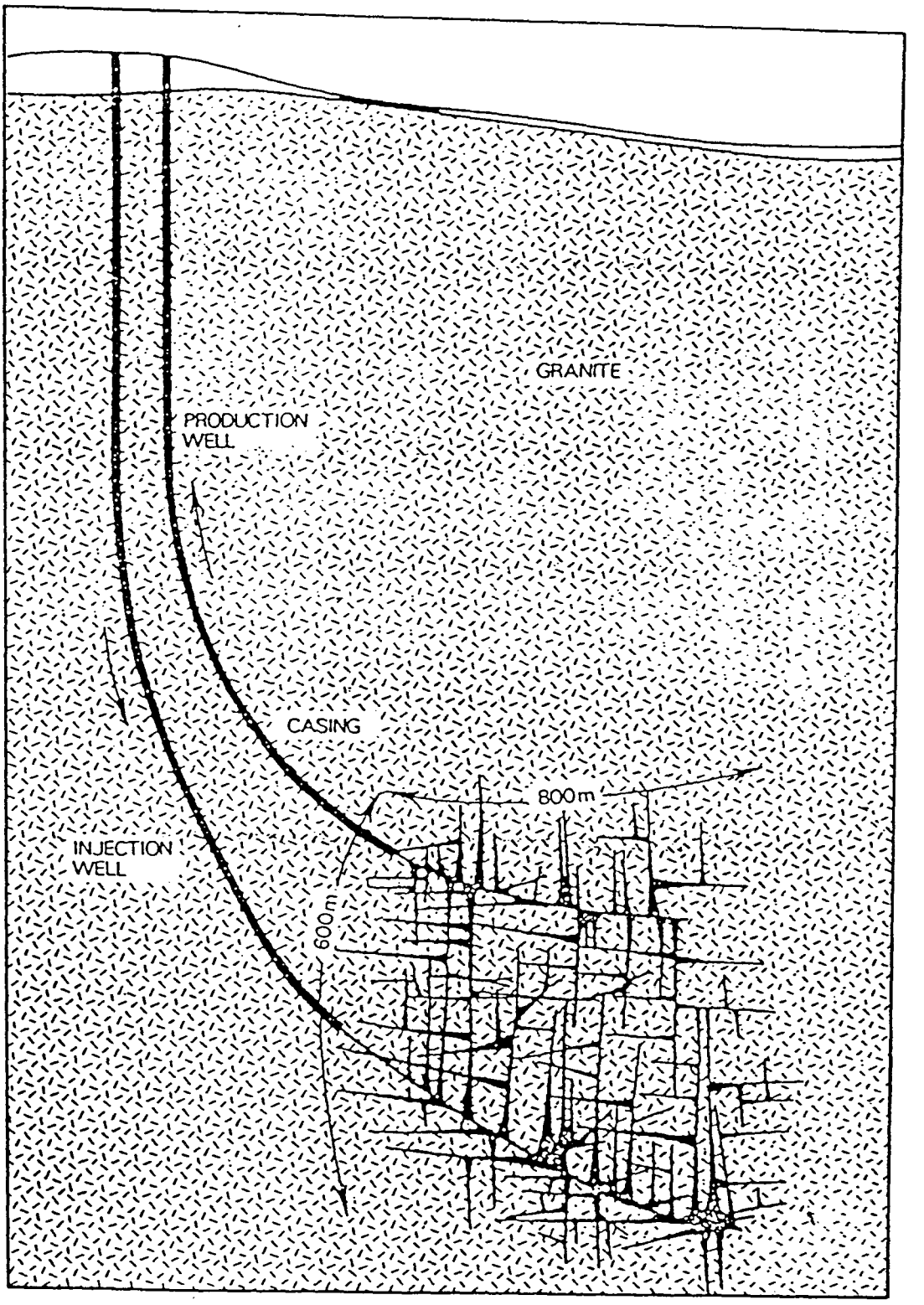


Figure 1.2 Hot Dry Rock Reservoir Formed by Stimulation of Natural Joints. (After Batchelor [1982]).

existing natural fissures by primary exposive pretreatment followed by hydraulic extension at the depth of about 2000 meters. The resulting reservoir is a fracture zone of high permeability and lower impedance linking two subparallel well-bores with a total vertical separation of 350 to 500 meters (Figure 1.2). Further in situ research is expecting to drill the well-bores down to the depth of 6000 meters.

In order to obtain efficient extraction of energy from hot dry rock it requires a very large heat-exchange surface owing to the low thermal conductivity of the rock. Hence the properties of the fractures become one of the most important factors controlling the whole process. In this application as well as in radioactive waste repository design, the properties of natural and induced dis-continuities in the rock masses are of primary importance.

1.2 Analysis of the Problems Involved Requiring Laboratory Investigations

To analyse Hot Dry Rock Geothermal Energy extraction processes, the properties of the rock and the rock masses must be known. Apart from the in-situ tests, which are usually very costly, general properties of the rock and rock masses can be determined by laboratory tests under the simulated field conditions. The rock mechanics problems involved in geothermal energy

extraction and some other related research fields, such as nuclear waste repository design, are mechanical properties of both rock and rock masses, hydraulic properties of the rock masses and joints, and thermal properties of the rock [Hudson and Boden 1982, Hudson 1983].

Several investigations may be carried out in the laboratory under simulated in-situ conditions. Although in some cases more satisfactory results could be obtained from in-situ tests, field tests are costly and sometimes difficult if not impossible to perform. However, for fundamental research, well controlled laboratory investigation are simpler, more accurate and convincing; particularly for the cases of investigating coupled hydro-thermo-mechanical properties of single joints in granite.

In order to explore the rock properties, laboratory investigations on mechanical properties of rock and rock joints, hydraulic properties of rock joints, thermal properties of rock material and thermal energy extraction by circulated fluid are needed. Hence the following tests are required to be conducted on some advanced testing facilities:

1) triaxial tests at room temperature and at elevated temperatures, by which the strength characteristics of the rock can be determined. This in term will allow studies to be made of the stability and failure of well-bores at depth and the stresses

required to fracture the rock;

2) shear tests on rock fractures and joints, by which the fracture shear strength and deformation can be determined;

3) normal loading tests on the rock discontinuities, particularly the deformation characteristics of the fractures and joints, which in practice, is the most important factor controlling the joint opening. A certain joint aperture should have to be maintained for effective geothermal energy extraction from the Earth's crust. However, this property of fracture deformation can also be studied by compressive loading in conjunction with permeability tests;

4) thermal conductivity and diffusivity of the rock. The determination of these coefficients, apart from being of general interest, are required later for rock-fluid heat transfer studies and the efficiency of thermal energy extraction;

5) thermal expansion, cracking of the rock and of the joint surface during heating and heat exchange. These properties will effect the joint opening, fluid passage and the whole hydromechanical behaviour of the rock joint;

6) permeability or hydraulic conductivity tests on the rock joint. Since the joint is thousands of orders

more permeable than the rock matrix, the flow of fluid will be centralized along the joints [Louis 1969, Maini 1971b and Wittke 1973]. Hence knowledge of the permeabilty of the rock joints under various stress and temperature conditions will be required for the study of the flow of the working fluid circulated within the geothermal extraction system;

7) rock-fluid heat transfer tests coupled with hydraulic tests at elevated temperatures. These tests will provide essential knowledge of the efficiency of Hot Dry Rock Geothermal energy extraction in relation to joint apertures, flow rate and other important factors.

1.3 Laboratory Determinations of Hydro-mechanical Properties of Rock Discontinuities

As noted in section 1.2, the study of fluid flow in rock joints is required by the recent development of research on HDR geothermal energy extraction and on radioactive waste repository design. The research reported in this thesis is a laboratory study of fluid flow in rock joints under simulated stress and thermal conditions.

In the past laboratory tests have been performed on a variety of "discontinuities" mainly to check the validity of theoretical flow laws and to assess the effects of discontinuity geometry. Baker [1955] and

Louis [1969] used rough cast concrete as a model rock material containing simulated discontinuities. Lomize [1951] created roughness by casting regular patterns in concrete. Huitt [1956], in an attempt to model rough joints, glued uniform sized sand particles to two steel plates. More recently, tests have been performed on extension fractures created in intact samples of rock. Gale [1975] and Iwai [1976] tested single fractures created in samples of granite, basalt and marble for linear and radial flow regimes. Heimili [1972] and Detournay [1980] investigated flow in "closed" discontinuities using extension fractures in blocks of granite. Kranz et al [1979] tested joints with grit surfaces and whole rock, and Johnson [1983] used a "simulated" fracture which consists of a monolayer of small glass spheres sandwiched between two halves of either a steel or quartzite longitudinally split cylinder. Maini [1971a] performed tests on an epoxy resin model of an actual discontinuity and showed, amongst other things, that the flow within a discontinuity is three dimensional with the fluid flowing along clearly defined paths.

A few laboratory investigations have been performed on natural joints. Sharp [1970] carried out tests on samples of rock containing weathered natural joints. Gale [1975] tested natural joints for comparison with induced tensile fractures in order to study the effects of fracture type. Raven and Gale [1985] studied water flow in a natural rock fracture as a function of

stress and sample size. Schrauf [1984] performed tests on natural joints to study the relationship between hydraulic conductivity and geometry of the fracture. The author has been involved in a very recent investigation on natural granite joints conducted by Boodt and Brown [1985] and Elliott et al [1985].

Barton et al [1985] related the joint roughness to the strength, deformation and conductivity coupling of rock joints. Witherspoon et al [1980] and Elliott et al [1985] suggested that a factor should be introduced into the theoretical parallel plate theory (the cubical flow law, see section 2.1) by taking account the joint surface properties. Hardin et al [1982] performed fully-coupled hydro-thermo-mechanical joint behaviour tests on a rough joint and found a considerable reduction in hydraulic conductivity due to an increase in temperature.

The research project described here is a laboratory study of hydro-thermo-mechanical properties of rock joints under simulated stresses and thermal conditions. The investigations will consist of studies on surface geometrical properties of joints in Carnmenellis granite, from Cornwall, SW England; tests on joint deformation under normal stresses coupled with studies on fluid flow in the joints in granite both at room temperature and at elevated temperatures of up to 200°C; and rock-fluid heat transfer in corresponding with the fluid flow tests. The presentation of this research study is briefly described in the following section.

1.4 Structure of the Thesis

The thesis is divided into 8 chapters. In Chapter 1, an introduction to the whole concept of thesis has been given, together with a discussion of Hot Dry Rock geothermal energy extraction and related problems.

Chapter 2, presents an introduction to the fundamentals of fluid permeability determinations, and ideas on the hydro-thermo-mechanical properties of rock fractures and the effects of stress, joint surface properties and temperature. Previous work on the subject and physical models that have been proposed are reviewed. Also, a concept of Joint Matching Coefficient (JMC) is proposed.

The testing facility is described in Chapter 3, with details of pressurizing, heating and measuring systems, at both room temperature and elevated temperatures (up to 200°C). At the end of the chapter, the method of data collection and errors which may be induced during testing are discussed.

In Chapter 4, the experimental programme and techniques are described. It includes rock material and joint surface description, sample preparation and test set up, testing procedures at various temperatures, confining pressure and differential pressure ranges.

Chapter 5 deals with the joint surface geometrical properties and joint hydro-mechanical properties. The chapter includes experimental data and

observations, methods of calculation, results and discussion. The results are compared with previous models. A simple logarithmic model is developed to fit the test results to the joint mechanical properties. Relationships between the joint surface geometrical properties and joint mechanical behaviour are proposed and discussed.

Chapter 6 presents studies of inter-relations of joint hydro-thermo-mechanical properties (including surface and mechanical). Based on the experimental results, an empirical relation coupling joint hydro-thermo-mechanical and joint surface properties (including joint matching) is established and discussed. Scanning Electron Microscope observation of thermal cracking are presented and a concept of joint thermal expansion is proposed.

Chapter 7 deals solely with thermal energy extraction. It starts with the fundamental concepts of solid-fluid heat transfer. Experimental measurements of thermal conductivity of the granite and analytical solutions for heat transfer (convection) coefficients are presented and discussed. The influences of joint apertures, flow velocities and temperatures on the rate of rock-fluid heat transfer are discussed.

In the final chapter, Chapter 8, the conclusions of the study are presented, possible applications of the experimental results to the hot dry rock geothermal energy extraction are considered. And topics for further research are recommended.

Chapter 2

FRACTURE PERMEABILITY AND DEFORMATION

2.1 Permeability Determination

As noted in section 1.4, this chapter is intended to introduce the fundamentals of fluid permeability, and the background and ideas on the hydro-thermo-mechanical properties of rock joint. In order to study those properties, a basic knowledge of the concept of permeability and of permeability determination is required.

2.1.1 Equations of permeability

Consider a cylindrical sample of soil or rock under the different water pressure heads h_1 and h_2, shown in Figure 2.1. In one dimension, steady water flows through the fully saturated sample without affecting the structure of the soil or rock in accordance with Darcy's empirical law,

$$Q = A\,k\,i \qquad (2.1)$$

where Q = volume of water flowing per unit time,

A = cross sectional area of sample corresponding to the flow,

k = coefficient of permeability,

i = hydraulic gradient = $(h_1 - h_2)/L$,

L = length of sample.

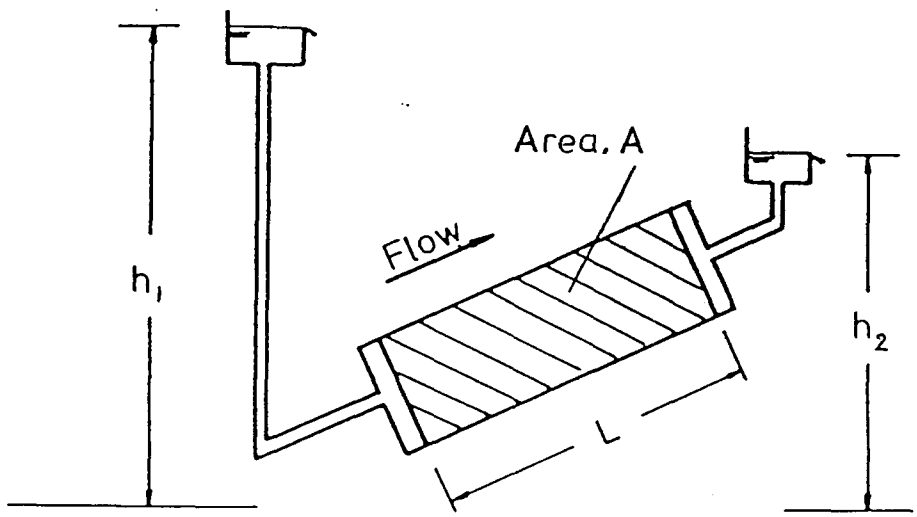


Figure 2.1 Darcy's Experiment

Hence $$k = \frac{Q}{A\ i} = \frac{Q\ L}{A\ (h_1 - h_2)} \qquad (2.2)$$

The coefficient of permeability k is a constant. Experiments have shown, however, that its value depends not only upon the character of the soil or rock, but also upon the properties of the fluid percolating through it. The value of k is inversely proportional to fluid kinematic viscosity, ν, which can be expressed [Lamb 1932] as,

$$k = K\ g/\nu \qquad (2.3)$$

where g = gravitational acceleration,

K = the intrinsic permeability, and is a property

of the material only, with dimension of L^2.

For the flow of a viscous fluid through the narrow interspace between two closely spaced parallel plates, the intrinsic permeability is [Todd 1959, Verruijt 1970],

$$K = d^2/12 \tag{2.4}$$

where d is the thickness of the fluid lamina, i.e., the distance apart of the two parallel plates.

Hence equation (2.3) can be rewritten as

$$k = \frac{g\, d^2}{12\, \nu} \tag{2.5}$$

for laminar flow through smooth parallel plates. This is often called the "parallel plate theory" in the hydrology of rock joints. A laminar flow through smooth parallel plates is a potential flow with its Reynolds number $\leqslant 2300$ (see Louis [1969] or Massey [1975]).

By inserting Equation (2.5) into (2.1), the equation becomes

$$Q = \frac{A\, i\, g\, d^2}{12\, \nu} \tag{2.6}$$

Since the area A is the flow passage which is equal to the width w times to the aperture of the parallel plates, d, Equation (2.6) may be written

$$Q = \frac{w\, i\, g\, d^3}{12\, \nu} \tag{2.7}$$

Equation (2.7) is identified as the "cubic flow law" which is widely used to describe the flow of fluid through rock joints.

For a planar array of parallel smooth openings, the equivalent permeability parallel to this array is given as

$$k = \frac{d^3}{12\ b} \qquad (2.8)$$

where b is the spacing between openings.

Equation (2.7) shows that the flow rate is extremely sensitive to the aperture of the opening. In practice, this opening is governed by the deformation characteristic of the discontinuities. Since this deformation is highly stress-dependent, the permeability of rock mass will also be very sensitive to stress level.

2.1.2 Laboratory tests on single joint

Almost all the measurement from field permeability tests are of rock mass permeability or of joint permeability, since the tests are often involved with a huge scale. The fact that rock masses owe their permeability mainly to the joints and fractures makes the problem of in-situ determination of permeability very erratic and sometimes senseless [Laghina Serafim 1968]. Tests conducted in the laboratory will generally be on a

small scale and will be concurred with the determination of intrinsic and of single joint permeabilities.

Intrinsic permeability

Intrinsic permeability can be measured directly by injection of air or water through a cylindrical specimen contained in an impermeable membrane (see Figure 2.1). Then, the coefficient of permeability is given by Darcy's law as

$$k = \frac{Q\ l}{A\ \Delta h} \qquad (2.9)$$

where Δh = differential head pressure,

$= h_1 - h_2$,

Q = the volume flow rate,

L = specimen length,

A = specimen cross-sectional area.

Directional permeabilities can be obtained by specifying the specimen orientation.

Determinations of the intrinsic permeability can also be made using radial flow method. This is very much like the field injection test [Attewell and Farmer 1976, Roberts 1977]. The inlet pressure p can vary while the outflow pressure remains constant, and both p and Q are measured when the system is in a steady state.

Laboratory tests can hardly be carried out for investigating the permeability of rock masses, though tests in a large testing cell on crushed rock masses

seems to be possible. But by using the same equipment mentioned above for intrinsic rock sample, permeability tests can be easily conducted on single fractured rock samples.

Direct injection method

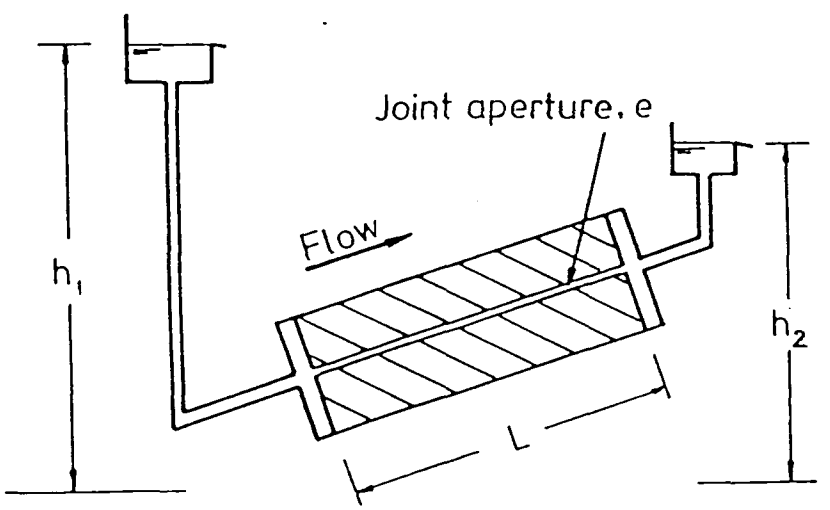


Figure 2.2 Direct Injection Method of Joint Permeability Determination.

This method of determining single fracture permeability is based on the intrinsic rock material test. It is required that the fracture lies along the cylinder length, and again, air or water is directly injected through the fractured sample contained in an impermeable seal. By adopting the cubic flow law stated earlier on the basis of laminar flow discharge, and neglecting fracture wall surface roughness and mismatching effects, then for the case defined in Figure 2.2,

$$Q = \frac{w\ i\ g\ e^3}{12\ \nu} \qquad (2.10)$$

and

$$k = \frac{g\ e^2}{12\ \nu} \qquad (2.11)$$

where e is the fracture aperture.

The test allows the confining pressure to be varied and its effect on the deformation and on the hydraulic properties of the fracture to be studied.

Radial flow method

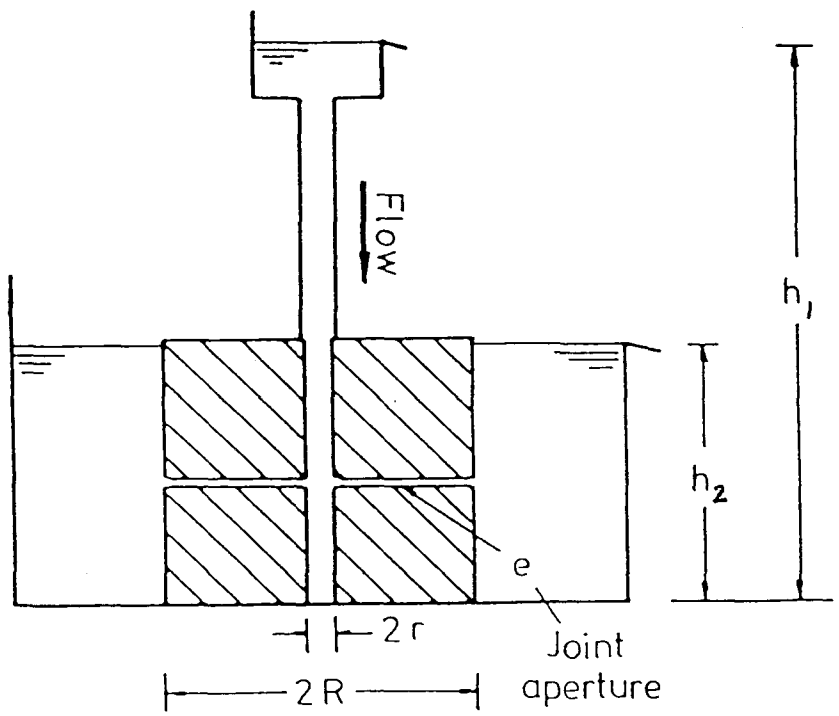


Figure 2.3 Radial Flow Method of Joint Permeability Determination.

It is also possible to use the radial flow method with the fracture perpendicular to the axis. This test allows one to study the deformation and hydraulic properties of the fracture under normal stresses if a load is applied on the top of the sample, as shown in Figure 2.3. The flow rate Q becomes [Gale 1982]

$$Q = \frac{2 \pi w i g e^3}{12 \nu \ln(r/R)} \qquad (2.12)$$

Hence, $$k = \frac{2 \pi g e^2}{12 \nu \ln(r/R)} \qquad (2.13)$$

where R = radius of fractured sample,

r = radius of the central hole.

Both direct injection method and radial flow method are developed from Darcy's law and the parallel plate theory. Therefore, the limitations for Darcy's law and for the parallel plate theory is also applicable to these methods. As noted earlier, the parallel plate theory is for the flow of a viscous fluid through the narrowly interspaced parallel plates; thus the joint should be in a state that it is not held widely open. A steady state of flow and of flow path structure must be maintained [Verruijt 1970]. By noting equation (2.12), when R, the outer radius becomes infinitely large, then $\ln(r/R)$ tends to $-\infty$ for the values of r. This means that it is impossible to inject water at a steady state. However, this does not occur in practical cases [Todd 1959].

One of the major problems involving the tests is to hold the flow path (i.e. the discontinuity) geometry at a steady state. This may be achieved by application of constant effective normal stress (usually taken as the total normal stress less the joint fluid pressure [Terzaghi 1943, Terzaghi and Peck 1967, Jaeger and Cook 1979]) at normal temperature environment. Problem arises in elevated temperature tests as thermal cracks initiating and propagating continuously alter the joint state. In the present study, the effective normal stress approach is adopted in experimental works and in analysis. The radial flow method may encounter the difficulty of objecting the effect of the radial flow (variation of the velocity in the flow direction). A theoretical correct equation for the influence is given by Wittke and Louis (see Louis [1973]).

2.2 Joint Surface Properties

Evidence that rock joint hydro-mechanical properties are dependent on joint surface characteristics such as roughness, matching and wall strength were obtained by Jaeger [1959], Patton [1966], Louis and Maini [1970], Barton [1971], Maini [1971b], Goodman [1976], Tsang and Witherspoon [1982].

2.2.1 Joint roughness

Roughness is a measure of the inherent surface unevenness and waviness of the discontinuity relative to

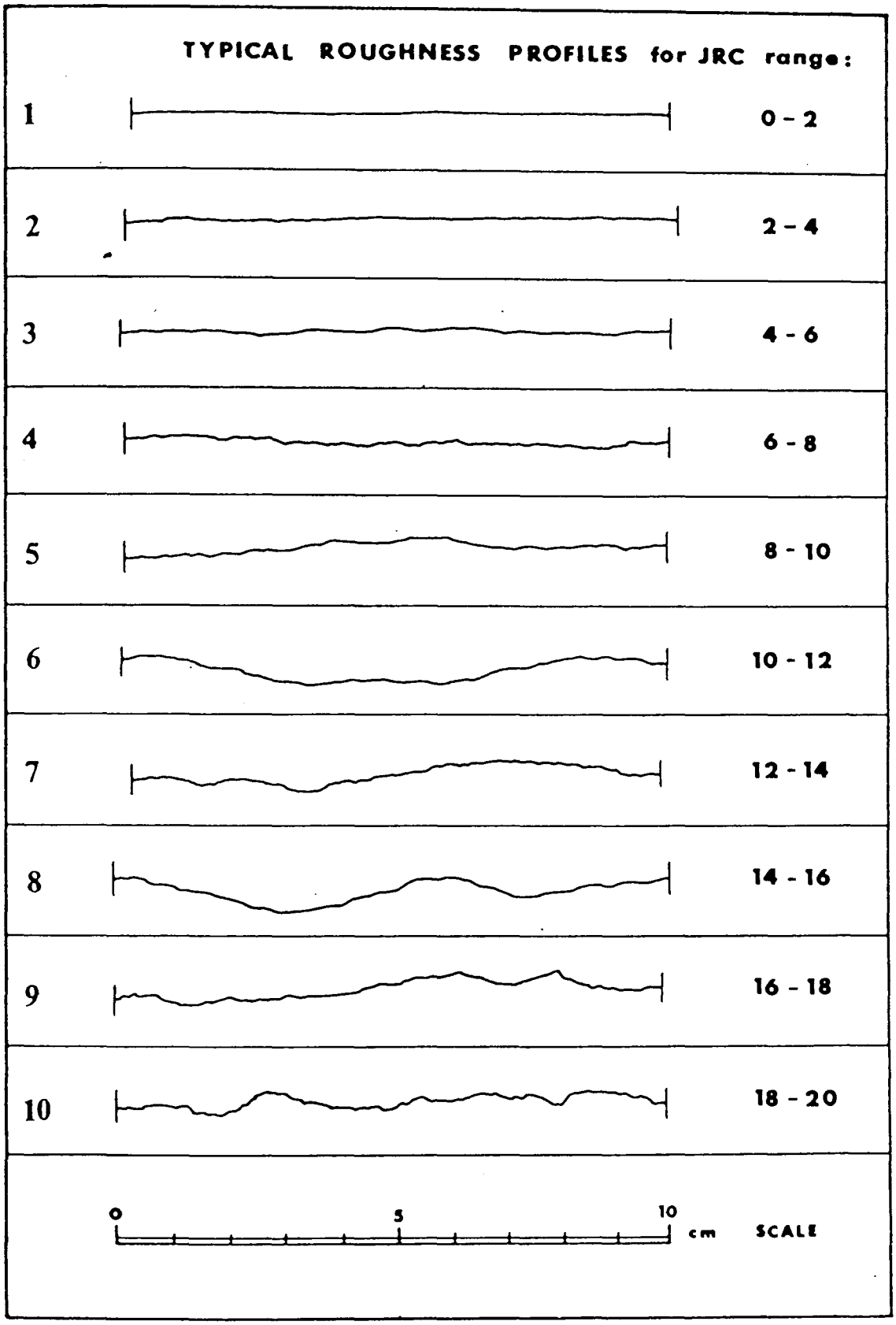


Figure 2.4 Typical Roughness Profiles and Corresponding Range of JRC (after Barton and Choubey [1977]).

its mean plane [Louis 1969]. It is a potentially important component of shear strength, especially in the case of undisplaced and interlocked fractures (e.g. unfilled joints). The importance of wall roughness declines as aperture, or filling thickness, or the degree of any previous displacement increases.

Barton [1972, 1973, 1976], Barton and Choubey [1977] proposed a Joint Roughness Coefficient (JRC) to describe the surface roughness scaled from 0 to 20. Typical roughness profiles for the entire JRC range are represented in Figure 2.4. The measurements of this index are estimated by using the direct profiling method for the joint.

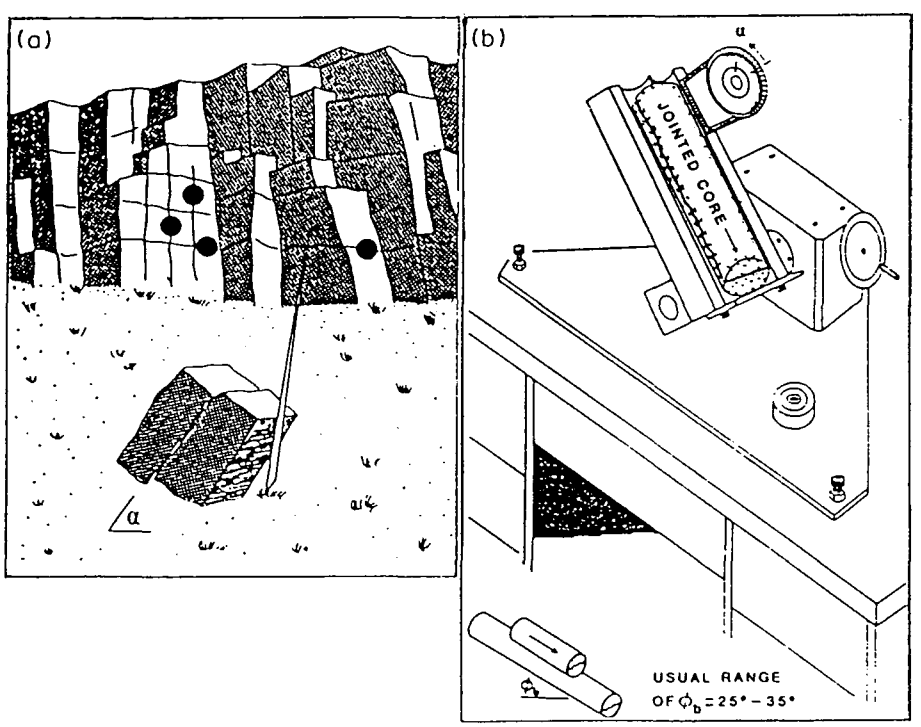


Figure 2.5

Tilt Test (After Barton and Choubey [1977]).

A indirect method of estimating the JRC is described by Barton and Choubey [1977] and developed in Norwegian Geotechnical Institute (NGI). By perform the Tilt Test on a rough joint as illustrated in Figure 2.5, together with Schmidt Hammer Index Tests and the Tilt Test on sawn rock surface, the JRC value can be easily and conveniently estimated.

The ISRM Commission [Brown 1981] recommended that in general terms the roughness of the discontinuity walls can be characterized by a "waviness" (large scale undulations which, if interlocked and in contact, cause dilation during shear displacement since they are too large to be sheared off) and by an "unevenness" (small scale roughness that tends to be damaged during shear displacement unless the discontinuity walls are of high strength and/or the stress levels are low, so that dilation can also occur on these small scale features).

The Commission suggested that the roughness can be described on two scales of observation based on the small scale (several centimetres) and the intermediate scale (several metres) as shown in Table 2.1 and Figure 2.6 which shows the typical profiles.

The intermediate scale of roughness is divided into three degrees: stepped, undulating and planar, and the small scale is also divided into three degrees: rough (or irregular), smooth and slickensided. The term "slickensided" should only be used if there is clear evidence of previous shear displacement along the

Table 2.1 ISRM Descriptive Terms for Joint Roghness
(After Brown [1981])

	Small scale (several centimeters)	Intermediate (Several meters)
I	Rough (or irregular)	Stepped
II	Smooth	Stepped
III	Slickensided	Stepped
IV	Rough (or irregular)	Undilating
V	Smooth	Undilating
VI	Slickensided	Undilating
VII	rough (or irregular)	Plannar
VIII	Smooth	Plannar
IX	Slickensided	Plannar

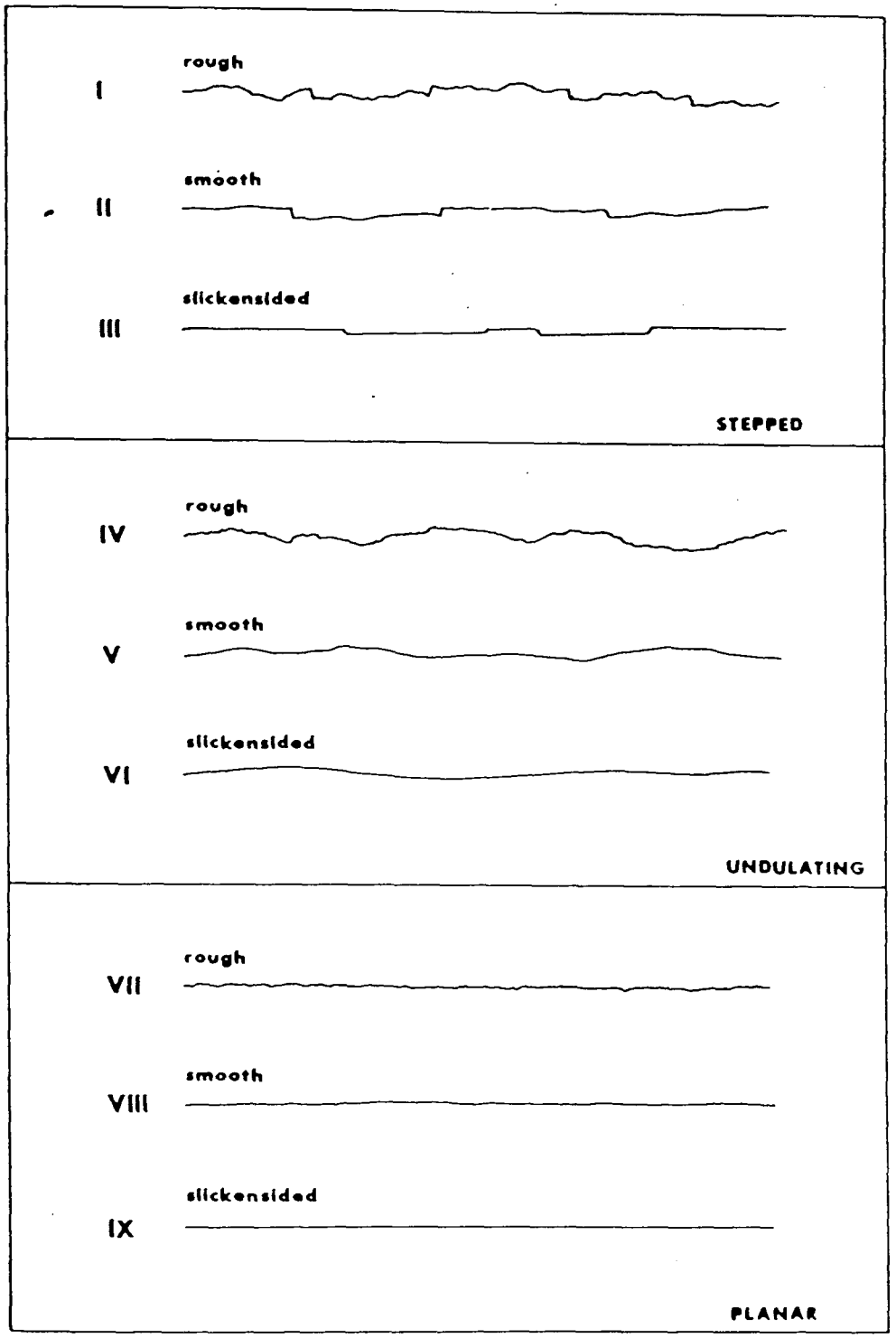


Figure 2.6 Typical Roughness Profiles and ISRM Suggested Nomenclature (after Brown [1981]).

discontinuity.

2.2.2 Joint wall compression strength

The compression strength of the rock comprising the walls of a discontinuity is a very important component of shear strength and deformability, especially when the walls are in direct rock to rock contact as in the case of unfilled joints. Slight shear displacement of individual joints caused by shear stresses within the rock mass often results in very small asperity contact areas with the stresses locally approaching or exceeding the compression strength of the rock wall material, producing asperity damage.

Rock masses are frequently weathered near the surface, and are sometimes altered by hydro-thermal processes. The weathering and alteration generally affects the walls of the discontinuities more than the interiors of rock blocks. This results in a wall strength that is some fraction of what would be measured on the fresher rock found in the interior of the rock blocks, for example that sampled by core drilling.

There are two main results of weathering: one dominated by mechanical disintegration, the other by chemical decomposition including solution. Generally, both mechanical and chemical effects act together, but, depending on the climatic regime, one or other aspect may be dominant. Mechanical weathering results in the opening of discontinuities, the formation of new discontinuities

by rock fracture, the opening of grain boundaries, and the fracture or cleavage of individual mineral grains. Chemical weathering results in discolouration of the rock and leads to the eventual decomposition of silicate minerals to clay minerals. Some minerals, notably quartz, resist this action and may survive unchanged [Morey and Hesselgesser 1951].

2.2.3 Fracture aperture

Aperture is the perpendicular distance separating the adjacent rock walls of an open discontinuity, in which the intervening space is filled with air or water. Aperture is thereby distinguished from the width of a filled discontinuity [Brown 1981, Brady and Brown 1985].

A large aperture can results from shear displacement of discontinuities having appreciable roughness and waviness, from extensive opening, from outwash, and from solution. In most subsurface rock masses apertures are small and will probably be less than half a millimeter, compared to the tens and hundreds of millimeters width of some of the outwash or extension varieties. However, indirectly as a result of hydraulic conductivity, even the finest may be significant in changing the effective normal stress [Hudson 1987] and therefore also the shear stress [Barton et al 1985, Barton 1986].

Apertures are recorded from the point of view

of both their loosening and conducting capacity [Brown 1981]. Joint water pressure, inflow of water and outflow of storage products (both liquid and gas) will be effected by aperture. The influence of aperture on the permeability or hydraulic conductivity of the discontinuity and of the rock mass is according a cubic flow law. For laminar flow, the hydraulic conductivity of a single discontinuity with plane, parallel sides is given by

$$k = \frac{g\ e^2}{12\nu} \qquad (2.11)$$

2.2.4 Joint matching

Geologically, joints may suffer weathering, shearing, previous loading or thermal cycles, all of which may change the joint, normally in a very similar way, that is, they may smooth the joint surface. The effects also crush some of the asperities, which in turn affects the matching of the joint surfaces. In the general case, the joint that have been weathered, sheared or under loading and thermal cycles are smoother in roughness but poorer in matching compared to fresh extension fractured joints. Hence, it is not possible to represent the degree of matching by the degree of roughness. Both may have a significant influence on the mechanical, hydraulic and thermal properties of a joint.

A larger joint aperture and joint hydraulic conductivity may be associated with poorer matching of

the joint, and the mechanical behaviour may also differ due to different degrees of matching. It will be shown later that the joint closure - effective normal stress behaviour is virtually controlled by the contact area between the two surfaces of the joint.

Tsang and Witherspoon [1982] used a numerical investigation to correlate the relationship between fracture roughness characteristics and fracture mechanical and hydraulic properties using their model (see section 2.4). They used the term aperture density n(b), the number of discretized units with the aperture, to describe different matching for the same fracture surface roughness. The results showed that both mechanical fracture closure and normalized flow rate were effected by different matching of the fracture. Their investigation showed that as the mismatching between the top and bottom joints increases, the aperture distribution broadens and the variation of normal stress with aperture closure becomes less steep; or in other words, softer mechanical properties is predicted for the more mismatched fractures. It also showed that the flow drop with normal stress becomes progressively slower from well matched joint case to mismatch joint case as the rise in the aperture distribution becomes less steep. The flow approaches zero asymtotically as the fracture closure becomes complete. Such asymtotic had been observed (e.g., Iwai [1976] and Kranz et al [1979]). Goodman [1976] and Bandis et al [1983] showed that a mismatched joint has mechanical characteristics similar

to those identified by Tsang and Witherspoon.

All these observations suggest that a numerical index is required to represent the condition of joint matching. The degree of joint matching is a combination of the following two factors:

1) the matching of joint waviness, i.e., in the medium to large scale (1/10 m to m);
2) the degree of the joint roughness, i.e. on the small scale (mm to 10 mm).

To represent this numerical index, a Joint Matching Coefficient is developed to couple with the existing Joint Roughness Coefficient [Barton 1972, Barton 1973, Barton 1976, Barton and Choubey 1977] to provide a suitable parameter for correlating joint surface properties. It will therefore be easier to use if JMC has chosen the same measure as JRC. The defined Joint Matching Coefficient (JMC) scaled from 0 to 20 is presented in Table 2.2 and Figure 2.7 and Figure 2.8 which shows typical joint profiles for the various cases. Clearly, fresh extension fractures (Figure 4.4) are placed in the category of "very good" joint waviness matching, with some exceptional ones falling into the category of "good" waviness matching. Natural joints (Figure 4.5) can have joint waviness matching down to the "very poor" category dependent upon previous geological conditions as indicated earlier.

Table 2.2 Joint Matching Coeffient (JMC)

Joint Surface Roughness (JRC)	Joint Waviness Matching, good→poor				
	1*	2	3	4	5
Slickensided(1-3)	1-2	1-3	2-4	2-4	2-5
Smooth(4-7)	2-3	3-4	4-6	4-7	5-8
Rough(8-11)	3-5	4-6	6-8	7-10	9-13
Very rough(12-15)	5-7	6-9	8-11	10-13	13-17
Stepped rough(16-20)	7-10	9-12	11-14	13-17	16-20

* 1-very good, 2-good, 3-fair, 4-poor, 5-very poor.

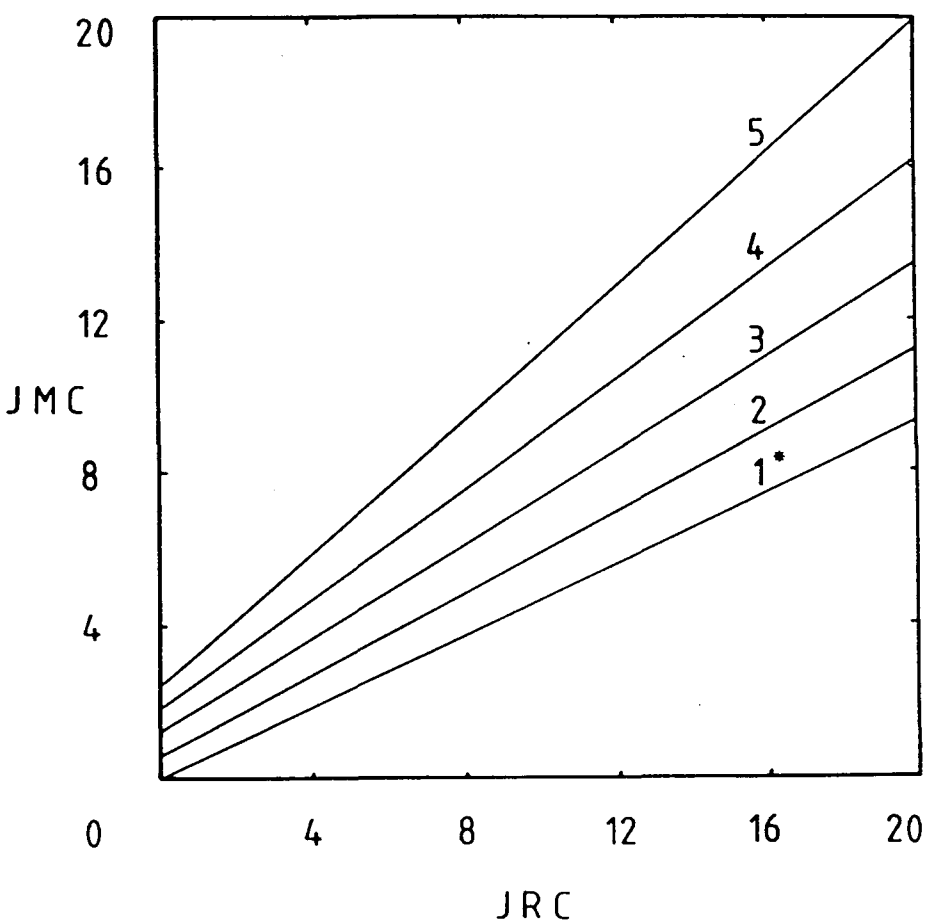


Figure 2.7 Joint Matching Coefficient.

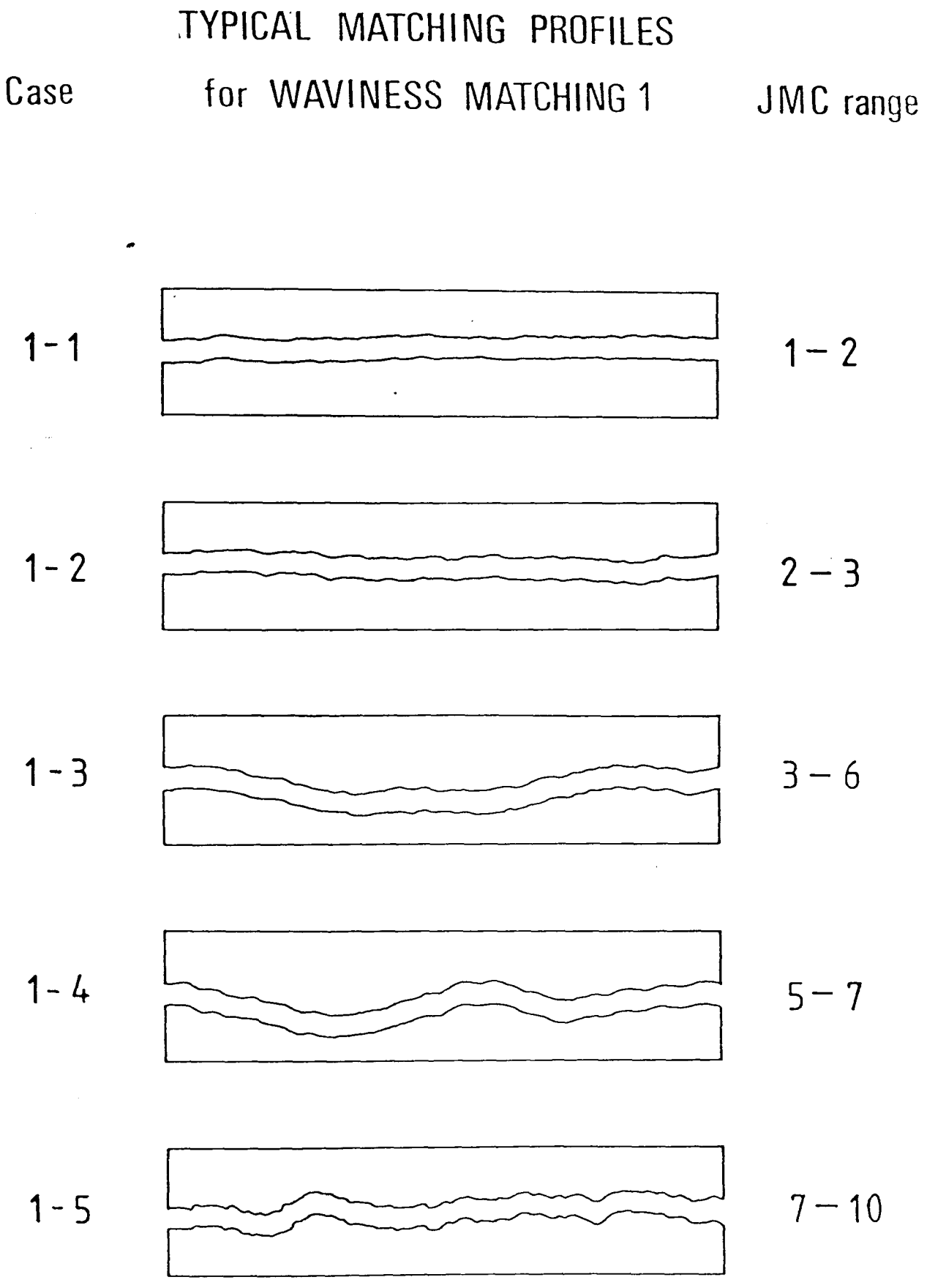


Figure 2.8 Typical Joint Profiles with JMC Ranges.

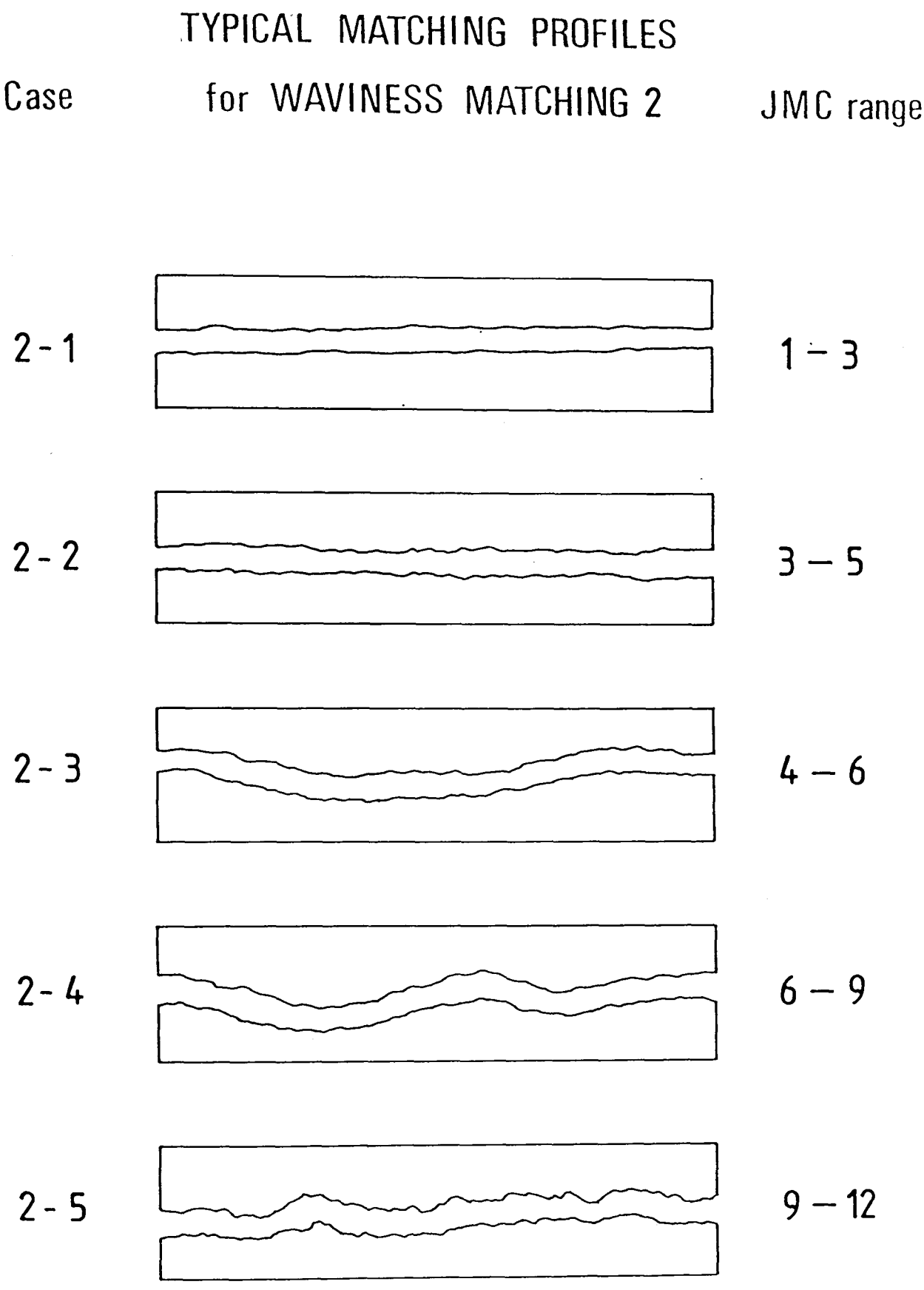


Figure 2.8 (continued).

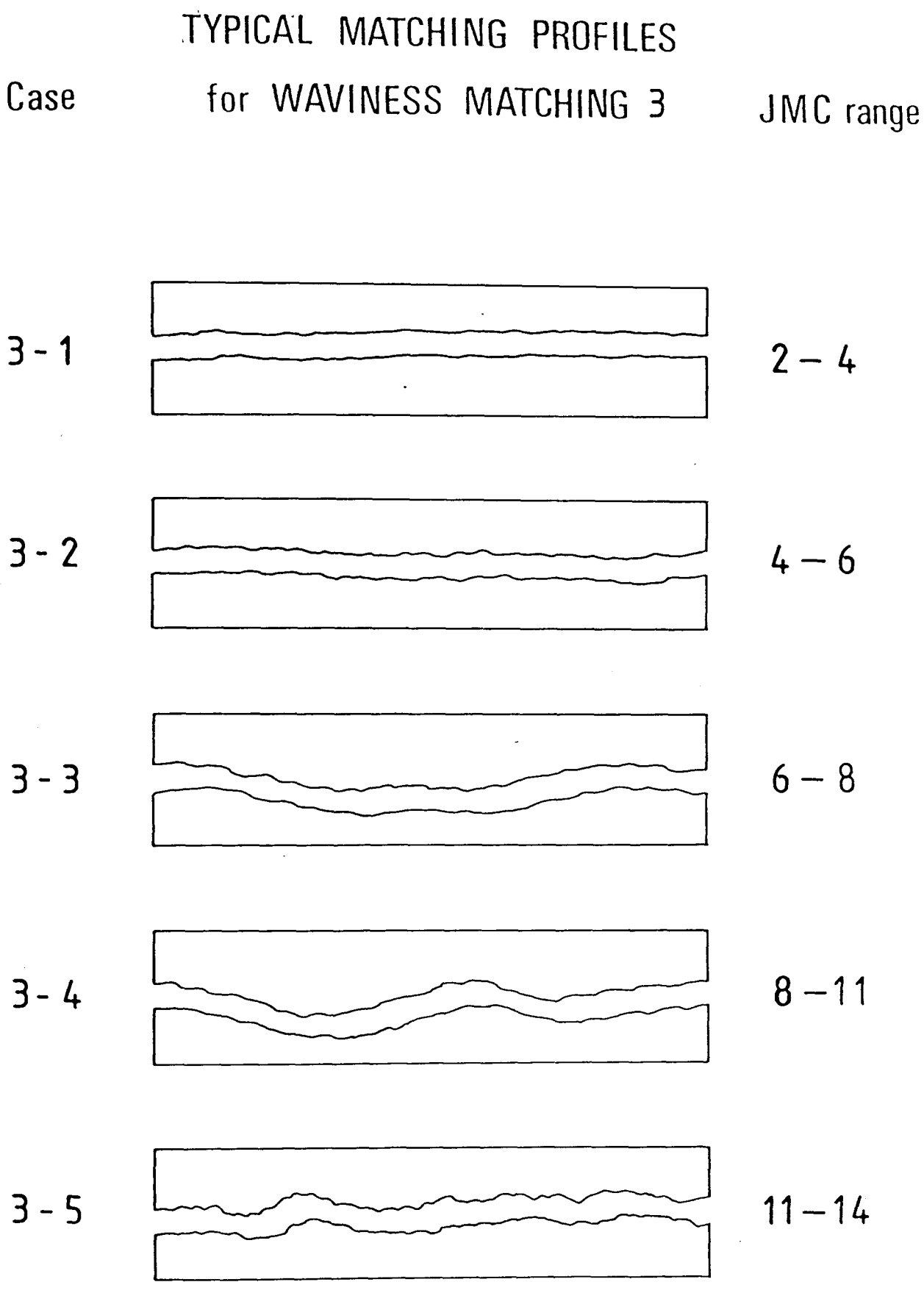


Figure 2.8 (continued).

TYPICAL MATCHING PROFILES

Case for WAVINESS MATCHING 4 JMC range

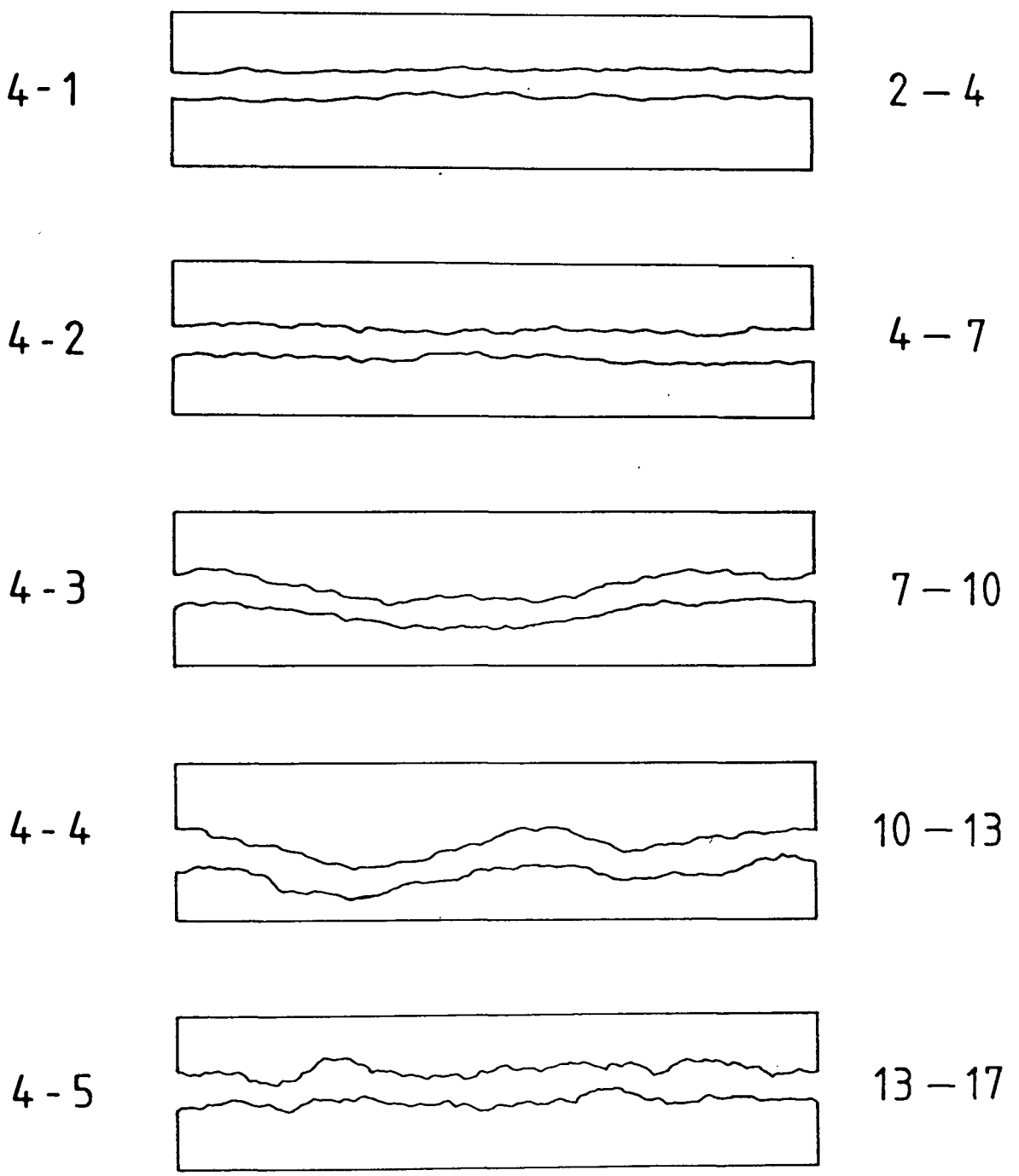


Figure 2.8 (continued).

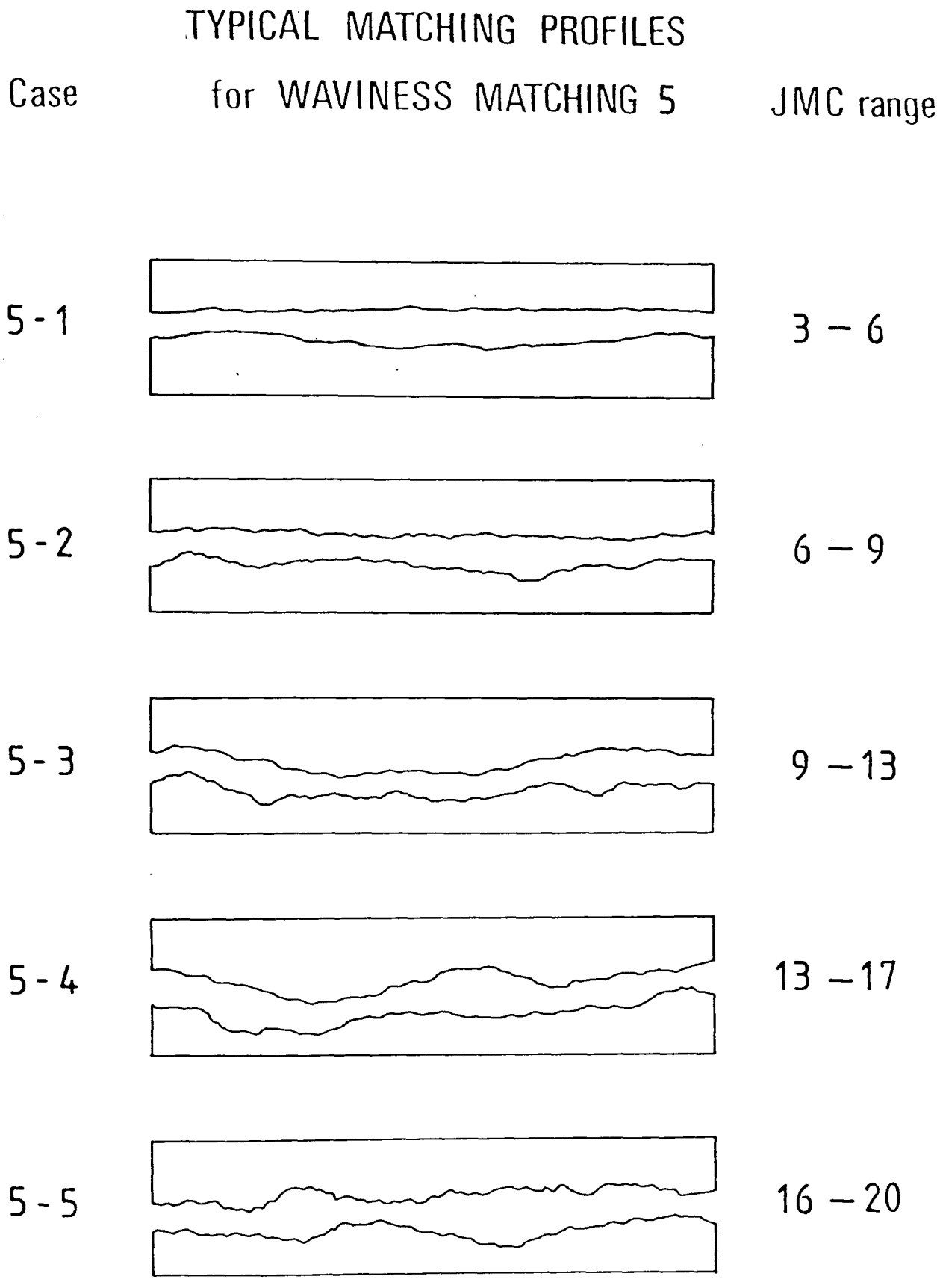


Figure 2.8 (continued).

2.3 Hydro-mechanical properties of single joint

2.3.1 Modification of the parallel plate theory

As stated earlier in this chapter (section 2.1.1), parallel plate theory is widely adopted for the analysis of viscous fluid flow in joints. When a liquid flows under different pressures, the flow rate Q per unit area A normal to the flow is related to the hydraulic head gradient i, in the direction of fluid flow. Hence,

$$\frac{Q}{i} = C\, e^3 \qquad (2.14)$$

and

$$C = \frac{w\, g}{12\, \nu} \qquad (2.15)$$

where g = acceleration due to gravity,

ν = kinematic viscosity of the fluid,

w = width of the joint,

e = aperture of the joint.

When this theory is applied to actual rock joints with rough surfaces, of which the walls are far from smooth [Louis 1969, Sharp 1970, Maini 1971, Hoek and Bray 1981, Blyth and De Freitas 1984], the equation does not truly represent the real case. The original equation therefore, does not account for the deviations from the ideal conditions due to the joint surface geometry and other effects. Somehow, modification has to be introduced to reflect the effects of joint roughness, surface matching, joint stiffness, deposits of detritus, loading

history, sample disturbance, sample size and temperature [Witherspoon et al 1980, Elliott et al 1985].

Sharp [1970] and Sharp and Maini [1972] proposed an empirical flow law for natural joint fractures disputing the validity of the cubic flow law and suggesting that for their particular conditions, the exponent in the flow equation (2.14) should be 2. In reviewing these results, Gale [1975] pointed out that the cubic law is still valid if one correlates their flow rates corresponding to the apertures that are actually presented (i.e., the real aperture). Witherspoon et al [1980] examined the validity of the cubic flow law through a rough walled fracture and showed that an equivalent cubic law may be used. The flow cubic law for rough joints then can be written as

$$\frac{Q}{i} = \frac{C}{F} E^3 \qquad (2.16)$$

where F is a factor that accounts for deviations from the ideal conditions that are assumed in the parallel smooth plate theory.

2.3.2 Elastic and Non-elastic Behaviour

The relationship between normal displacement and effective normal stress is well established, e.g., by Goodman [1976]. The elastic modulus of jointed rock, as always, is less than that of the intact rock. Typical normal stress-displacement curves for intact rock and

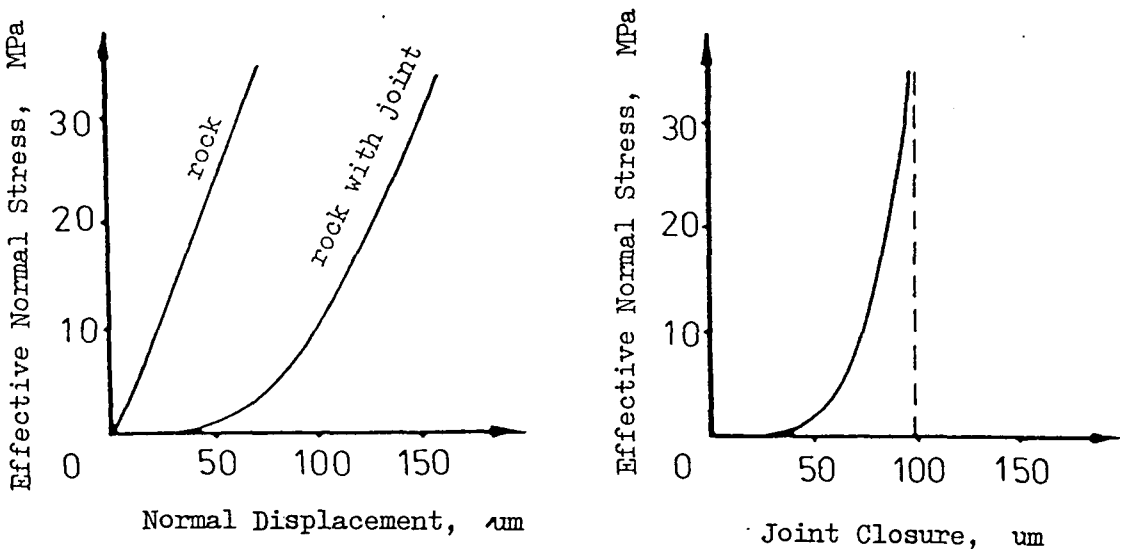


Figure 2.9 Typical Joint Closure-Normal Stress Behaviour.

jointed rock are shown schematically in Figure 2.9. The slopes of these curves clearly demonstrate that at low stress, the Young's modulus for the jointed rock is much smaller than that of the intact rock [Maini 1973]. As normal stress level increases, the modulus increases and approaches the value of the intact rock at higher stresses.

If a small block is placed slightly with its own weight on a rough surface, the contacting area is virtually zero in proportion to the total area, since the block is only in contact with the rough surface in three or more points. The entire load is hence sustained at the contacted asperities. The points of contact and their areas are enlarged by elastic deformation, crushing and tension cracking. By taking account of two physical constraints on normal deformation in discontinuities, first, an open joint has no tensile strength and secondly, there is a limit to the amount of compression closure, which must be less than the "thickness" of the

joint, Goodman drew that a simple relationship satisfying these conditions is the hyperbola

$$\frac{\sigma' - \zeta}{\zeta} = S\left(\frac{\Delta V}{V_{mc} - \Delta V}\right)^t \qquad (2.17)$$

where ζ = the seating pressure, defining the initial conditions for measuring the joint normal deformation V,

V_{mc} = joint maximum possible closure,

σ' = effective normal stress,

ΔV = joint normal closure,

S, t = constants.

2.3.3 High temperature mechanical, physical and thermal properties of granitic rock

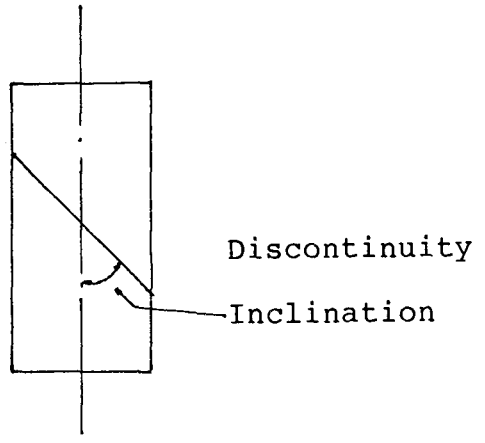
Extensive studies have been undertaken by a large number of previous workers on high temperature mechanical, physical and thermal properties of granitic rock. A review was given by Heuze [1983].

Compressive Strength

Comprehensive triaxial compression test results [Borg and Handin 1966, Tullis and Yund 1977, Jaeger and Cook 1979, Friedman et al 1979, Bauer et al 1981] on some granitic rock showed a significant decrease in rock strength at elevated temperatures. At low confinement less than the required threshold stress for thermal cracking, this decrease was even greater. Test

Table 2.3 Mechanical Properties of Cornish Granite (after Elliott [1984]).

Sample Temp. (°C)	Conf. Pres. (MPa)	Young's Modulus (GPa)	Poisson's Ratio	Max. Dev. Stress (MPa)	Residual Strength (MPa)	Discont. Inclin.
25	0	47.1	0.22	136.5	---	--
23	15	53.0	0.30	256.0	85	(32)
20	30	49.8	0.26	328.4	120	(31)
24	45	51.6	0.23	376.9	150	(29)
25	60	48.9	0.21	448.0	210	(27)
200	0	51.3	0.38	119.1	---	--
200	15	49.8	0.33	224.4	---	18
200	30	54.5	0.31	295.1	120	29
200	45	59.2	0.27	379.1	---	34
200	60	(57.8)	(0.38)	442.3	---	27



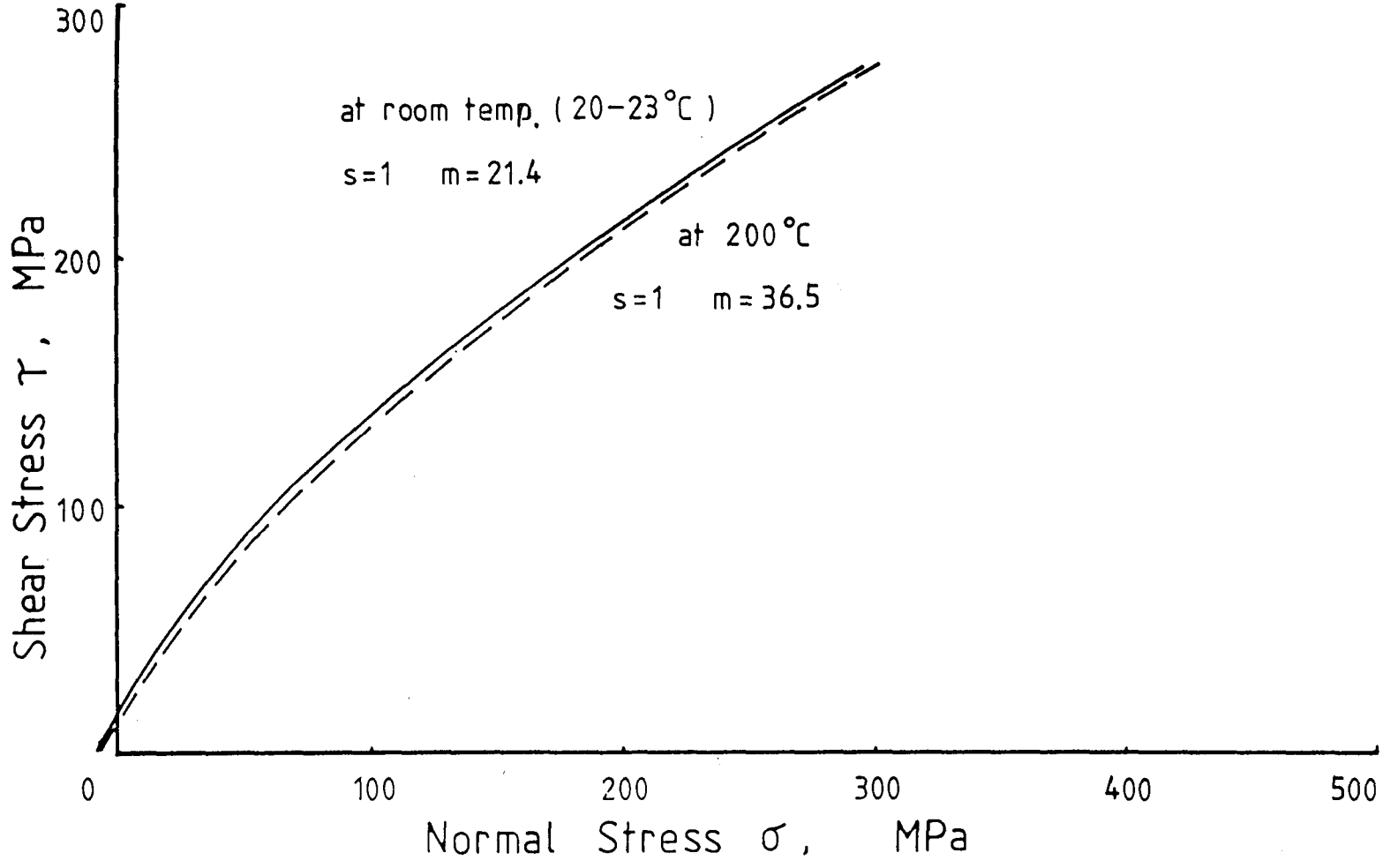


Figure 2.10 Cornish Granite Failure Envelope at Test Temperature of 20°C and 200°C (after Elliott [1984]).

results on Silver Phime granite at confining pressure of 0.1 MPa [Borg and Handin 1966] showed a reduction of as much as 50% on ultimate strength from room temperature to 400°C. However, at higher confinement, this reduction was smaller. Results on Cornish granite up to 200°C [Elliott 1984] also showed a reduction of up to 12% on uniaxial strength and up to 1.5% on ultimate strength at 60 MPa confinement, as shown in Table 2.3.

The Hoek and Brown [1980] failure envelope for those Cornish granite samples tested at 20°C gave m=21.41 and for those samples tested at 200°C gave m=36.52; S=1 since intact samples were tested. Despite this variation in the m value for the two sets of samples, the failure envelope for the samples tested at 200°C seemed to be almost identical to that for the samples tested at 20°C (Figure 2.10). The deformation mechanism seemed to be unaffected by the test temperature [Elliott 1984].

Young's Modulus and Poisson's ratio

Results obtained on numerous granites [Kaye and Lamb 1966, Swan 1978, Bauer and Johnson 1979, McLaren and Titchell 1981, Page and Heard 1981, Elliott 1984] show that the Young's modulus is temperature- and pressure-dependent. A decrease of Young's modulus with increase in test temperature is evident. This decrease continues after the temperature above the $\alpha-\beta$ transition of granite (573°C at atomspheric pressure). Results on Charcoal granite obtained by Bauer and Johnson [1979] clearly show that increased pressure tends to retard the

decay of elastic modulus, when temperature increases.

Previous tests have not shown a clear dependence of Poisson's ratio, ν, either on pressure or on temperature. However, Swan [1978] showed that for Stripa granite, at atomspheric pressure, ν decreased from 0.21 at 10°C to 0.13 at 200°C. On the contrary, the results obtained from Cornish granite [Elliott 1984] showed a general increase of ν with temperature from 20°C to 200 °C at each confining pressure ranging from atomspheric pressure to 60 MPa. It indicates that the variation in the measured values of Young's modulus and Poisson's ratio seems to be more dependent on the environmental conditions.

Thermal Expansion

The increase of the linear thermal expansion coefficient, α, with temperature has been investigated for numerous granites [Richter and Simmons 1974, Cooper and Simmons 1977, Wong and Brace 1979, Heard 1980]. The increase occurred at various pressures. The thermal expansion tests conducted above $\alpha-\beta$ transition temperatures [Van Der Molen 1981] at atmospheric pressure indicated a sharp increase in expansion just beyond the $\alpha-\beta$ transition. However, studies made by Van der Molen [1981] revealed that the linear thermal expansion coefficient would be greatly reduced beyond the $\alpha-\beta$ transition temperature. This reduction was further enhanced by increasing pressure. However, at temperatures

under the transition temperature and for pressures large enough (well above threshold stress) to prevent thermal cracking, the pressure dependency of thermal expansion has been shown to be quite small in tests on Westerly granite [Wang and Brace 1979] and Climax granite [Heard 1980, Durham and Abey 1981a]. In general, the effect of pressure is to increase the $\alpha-\beta$ transition temperature and to lower the peak thermal expansion.

Thermal properties

The results for specific heat, c_p, for different granites obtained by different types of test are quite consistent [Lindroth 1971, Dmitriyev et al 1972, Klett 1974] except after the $\alpha-\beta$ transition temperature. The specific heat increases linearly with temperature until the transition point. The results after the transition are apparently quite uncertain. All the data reported were obtained at atomspheric pressure; as yet no results have been obtained at elevated pressures.

The thermal conductivity is reduced by increasing the temperature, as a result of thermal cracking [Kaye and Lamb 1966, Walsh and Decker 1966, Jeffry et al 1979, Pratt et al 1979, Durham and Abey 1981a, Durham and Abey 1981b]. No results were found above the $\alpha-\beta$ transition temperature. However, the increase in confining pressure produced a modest increase in k [Walsh and Decker 1966].

The results obtained for thermal diffusivity

showed similar pressure and temperature dependencies as did the thermal conductivity [Hanley et al 1978, Jeffry et al 1979, Durham and Abey 1981a, Durham and Abey 1981b]. Moreover, the data consistently showed a minimum of thermal diffusivity at the α-β transition at various pressures.

Permeability

Permeability of the intact rock depends on the interaction between the water and the rock. Porosity measurements are generally used to calculate an estimated permeability K [Page and Heard 1981]. This permeability K is predicted to increase with temperature since the porosity would be increased as a result of thermal cracking and expansion [Summers et al 1978, Brace 1980].

The granite mass permeability is dominated by the water conducted through fractures (joints) [Louis 1969, Maini 1971a, Wittke 1973]. As for the granite mass as a whole, thermal expansion would tend to close the existing joints thus reducing the overall permeability [Lundstrom and Stille 1978, Ballou 1979, Voegele et al 1981]. A 10-fold reduction was also observed in-situ, in the Idaho Springs granite gneiss for an increase in temperature from 41°C to 73°C [Voegele et al 1981].

The effect of pressure is obviously to reduce the permeability for both intact rock and the rock mass by closing the pores and fractures [Maini 1973, Brace 1980]. Results of permeability test of whole Barre

granite showed a reduction of 2.5 fold as effective normal stress increased from 5 to 10 MPa [Kranz et al 1979]. Discussions of the influence of effective normal and temperature are presented in Chapter 5 and Chapter 6.

2.3.4 Stress, joint surface properties and temperature coupled effects on joint hydro-mechanical behaviour

Stress

In an earlier section (2.3.2), the effect of stress on the joint mechanical properties was stated, as shown in Figure 2.9. Goodman drew a simple hyperbolic relation between effective normal stress and joint closure. By using the equivalent cubic flow law, the flow rate is proportional to e^3, where e is joint opening. The joint permeability thus is proportional to e^2. The stress has a dominating effect on the joint closure hence on the joint hydraulic permeability [Sharp et al 1972].

Joint surface properties

The effects of joint surface properties are due to three components -joint surface roughness, joint surface matching and joint wall strength. The first two could alter the mechanical and hydraulic behaviour of the joint in a similar way. Basically, high roughness and non-matching lead to large joint aperture and greater joint conductivity. Larger mechanical and hydraulic

aperture closures occur at higher applied effective normal stresses. This has been demonstrated by Goodman [1976], Bandis et al [1983] and Tsang and Witherspoon [1981] by mismatching the joint. Barton et al [1985] also concluded that joint with high roughness coefficient can produce both large hydraulic and mechanical aperture (see section 5.2.4) or the change of those apertures under the effective normal stress. But it would become complicated when wall strength is also under consideration. Samples with the same roughness and matching may still have quite different behaviour if one of them has been weathered or has experienced stress and thermal alterations. Therefore one should expect that natural joints will sustain a larger change in apertures than those artificial extension fractures under the same increment of effective normal stress, even if they have the same roughness coefficient and matching quality.

Temperature

Only a few studies on the fully coupled, hydro-thermo-mechanical joint behaviour have been conducted previously. Handin et al [1982] reported for a rough, mineralised joint in gneiss, a thirty-fold reduction in flow conductivity when temperature increased from room temperature to 74°C. The reduction of flow conductivity and of flow aperture with temperature was interpreted by Barton and Lingle [1982] as improved mating of the opposing joint walls.

2.3.5 Joint Condition Factor, JCF

As mentioned in section 2.2.1, Gale [1975] and Witherspoon et al [1980] pointed out that the cubic flow law derived from smooth parallel plate theory is still valid if one correlates their flow rates correspondingly to the real aperture. Hence for flow Q through a rough-wall fracture with real aperture E, the equivalent cubic flow law becomes

$$\frac{Q}{i} = \frac{C}{F} E^3 \qquad (2.16)$$

where F is a factor that accounts for deviation from the ideal conditions which are assumed in the smooth parallel plate theory. Elliott et al [1985] termed the factor F, the joint condition factor (JCF). This modification is to reflect the effects of joint roughness, surface matching, joint wall strength, deposits of detritus, loading history, sample disturbance, temperature and sample size. In the general case of rough walls, $F \geq 1$.

$$\text{By assuming } F = 1/f^3 \qquad (2.18)$$

Equation (2.16) becomes

$$\frac{Q}{i} = C \ (f\,E)^3 \qquad (2.19)$$

By comparison with the cubic flow law for smooth parallel plates, Equation (2.14), it is seen that

$$fE = e \quad \text{or} \quad e/E = f \tag{2.20}$$

where e is the theoretical hydraulic aperture.

Witherspoon et al [1980] have determined the value F using a least squares method to fit their data, and found that F is a constant greater than or equal to one. Hence, for a samples at different apertures without change of joint conditions, F is a constant. The ratio of theoretical hydraulic aperture to the real mechanical aperture is also a constant.

The value of JCF is affected by joint conditions. Witherspoon et al [1980] reported that the F value was greater when the joint is rougher. Joint matching may control JCF to the same extent as roughness does, though so far no previous study of this has been found. Witherspoon et al [1980] also reported that the F value was reduced by cyclic loading. This reduction may be due to the better mating of the opposing joint walls. The results obtained and presented in Chapter 5 suggest a conclusion that is quite the opposite of the one drawn by Witherspoon et al. In general, the F value is increased after the first loading. When the joint is loaded normally up to 30 MPa, some of the asperities fractured or crushed. The increase in the F value can be accounted for in three ways: better mating, weaker wall strength and production of detritus. As a combination, the results may worsen the total joint condition. Thermal effects somehow influence the JCF in a similar way to loading. Localised better mating may occur due to thermal

expansion into the fracture. Together with the deposition of detritus, this may reduce the flow conductivity. However, the overall joint is expanded by the contact asperities being pushed apart (see section 5.7). Thermal cracks occurring perpendicular to the joint surface can also decrease the joint wall strength (see section 5.7). Hence, heating up the joint or subjecting the joint to a thermal cycle would be expected increase the value of JCF.

2.4 Review of Previous Work and Models of Joint Hydraulic Behaviour

2.4.1 Review on previous work

Louis [1969] started his comprehensive research on rock joints hydraulics at the Technische Hochschule Fridrieiana in Karlsruhe, Germany. He found that for a single fracture, if the fluid flow in a laminar state, the mean velocity of the flow through the joint with mean aperture of E is

$$V = \frac{k\ g\ i\ E^2}{12\ \nu\ C} \qquad (2.21)$$

where k is the degree of continuity of the fracture (ratio of the open surface to the total surface of the fracture), ν is the kinematic viscosity of the fluid. C is a coefficient which depends on the relative roughness K/D_h of the fissure, and is given by

$$C = 1+8.8\ (K/D_h) \qquad (2.22)$$

where K is the absolute roughness of the joint walls and D_h is the "hydraulic diameter". In the case of planar joints, $D_h = 2e$, and K is represented by the height of asperities.

By rewritting Louis' equation as

$$Q = \frac{w\ g\ i\ k\ E^3}{12\ \nu\ C} \qquad (2.23)$$

one can instantly see that C/K=JCF by comparison to Equation (2.16).

Louis [1969, 1973] and Louis et al [1976] also investigated turbulent flow , giving

$$V = 4\ k\ \sqrt{g\ k}\ \log_{10} \frac{1.9}{K/D_h} \sqrt{i} \qquad (2.24)$$

for a relative roughness $K/D_h > 0.033$.

In addition he found that for the fluid flow in a fracture, the transition from laminar to turbulent flow takes place at very low values of the Reynold's number (2300 for parallel smooth plates). The Reynold's number would be as low as 100 or even 10 for flow from laminar to transitional in a rough fracture and decreases as the relative roughness of the fracture increases. The Reynold's number, defined by the relation $Re = \mu\ D_h/\nu$, in fact has a value that is extremely difficult to determine in the case of rock fractures, since for a given type of flow it can vary enormously from one point to another

along the same fracture. Louis argued that roughness increases the flow path and causes curvature loss because of the inherent changes in direction of the flow. Great energy losses will occur in addition to friction losses. These energy losses are caused by the formation of eddies which are in turn caused by the curves and contractions in the flow channels. Hence, he concluded that the flow process within the fracture cannot be determined analytically, but must be studied experimentally.

Louis conducted his experimental study using two concrete slabs with rubber seals between them. However, the joint was held open by the rubber seal, which is hardly the case occurring in nature. Therefore the results that Louis obtained are not discussed here.

Kranz et al [1979] conducted permeability tests on whole (intact) and jointed Barre granite. Their results showed that the permeability K was a function of many variables, the most important of which were evidently confining pressure, internal fluid pore pressure, temperature and, in the case of joints, surface roughness. They found that jointed rock was much more sensitive to effective normal stress than intact rock and that the decrease in permeability was greater for joints than for whole rock. That is, the aperture closes more readily under pressure than do cracks within the whole rock. In addition, the joint surface has an effect on the decline of permeability with the effective normal stress. For the whole sample the aperture is small so the joint

closes rapidly at low pressures until enough of these asperities make contact with the opposing surface to increase the flow tortuosity and decrease the closure rate. In contrast, where the aperture is larger and tends to prop the joint open, thereby diminishing the rate of permeability decline diminishes as the effective normal stress is raised.

Iwai [1976] investigated the effects of contact area and aperture geometry on the permeability of rock fractures. He found that at low effective normal stress (0.26 MPa) the real area of contact of a granite fracture was less than 0.1% of the apparent total area and increased to 10 - 20% at 20 MPa, and also derived that the contact area increased linearly with effective normal stress. This was consistent with the results of Bowden and Tabor [1950] who showed that, neglecting time effects, the real area of contact

$$Ar = N/h \tag{2.25}$$

where N is the average normal load on an aperture and h is the indentation hardness for the asperity material.

Iwai found that the relationship between the permeability and the contact area could be expressed by an empirical form

$$\gamma \frac{K}{K_o} + 1 = \frac{\phi}{\gamma\, Ar/A + 1} \tag{2.26}$$

where γ and ϕ are empirical constants, K_o is the pressure permeability at zero pressure, Ar is the real area of

contact and A is the aperture joint surface area.

A series of conductivity experiments under straight flow conditions were performed on an artificial granite fracture closed under various compression stress by Detournay [1980]. Regression analysis carried out on the calculated conductivity coefficients and the joint closure data showed that the parallel-plate cubic law was applicable to closed joints provided that one introduces an initial aperture (corresponding to zero stress across the fracture), which was computed from the conductivity-closure data. Detournay also found that with a constant load applied on the sample, the relationship between discharge and head gradient was linear only at low pressure gradients. A conductivity coefficient could be computed by linear regression. The discharges observed at high pressure gradients were consistently greater than what could have been expected from extrapolation of the linear regression.

However, this observed non-linearity between the discharge and the head gradient was quite certainly attributable to the deformation of the joint caused by a change of the effective stress across the fracture. Apparently, in his tests, Detournay increased the head gradient at a constant normal stress. The increase of head gradient caused an increase in pore pressure, which in turn reduced the effective stress. The joint aperture was thus enlarged, which led to a greater discharge being observed. This non-linearity can hence be overcame by

keeping the effective stress constant rather than by holding the external normal stress constant. This non-linearity will occur at a high fluid pressure gradient when the flow becomes turbulent as discussed earlier in this section.

Gale [1982] studied the effects of fracture type on the normal stress - fracture permeability relationship by testing granite samples containing natural joints and tensile induced fractures. The results showed that the induced fractures gave lower initial (at low normal stresses) and lower final (at maximum normal stresses) flow rates, than the natural joints. Gale suggested that natural joints are stiffer than induced fractures and that fracture closure at a given normal stress will be less for natural fractures. Both types of fracture exhibited permanent nonlinear, with distinct hysteresis, loading and unloading flow rate - normal stress curves. The results suggested that the cubic flow law, or the approach to check the validity of cubical law, was not applicable to rough, deformable, induced or natural fractures when the residual apertures were computed on the basis of flow rates measured at stress levels equal to or greater than 30 MPa. However in most cases, when lower normal stresses were used, for purposes of computing the residual aperture, the aperture flow rate data approaches a cubical relationship. Hence, Gale proposed a simple relationship relating the fracture hydraulic permeability (K_f) to normal stress in the form of

$$K_f = s\,\sigma^{a} \qquad (2.27)$$

where s is the value of K_f at a normal stress σ of 1.0 MPa.

Raven and Gale [1985] studied size effects by studying water flow in a natural fracture as a function of stress and sample size and found that fracture flow rate decreased with increasing sample size and with each additional loading cycle. In addition, the deviation of the relation between fracture flow rate and fracture deformation from the behaviour predicted by a parallel plate model increased with sample size and number of loading cycles. The effects were attributed to the roughness or asperity characteristics of the fracture surfaces. The data indicated that the smaller fracture surfaces may be characterized by a few high asperities unevenly distributed over the sample, while the larger fracture surfaces may be typified by a greater number of more variable height asperities more evenly distributed over the sample. With the application of normal loading, the larger samples have more asperities in contact and therefore lower contact point stresses and more tortuous flow channels. This results in less permanent fracture deformation, lower flow rates and deformation hysteresis between loading and unloading cycles and greater deviation of the data from the cubical flow law.

From Raven and Gale's results, in order to extrapolate laboratory test results of the type undertaken in their study to the field condition, it is

necessary to understand fully the relations between measured roughness and the effective normal stress - permeability properties of fractures and also the scale and variation of surface characteristics of natural fracture planes. Although theoretical effective normal stress - deformation and effective normal stress - permeability models (sections 2.4.1, 2.4.2 and 2.4.3) may provide clues to the roughness or asperity characteristics of fractures based on observed deformation and flow rate behaviour, actual measurement of fracture surface properties are required.

Barton et al [1985] studied strength, deformation and conductivity coupling of rock joints in an attempt to relate these to the joint surface roughness. A relationship between theoretical hydraulic aperture and real joint aperture based on the Joint Roughness Coefficient (JRC) was proposed by Barton and Choubey [1977]:

$$e = \frac{JRC^{2.5}}{(E/e)^2} \qquad (2.28)$$

where e is the theoretical hydraulic aperture and E is the real mechanical aperture of a joint. However, data on which the equation is based seem to be scarce.

In these studies, it was observed that closure under load was more complete in smooth joints than in rough joints. Conversely, rough joints in strong rocks close least under normal stress. The initial normal

stiffness and maximum closure were dependent on roughness (JRC) and wall strength (JCS).

The effect of joint surface mismatch was noticed. Earlier experiments performed by Bandis [1980] suggested that when mismatch occurs the number of contact points may reduce, although the individual areas of contacting asperities may become larger.

Fully-coupled, hydro-thermo-mechanical joint behaviour tests were conducted on a rough joint in gneiss by Hardin et al [1982]. The test joint exhibited a four-fold reduction in hydraulic conductivity when loaded from 0 to 6.9 MPa under ambient conditions, and a thirty-fold reduction when temperature was also increased to 74 °C. Increased temperature alone, with no change in normal stress, reduced the hydraulic conductivity ten-fold. This reduction of conductivity and in turn the hydraulic aperture with temperature was suggested by Barton and Lingle [1982] to be the result of improved matching of the opposed joint walls.

2.4.2 Gangi's "Bed of Nails" model

As stated in section 2.1.1, steady laminar flow of a viscous incompressible fluid in a fracture composed of two smooth, parallel walls separated by a distance e obeys the cubical law; that is, the flow rate is proportional to e^3. In actual rock fractures, the walls are far from smooth. This rough wall fracture may be suitably modelled using a mathematical expression.

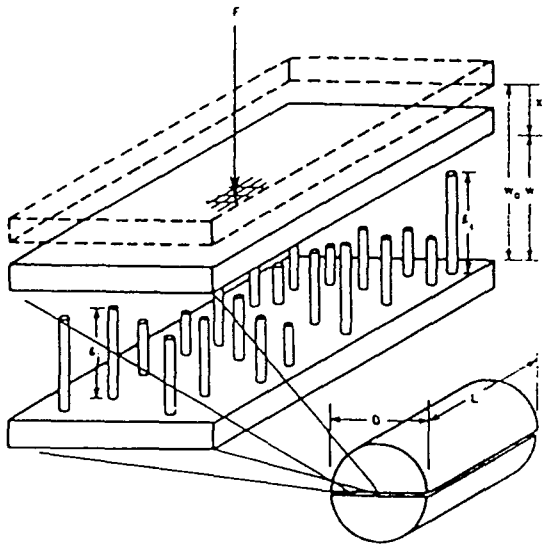


Figure 2.11 "Bed of Nails" Model (after Gangi [1978]).

The mechanical properties of this crack can be determined by using complex mathematical techniques, such as Maskhelishvilli's method of singular Integral Equations [see Mavko and Nur, 1978], but the essential properties can possibly be determined using a much simpler method which treats the problem as a statistical one. Gangi [1975, 1978, 1981] proposed a "bed of nails" model (Figure 2.11) based on the assumptions that:

1) the crack has a very small aperture, consequently the flow is laminar and slow, without turbulence;
2) the surface roughness has little effect on the flow which can be considered to be laminar between parallel plates;
3) the angles of the fracture surfaces relative to a plane (or smooth) surface are small;
4) the two surfaces of the fracture do not make a perfect fit.

The variation of fracture permeability with pressure can be described by the "bed of nails" model to represent the asperities on the fracture surface by a distribution of rods. Simple theoretical variation was obtained if a power-law distribution function for the asperity heights is assumed. These asperity height distribution functions should provide accurate representation of the actual asperity height distribution functions since they need to represent the actual distribution only over a limited range (generally less than 1/2) of the asperity heights. The use of the asperity height distribution functions provides insight into the reason why the pressure variation of permeability is different (for the same sample) on the second loading cycle than it is on the first loading cycle. In addition, it allows one to predict what would happen on subsequent loading cycles whether the normal stress variation on the first cycle is exceeded or not.

In Gangi's "bed of nails" model, the closure of the fracture under effective normal stress was ascribed to the elastic compression of the asperities, and the 'softness' of the fracture was said to result from the small number of asperities that were in contact. These contact areas therefore sustained much higher stress than that measured by the total load divided by the total fracture area. As a result, the strain of the asperities in contact was expected to be larger than the strain in the intact rock under the same effective normal stress.

The theory gives the result

$$\frac{K}{K_o} = \left[1 - \left(\frac{\sigma'}{D}\right)^{1/n} \right]^3 \qquad (2.29)$$

where K_o = joint permeability at zero effective normal stress,

K = joint permeability at effective normal stress σ',

D = material constant, being the effective modulus of the asperities,

n = constant.

With this model, Gangi obtained a very good fit to flow data for a fractured sandstone [Nelson 1975].

2.4.3 "Asperity or voids" model proposed by Tsang and Witherspoon

When Tsang and Witherspoon applied Gangi's "bed of nails" model to both the flow data and normal stress-deformation measurements for a granite fracture [Iwai 1976], some difficulties were encountered. They found that in order to obtain a result that was quantitatively compatible with Iwai's flow data [Iwai 1976], they arrived at a contact area that, at the maximum experimental stress level of 20 MPa, was only 0.001 of the total fracture area. In contrast, Iwai's experimental results for contact area ratio at this maximum stress were between 0.1 to 0.2. Furthermore, when they required the theoretical fractional contact area to conform to Iwai's measured values, no agreement between

calculated and measured flow rates could be obtained. To force an agreement required adopting a value of Young's modulus for each asperity that was two orders of magnitude greater than that of the intact rock, which did not seem to be reasonable. Tsang and Witherspoon therefore proposed an "asperity and voids" model by introducing a statistical average for the variation in aperture [Tsang and Witherspoon 1981]. The model can be used to determine the hydro-mechanical behaviour of a single fracture under normal stress.

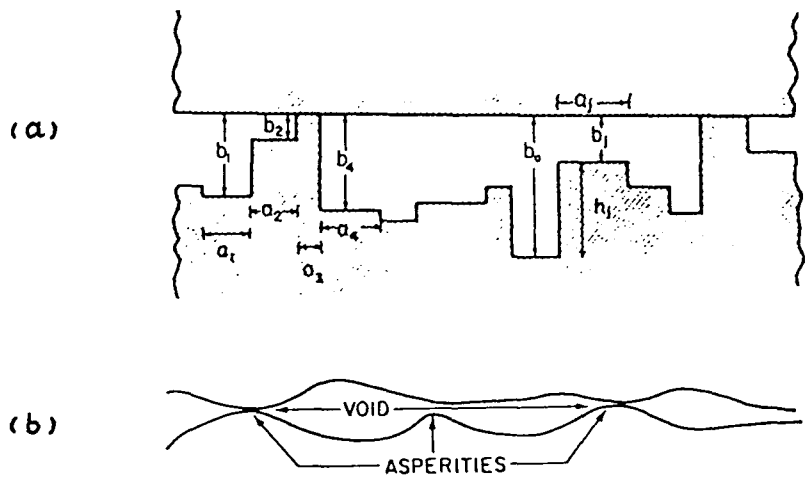


Figure 2.12 "Asperity and Void" Model (after Tsang and Witherspoon [1981]).

The asperities protruding into the flow stream varied in height and could have the same order in measurement as the fracture aperture e itself. It appeared that an equivalent cubic flow law may be used as long as the typical size of the asperity (the typical distance over which aperture may be considered constant) is small compared to the scale of the flow region under

study. When this physical constraint was satisfied, the effect of fracture roughness entered into the flow equation by introducing a statistical average for the variation in aperture. A schematic model of a fracture consisting of a smooth top slab and a rough bottom slab with asperities of different heights (h_i) is shown in Figure 2.12a. The configuration of asperities gave rise to a fracture with variable apertures (b_j). Though an asperity model for a fracture seemed to be the natural candidate for the study of fluid flow through fractures, it was not suitable for the interpretation of the mechanical property of a single fracture under stress. In their study, Tsang and Witherspoon considered the closure of a fracture as resulting from the deformation of "voids" or "cracks" between the asperities. The physics of this void model predicted a very soft elastic property at low stresses; it also predicted a gradual increase in the effective Young's modulus to approach the intrinsic value of solid rock in accordance with the behaviour displayed in Figure 2.9. Geometrically, one may either imagine a single fracture as being composed of a collection of voids or of a distribution of asperities, as illustrated in Figure 2.12b. The asperity model and the void model are entirely interchangeable as far as the geometry of the fracture is concerned.

It was suggested by Tsang and Witherspoon [1981] that the theory utilises the void model to describe the behaviour of the fracture under normal stress and the asperity model to describe the flow through a rough-wall

fracture. They also developed a mathematical correspondence between the void model and the asperity model. This correspondence allowed the prediction of the flow rate as a function of normal stress. As no arbitrary adjustable parameter was employed in the validation of the theory, their model probably contained the essential physics relevant to the problem of fluid flow through a single fracture under normal stress.

2.4.4 Other models

A number of models have been proposed to analyse theoretically the effect of porosity upon the deformation of rock. These analyses were generally based on a model in which the pore phase was assumed to be a population of cavities of specified shapes dispersed in an elastic matrix, e.g., Walsh [1965] and O'Connell and Budiansky [1974]. These models had two main limitations. Firstly, the models could not be used to study transport properties of rock because these properties require that the pore phase be continuous. Secondly, the pore phase was a tangle of connected irregularly shaped cavities and crack radii, crack density and the shapes of individual cracks which were needed for evaluating theoretical results could not be measured objectively.

Walsh and Grosenbaugh's model [1979] bypassed some of these problems by assuming that the asperities were sufficiently separated that the stress field from one does not significantly affect that of a neighbour.

Whether the pore phase was connected or not was immaterial, and so the model can be used to study both interconnected microcracks and joints. In the model the mechanics of elastic deformation of two rough surfaces in contact was analysed by Greenwood and Williamson [1966] assuming that all tips of the asperities have the same radius of curvature and that the heights vary according to a distribution function which can be specified independently. From the measurements of topography of joint surfaces, they assumed that the heights of asperities were distributed according to an exponential or Gaussian distribution function. These two distribution functions were found to give nearly identical results except at the very lowest loads. Though they compared theoretical results with experimental data and found good agreement, the model is probably suitable only for the use in studying the mechanical behaviour of interconnected microcracks, since the model is rather based on microphenomena.

Walsh [1981] later derived an effective pressure model for fracture hydraulic behaviour based on his fracture asperity height distribution model [1979]. It related the flow rate Q and effective normal stress σ' in the form of

$$\left(\frac{Q}{Q_1}\right)^{1/3} = \left(1 - 2\sqrt{\frac{h}{e}\ln\frac{\sigma'}{\sigma'}}\right) \qquad (2.30)$$

where Q_1 = the flow rate at a reference effective normal stress σ_1',

e = the initial fracture hydraulic aperture,

h = r.m.s of the asperity height distribution.

An "aperture frequency" model for flow in a fracture was proposed by Neuzi and Tracy [1981], wherein the fracture was represented by a set of parallel plate openings with different apertures. The model led to a modified Poiseuille equation for flow which included an aperture frequency distribution for the fracture. Any arbitrary aperture distribution can be used; in order to specify computation and demonstrate the properties of the model, a log-normal form of distribution was assumed. However, even when an analytical form of the distribution was assumed, two parameters rather than a single value representing aperture size were required to determine flow rate. Models of aperture change for a fracture undergoing compression (fracture walls deforming) and extension (fracture walls separating) were developed which constrain the additional parameter and allow calculation of flow rate as a function of mean aperture. However, the model had an obvious limitation that the distribution of aperture was only along the cross section of the flow channel, and did not take into consideration of the variation of aperture along the flow. Often in real cases and laboratory testing of a single joint the flow length is greater than the width, and the importance of the aperture variation along the flow length can not be possibly neglected.

Swan [1983] proposed a "joint contact" model based on the "half joint" model of Greenwood and

Wiliamson [1966] and on the "full joint" model of Greenwood and Tripp [1971]. The model proceeded from a measured joint profile. The linear profile of the joint sample was presumed to contain information representing the distribution of peaks and valleys over the area of the joint surface. Equations were derived from an elastic model of contact deformation. The equations formed the basis for discrete numerical models from which both "half joint" and "full joint" behaviour may be predicted. The models can be applied to peak contact and equally to peak on valley or what may be termed all-ordinate contacts. In reality, two surfaces in contact will contain a mixture of contact possibilities. Depending upon which condition is modelled so an initial aperture E_o can be established numerically by simulating a shear motion starting from the mated full-joint. This was done by shifting two identical roughness profiles relative to one another multiplies of the sample interval. For a desired aperture normal loading was next simulated by stepping the profile multiplies of each asperity height interval and at each step locating the initiation of contact. Each step was accompanied by a calculation of normal stress, aperture, contact area and contact stresses for the desired nominal joint area. One can easily see that with this model it is only possible to determine the upper and lower limits to bound the joint mechanical behaviour by referring to the peak-peak contacts and all-ordinate contacts. However, by measuring the joint profile of both joint surfaces, a true

possibility of joint contact can be known, which may lead to the determination of more accurate properties of the rough joint. Based on this model, Swan [1983] proposed a simplified model for the determination of the joint hydraulic behaviour relating to the normal stress as

$$K/K_o = c - m \ln \sigma' \qquad (2.31)$$

where K_o= joint permeability at zero effective normal stress,

K = joint permeability at effective normal stress σ',

c, m = constants.

2.5 Summary and Topics for Investigation

By reviewing the previous studies, the following summary can be drawn:

1. The mechanical behaviour of joints under normal stress is non-linear. It is commonly agreed to satisfy the conditions of a hyperbola, proposed by Goodman [1976], or of a logarithmic relation.

2. At present, there are a number of major models dealing with the hydro-mechanical behaviour of joints. However none of these models take account of the measurement of true joint surface properties.

3. Previous studies by a number of investigators have shown that the hydromechanical behaviour of a joint can be affected by the joint surface properties

[Louis 1969, Maini 1971b Louis 1973, Gale 1975, Iwai 1976, Barton and Choubey 1977, Detournay 1980, Tsang and Witherspoon 1982, Barton et al 1985, Elliott et al 1985, Hudson 1987]. Some relationships have been proposed [Sharp and Maini 1972, Gangi 1978, Walsh 1981, Tsang and Witherspoon 1982, Swan 1983, Barton et al 1985, Elliott et al 1985]. The most rational one is considered to be the idea of a Joint Condition Factor.

4. The cubic flow law derived from smooth parallel plate theory is validated as long as a factor is introduced to account for the joint condition. This factor can be termed the joint condition factor.

5. An increase in sample size and in loading cycles reduces the flow rate and causes higher deviation from the relation between fracture flow rate and fracture deformation predicted by the cubic flow law.

6. Few studies have been conducted on the thermal effect. One test showed that the hydraulic conductivity was reduced considerably by raising the temperature. Further detailed research therefore is required.

7. So far, no study has been attempted which relates the differences in the hydraulic and mechanical behaviour of joints to the joint surface properties in a precise way, i.e. pre-test determinations of initial aperture and joint condition factor are not possible.

The objective of the investigation is to verify

and further the studies and models proposed by previous research workers and to initiate studies of temperature related and joint surface geometrical properties. In particular, the importance of the effects of joint surface geometrical properties on the hydro-thermo-mechanical behaviour of joints will be emphasized and an attempt will be made to develop an empirical model which will be able to account for these properties.

CHAPTER 3

JOINT PERMEABILITY AND DEFORMATION TESTING SYSTEM

3.1 Test Requirements and Introduction to the Testing Facility

3.1.1 Test requirements

The principal aim of the research is to study the hydro-thermo-mechanical properties of rock joints and the effects of temperature on these properties. The requirements for the tests must include the ability to:

1. measure the mechanical properties of joints, that is the deformation of joints under effective normal stress;

2. create fluid flow, measure the flow rates, and measure joint fluid pressures and differential pressures;

3. conduct tests at elevated temperatures; thus the rock sample inside the testing cell must be heated up to a predetermined temperature, and measurements of the temperature taken at desired points;

4. couple all the effects and properties, requiring

that all tests must be carried out within the same testing cell using the same testing facility.

3.1.2 Features of the testing facility

All the tests are to be conducted on the Terra Tek Systems Geothermal Rock Testing Facility in the Department of Mineral Resources Engineering at Imperial College of Science and Technology [Enniss 1979a, Enniss 1979b, Elliott and Brown 1985] (Figure 3.1). The system comprises a triaxial compression testing machine with provisions to raise the sample temperature above room temperature and to include pore pressure within the sample. In addition, there is an automatic data collection and recording facility with data processing and output in the form of graphs or data listings [Elliott and Brown 1985]. Using this complex servo-controlled high pressure - high temperature testing facility, the following geothermal material properties can be determined [Enniss 1979b]:

Mechanical properties: complete stress-strain response including longitudinal and lateral strain (volume response) and pore fluid pressure;

Thermal properties: thermal conductivity, thermal diffusivity, thermal expansion coefficient;

Matrix and fracture permeability/conductivity to gas and liquids.

For triaxial tests, axial loads are applied

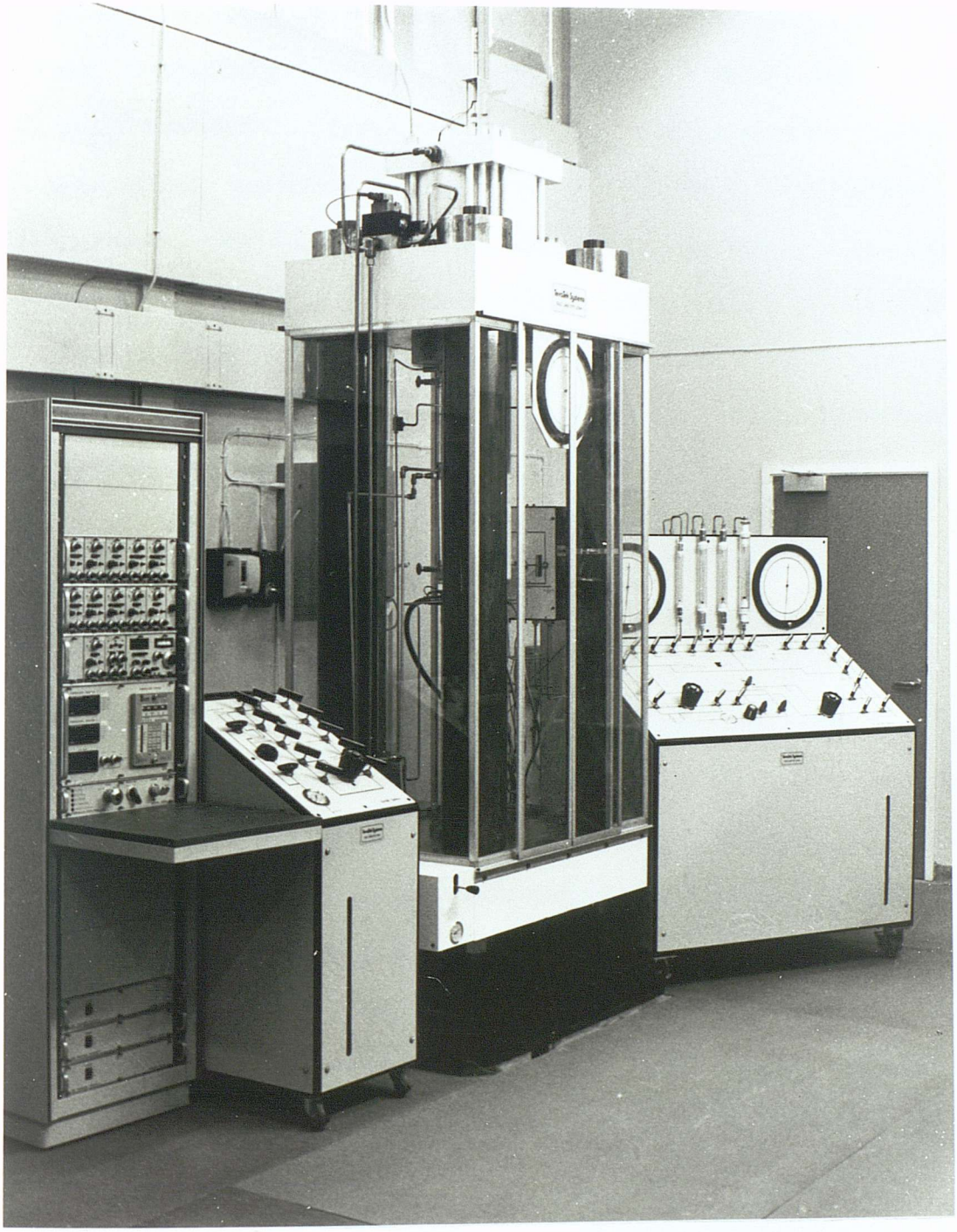


Figure 3.1 Geothermal Rock Testing Facility.

using a 2.67MN servo-controlled ram. During each triaxial test, the sample is located within a 105 MPa fluid pressure capacity triaxial cell (Figure 3.2). This cell may accommodate, together with load, axial and lateral displacement, temperature and ultrasonic velocity measuring equipment, samples of 51mm x ϕ 102mm (2 x 4 inches), or 102mm x ϕ 204mm (4 x 8 inches). The sample stack is sub-merged within the cell in a light lubricating oil, and confining pressures are generated and maintained by an independent servo-controlled system (Figure 3.3).

A coil heater located around the base of the sample is capable of heating the oil around the sample up to 400°C. Heat losses are reduced by using a series of ceramic shrouds which act as heat baffles. Sample temperatures may be ramped and held by using a dual-channel programmable heater controller (Figure 3.4). This controller was broken down during the late stage of the investigation and a manual device was adopted to control the heater. The device was to generate the same signal current which would be sent by the heater controller using a voltage and current controller and a current digital meter.

Pore pressure, and permeating fluid pressure within the sample are created using a 70 MPa manually controlled system that generates independent up-stream and down-stream fluid pressures (Figure 3.5). The fluid may be either liquid or gas, although only liquids have the facility to be heated up to 120°C prior to entering

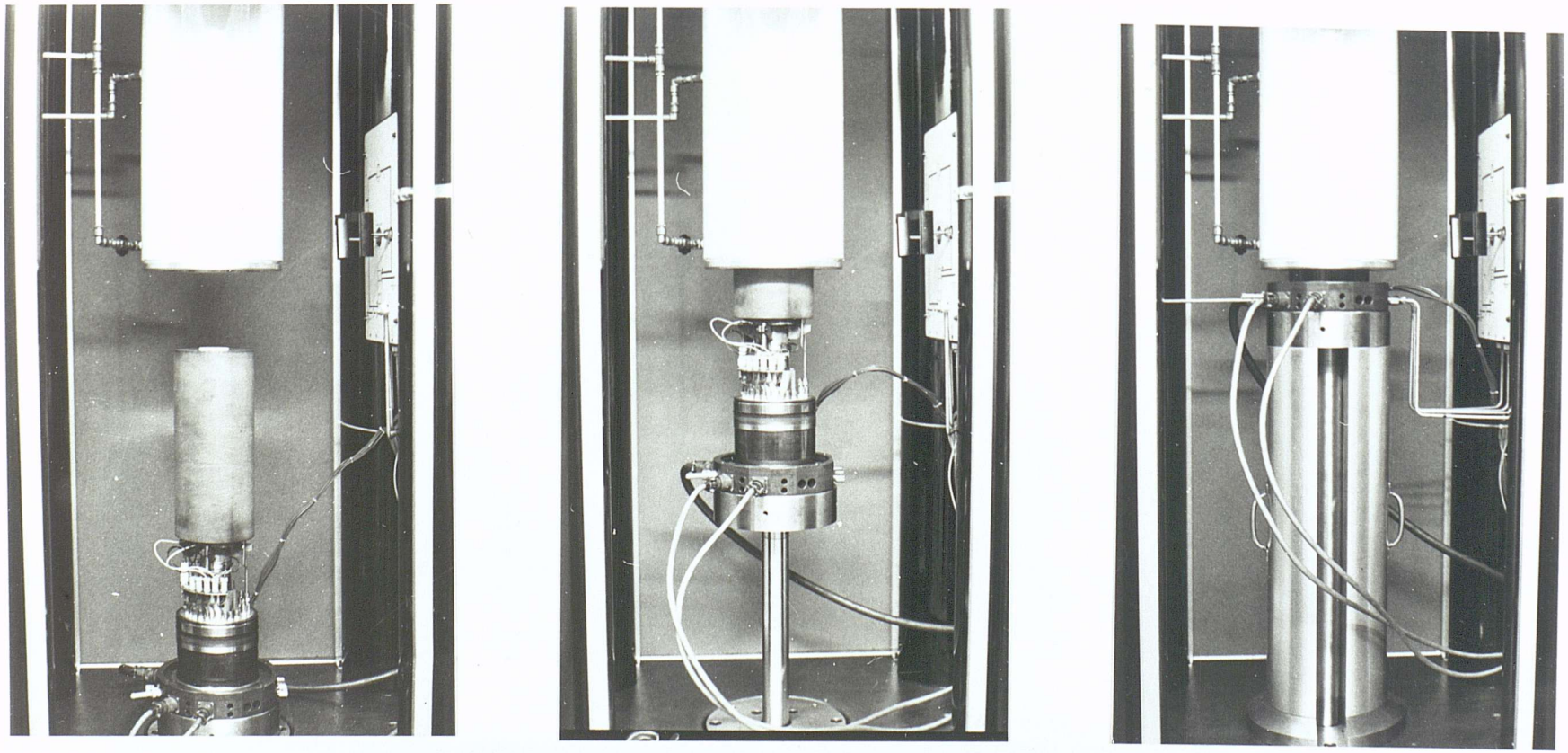
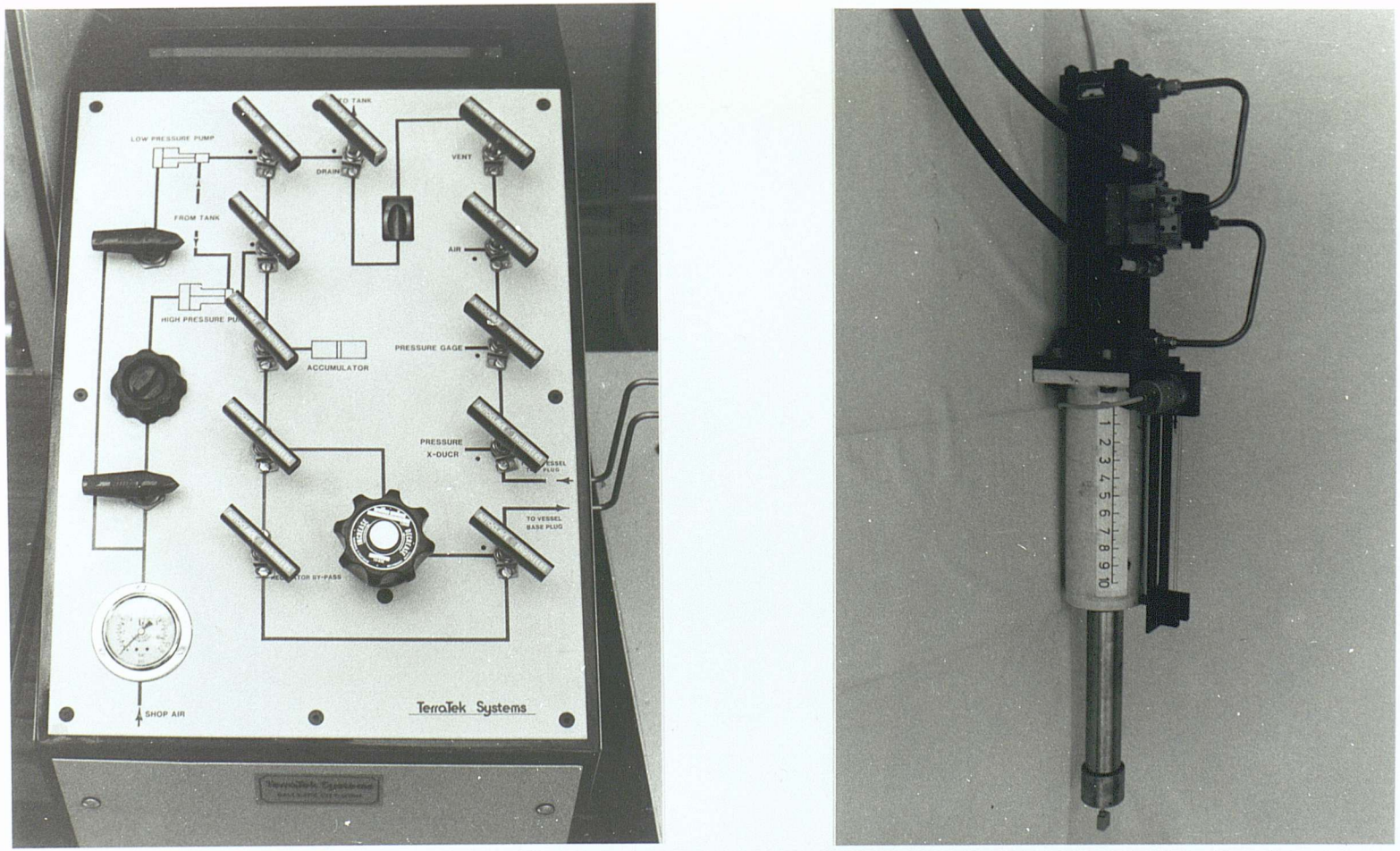


Figure 3.2 Test Configurations Inside Load Frame.



a b

Figure 3.3 Confining Pressure Cart and Pressure Intensifier.

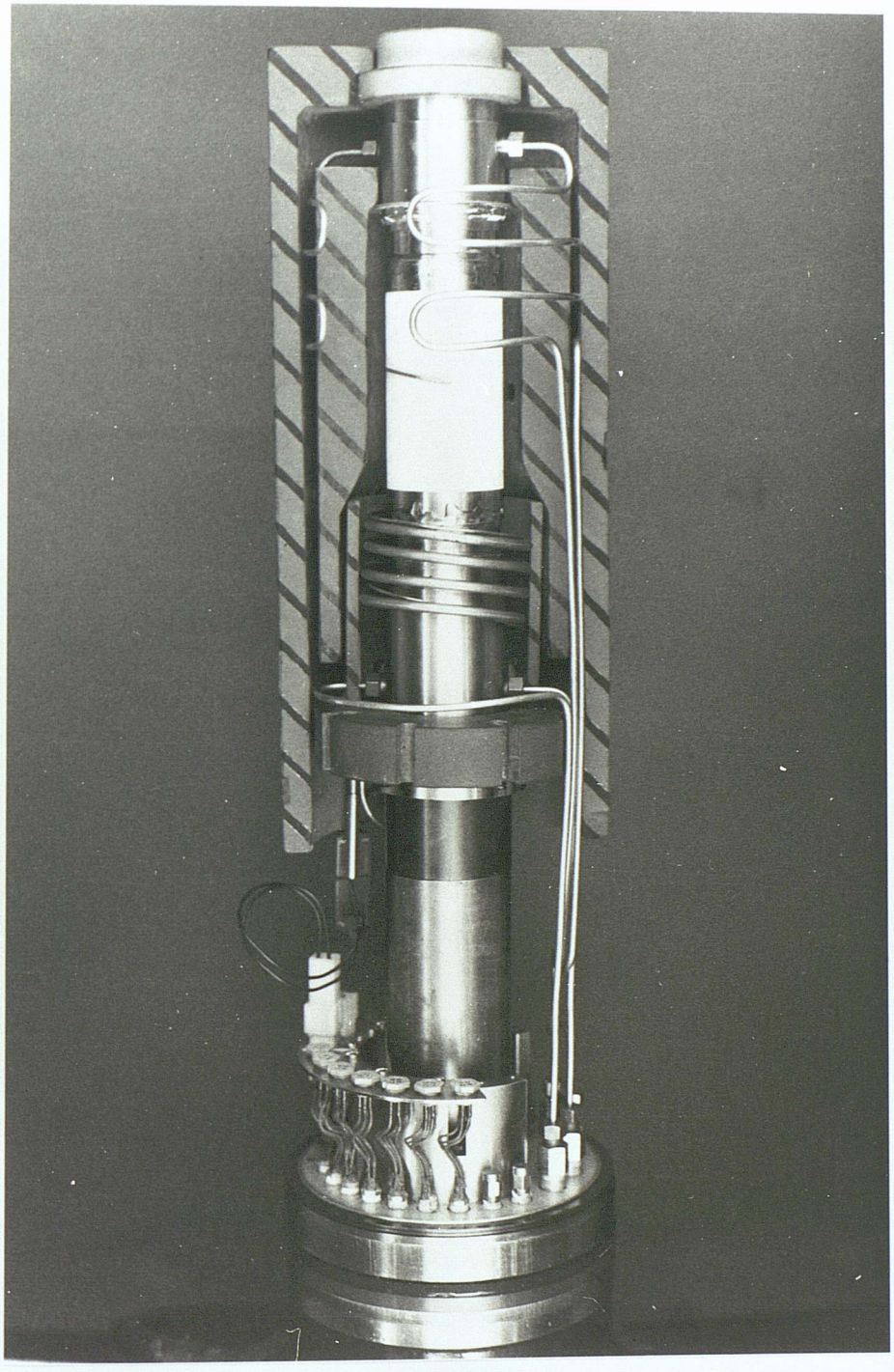


Figure 3.4 Hydro-thermo-mechanical Test Stack Assembly.

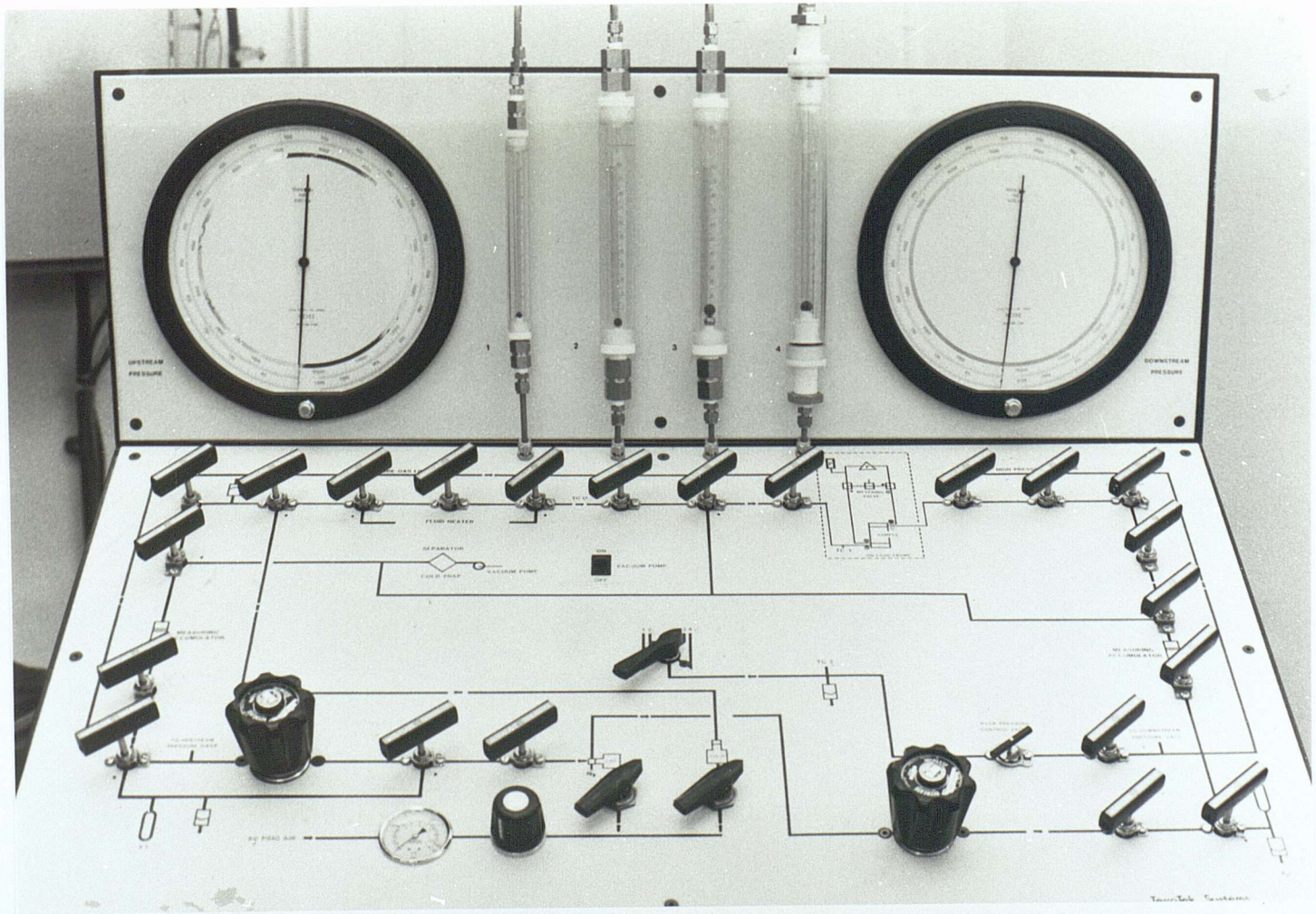


Figure 3.5 Permeating Pressure and Joint Fluid Pressure Cart.

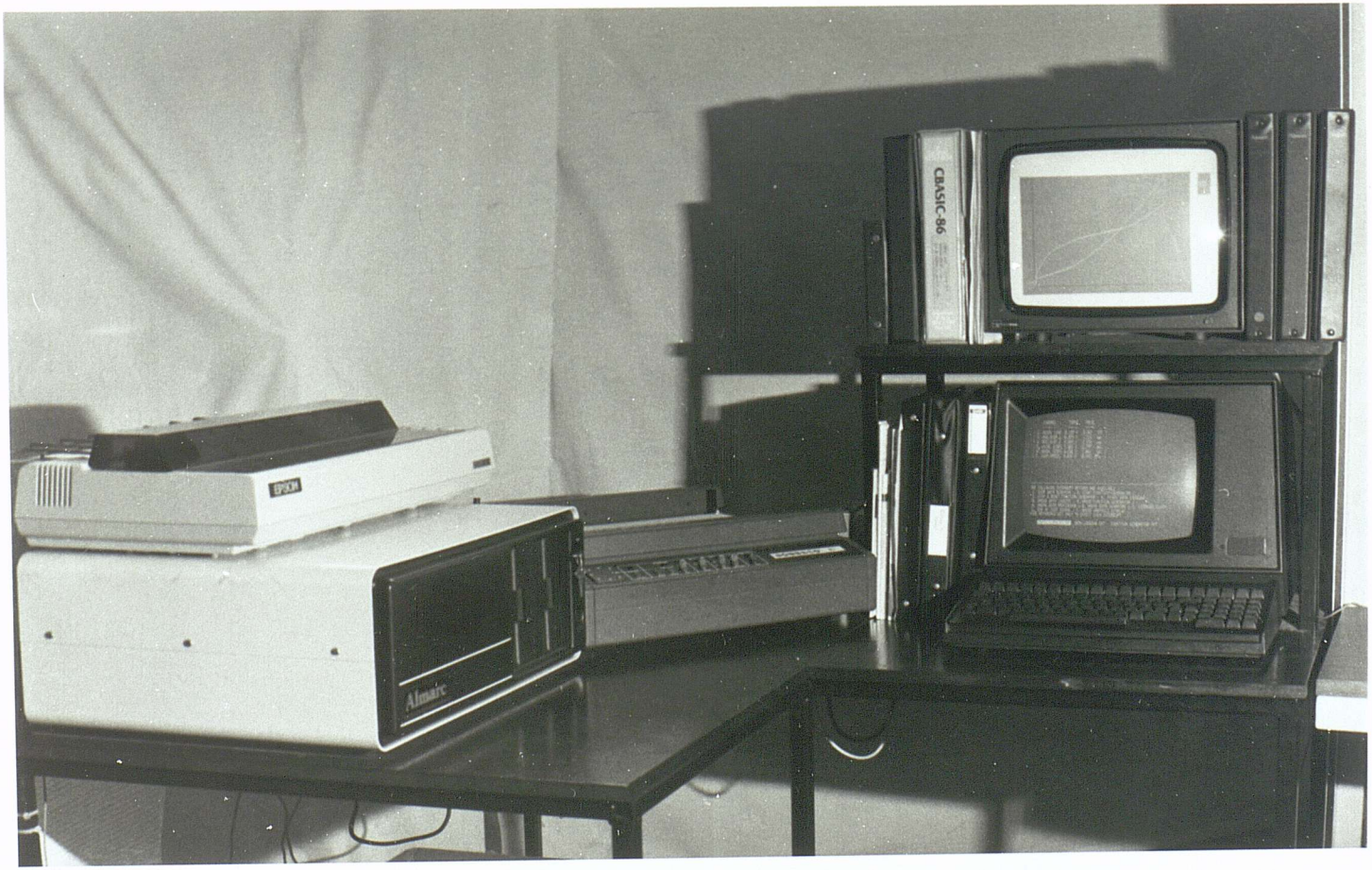


Figure 3.6 Data Acqisition and Display System.

the testing cell.

Data on measured loads, displacements, temperatures and pressures are automatically collected, processed and output in the form of data listings and/or graphs using a 16 bit micro-processor facility equipped with a 16 channel, 12 bit A-D converter (Figure 3.6).

3.2 Arrangement of the Testing System at Room Temperature

3.2.1 Arrangement of the testing cell

The load frame consists of four columns, which have a rated stiffness of 5.25 GN/m, attached to end platens having a clearance of 1744 mm between the faces. On top of the top platen is fitted a servo-controlled hydraulic ram that can apply forces of up to 2.67 MN from a 21 MPa hydraulic power unit; this ram is used to apply compressive loading along the axis of the sample. This ram passes through the upper platen and past seals into the barrel of the testing cell which is fixed at its upper end to the underside of the upper platen of the loading frame. The barrel of the cell has a bore of 152.4 mm and an internal operational length of 560 mm. The testing cell is designed for a maximum working internal pressure of 105 MPa (Figure 3.2).

A second sleeve around the outside of the cell contains helical passages through which running cold water may be circulated continuously. This system keeps

the cell cool during heating tests. The base plug of the cell contains a sufficient number of sealed, insulated electrical and hydraulic feed-throughs to allow for confining fluid entry, four pore fluid lines, six thermocouples, two heating elements and up to nine four-lead in-cell analogue measuring devices (Figure 3.4). During test operation, the underside of the cell base is about 768 mm above the lower platen of the load frame. This space is filled by an aluminium and steel spacer which provides transmission of the loads from the base plug to the lower platen of the load frame (Figure 3.2). The spacer can be removed while a test is not being conducted, and the base plug can be lowered by using a hydraulic actuator mounted under the lower platen. This allows easy access for dismantling of the stack assemblies.

3.2.2 Confining pressure system

During the hydro-mechanical and permeability test on fractures, only hydrostatic loading is generated by fluid pressure bearing on the boundaries of the sleeved sample. During the tests, the testing cell is filled with an hydraulic oil (Multitherm PG1) from a storage tank using an air driven centrifugal pump. The confining oil pressure is raised either manually using an air driven booster pump and pressure regulator, or automatically using a servo-controlled liquid pressure intensifier. An enclosed unit that contains the items mentioned above together with the necessary shut-off

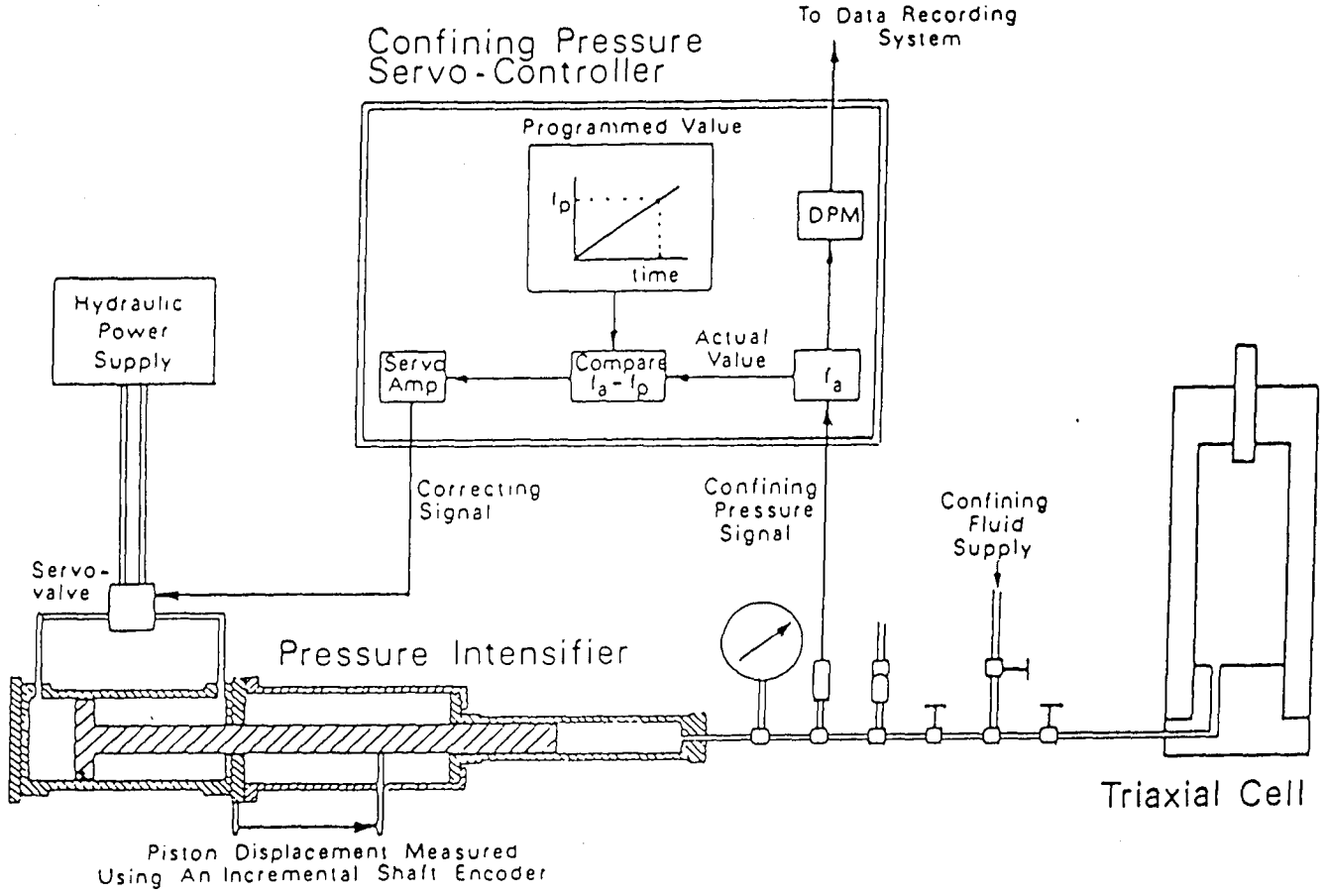


Figure 3.7 Schematic of Confining System.

valves, pressure transducers and burst discs is located next to the load frame (Figure 3.3). The arrangement of the confining pressure system is shown in a schematic drawing as Figure 3.7.

The servo-controlled pressure intensifier utilises the mechanical advantage of two pressure cylinders of different bores connected by a steel ram. A standard 21 MPa hydraulic power unit supplying oil to the larger bore cylinder is then able to generate much higher pressures in the oil contained in the smaller bore cylinder. The smaller bore cylinder has a large length and small cross-sectional area; this enhances smooth pressure control with very low amplitude pressure oscillation, and also improves the precision of making measurements of fluid volume changes. The intensifier has an output pressure capacity of 140 MPa and a controlled ramp rate of approximately 10 MPa/sec. A high precision is used to hold pressures constant to with-in ± 6 KPa and to reset the pressure after ramping to within ± 15 KPa.

3.2.3 Permeating fluid pressure and pore pressure system

The system may be used for saturating a sample, or for permeating a selected fluid (liquid or gas) through the sample, and allows manual regulation of the pore pressure. A separate system independently controls the injection and back-up fluid pore pressures up to 70 MPa. By isolating the injection and back-up pressure

systems in this way, differential pressures across the sample may be generated and sample permeabilities measured (Figure 3.5). The system is contained in a permeability cart unit located next to the load frame, and is connected to the triaxial cell base plug by standard high pressure pipework. From the cell base plug, the pressure is applied to the sample end platens inside the cell. The unit has pressure gauges for visual indication of the injection and back-up pore fluid pressures. The injection or pore pressure is measured by a diaphragm pressure transducer, and a magnetic reluctance transducer measures the differential pressure across the sample with high precision even when high mean pore pressures are used. Gas injection and back-up pressures are generated by manual gas regulators supplied by separate high pressure gas storage. A needle valve in the back-up system discharges the excess collected gas that has passed through the sample into a bank of four calibrated gas flow tubes (Figure 3.8). The system can measure flow rates in the range 1.7 ml/sec to 60 litres/sec. Liquid pressures are generated by applying the separate high pressure gas systems to one side of two high pressure cylinders containing free moving pistons. The liquid in the other side of each cylinder is then compressed to the same pressure less a small component needed to overcome the friction between the piston seal and the bore. The measurement of fluid flow rate through the sample is made by using large LVDT's contained in each cylinder to measure the piston displacements with

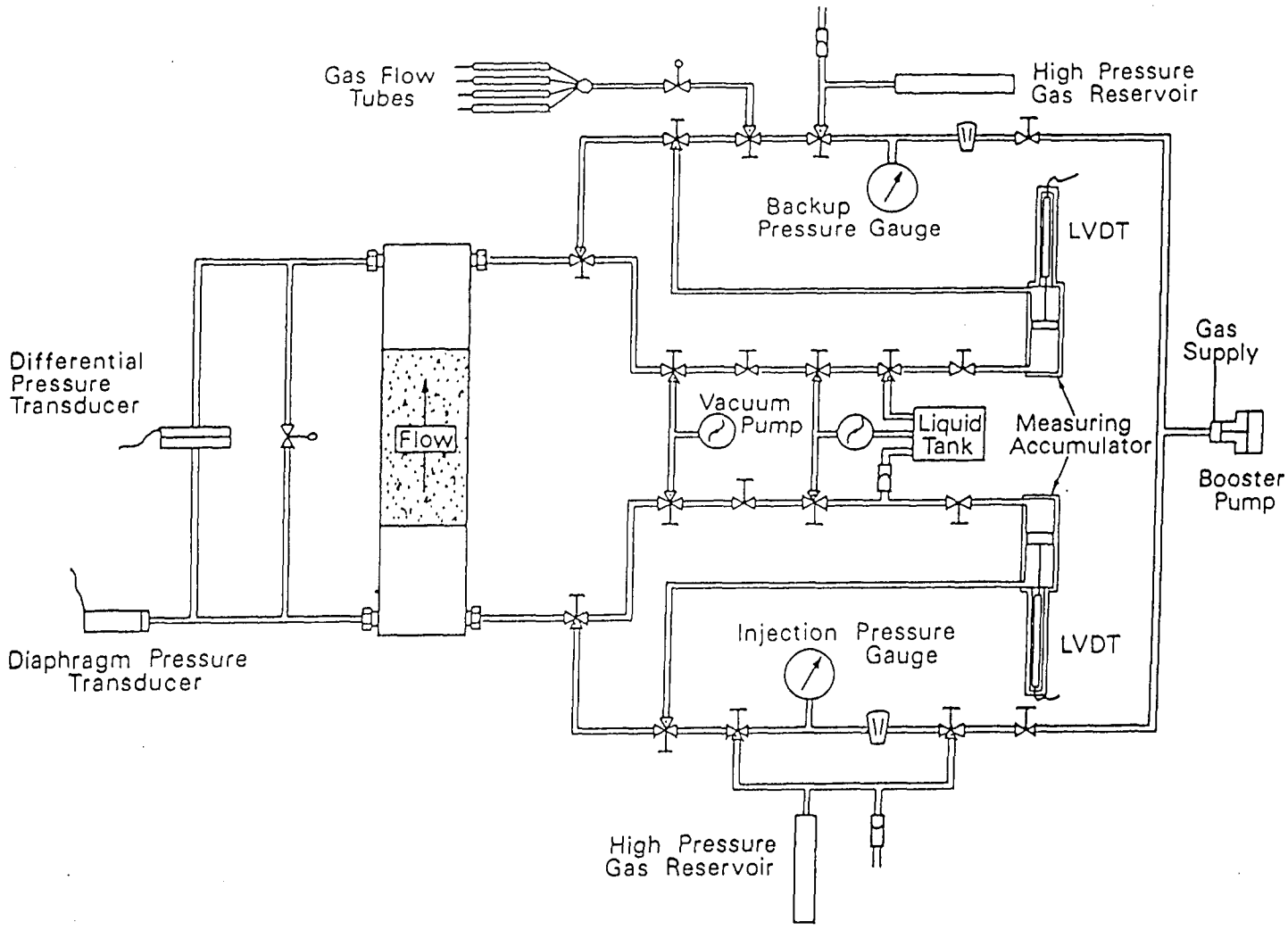


Figure 3.8 Schematic of Permeating Pressure and Pore Pressure System.

time. This method of flow measurement is suitable for liquid flows in the range 0.005 ml/sec to 10 ml/sec.

3.3 Tests at Elevated Temperatures

3.3.1 Heating system

Sample temperatures are generated by heating the oil surrounding the sample in the cell. A 3.5 KW coil heater is located around the lower platen and the lower part of the sample. A series of insulating shrouds are included in each stack assembly in order to improve the efficiency of the immersed heater, and in order to minimize the total heat energy stored within the cell during high temperature tests (Figure 3.4). These shrouds are geometrically designed to provided a close fitting capsule around the sample inside the cell. The shrouds are made of PTFE (for temperatures up to 200°C) or a silicon rich ceramic (for temperatures up to 400°C). They contain the heat generated by the heater and prevent widespread thermal currents and heat flows. The cooling water circulated inside the cell wall forms an efficient heat sink for heat escaping from the series of shrouds. This arrangement enables maximum sample temperatures of up to 400°C to be generated and dissipated quickly, while leaving the greater proportion of the oil outside the shrouds at temperatures not exceeding 60 °C. This low temperature region includes the cell base plugs and wirings.

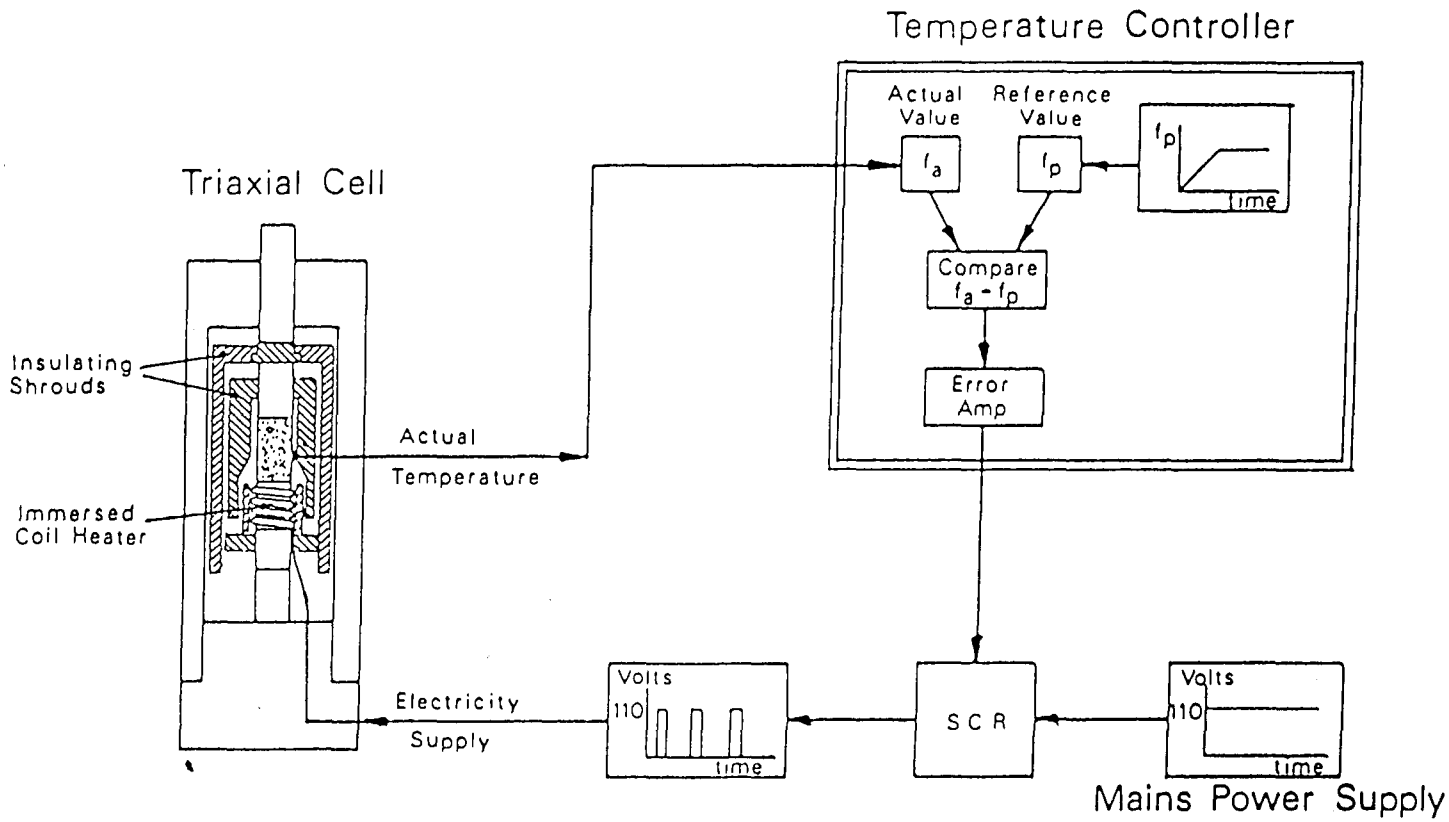


Figure 3.9 Schematic of Heating System.

A pulsed 110 V electrical power supply is fed through the cell base to the heater from a Silicon Controlled Rectifier (SCR) unit. A 4-20 mA current supply regulates the proportion of each one second interval that the SCR switches the 110 V power supply on to the heating coil. A dual channel programmable controller links the closed-loop Temperature Control System (Figure 3.9). The temperatures inside the cell at desired points are measured and monitored by K-type thermocouples and accepted as input to the control system. The system automatically regulates the output to the SCR depending on input value and a programmed reference value. Alternatively, the controlling current output may be controlled manually at any desired interval between 4 to 20 mA by connection to a digital current meter.

3.3.2 Rock-fluid heat transfer measurement

Rock-fluid heat transfer data can be calculated from the measured inlet and outlet temperatures of the working fluid. The rate of heat energy extracted, P, by the fluid with flow rate Q and specific heat c_p can expressed as

$$P = Q\, c_p\, (t_2 - t_1)$$

where t_1 and t_2 are the inlet and outlet temperatures. Detailed analysis and discussion on heat transfer are presented in Chapter 7.

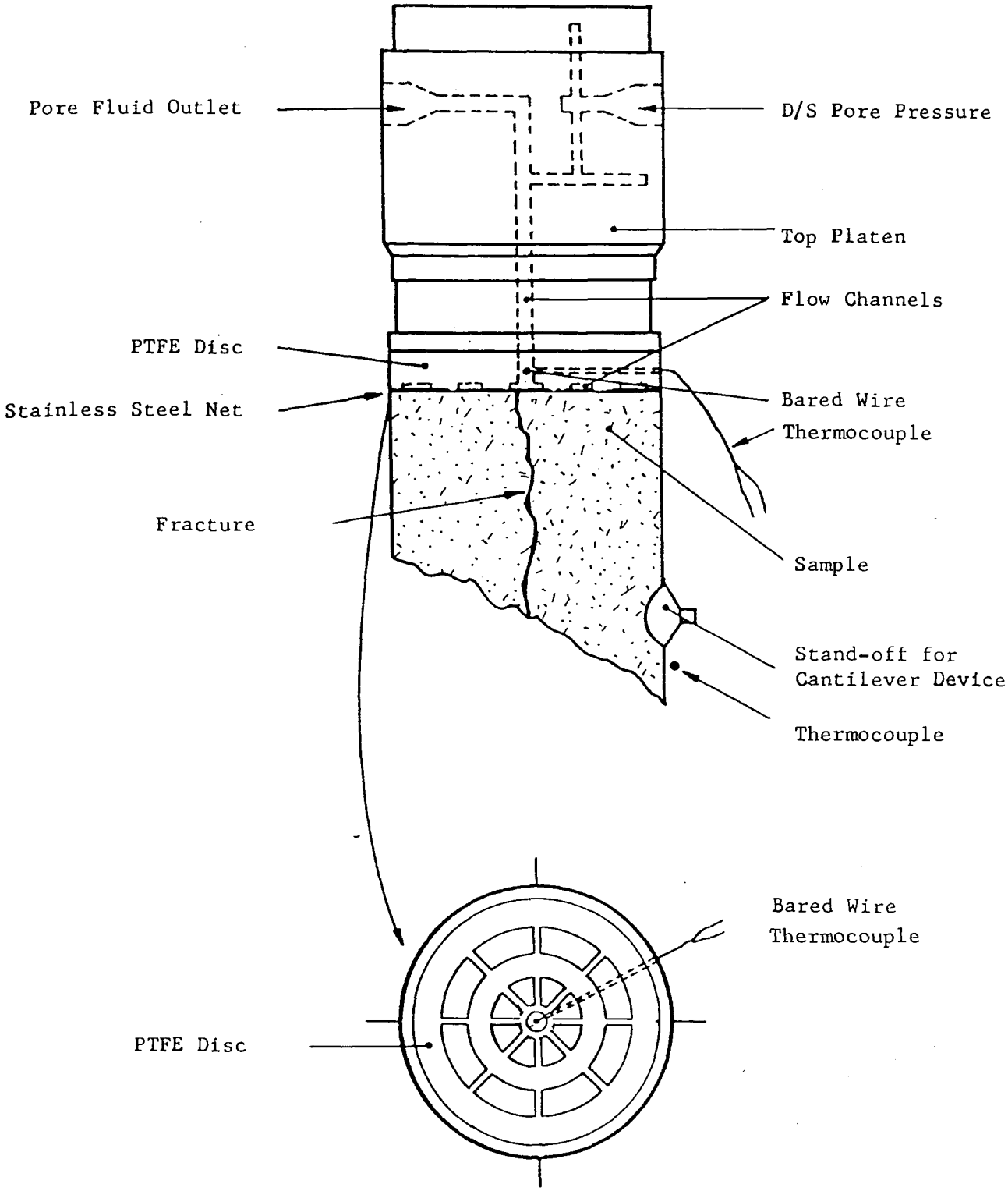


Figure 3.10 Rock - fluid Heat Transfer Temperature Measurement Assembly.

Experience indicated that errors in measurements may be introduced by the two heated steel endcaps through which the fluid is injected and collected from the samples. After a few trials on different methods of avoiding these errors, PTFE insulators were sandwiched between the steel endcaps and the sample (Figure 3.10). Bared wire K-type thermocouples are placed in the fluid passage through specially arranged holes on the PTFE insulating disc. The thermocouples are only about 2 mm away from the rock joint, and since the PTFE disc acts as an insulator, the temperatures measured by the thermocouples are very close to the water temperatures at the entrance and immediately after passing through the joint. The temperatures of the working fluid (water) at inlet and outlet, together with other known conditions, the rate of heat transfer between rock and fluid can be easily determined as shown in a later chapter (Chapter 7).

3.4 Measurements and Calibration

3.4.1 Measurements and calibrations at room temperature

1. Axial loads are measured by using a solid steel strain gauged load cell located just beneath the sample platen in the test stack (Figure 3.11). The gauges are wired in an active bridge configuration. The loads measured can therefore be related to the magnitude of the

deviator stress. Measurement of the axial loads in this manner eliminates the possibility of seal friction error. The load cell is calibrated against a proving ring to give a full range of output of 320 KN with a coefficient of correlation of better than 0.9999 [Elliott and Brown 1985].

2. Confining pressure is measured using a diaphragm transducer located within the the pressure control system (Figure 3.7). It is accurate to within +1 percent of the measured value. This is calibrated using a dead-weight tester to give a full range output of 100 MPa with a coefficient of correlation of better than 0.9999.

3. Axial displacements are measured by taking the mean displacements of two diametrically opposed LVDTs (Linearly Variable Differential Transformers) contained in the lower vessel closure (Figure 3.11). These transducers are connected to the sample top end platen by quartz rods. Quartz is selected because of its very low variation of thermal expansion coefficient under different temperature conditions. Each LVDT is calibrated using a travelling micrometer to give a full range of 5 mm with a coefficient of correlation of better than 0.9999.

4. Lateral strains are measured by taking the mean diametral displacement of a pair of orthogonally positioned built-in cantilever devices with long, stiff cantilever arms and a strain-gauged section near the bottom (Figure 3.11). The cantilever is located outside

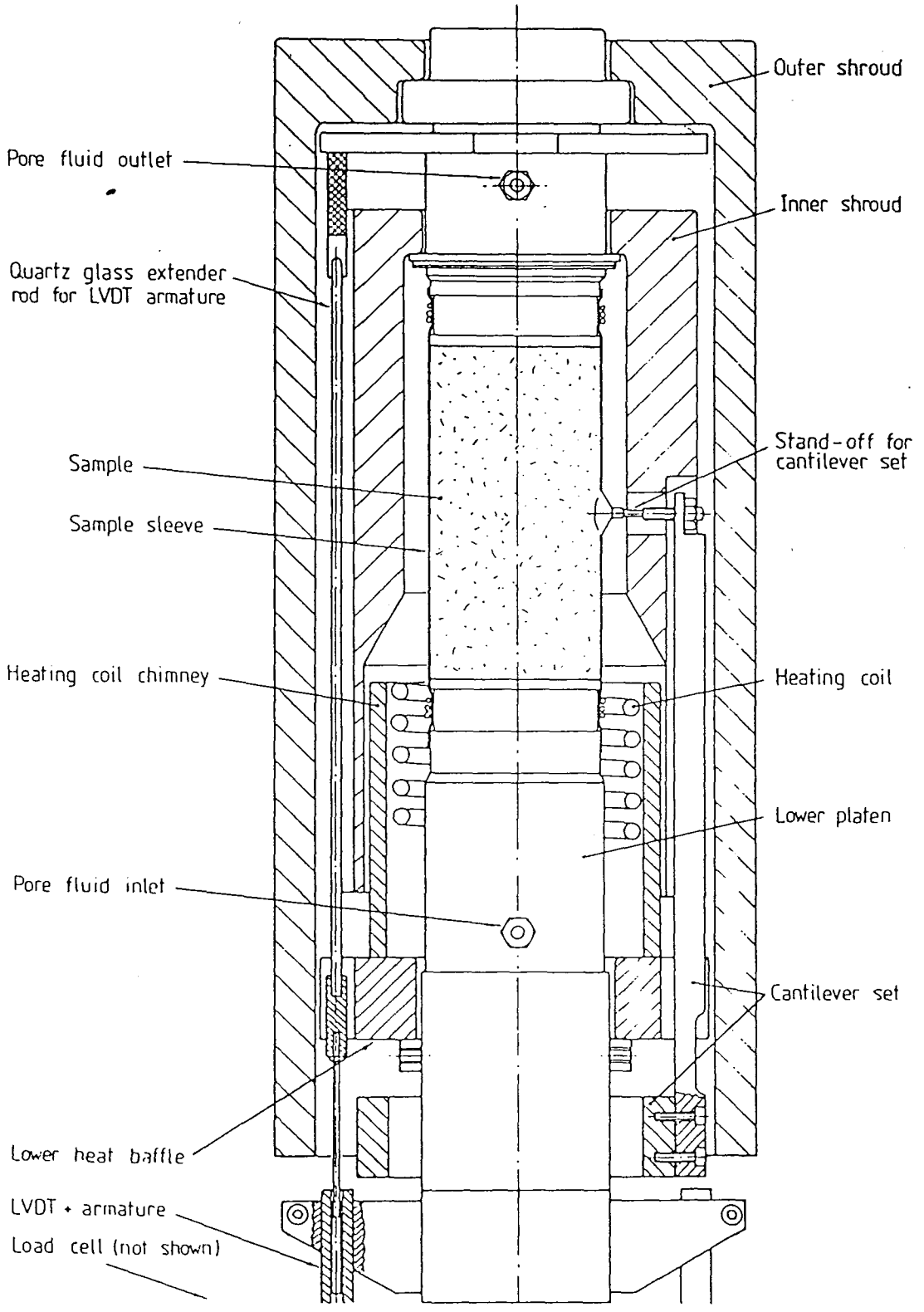


Figure 3.11 Stack Assembly for Triaxial Compression Test.

the inner shroud and in the lower part of the pressure vessel. This location ensures that the strain-gauged section is outside the high temperature environment. These are mounted on the sample at mid-height where stand-offs were glued on. Each cantilever device is calibrated using a micrometer to give a full range output of 2.25 mm with a coefficient of correlation of better than 0.9996.

5. Pore pressures are measured by using a diaphragm transducer located within the internal pressure control system connected to the upper and lower platens through pipelines and holes attached to the sample (Figure 3.8). This is also calibrated using a dead-weight tester to give a full range output of 20 MPa with the accuracy of within ±1 percent.

6. Fluid permeating pressures, or the differential pressures, are measured and read from the display on the electronic system, using a magnetic reluctance transducer located within the permeating pipe system with the ends connected to the upper and lower platens where the differential pressure was set up (Figure 3.8). The measurement is calibrated against the pore pressure transducer measurement by letting the outlet end pressure be zero; the differential fluid permeating pressure is equivalent to the pore pressure under this condition.

7. The volume of fluid passing through the sample is obtained from the dis-placements of the pistons

in two accumulators measured using two large LVDTs. This system will measure changes in volume as small as 0.127 ml. The minimum measurable flow rate is a function of the duration of the test. This method of flow measurement is suitable for liquid flows in the range 0.005 ml/sec to 10 ml/sec. Each LVDT is calibrated against a travelling micrometer to give a full range output of 500 ml with an accuracy of within ±1 percent.

3.4.2 Temperature measurements

Six thermocouple plugs are fixed to the base plug of the testing cell. They are used for K-type thermocouples to measure the temperatures at selected points inside the cell. Thermocouples are allocated usually at mid-height of the testing sample, at three-quarters height of the sample, around the heating coil, and outside the insulating shrouds. The remaining two are used to measure the inlet and outlet working fluid temperatures at points close to the rock joint (Figure 3.10). The temperatures measured are shown as digital signals on the Electronic Cart. One of them, usually the temperature at the mid-height of the sample, is connected to the closed-loop Temperature Control System (Figure 3.9) and used as the actual value to be compared with the reference value by the controller; their difference provides the basis for regulating the power output to the SCR and hence to the heating element.

3.4.3 Errors introduced in the tests

Errors introduced by data logger

A common limitation of the accuracy of the data recorded is introduced by the data logger. The logger only recorded a four digital representation of the input analogue voltage which is proportional to a preset maximum voltage input on the channels of confining pressure, lateral displacement and pore pressure. As noted previously, coefficients of inaccuracies could be 0.01% for confining pressures, 0.04% for lateral displacements, 1% for pore pressures and 1% for the volume of fluid passing through the sample. The temperature display give digital integral degrees (centigrade); hence it could have the maximum inaccuracy of $\pm 0.5\ ^{\circ}C$. Permeating pressures or the differential pressures are calibrated against pore pressures; hence the inaccuracy could be as great as that for the pore pressures.

Error induced by electrical "drift"

It is observed that the recorded readings varies due to the drift of the currents and voltages in the electric circuits. Once the initial readings are offset, electrical measuring devices are not re-offset until the test is completed. A complete test often last more than two days, and during this long period, change of nearby usage of electrical machines may influence the

voltages and currents in the circuits. This change in the circuits may drift the readings recorded by the testing system built-in electrical devices. The measuring system is calibrated before and after each test period, which generally last for about a month. Once calibrated, the system is not re-calibrated until the end of the period. Regular visual checks are made of the consistency of the calibrations, and no abnormal deviations are observed. Nevertheless, errors are induced by the drift occasionally. This is due to the design and limitations of the electric measuring devices, as well as the present electric circuits.

Influence of confining pressures and pore pressures

When Boodt and Brown [1985] conducted hydraulic tests using manually controlled confining pressures, errors were caused by variation in the confining pressures. Errors in recorded lateral displacements were due to the delayed reaction of the joint changes in the confining pressures. The errors seem to be overcome by introducing a pressure intensifier into the testing system (Figure 3.7). However, within the control loop, the oil pressure oscillated in order to achieve the programmed value. It is known [Massey 1975] that pressure waves travel at approximately 1500 m/sec. through oil, and hence the time during which a pressure wave was set up by a sample lateral increment and is detected by the pressure transducer would have been very small compared

to the response time of the pressure control loop. However, coupled with the fact that sample lateral displacement changes are gradual there is sufficient justification to assume that pressure waves offered negligible contribution to errors in the lateral displacement measurements.

Influence of temperature measurements and heating

In elevated temperature tests, it is observed that the temperatures have a significant affect on the sample lateral displacement measurements. Generally, a rise of 1°C in testing temperature can result in several to tens of micrometers of expansion. As noted earlier, the temperature measurements are displayed in digital integral figures with an accuracy of ±0.5 °C; this inaccuracy will therefore affect the recorded measurements of joint displacements.

The temperatures controlled by the heater are often ramped due to delayed reaction of the closed-loop Temperature Control System (Figure 3.9). The temperatures are well controlled to within ±2 °C of the desired values. However, the ramping may cause errors in the displacement measurements. Similar errors may have also occurred when cold water is injected into the sample, and cooled the sample internally.

3.5 Electrical Output and Data Acquisition

The testing facility has 21 signal conditioning units used for a variety of electrical measuring devices and for calibrating and processing the return signals. The electrical analogue output of each unit is 10 V maximum. The units are interfaced with the micro processor which operates all the automatic data acquisition, display and processing functions. The 16 bit micro processor is fitted with a 16 channel 12 bit A-D converter which is the only connection unit and has no provision for digital interfacing. The full micro processing computer includes a VDU and keyboard, twin floppy disc drives, a high resolution 8 colour graphic monitor and control board, a flat bed plotter and a matrix printer (Figure 3.6).

During the experiments the test system is scanned continuously. The analogue input voltages are converted into measurements in Engineering Units by a software programme written specifically for the system by Elliott [1984]. The collected data are then displayed digitally on the VDU and on the colour monitor in graphic form as output voltage against real time plots. Selected data may be stored on floppy disc files so that upon completion of a test, the results may be plotted or printed. The presentation of results may be in the form of suitably annotated graphs of report quality, or as printed data listings. Since the test system configuration is such that the sample is located inside

the cell and remote from the test operator, this data acquisition facility provides essential visual aids for setting up and monitoring the progress of the tests, as well as for diagnosing faults.

Chapter 4

EXPERIMENTAL PROGRAMME AND TECHNIQUES

4.1 Outline Plan

As noted in Chapter 3, it was necessary to undertake an experimental programme that would provide suitable data which could be used to assess the theoretical assumptions outlined in Chapter 2. The data obtained from the tests should provide reliable information on the mechanical, hydraulic and thermal behaviour of rock joints and the effects of temperature on these properties.

It was intended to relate the joint surface properties to the hydro-thermo-mechanical properties of the joint as stated in Chapter 2, and to investigate the differences in behaviour of joints of different origins. An initial programme of room temperature experiments was planned using natural joints and induced extension fractures in Cornish granite under varied confining pressures and differential pressures. Some tests on natural joints had been carried out previously by Boodt and Brown [1985] who concentrated on the determination of conditions of laminar flow in natural rock joints. Little

was known about the influence of temperature on joint properties. Accordingly, the present experimental programme consisted of testing the joints at elevated temperatures; these tests also allowed the rock-fluid heat transfer characteristics to be investigated. Although tests involving the complete range from laminar to turbulent flow were conducted occasionally, the tests were mainly restricted to laminar flow both at room temperature and at elevated temperatures.

Initial experience indicated that errors in fluid temperature measurements may be introduced by the original steel endcaps, through which the fluid is injected into and collected from the test samples. Thus a new system of measuring the inlet and outlet fluid temperatures had to be developed to ensure that it would provide the quality of data required (section 3.3.2). The measurements are to be used to determine the rate of rock - fluid heat transfer and of thermal energy extraction by the water.

It was initially proposed that the acoustic emission technique would be used to detect the possible thermal cracking induced when cold water was injected into heated joints. Trials were carried out with the acoustic emission technique. This technique detects the sound released by the cracking of test sample (Yong and Wang 1980, Atkinson et al 1981). The servo-controlled testing machine produces high degree of noise by the servo-controller and the pressure intensifier. This noise has a frequency close to that of the noise released by

TABLE 4.1 Tests Conducted on Natural Joints and Extension Fractures in Carnmenellis Granite

Sample No.	Maximum Temp.°C	Load. Cycle	Maximum Pc (MPa)	Maximum dP (MPa)	Pc at Max. dP (MPa)
Natural Joints					
NJ1	room	1	30.0	4.828	10.0
NJ3	200	2	30.0	5.517	30.0
NJ4	180	1	7.0	1.186	7.0
NJ5	140	2	20.0	0.345	7.0
NJ6	100	1	20.0	0.759	6.0
NJ2	room	1	7.0	0.083	3.5
NJ13	room	1	8.0	0.083	4.0
NJ14	room	1	15.0	5.517	15.0
NJ15	room	2	10.0	6.207	10.0
Extension Fractures					
TF2	room	1	40.0	0.172	7.0
TF3	100	1	2.5	0.138	2.5
TF5	180	1	30.0	2.760	10.0
TF6	180	1	0.8	0.375	0.8
TF7	180	1	30.0	2.760	15.0
TF9	140	4	30.0	1.380	20.0
TF10	120	2	25.0	0.140	5.0
TF11	100	2	25.0	0.345	1.5
TF12	120	2	20.0	1.724	10.0
TF13	120	2	30.0	1.724	7.0
TF15	140	1	25.0	0.345	8.0

cracking. Difficulty arose in isolating the disturbance from the testing machine, and so the ambition of using the acoustic emission technique was not realized.

However, it was important to understand the physical and structural changes occurring in the rock joint after it had been heated and in contact with cold fluid, since this may provide the reason for any observed change in joint properties. Accordingly, thin sections were made from the tested samples and examined by both ordinary microscopy and Scanning Electron Microscopy (SEM) in order to make up a deficiency from a detection by acoustic emission.

Due to the shortage of suitable naturally jointed samples, work at elevated temperature and with multi-loading cycles was concentrated on induced extension fractures. A total 3130 tests runs on 9 naturally jointed samples and 11 fresh extension fractured samples were carried out during this experimental study. The sample tested with their temperature and pressures ranges are listed in Table 4.1.

4.2 Description of Rock

The Carnmenellis Granite is part of the exposed Cornubian granite batholith, forming a circular granite boss, which underlies most of Cornwall, South-west England. The Carnmenellis pluton was emplaced into sedimentary and volcanic country rock laid down in the

Devonian Period about 285 million years ago, and subsequently metamorphosed [Brown et al 1982].

The rock is a coarse to medium grained (2-5 mm) biotite-muscovite granite with potassium feldspar phenocrysts [Hill and MacAlister 1906]. The phenocrysts are up to 20 mm long and randomly oriented in a predominately coarse groundmass of plagioclase feldspars, quartz, biotite, muscovite and tourmaline. The granite contains about 55% of feldspars, 30% of quartz and rest of others. There has been post-magnetic growth and recrystallization of quartz and feldspar which has resulted in a complex fabric with strongly convoluted crystal boundaries [Beswick 1982]. Tunbridge and Richards [1983] describe the rock mass as being faintly weathered. Although hand specimens appeared fresh, feldspar and micas showed signs of weathering and the rock exhibits hydro-thermal alteration.

Some studies of rock mass structure and in situ stress have been carried out at an experimental site in the granite [Cooling et al 1984]. The site comprises a series of tunnels totalling 150 - 200 meters long [Brown et al 1982], roughly at right angles to each other (Figure 4.1), entered at ground level at the base of a quarry wall. The tunnels are at a maximum depth of approximately 34 meters below the surface. A block of rock (indicated on Figure 4.1) was selected for a series of experiments to assess the properties of rock masses, especially those of its discontinuities because these

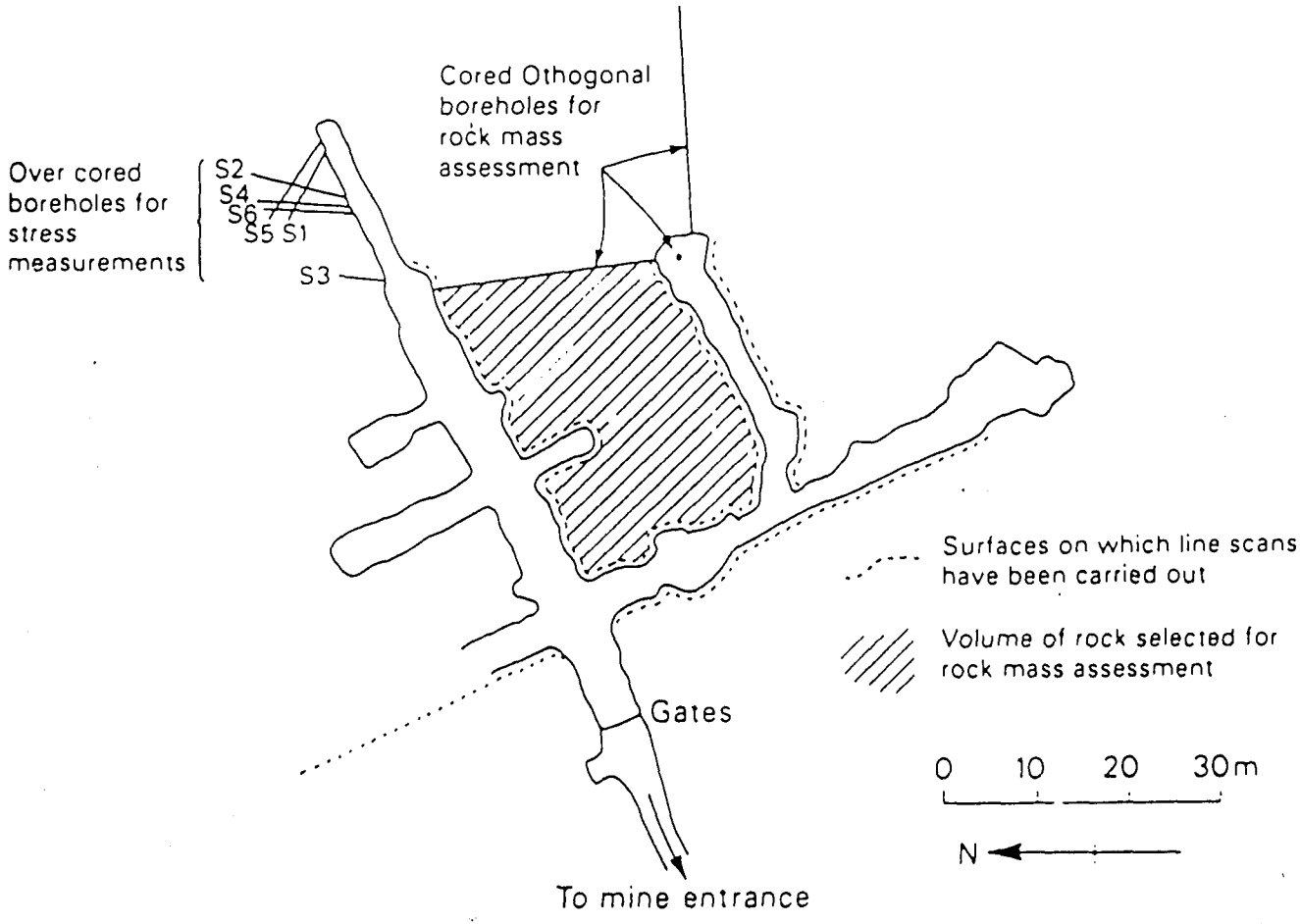


Figure 4.1 The In-situ Experimental Site at Cornwall, SW England (after Cooling et al [1984]).

control amongst other things, anisotropy in the mechanical and hydro-geological properties of the rock mass. Structural mapping at the site and at underground exposures revealed two major sets of steeply dipping discontinuities [Cooling et al 1984].

The mechanical properties of the Carnmenellis granite at the Rosemanowes quarry site has been determined by Pine and Batchelor [1982] to be the following:

1. the intact granite has an average uniaxial compressive strength of 135 MPa for 42 mm diameter cores;

2. a typical deformation modulus determined by uniaxial loading of 42 mm diameter core was 65 GPa with a Poisson's ratio of 0.2; there was no significant anisotropy in the modulus;

3. an average tensile strength of 10 MPa was measured by Brazilian tests and an average tensile strength of 15 MPa measured by the hydraulic fracturing method;

4. permeability of the rock fabric of 10 microdarcies (10^{-17} m^2) was determined by water diffusion.

Elliott [1984] carried out some further tests to determine the mechanical properties of the granite at elevated temperatures up to 200°C. The results showed little increase in the deformation modulus and Poisson's ratio and little decrease in uniaxial strength at high

temperatures, as shown in Table 2.3. He concluded that the deformation mechanism seem to be unaffected by the temperature of the test, since the failure envelope for the samples tested at 200°C was almost identical to that for the samples tested at 20 °C (Figure 2.10). The variability in the measured values of Young's modulus and Poisson's ratio seemed to depend more on the structure and composition of the sample than on the environmental conditions of the test.

4.3 Sample Preparation and Joint Appearance

4.3.1 Natural joints

Samples of a natural horizontal discontinuity were taken from unused core obtained from a 102 mm diameter horizontal borehole drilled in the rock mass of granite at Troon , Cornwall. Short lengths of core containing the fracture were re-cored using an hydraulically driven diamond drill to obtain 51 mm diameter cylindrical samples of 102 mm in length with the discontinuity approximately parallel to the axis of the sample. The parts of the specimen were taped together during the coring to prevent the surfaces from becoming damaged or displaced relative to each other. The cored granite was then retaped and cut to the required length and finished on a surface grinder to ensure parallelism of the ends.

Visual inspection of the tested samples showed

the joint to be clean and fairly matching with little of sign of previous shearing. Figure 4.2 shows a typical profile of a natural joint obtained as described in section 4.4.

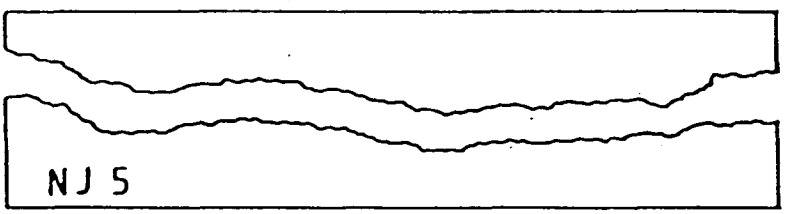


Figure 4.2 A Typical Profile of a Natural Joint.

4.3.2 Artificial extension fractures

Artificial extension fractures were prepared by splitting the rock core along its diameter. The 51 mm diameter core was taken from a rock block and then cut into lengths of 102 mm in which discontinuities were induced. Each granite core was loaded between two sharp edged steel cutters across its diameters. During splitting the core, little shearing occurred, and the joint produced was a purely extension fracture.

The joint was a typically fresh extension fracture joint showing no signs of mechanical deformation and weathering or other alteration. The joints surfaces were generally rough, with high unevenness over their lengths. The two faces of each joint were precisely matched. A typical profile of an induced extension fracture is shown in Figure 4.3.

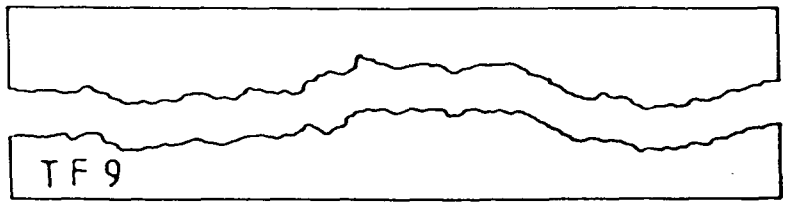


Figure 4.3 A Typical Profile of an Extension Fracture.

4.4 Measurement of Joint Properties

In this thesis, the joint surface geometrical properties are taken to be a combination of two measurements -joint roughness and joint matching. A coefficient for the first of these was proposed by Barton and Choubey [1977] and the latter is a measure of the degree of the matching of two surfaces. Both coefficients will be discussed in detail in Chapter 5; this section describes the methods used to measure these properties.

The measurements on natural joints were made after the test in order to avoid introducing disturbance to the test sample. Measurements on the split samples were made immediately after splitting. The actual surfaces of the joints and the fractures are shown in Figure 4.4 and Figure 4.5. Measurements were made on both sides of the joint surfaces, at exactly matching lines across the length for all the samples. Generally, readings were taken along 3 pairs of matching lines for each pair of joint surfaces, with one approximately lying along the centre.

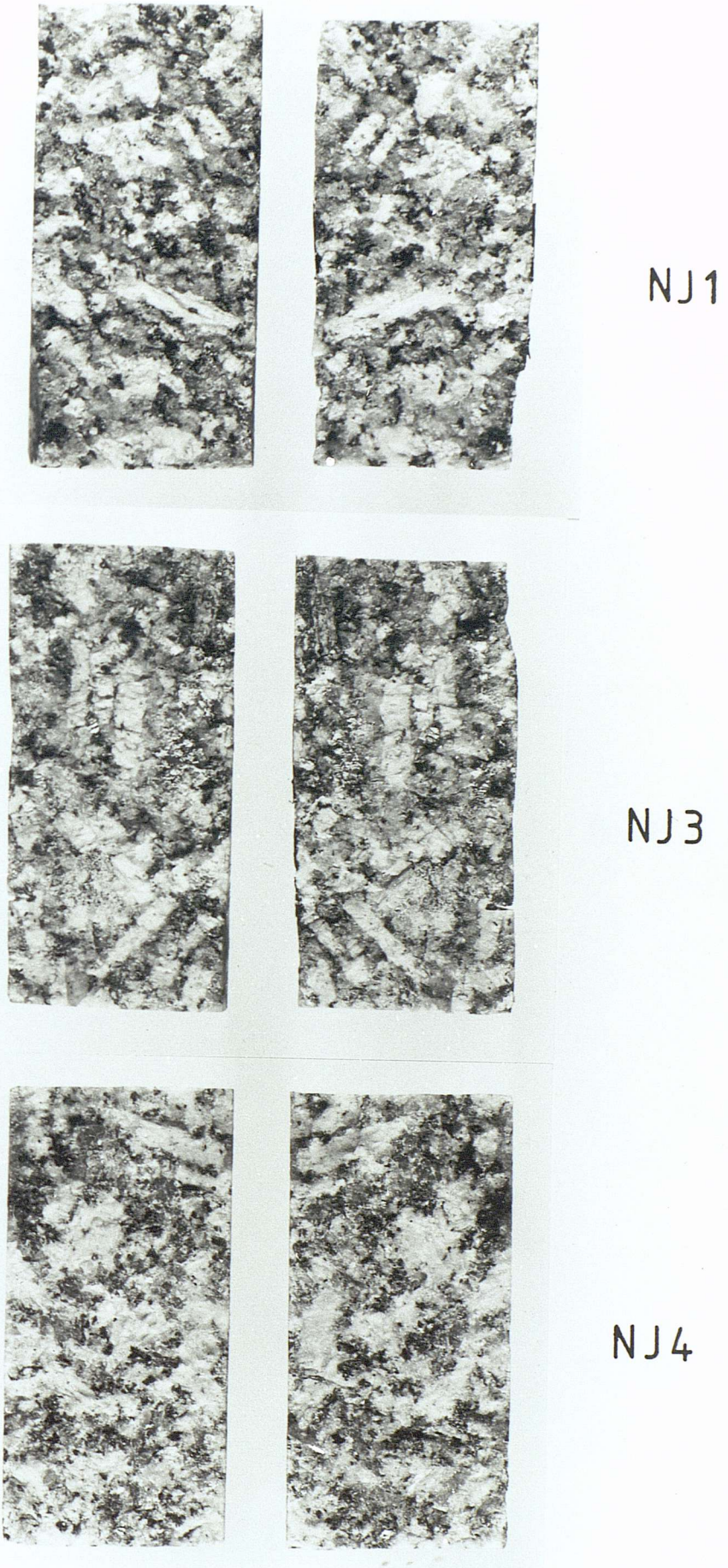
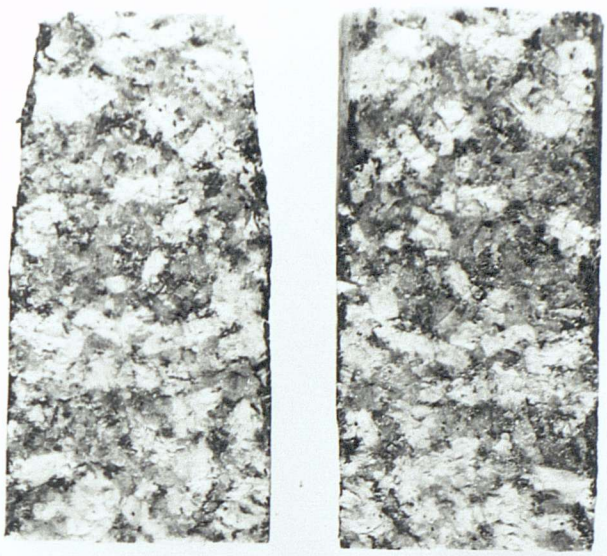
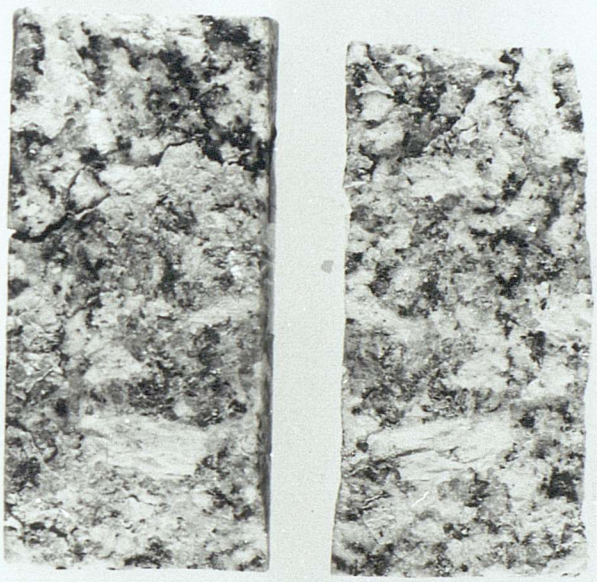


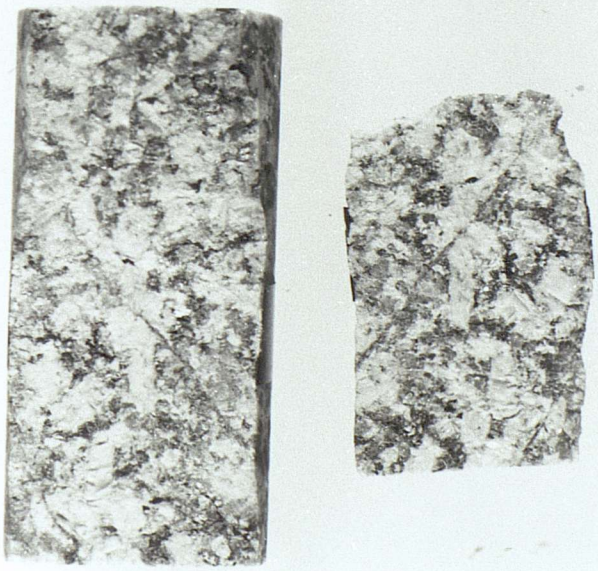
Figure 4.4 Tested Natural Joints Surfaces.



NJ5

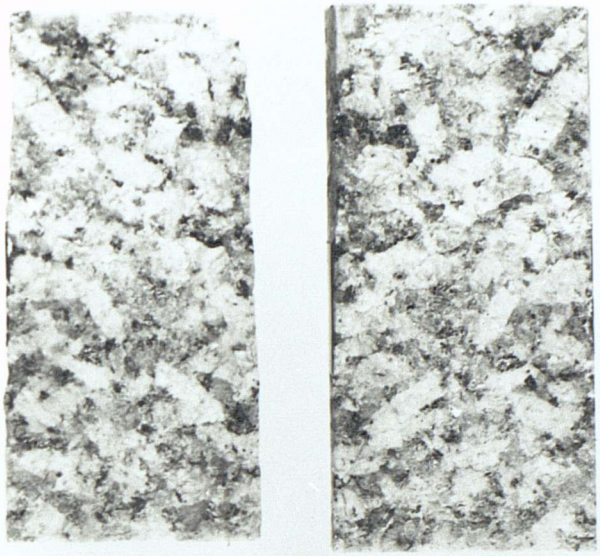


NJ6

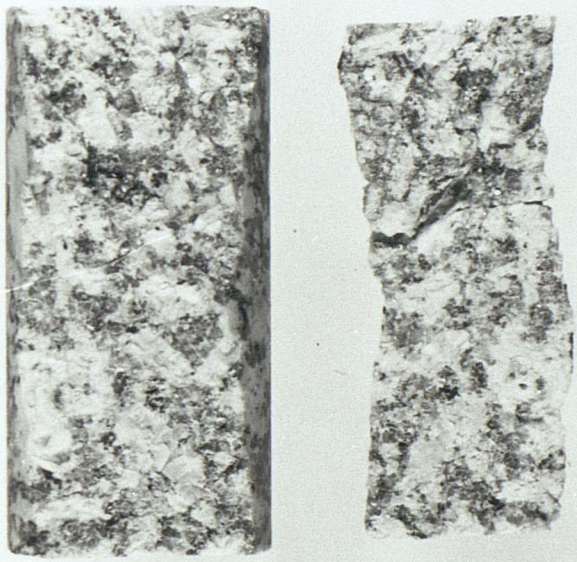


NJ12

Figure 4.4 (continued).



NJ13



NJ14



NJ15

Figure 4.4 (continued).

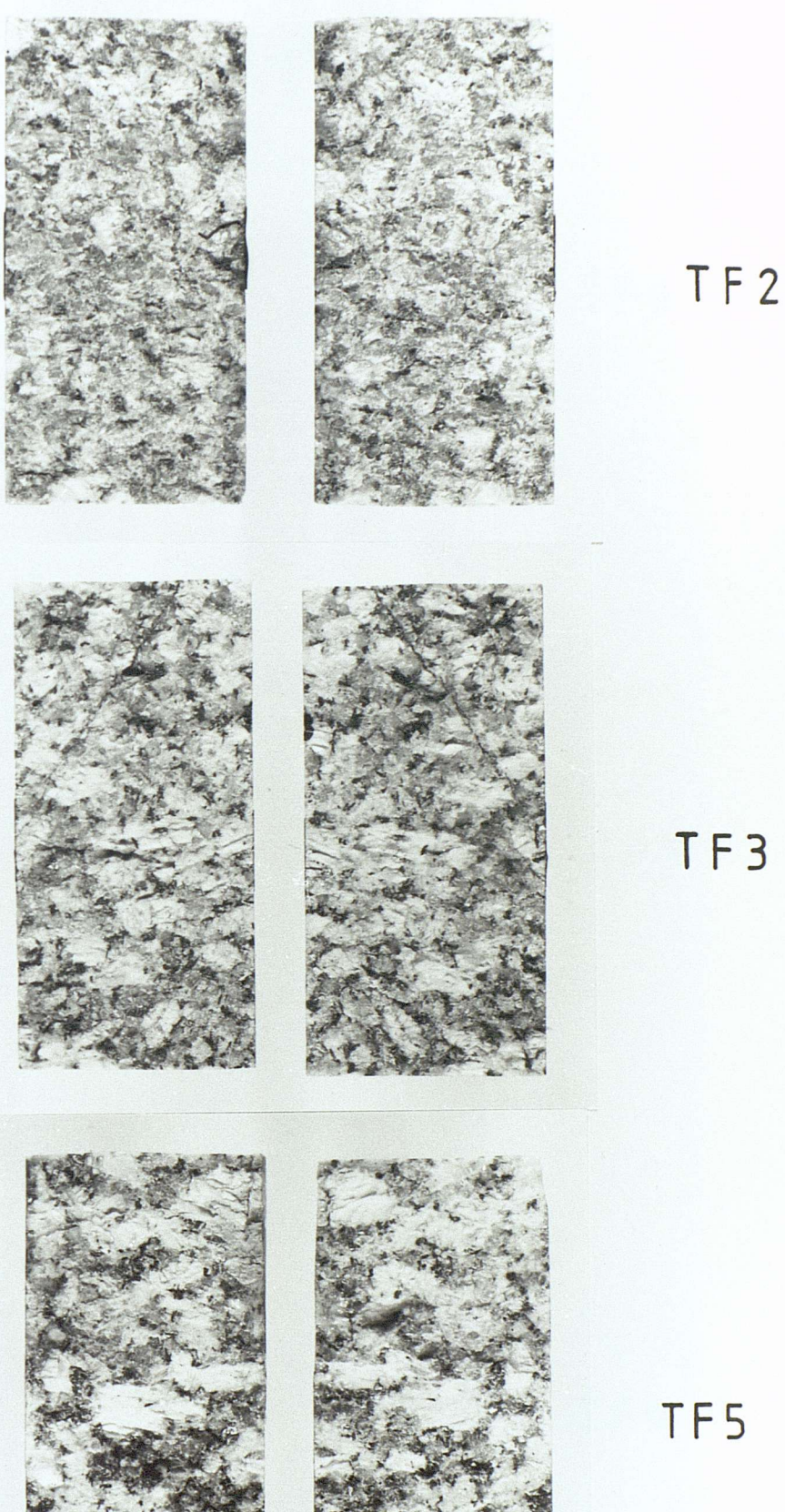
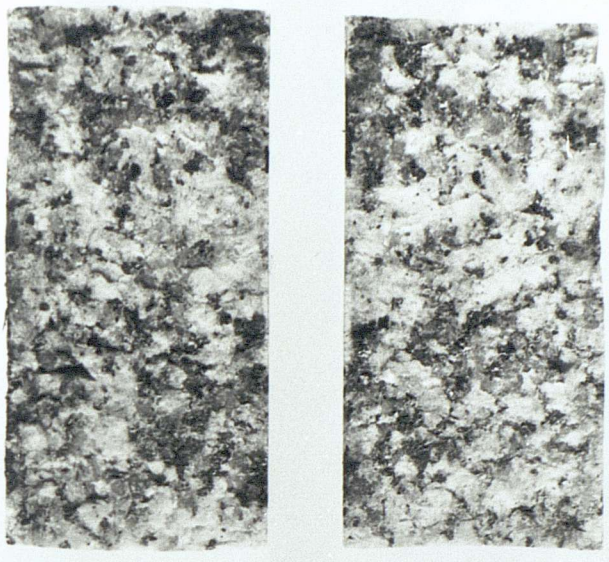
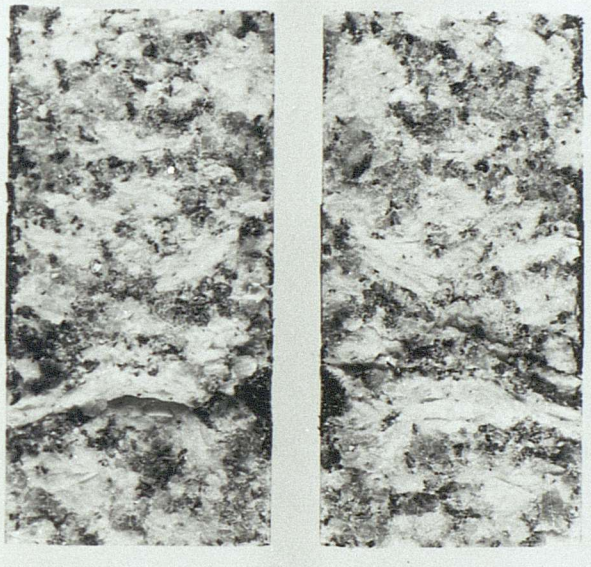


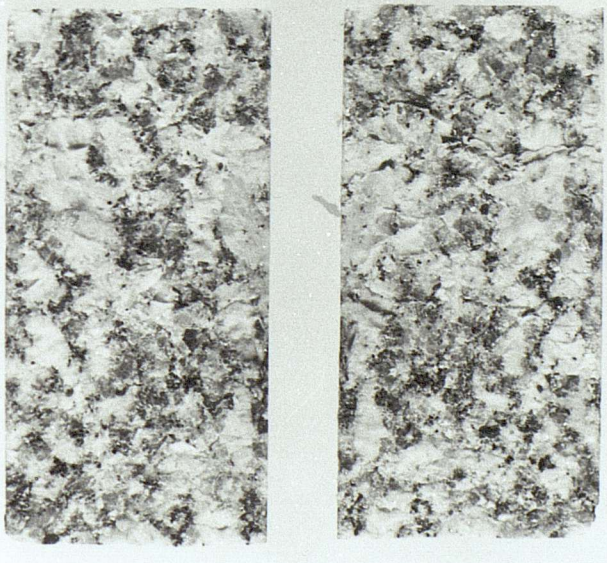
Figure 4.5 Tested Extension Fractures Surfaces.



TF6



TF7

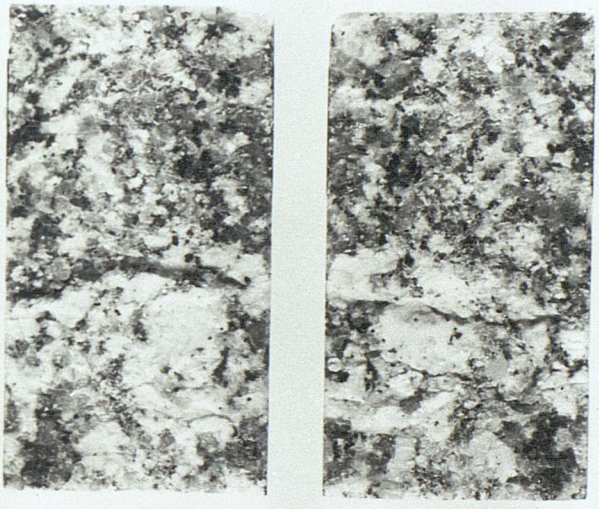


TF9

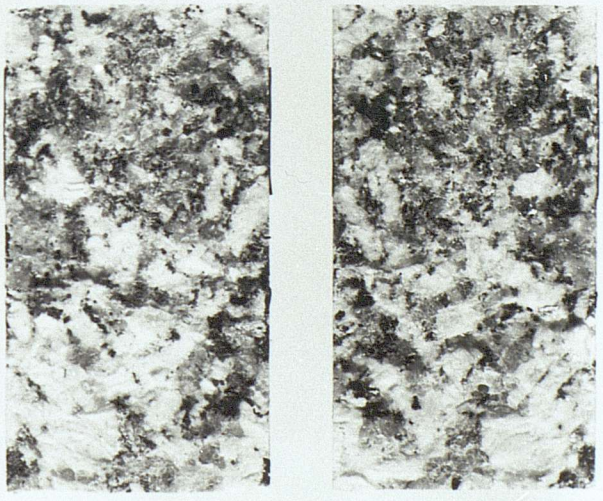
Figure 4.5 (continued).



TF10

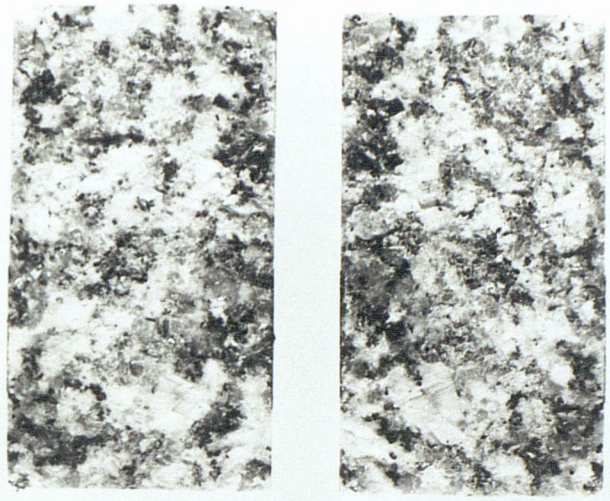


TF11

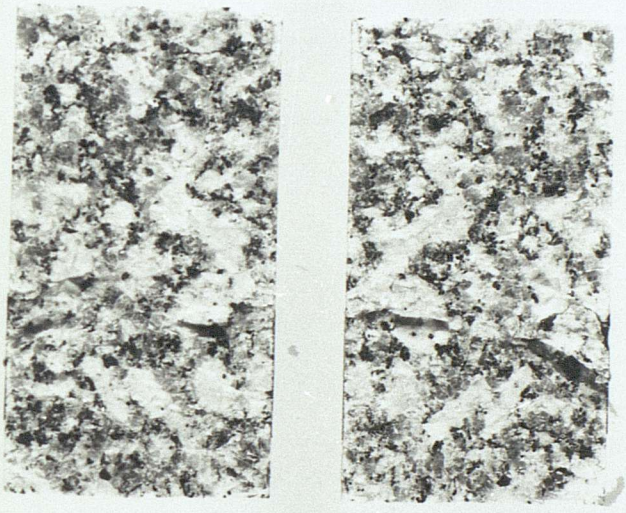


TF12

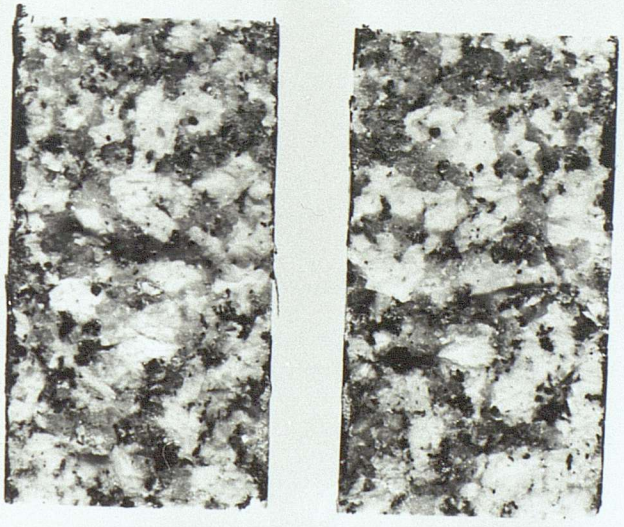
Figure 4.5 (continued).



TF13



TF14



TF15

Figure 4.5 (continued).

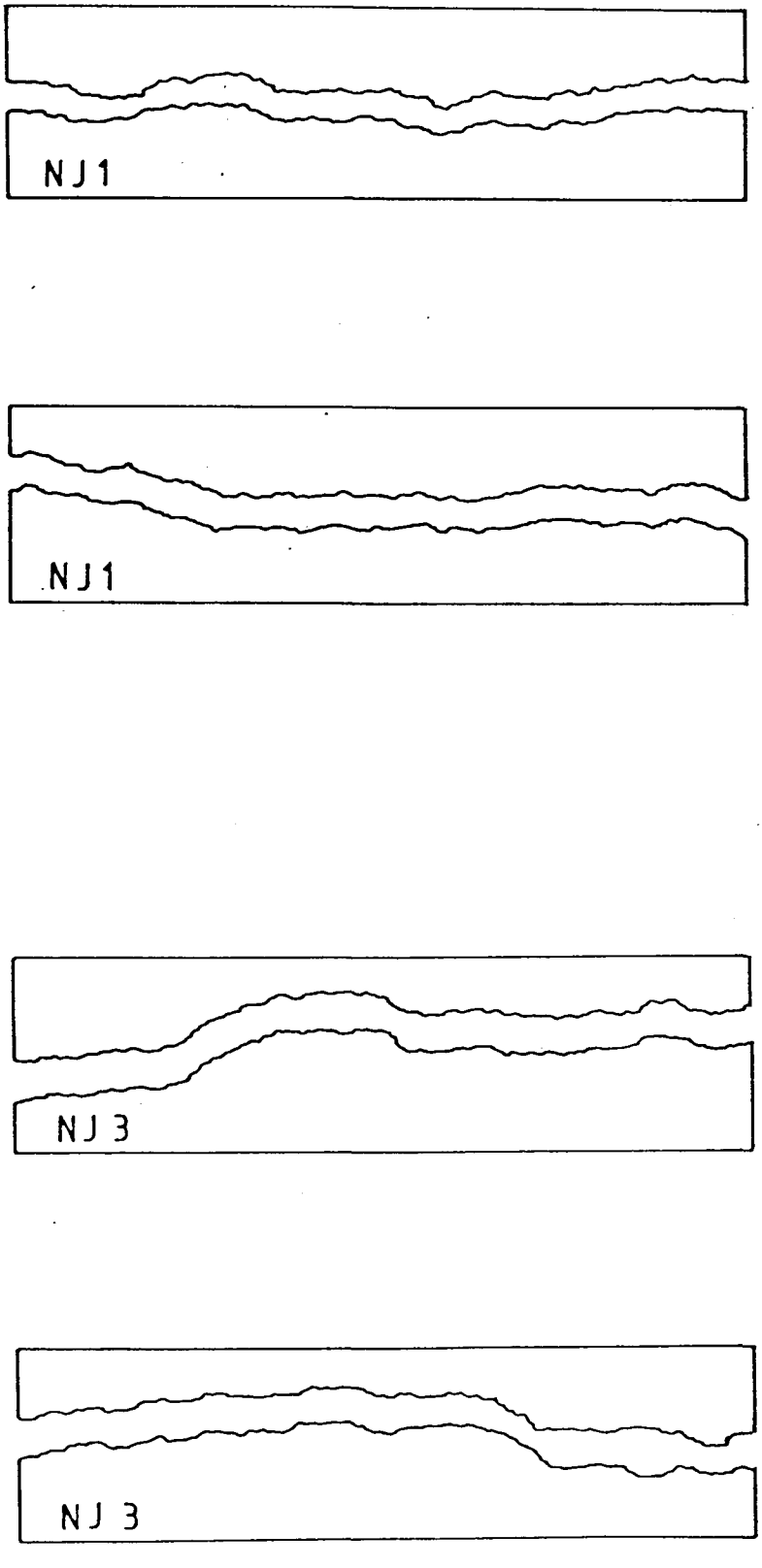
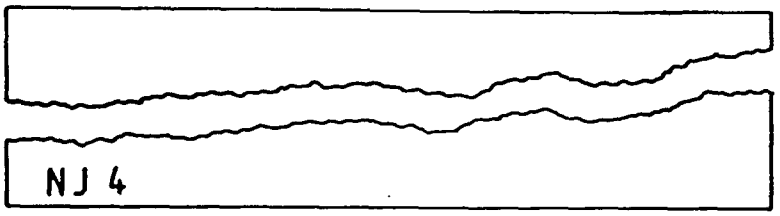
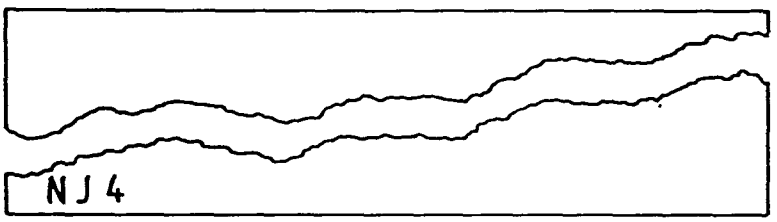
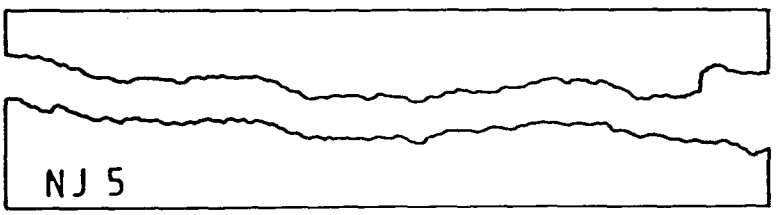


Figure 4.6 Surface Profiles of Natural Joints.







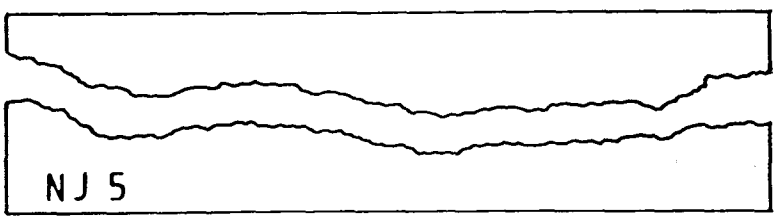
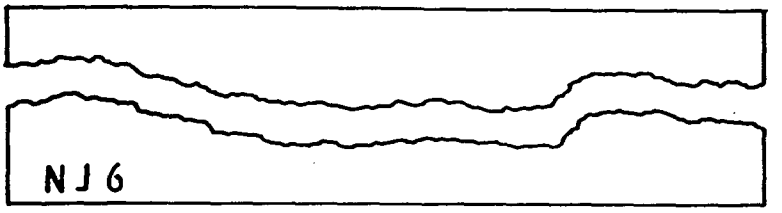
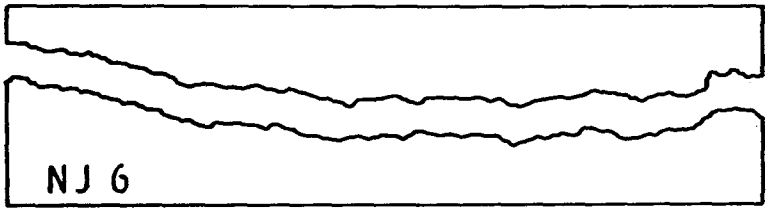
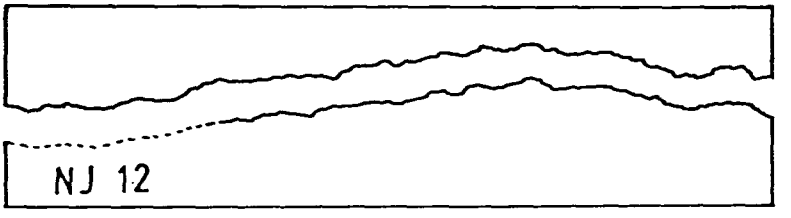


Figure 4.6 (continued).







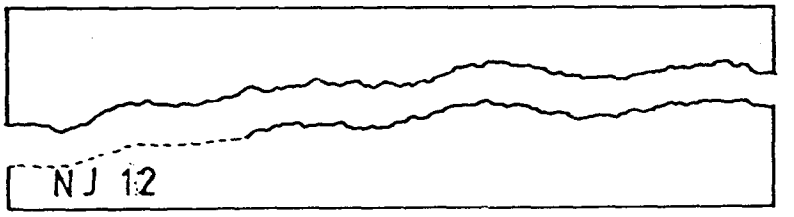
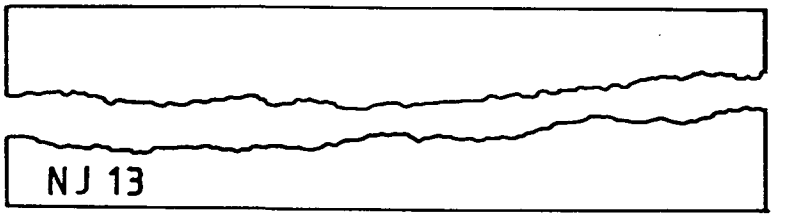
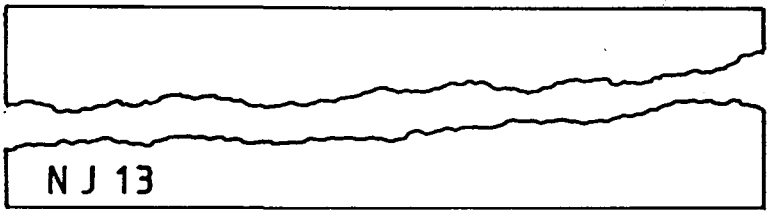
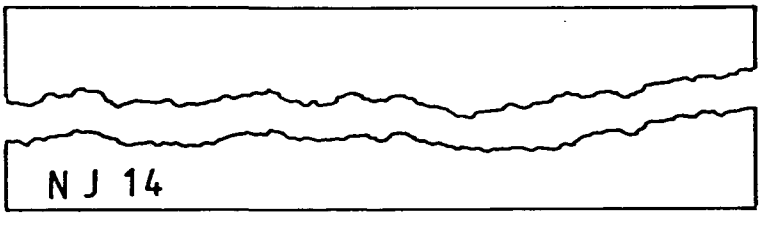


Figure 4.6 (continued).







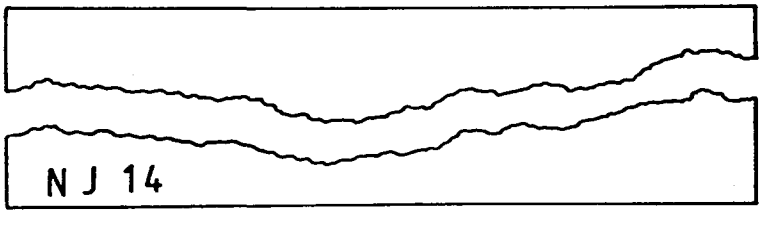


Figure 4.6 (continued).

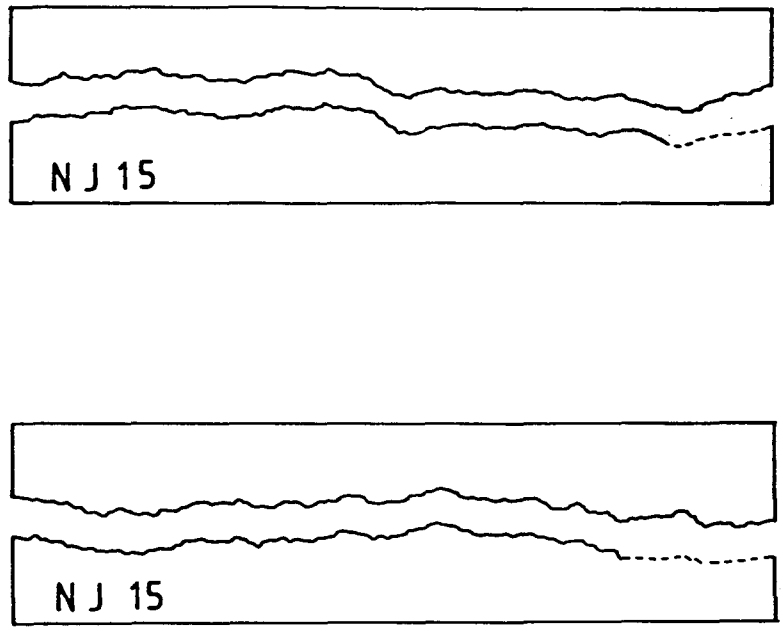


Figure 4.6 (continued).

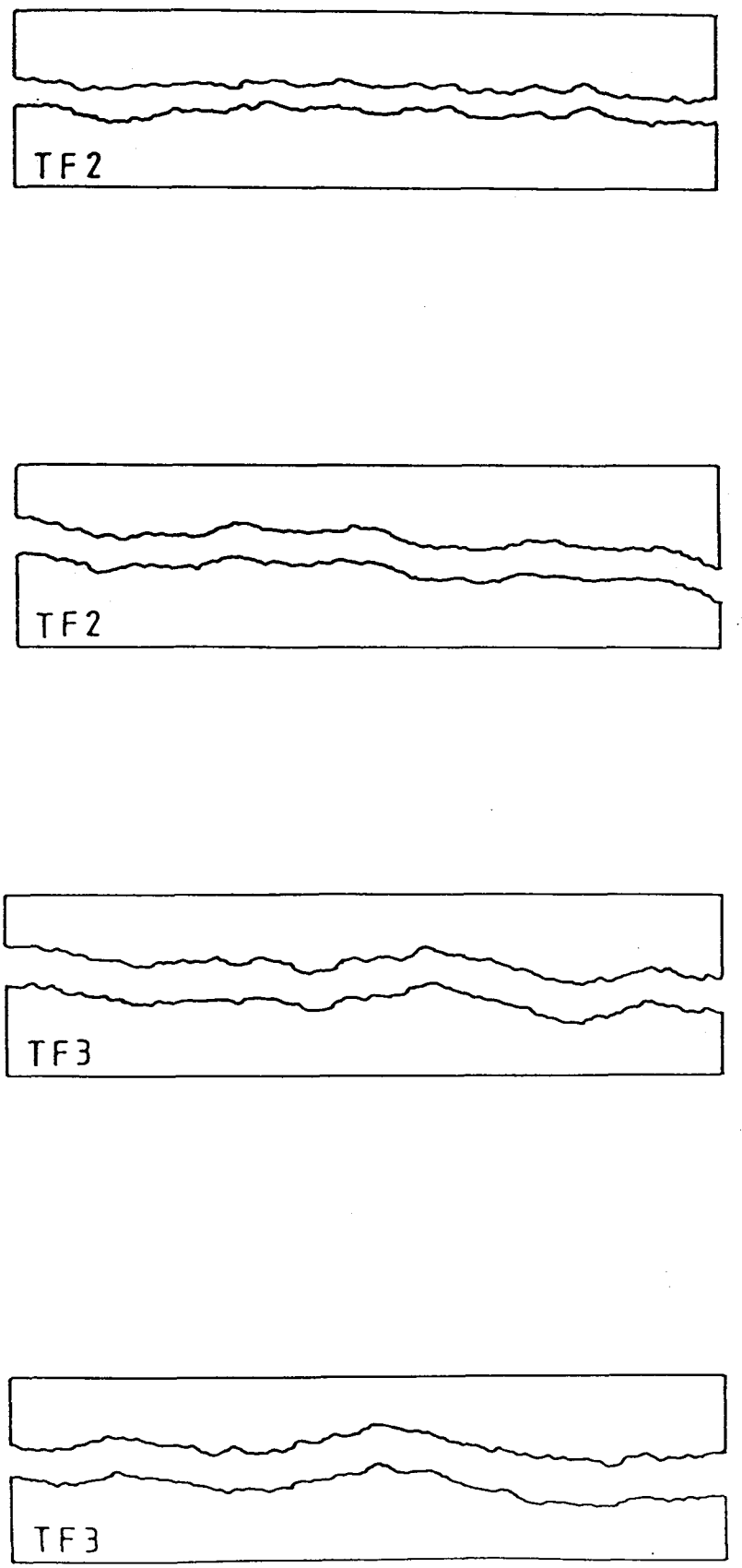
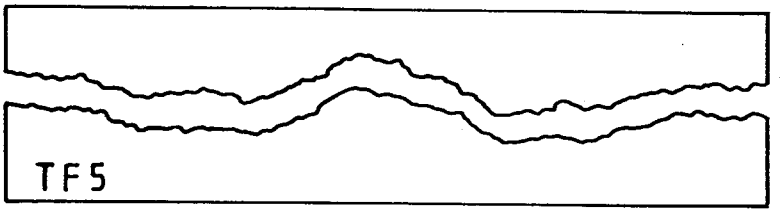
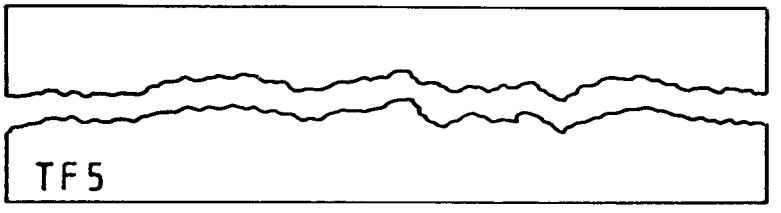
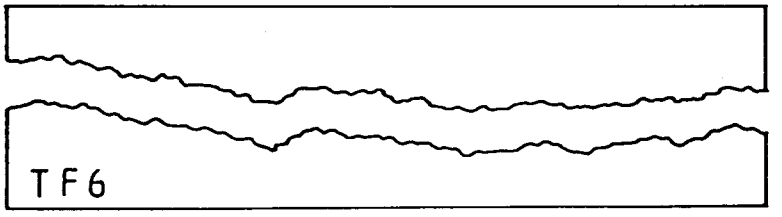


Figure 4.7 Surface Profiles of Extension Fractures.







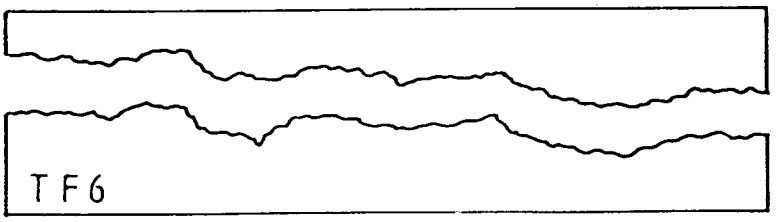
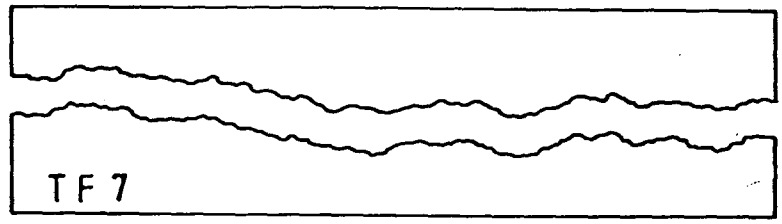
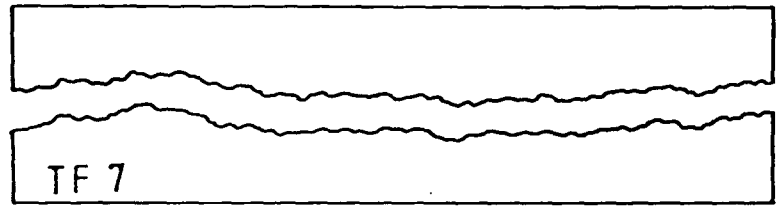
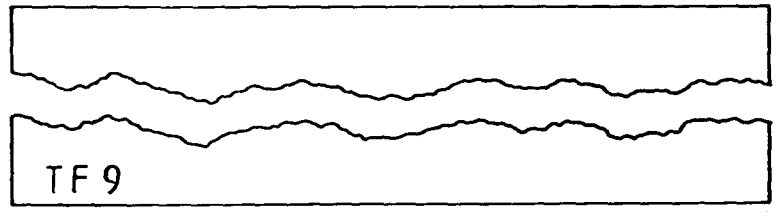


Figure 4.7 (continued).







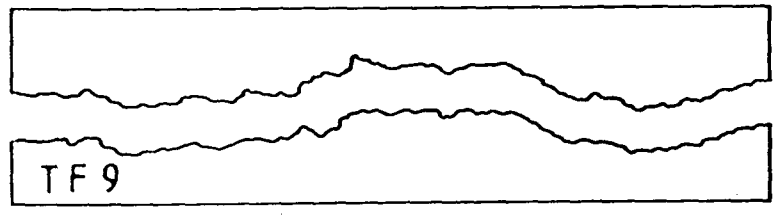


Figure 4.7 (continued).

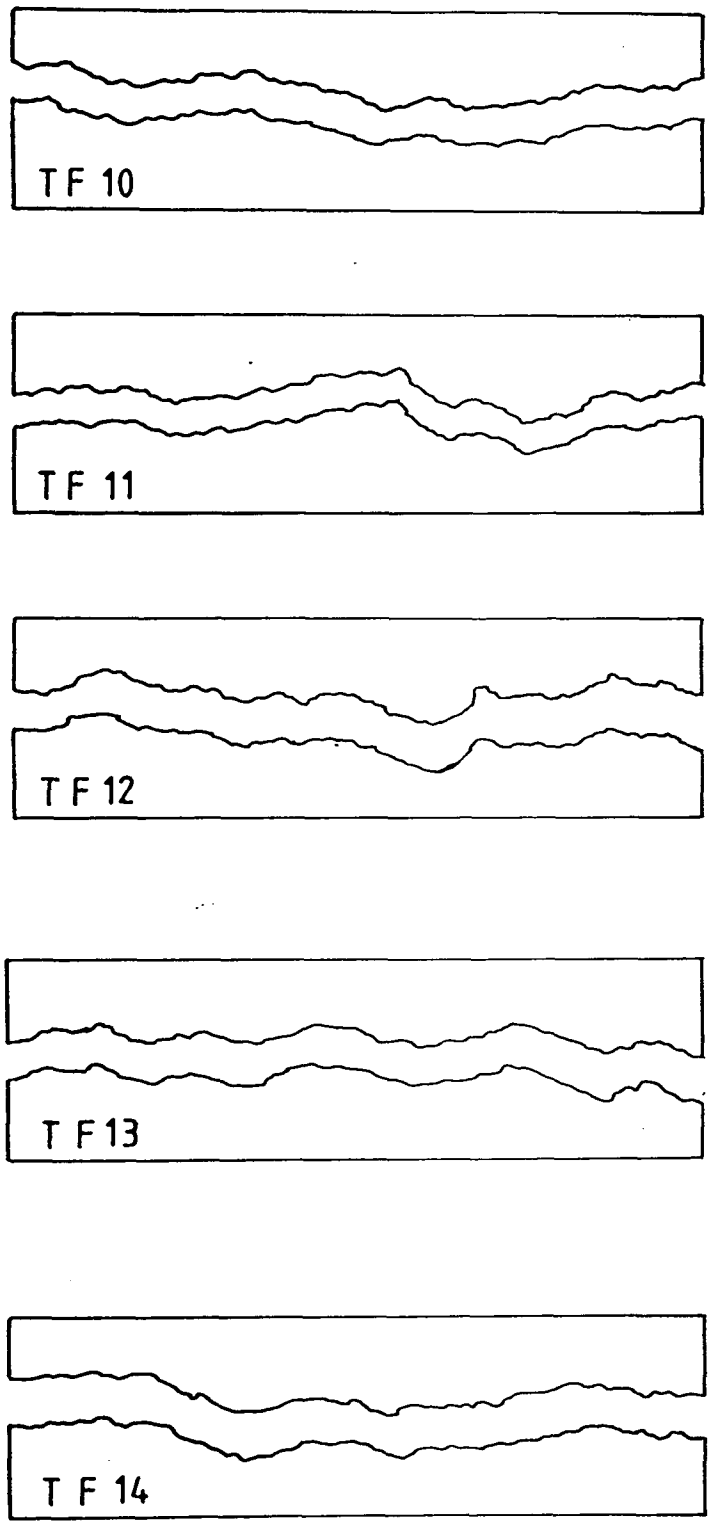


Figure 4.7 (continued).

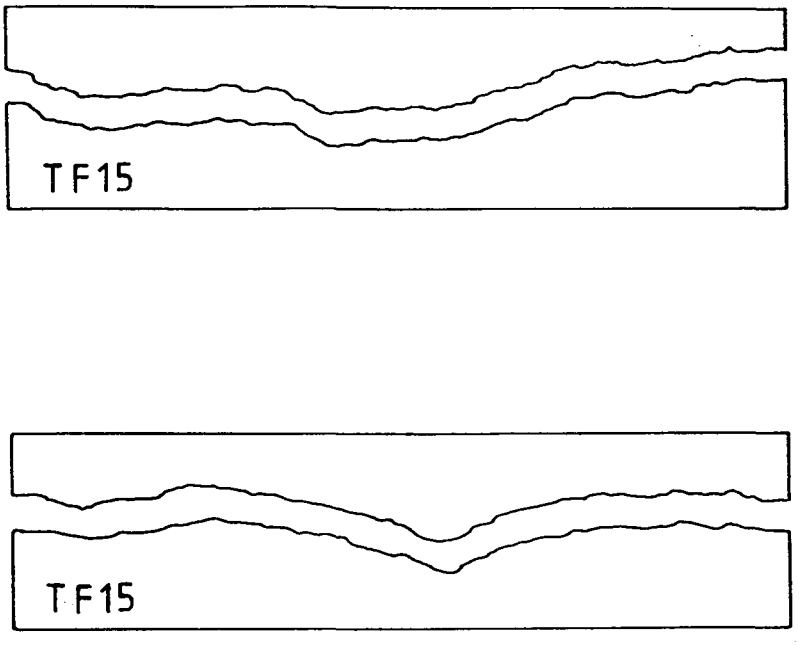


Figure 4.7 (continued).

A linear measuring and profiling method was adopted to determine the geometrical properties of joint surfaces. A strain gauge was attached to a travelling micrometer, and the heights of asperities were noted at each mm along a straight line along the sample length. The measurements were then plotted to present the surface profiles on same horizontal and vertical scale (Figure 4.6 and 4.7). The Joint Roughness Coefficients were determined from these profiles by comparing them with Barton and Choubey's chart [1977] shown in Chapter 2. The Joint Matching Coefficient were determined by fitting the upper and lower parts of the joint surface profiles and comparing with the chart given in chapter 5.

4.5 Sample Setting Up

Each prepared sample was left to air dry for a few days before being set up for the test. The joint trace which appeared on the outside of the curved cylindrical surface was sealed with adhesive tape. Two stand offs for the cantilever device were glued at the mid-height of the sample in a position perpendicular to the fracture plane, in order to measure the normal displacement of the joint under stress. The sample then was attached to the stainless steel end platens, with a stainless steel mesh net between the ends of the sample and the endcaps. The sample stack then was sleeved directly in silicon rubber and a heat-shrink plastic jacket. This provided good adhesion plus an ideal jacket

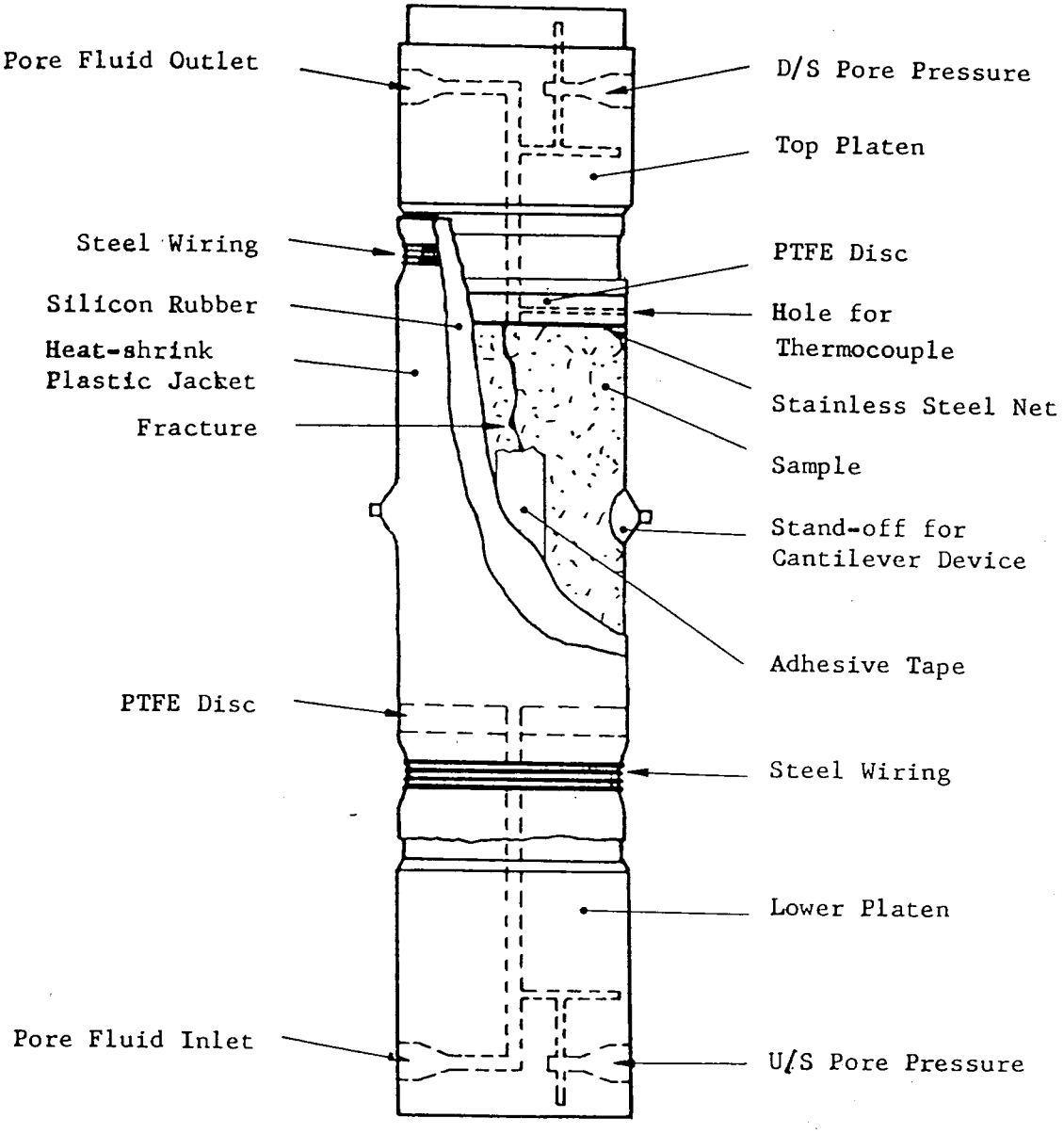


Figure 4.8 Details of Sample Set Up.

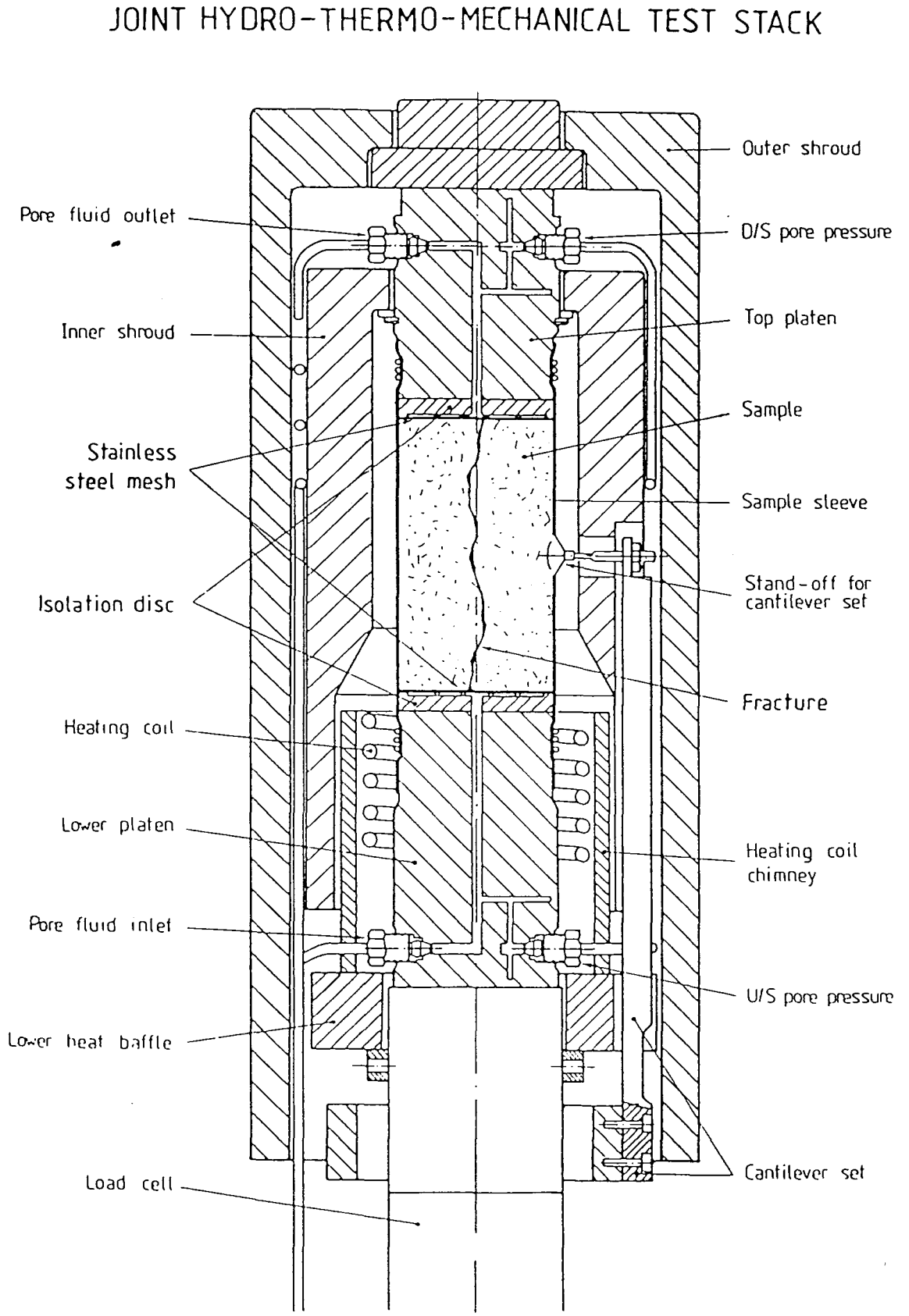


Figure 4.9 Stack Assembly for Hydro-thermo-mechanical Tests.

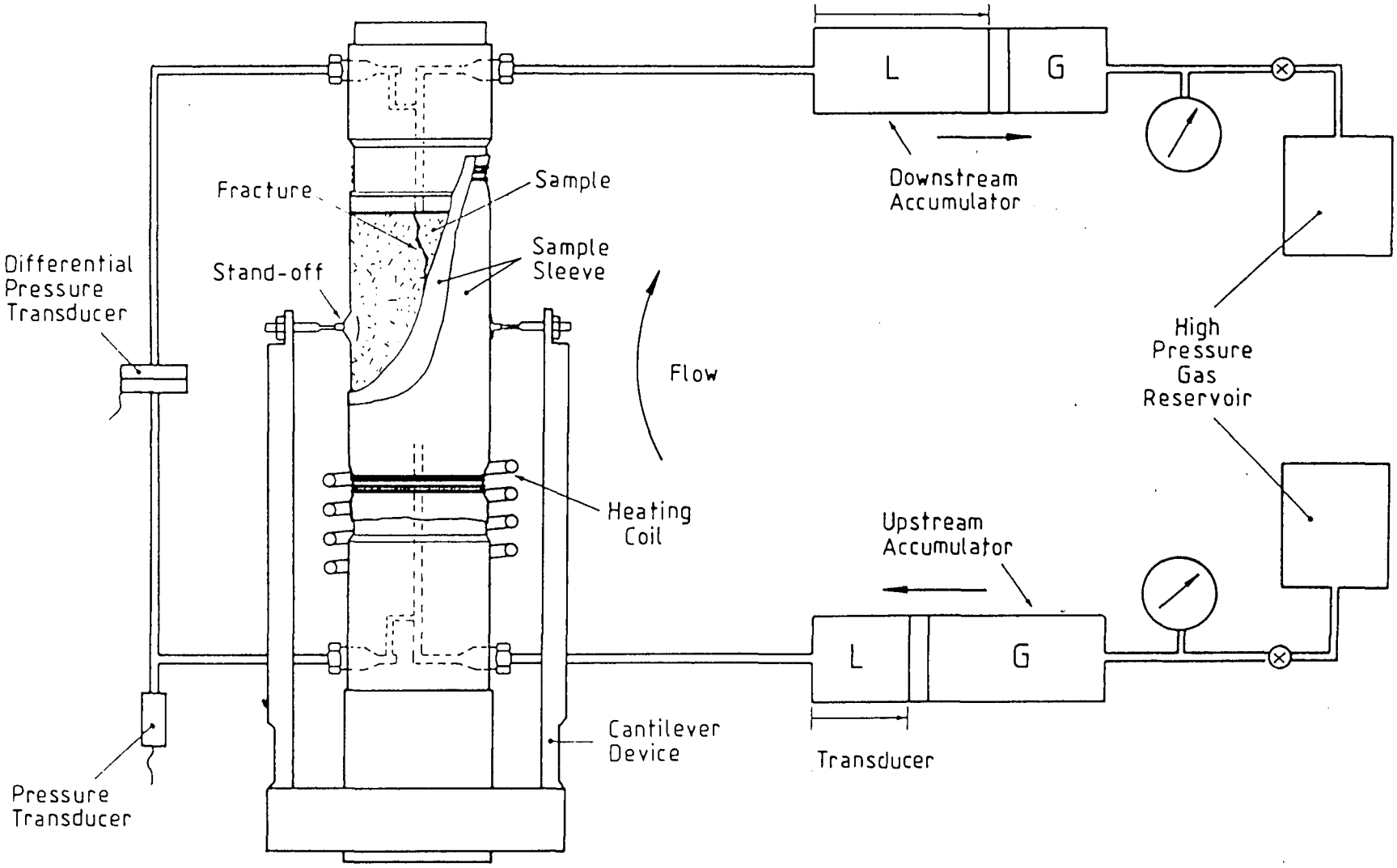


Figure 4.10 Schematic of the Arrangement for Hydro-thermo-mechanical Tests.

fit. End sealing was accomplished by wiring the jacket to the stainless steel endcaps (Figure 4.8). This method of sample sleeving has been developed by Terra Tek Systems, Utah, USA, and operated well within the environmental conditions used in the tests. The sleeving has been shown to have negligible influence on the strength and deformation response of tested rock samples [Enniss et al 1979b].

The sample stack was then placed into the triaxial cell base, a heater located over the lower part of the stack, a cantilever device connected to the stand-offs, thermocouples located at desired points and pipework fixed to the platens. The insulating shrouds were carefully placed around the sample stack before the assembly was raised into the testing cell and submerged in the confining oil (Figure 4.9 and Figure 4.10

4.6 Test Procedure

4.6.1 Testing at room temperature

After the testing cell was filled with confining oil (Multitherm PG1), the sample and the permeabilty pipework were evacuated to remove all the air. Then water was introduced into the sample with system at a very small pressure (<0.1 MPa), ensuring that the joint and pipelines were saturated with water. Initial tests at zero confining pressure showed early discontinuity dilation. So for all the samples the first

test runs were started at a small confining pressure of 0.1-0.2 MPa. When the confining pressure was established at its constant level by the pressure intensifier, the fluid pressure in the up-stream accumulator was increased to create a pressure gradient across the sample and data recording was started.

Readings were taken of confining pressure, joint normal displacement, pore pressure, and the volume of water in the up-stream and down-stream accumulators, according to the time, at each constant differential pressure. The volume of the accumulators often restricted the duration of the early tests at low confining pressures and of those with high differential pressures in which the flow rates were generally too high. In these tests readings were taken more frequently than in the longer tests so that approximately the same number of the readings were obtained for each test. Unless the flow rates were very low during later tests, particularly at very high confining pressure, the tests usually were stopped after 1000 seconds.

In general, between 5 to 15 tests at different differential pressures were performed at each confining pressure up to 20 MPa. The increment of confining pressure was small at the beginning and then increased at higher confining pressures. In most situations, the samples were tested at confining pressures of 0.1, 0.2, 0.3, 0.4, 0.5, 0.6, 0.8, 1.0, 1.2, 1.5, 2.0, 2.5, 3.0, 3.5, 4.0, 5.0, 6.0, 8.0, 10.0, 12.0, 15.0, 20.0, 25.0 and

30.0 MPa. However, the range of differential pressures varied according to the joint type, confining pressure, and were normally judged by experience and trial results. The procedure is shown schematically in Figure 4.11a. In general, the flow rates measured were extremely small (< 0.5 mm /sec) for the joints at the confining pressure above 8 MPa. Therefore, only normal deformation readings were taken at high pressures.

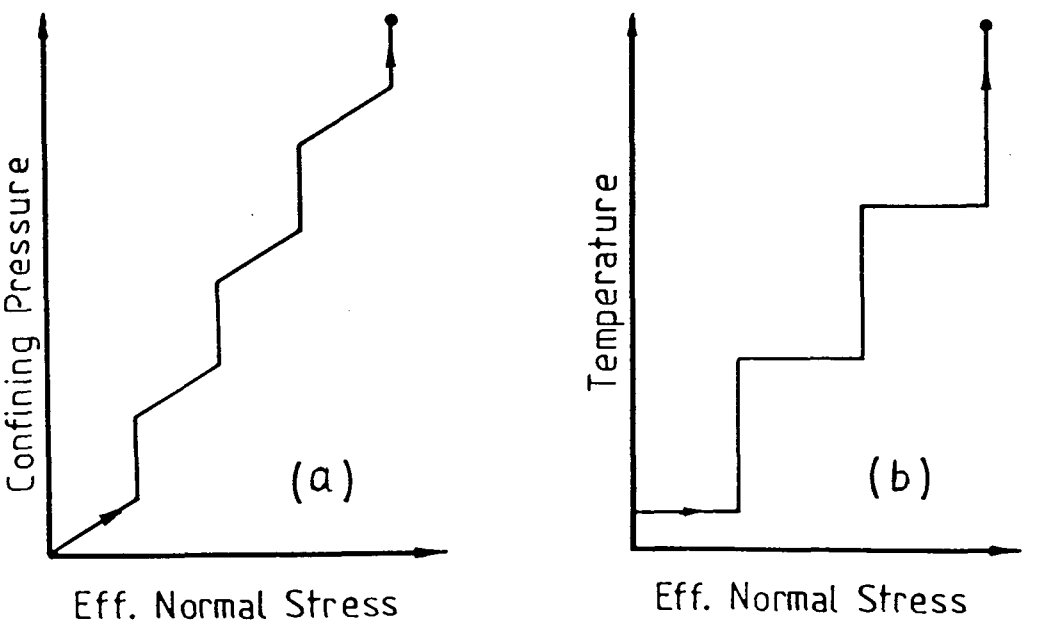


Figure 4.11 Schematic Representation of Test Procedures.

For natural joints, differential pressures were in the range of 0.003-0.276 MPa at early low confinement. This range, as well as the lower limit were both increased as the confining pressure increased. Sometimes the differential pressure applied during the test was as high as 2.8 MPa.

Extension fractures samples had well matched joints with narrower joint apertures, and hence considerably reduced water conductivities. The differential pressure for testing these samples ranged from 0.007 to 0.414 MPa at lower confining pressures. As a result of increasing the confinement, the differential pressure required to complete the tests might go as high as 4.1 MPa.

The choice of the differential pressure used was dependent on the flow rate that could be generated, but was kept as low as possible in an attempt to prevent the flow in the discontinuity from becoming non-laminar. However, in some cases, a larger number tests and higher differential pressures were used to demonstrate the effects of non-laminar flow. A plot of the flow rate against differential pressure was drawn immediately following each test performed to verify that the test remained in the laminar range.

4.6.2 Tests at elevated temperatures

Tests at elevated temperatures usually followed a few tests carried out at room temperature for the purpose of making comparisons. The procedure is shown in Figure 4.11b. After a few tests (or a series of tests) at room temperature, the confining pressure was held constant by the intensifier. The heater inside the testing cell described in section 3.4.1 was generated on by the Silicon Controlled Rectifier unit. Although the

power output could be controlled from the unit either manually or automatically using the built-in programmer, throughout these tests manual control was used to obtain precise heating rates and for maintaining constant temperatures. The heating rate was kept at about 1 C per minute in order to prevent the sample from being thermally cracked during heating [Lo and Wai 1982]. When the sample inside the cell reached the desired temperature, a constant temperature was maintained for at least 20 minutes in order to ensure that the whole sample was fully heated up and in a constant and uniform temperature condition.

The process used for permeating the fluid through the specimen was the same as that used at room temperature. Experience showed that as the temperature increased, the flow rate decreased. In order to obtain moderate flow rates and flow rate increments, differential pressure increments were also increased. Measurement of confining pressure, pore pressure, mechanical joint deformation, temperatures of the sample and of the inlet water and the water at discharge, and the volume of flowing water in the up-stream and down-stream accumulators were recorded against time during the tests. The permeability of the rock matrix was taken to be negligible [Pine and Ledingham 1983] in the evaluation on the experimental data.

In some cases the sample was heated in two stages, and at each constant temperature, a series of tests was carried out. The sample was then reheated to a

higher temperature in the same manner as for the first heating, as shown schematically in Figure 4.11b.

Samples could be loaded and unloaded repeatedly at constant temperature. However, the confinement affected the cell temperature. Usually a high confinement brought up the temperature at the same power output of the heater; that is, in order to maintain a constant sample temperature, the power output of the heater had to be lowered when the confining pressure was raised. During the tests, the variations in temperature were controlled to within ±2 and ±4 degrees at sample temperatures of 50 °C and 150 °C, respectively.

Chapter 5

RESULTS AND DISCUSSION --JOINT MECHANICAL AND HYDRAULIC PROPERTIES

5.1 Joint Surface Properties

5.1.1 Observations on joint roughness

As noted in section 4.3, joint surface roughness was measured using a linear measuring and profiling method. The surface roughnesses of natural joints were measured after the permeability tests, while those of extension fractures were measured before the tests. This is to introduce minimum disturbance to the samples.

Typical surface roughness profiles were presented in Figures 4.6 and 4.7 for both types of joints, corresponding to the samples shown in Figures 4.4 and 4.5. By comparing the profile obtained from the samples used in the test with the profiles presented by Barton and Choubey [1977] (see section 2.2.1), the Joint Roughness Coefficients for the rock fractures could be estimated.

Results are shown for pairs of surfaces from each side of the joints as described earlier. Hence the figures show not only the degree of roughness of the

joint surfaces but also the degree of matching of the joints. All the joints are rough; however, the roughness of the natural joints are lower than those of the induced extension fractures because the former have suffered a small degree of weathering and hydro-thermal alteration.

Natural joints are generally rough, with the Joint Roughness Coefficients from 8 to 11, and show quite rounded profiles at the tips of asperities. They are not as stepped as are fresh extension fractures, and the asperities are round and generally not of height. The joints appear to be naturally induced extension fractured joints with little signs of shearing. The signs of degradation of the asperities suggest that the joints have been subjected to previous weathering and hydro-thermal alteration. Damages induced by transportation, sampling and preparation were not found.

The surfaces of the extension fractures, are rougher than those of natural joints, with clear signs of sharp asperities and stepped roughness. The asperities are fresh and with no signs of wear or tear. The estimations show that, with few exceptions, the artificially induced extension fractures have Joint Roughness Coefficients between 12 and 20.

Because the granite samples containing natural joints and those containing extension fractures have the same grain size, the medium scale (in centimeters) profiles are fairly similar, since this medium scale

profile is mainly dependent upon the size of some large individual grains (particularly feldspar). However the roughness obtained on the small scale (millimeters) is greater for the fresh extension fractures.

5.1.2 Observations on joint matching

The profiles of joint surfaces presented in Figures 4.6 and 4.7 also show the degree of joint matching. Comparison of the profiles directly measured from the test samples with the typical joint matching profiles with the Joint Matching Coefficient ranges proposed in section 2.2.4, show that all the joints are fairly well matched or better. However, the fresh extension fractures are better matched as would be expected.

The waviness matching at degree of natural joints fair or good, the JMC of the joints ranging from 5 to 8. The extension fractures have good or very good waviness matching, but due to their high roughnesses, the JMC ranges from 4 to 10 mainly dependent upon the joint roughness.

Natural joints have undergone previous hydro-thermal alteration and perhaps some degree of mechanical deformation, but essentially, the joints are not sheared or heavily deformed. So both types of joints are fairly well matched. For the cases of the granite joints tested, the following approximations can be found by plotting JMC against JRC as shown in Figure 5.1:

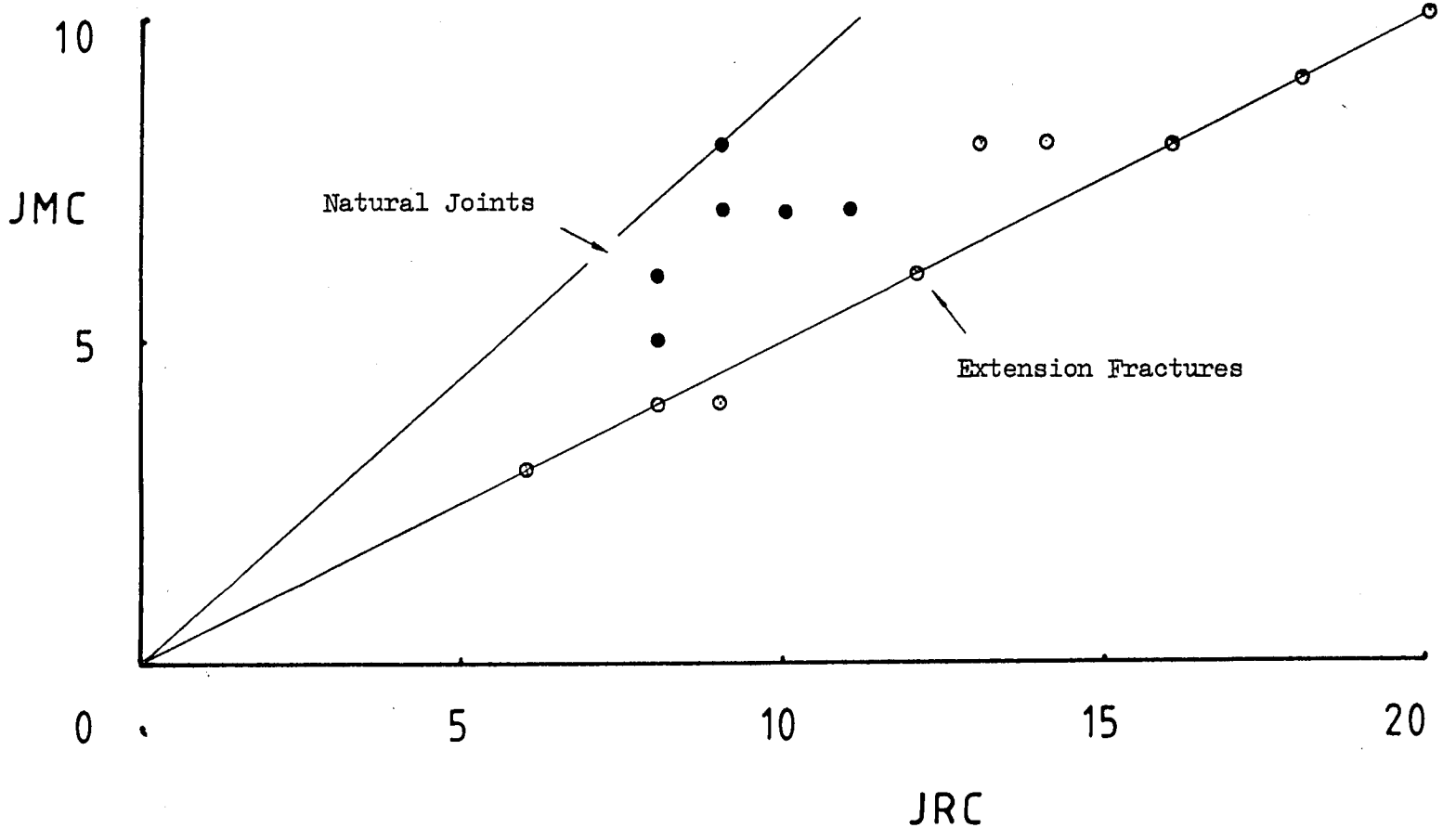


Figure 5.1 Plots of Joint Matching Coefficient (JMC) with Joint Roughness Coefficient (JRC) for Natural Joints and Extension Fractures.

Natural joints	JMC = 0.6 JRC to 0.8 JRC
Extension fractures	JMC = 0.5 JRC
and overall	JMC = 0.6 JRC

The expression for extension fractures is quite precise; that for natural joints depends on the extent of previous mechanical deformation and/or hydro-thermal alteration.

5.1.3 Discussion on joint surface geometrical properties

Joints are formed through fracture in tension, in shear, or through a combination of both. There are several possible modes of formation and modification of fractures and joints as summarized below [Denness 1969]:

(a) formed at the time of deposition or soon after by synizesis and/or change in salt chemistry of the depositional environment;

(b) formed or modified some time later than (a) by in situ physico-chemical changes through agencies such as groundwater, weathering, ion exchange;

(c) formed or modified by tectonic or earthquake stresses during folding, or shearing of the beds;

(d) formed or modified by non-diastrophic processes such as hill creep, rebound on unloading, stress release during erosion;

(e) inherited from underlying rocks.

In igneous rocks contraction-joints are formed as a hot mass cools and contracts. In an intrusive body such as a granite pluton, joint systems develop during the cooling of the mass after its emplacement. Cooling takes effect first near its roof and walls; movement of still liquid or plastic magma at a lower level may then give rise to fracturing in the outer, more solidified, part of the intrusion [Blyth and De Freitas 1984]. The joints in Carnmenellis granite are formed by such cooling effects, or later by tectonic stresses and modified by mode (b).

The fractures are formed at various stages and times. To this extent, the fractures suffer different degrees of weathering, alteration and deformation. These changes control joint surface properties such as wall strength, roughness and matching.

Discontinuity weathering is rather more insidious in that softer weathered zones may develop within the intact material on either side of a joint surface. On the appearance of groundwater, the flow washes away weathered softer layers and small particles. Weathering reduces the joint wall strength and roughness but increases some individual gaps. Alteration (including hydraulic and thermal alteration) affects the joint in a very similar way to weathering. Mechanical deformation with normal displacement only crushes some of the asperities. Shear deformation is more important since any shearing motion would either be over the protrusions or

through them.

As a result of their different histories of fracturing and alteration, joints which are weathered and unweathered, altered and unaltered, deformed and undeformed, will present different joint surface profiles on each side, and different degrees of matching. In practice, it is very common for joints to have the same degree of roughness but different matching. Correspondingly, joints having the same degree of matching may also present different degrees of roughness. Hence to represent the full discontinuity surface geometrical characteristics, both roughness and matching should be considered. The importance of roughness has been recognized for some time [e.g., Jaeger 1959, Patton, 1966, Louis 1969, Louis and Maini 1970, Sharp 1970, Maini 1971b, Barton 1971, Barton and Choubey 1977, Witherspoon et al 1980, Hoek and Bray 1981, Barton 1986]. However, it seems that the degree of matching may be no less important than the degree of roughness.

The Joint Matching Coefficient (JMC) proposed in section 2.2.4 is coupled with the existing Joint Roughness Coefficient (JRC) to fully describe the joint surface geometrical properties. It is a parameter that is practically easy to obtain, particularly if one also wants to assess the JRC. The method of obtaining JMC was described in section 4.4 by inspection. However, a indirect method may be developed by measuring the peak shear strength, residual shear strength, dilation in

shear tests, coupled with the measurements of joint roughness.

5.2 Initial Apertures of the Joints

5.2.1 Calculation of joint initial aperture

There are several possible approaches of obtaining the estimation of joint initial apertures. A direct approach used by Bandis [1980] consisted of measuring aperture with a taped feeler gauge, using plane sawn surfaces to gain access to the joint. The joints were interlocked, but under the very low normal stress generated by the self weight of the sample. Barton and Bakhtar [1983] developed an empirical equation for estimating the initial aperture E_o based on the values of JRC and JCS recorded by Bandis [1980]:

$$E_o = \frac{JRC}{5} \left(0.2 \frac{\sigma_c}{JCS} - 0.1\right) \qquad (5.1)$$

where σ_c = uniaxial compressive strength of the rock
and JCS = joint wall compressive strength.

By implication, when a joint is unaltered and unweathered, JCS = σ_c, and the initial aperture may be a function only of surface roughness.

For a real joint, the joint initial aperture can hardly be measured directly. Analysis of the data of Witherspoon et al [1980] revealed that the real

mechanical apertures were never measured, since the samples were not instrumented prior to fracture formation. Difficulties were also encountered in the present study in the measurement of initial aperture. The sample should be in an undisturbed condition before the hydro-mechanical tests. The direct method described by Barton and Bakhtar [1983] would somehow disturb the joints. Therefore, the method was not adopted for the test carried out in this study. However, the testing facility provides measurements on the joint mechanical deformation. Via back analysis, the joint initial aperture are estimated. The method is based on the following assumptions:

1) the initial aperture is equivalent in value to the maximum joint closure at an assumed "complete closure" state, provided that dilation does not occur;

2) the assumed complete closure state is that at which the hydraulic conductivity of the joint reaches zero, i.e., the hydraulic aperture equals zero;

3) the cubic flow law of the parallel plate theory is valid; this enables the equivalent hydraulic aperture to be calculated;

4) the form of the flow channel, i.e., the profile of the joint surfaces, does not vary at low normal stress, though in fact when the joint is closed, it produces more contact area; and the surface

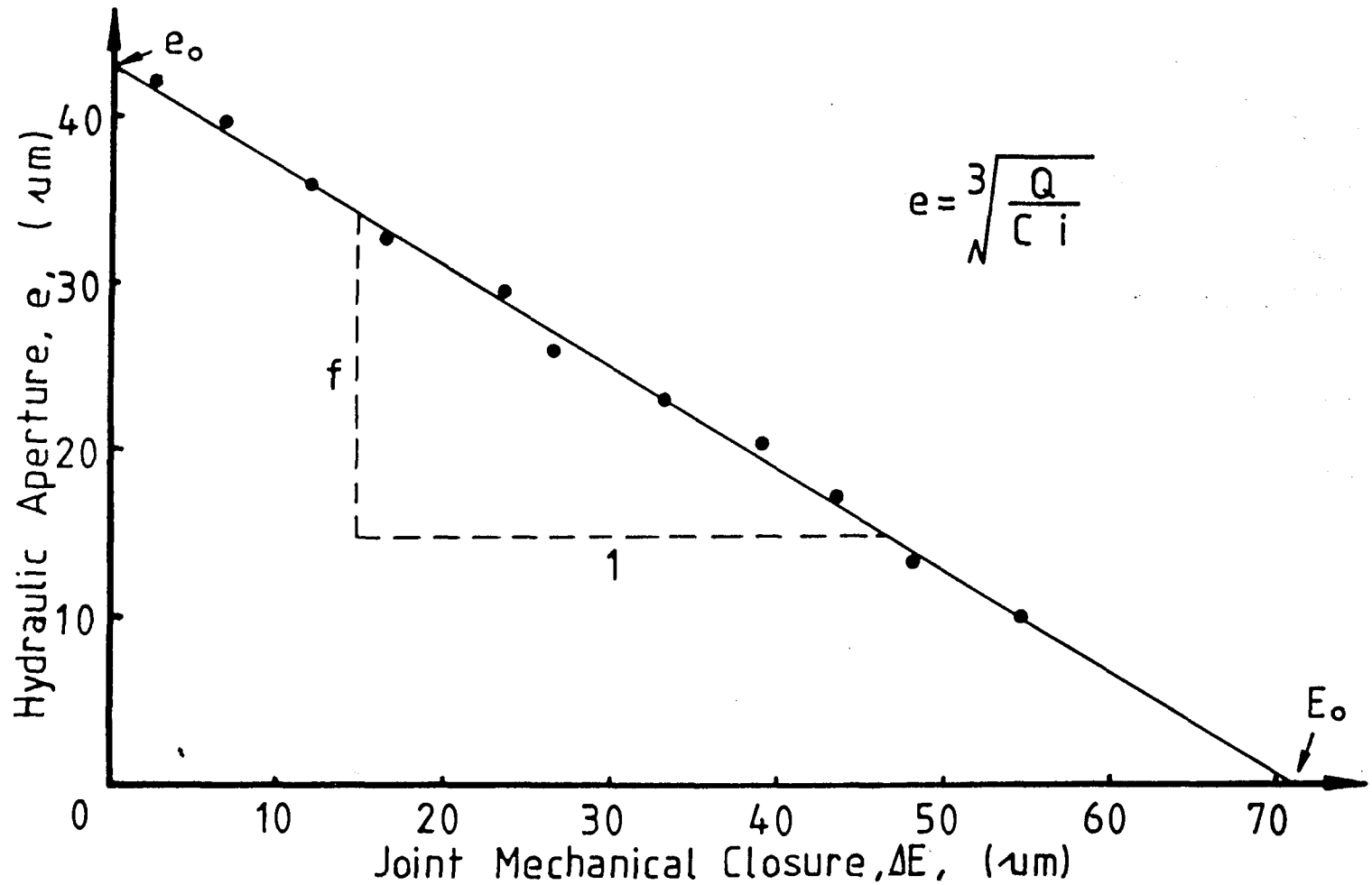


Figure 5.2 Typical Relation Between Hydraulic Aperture and Mechanical Aperture for a Rock Fracture.

properties of the joint remain unchanged at low stress. This provides the possibility of establishing a linear relationship between theoretical hydraulic aperture and the actual joint mechanical closure.

For each effective normal stress, the hydraulic aperture, e, calculated from the flow data by assuming the cubic flow law (see section 5.4), is plotted against the measured joint mechanical closure, ΔE, as shown in Figure 5.2.

The results show that at low normal stress (<10 MPa), the relationship between calculated hydraulic aperture and the measured real joint closure is more or less linear. In the experiments, it was not possible to reach the "complete closure" state, nor to undertake hydraulic conductivity tests at atmospheric pressure. By extrapolating the straight line to intersect the axes, the initial joint aperture and the initial hydraulic aperture of a joint can be calculated, as shown in Figure 5.2. The initial aperture of the joint is the intersection value on the horizontal axis where the hydraulic aperture is zero.

5.2.2 Joint initial aperture and relations with joint surface properties

The values of initial apertures of the joints appear to be very random, as shown in Table 5.1 and Figure 5.3. The values of the initial aperture E_o for the

Table 5.1 Values of Initial Mechanical Aperture E_o, Initial Hydraulic Aperture e_o, JRC and JMC.

Sample No.	E_o (μm)	e_o (μm)	JRC	JMC
Natural Joints				
NJ1	60.2	38.3	6	5
NJ3	25.1	46.1	11	7
NJ4	126.1	226.3	11	7
NJ5	73.2	71.4	9	8
NJ6	33.9	37.5	10	7
NJ12	160.2	148.0	9	7
NJ13	102.4	110.3	9	7
NJ14	168.1	70.9	8	6
NJ15	86.0	85.1	8	6
Extension Fractures				
TF2	60.0	64.0	8	4
TF3	48.9	91.0	12	6
TF5	71.1	43.3	18	9
TF6	52.5	50.5	12	6
TF7	56.1	62.3	9	4
TF9	118.8	93.6	14	8
TF10	142.2	136.0	13	8
TF11	30.7	14.6	20	10
TF12	40.4	25.9	18	9
TF13	81.4	65.8	16	8
TF15	137.1	93.0	18	9

natural joints are generally larger than those of the extension fractures; the means of the initial apertures are 92.8 and 76.3 μm for natural joints and extension fractures, respectively. The values of E_o for the extension fractures show a smaller range of variation.

The initial apertures E_o of the joints can be expected to be dependent not only upon the joint surface properties, but also upon their previous loading, on hydro-thermal alteration and on disturbance. If the data points for exceptionally small and exceptionally large values of E_o are ignored, Figure 5.3 shows that the value of E_o generally increases with an increase in Joint Roughness Coefficient, and is also related to the Joint Matching Coefficient. From the plots, it is evident that for a given JRC, the values of E_o increase with JMC. Hence an approximate relation may exist which can be used to estimate the value of E_o from measurements of JRC and JMC. A relationship is proposed and presented as a chart in Figure 5.4. In order to make this chart more accurate, much more data on measured joint surface properties and initial apertures are required.

The experimental data verified the general trend of Barton and Bakhtar's [1983] empirical relation. For natural joints, the estimated values of JRC are between 8 to 11, and the average value for estimated initial apertures is 92.8 μm. The fresh artificial extension fractures have relative high values of JRC ranging between 12 to 20, and average initial apertures

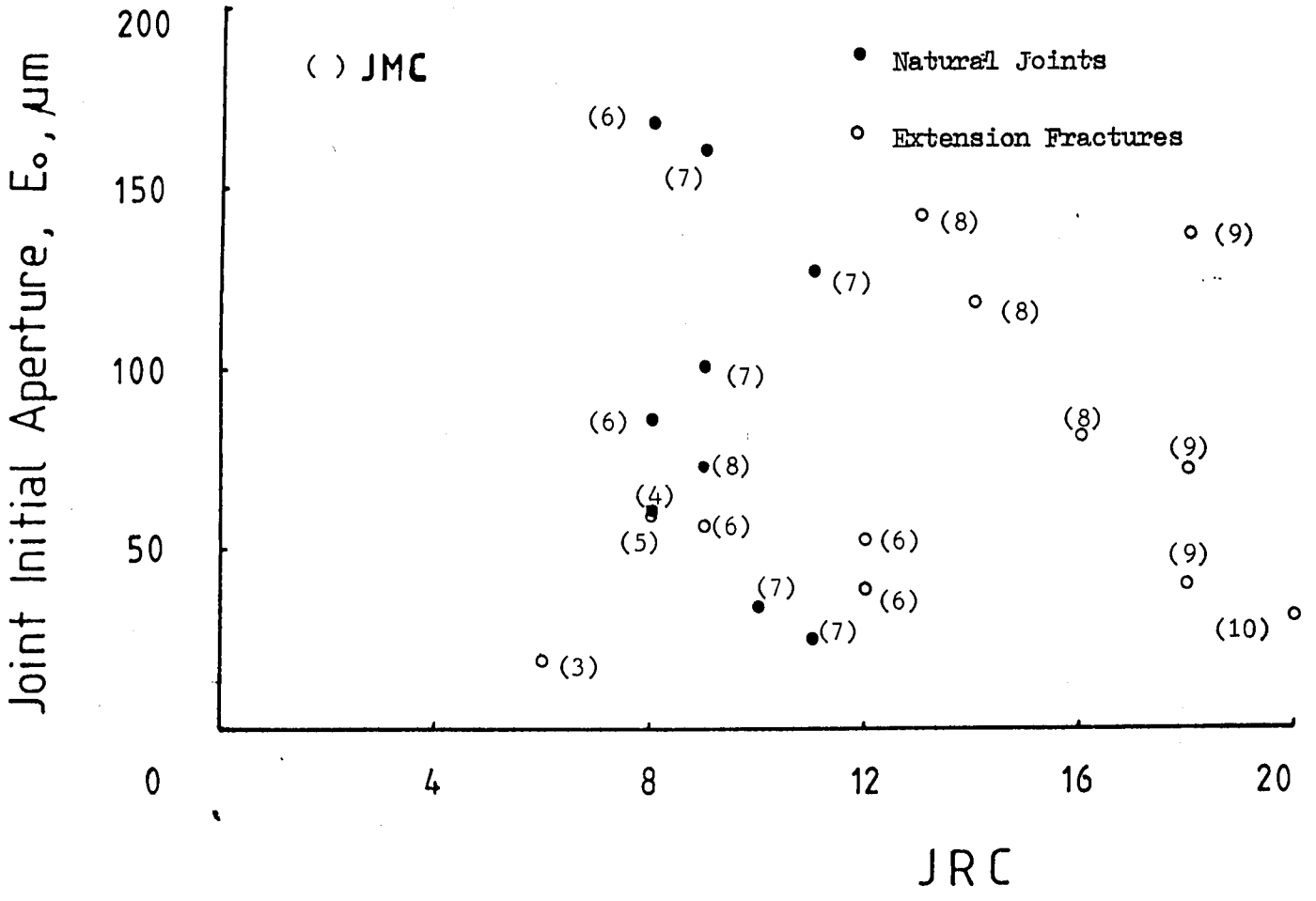


Figure 5.3 Plots of Joint Initial Aperture with JRC and JMC.

of 76.3 μm. This is consistent with the prediction of equation (5.1); the natural joint, which has been subjected weathering and alteration, has a relatively smaller JCS. However, the equation given by Barton and Bakhtar [1983] gives much higher values of the initial mechanical aperture than those estimated from the laboratory tests.

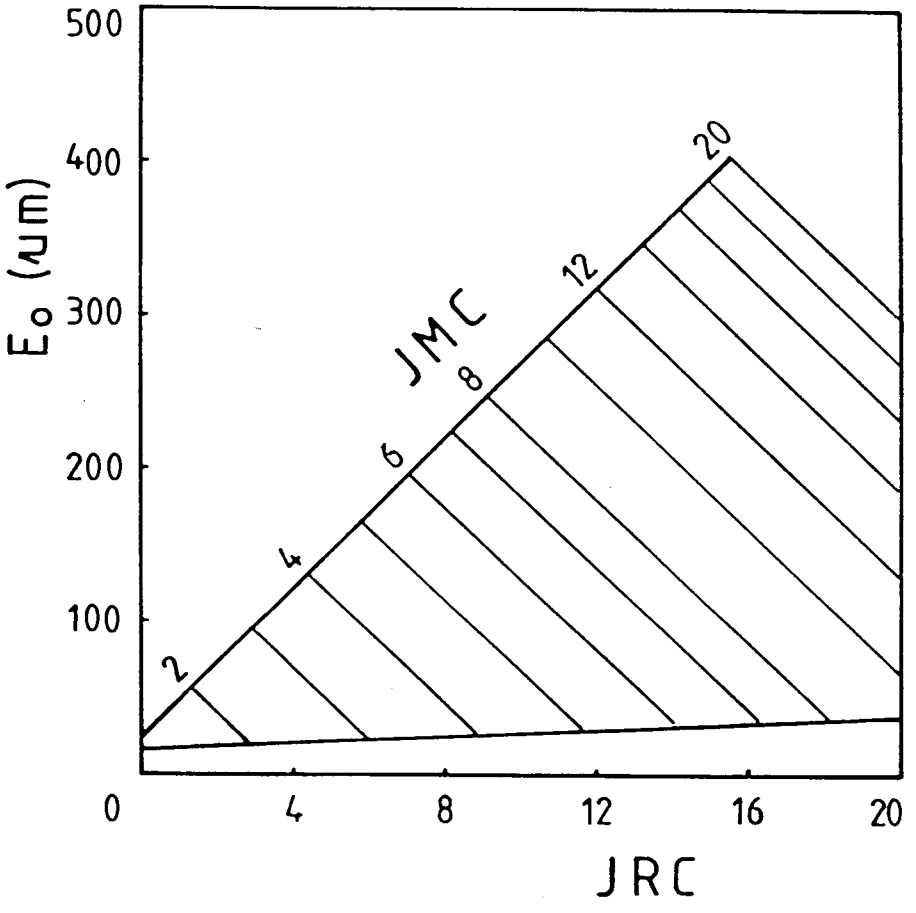


Figure 5.4 Chart for Relating Initial Aperture to JRC and JMC.

5.2.3 In-situ joint apertures

The definition of the initial aperture is the theoretical aperture at zero normal stress. In the

laboratory, it is rather dependent upon the reference seating effective normal stress; and in the field, it is dependent on the in situ stress. As shown earlier, the initial aperture obtained in this experimental study are back calculated. It is obviously, somewhat different from those directly measured. The back calculated value of the joint initial aperture is generally expected to be greater than that measured at a reference effective normal stress since the calculated E_o is at an assumed state of zero effective normal stress

In-situ joint apertures are generally measured in terms of hydraulic conducting aperture during permeabilty tests. Numerous tests performed at US dam sites [Snow 1968] in the depth range of 0 - 60 m indicated that most conducting apertures were in the range of 50 - 150 μm at this shallow depth. Borehole pumping tests performed across individual joints in crystalline rocks reported by Davison et al [1982] indicated a log - normal distribution of apertures over the depth range of 7 - 475 m, with a median value of only 25 μm. Extensive studies by Boodt and Brown [1985] showed that in the depth range of 2.42-23.64 meters, the in-situ joint apertures have a mean value of 15.93 μm indicated by constant head injection tests and of 91.73 μm by pressure drop tests. The results also showed that the apertures vary with the discontinuity orientation (Table 5.2). There is a hint of decrease of permeability with depth, but seems hardly enough to justify any exponential law suggested (e.g., Rice and Simons [1976]). Other

Table 5.2 In-situ Joint Hydraulic Apertures.

(After Boodt and Brown [1985])

Discontinuity Depth (m)	Discontinuity Orientation (Direction/dip)	Angle of Intersection	Hydraulic Aperture (μm)	
			C.H.I.T.	P.D.T.
2.42	185/76	21	20.66	69.21
2.43	194/84	11	20.66	69.21
5.94	114/89	79	19.96	152.99
6.07	111/89	82	19.96	152.99
6.20	226/60	47	19.96	152.99
6.65	149/80	46	19.96	152.99
6.75	152/78	44	19.96	152.99
7.48	175/69	31	0.00	47.05
13.86	177/34	62	26.39	55.35
14.18	149/73	49	26.39	55.35
15.82	207/76	24	6.70	38.23
16.27	170/90	24	6.70	38.23
19.48	240/35	71	16.08	70.41
20.44	261/82	69	13.28	117.85
22.08	257/62	70	9.72	78.40
23.64	198/76	20	8.60	46.31
		20		30.06

factors that influence in situ hydraulic properties must be considered [Maini et al 1972]. These in situ measurements could be generally greater than those estimated in laboratory owing to the larger scale of the formation of shearing of the joints in the field [Maini 1971b, Barton 1986].

5.2.4 The differences in hydraulic aperture, mechanical aperture and maximum closure

Aperture, as defined by the International Society for Rock Mechanics, is the perpendicular distance separating the adjacent rock walls of an open discontinuity, in which the intervening space is air or water filled [Brown 1981]. Aperture is thereby distinguished from the width of a filled discontinuity. Apertures are recorded from the point of view of both their loosening and conducting capacity [Brown 1981]. In general, the loosening of apertures of joints are termed mechanical or real apertures, while the conducting capacity of apertures are termed hydraulic or equivalent hydro-conducting apertures.

The maximum possible closure is one of the physical constraints on normal deformations in a discontinuity. It is a limit to the amount of compression possible of a joint can undergo, i.e., the maximum normal displacement before the rock joint deformation modulus reaches the Young's modulus of the rock material. The differences between mechanical aperture, hydraulic

aperture and maximum closure of a joint are schematically illustrated in Figure 5.5.

The mechanical aperture, which is recorded as the mean of the perpendicular distance between the joint walls, only concerns the average value of joint surface asperity heights, but not the arrangement of the asperity height distribution. Thus the matching joint and the non-matching joint illustrated in Figure 5.5 would give equal values of mechanical aperture. The hydraulic aperture, which reflects the ability of hydraulic conduction, is rather controlled by the arrangement of the asperity height distribution and contact area. As shown in the Figure 5.5, asperities in contact obstruct the flow pathways and produces a much smaller hydraulic aperture, despite the fact that it has an equal value of mechanical aperture. The initial hydraulic aperture is one of the most important factors control the discontinuities hydraulic properties (sections 5.5.2 and 5.6.2). When the discontinuity under increasing normal load, the total contact area enlarged by elastic deformation, crushing and tensile cracking [Goodman 1976]. However, for the deformation modulus of the joint to approach the elastic modulus of the comprising rock material, the entirely area of the discontinuity surface will have to be in contact. Thus, the values of the maximum possible closure are dependent on the distribution of asperities, the mean value of the asperity heights, and probably most importantly, the "thickness" of the discontinuity. The maximum closure has a controlling influence on the

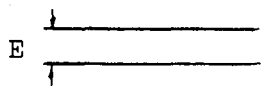
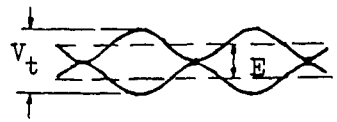
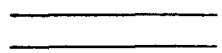
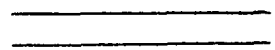
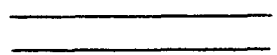
	Parallel Smooth Plates	Matching Joint	Non-matching Joint
Mechanical Aperture E	 Aperture = E	 Aperture = E	 Aperture = E
Equivalent Hydraulic Aperture e	 $e = E$	 $e \doteq E$	$e < E$
Maximum Possible Closure V_{mc}	$V_{mc} = E$	 $V_{mc} \doteq E$	$V_{mc} \geq E$ $< V_t$ (thickness)

Figure 5.5 Differences Between Mechanical Aperture, Hydraulic Aperture and Maximum Closure.

discontinuities mechanical behaviour [Goodman 1976].

5.3 Joint Mechanical Behaviour Under Normal Stress

5.3.1 Effective normal stress - joint closure relations

The deformation of the testing samples was measured by the cantilever device across the sample diameter and perpendicular to the joint surface. The deformation included the deformation of the joint and of the rock material. Hence the joint deformation is the measured total deformation less the deformation of the rock material estimated from the results of rock material loading tests [Elliott 1984].

The plots of joint deformation against effective normal stress are shown in Figure 5.6, where the effective normal stress σ' is taken as the total normal stress less the joint water pressure. The curves show the familiar form which can be fitted by a logarithmic function, or by a hyperbolic function such as Goodman's [1976]. Values for the constants in Goodman's function (Equation 2.17, section 2.3.2) are calculated and given in Table 5.3, for comparison with other published results. However, for engineering purposes, these curves can be approximated by a series of straight lines yielding joint stiffness values comparable with those measured for other granitic rocks. The curves show that at high normal stress, when the joint is highly closed,

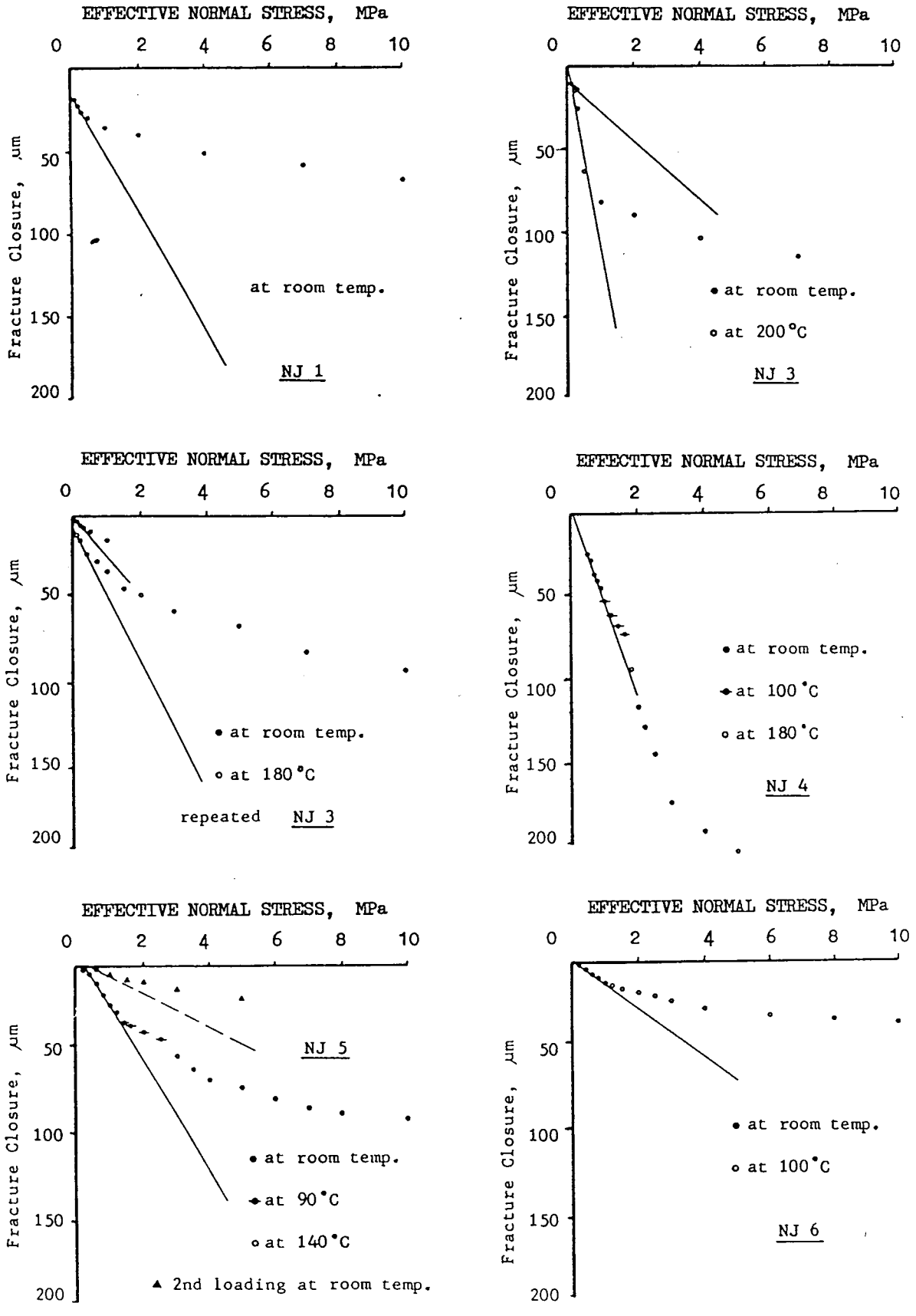


Figure 5.6 Test data of Effective Normal Stress - Joint Mechanical Closure Relation.

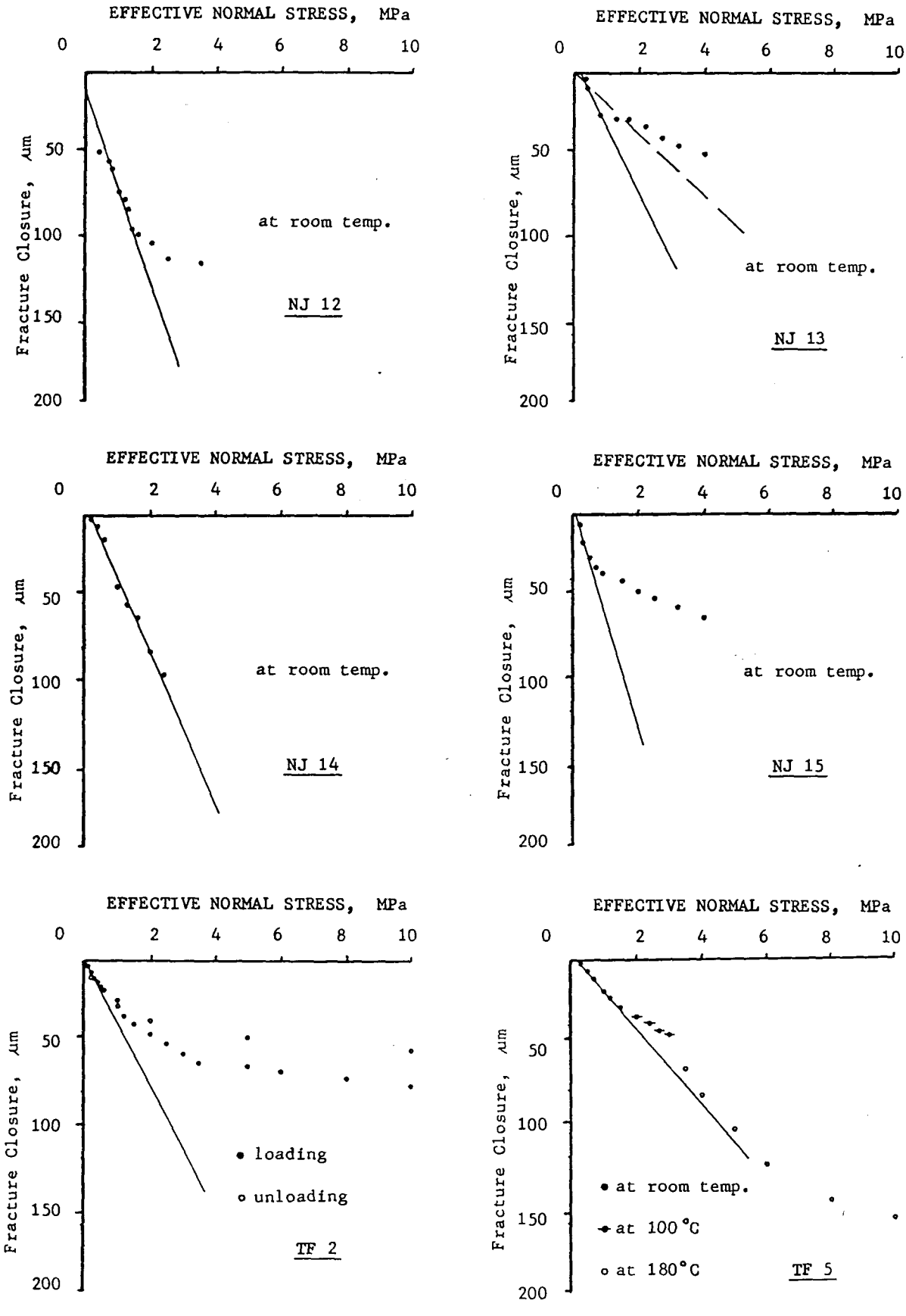


Figure 5.6 (continued).

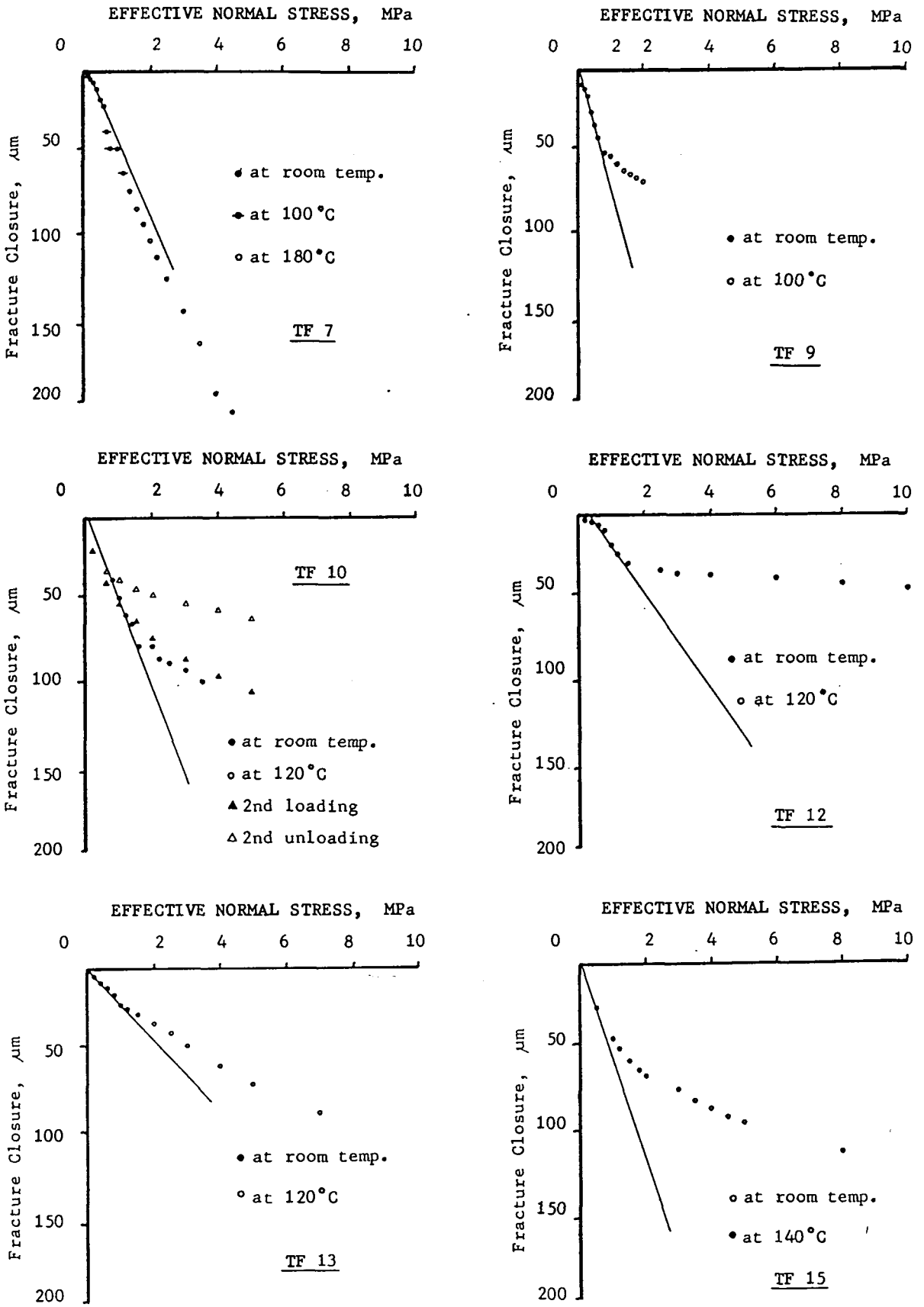


Figure 5.6 (continued).

the joint stiffness approaches the elastic modulus of the rock material. The range of joint apertures and closures measured are consistent with those inferred from the results of in-situ permeability tests conducted at the Carwynnen Quarry [Brown et al 1982] and hydraulic circulation tests carried out as part of the Camborne School of Mines Hot Dry Rock Geothermal Energy Project [Pine and Batchelor 1982].

5.3.2 Joint mechanical closure behaviour and comparison with Goodman's model

The results found and plotted in Figure 5.6 for the joint mechanical closure under effective stress are fitted by Goodman's hyperbolic relation. To fit the model, the mechanical initial apertures are used as a close approximation to the numerical values of the maximum possible closure, V_{mc}.

For joints suffering the same degree of alteration (mechanical, hydraulic and thermal), the mechanical closure behaviour under normal stress should be able to be related to the initial joint aperture (or the maximum possible closure) and the joint surface properties (JRC and JMC etc). In the laboratory studies, the joint surface properties were measured with the intention of investigating this relation. Goodman compared result obtained for induced fractures in granodiorite with mating faces and non-mating faces; he found that for the fracture with non-mating faces, much

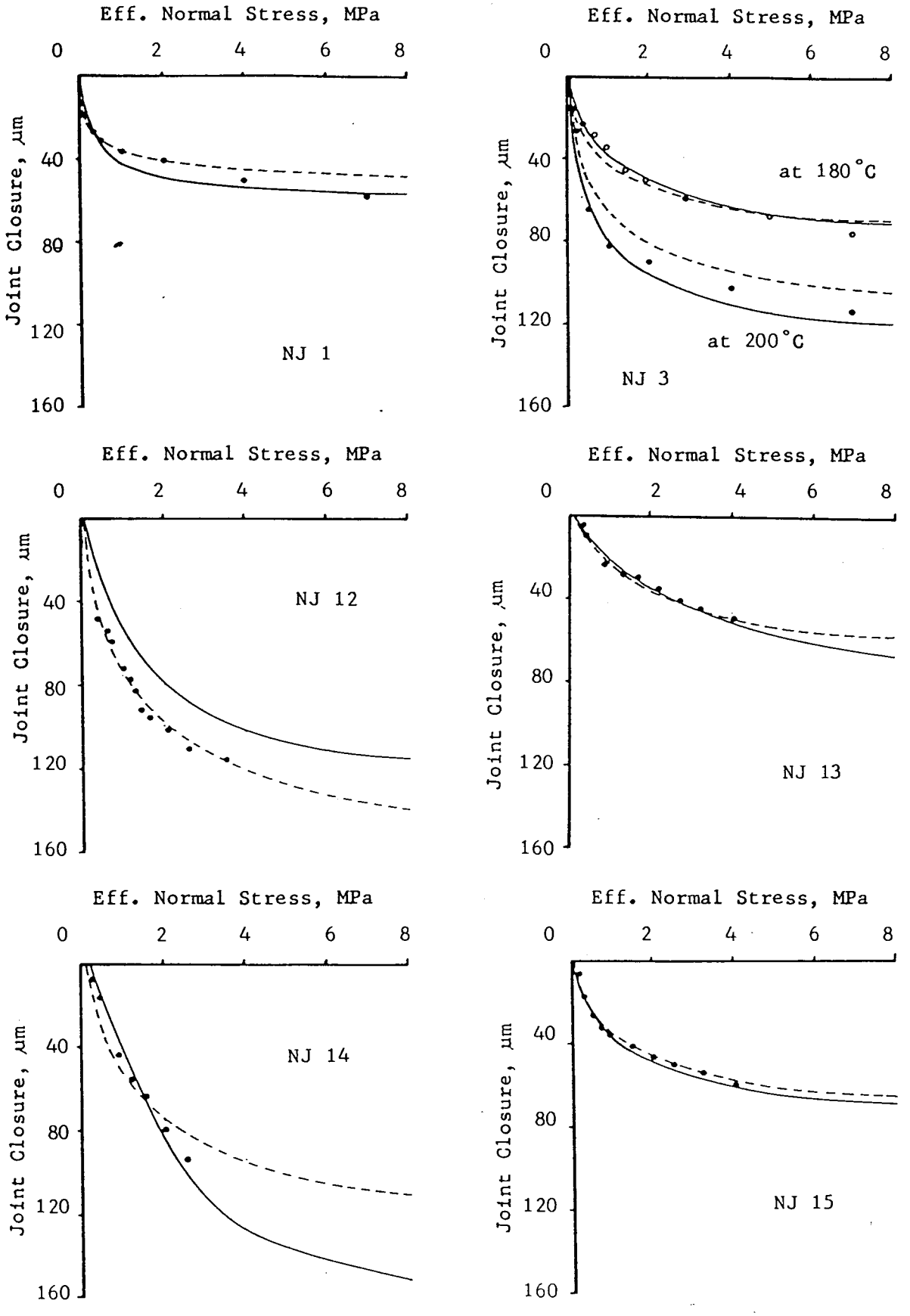


Figure 5.7 Experimental Results Compared with Goodman's Model and the Logarithmic Relation.

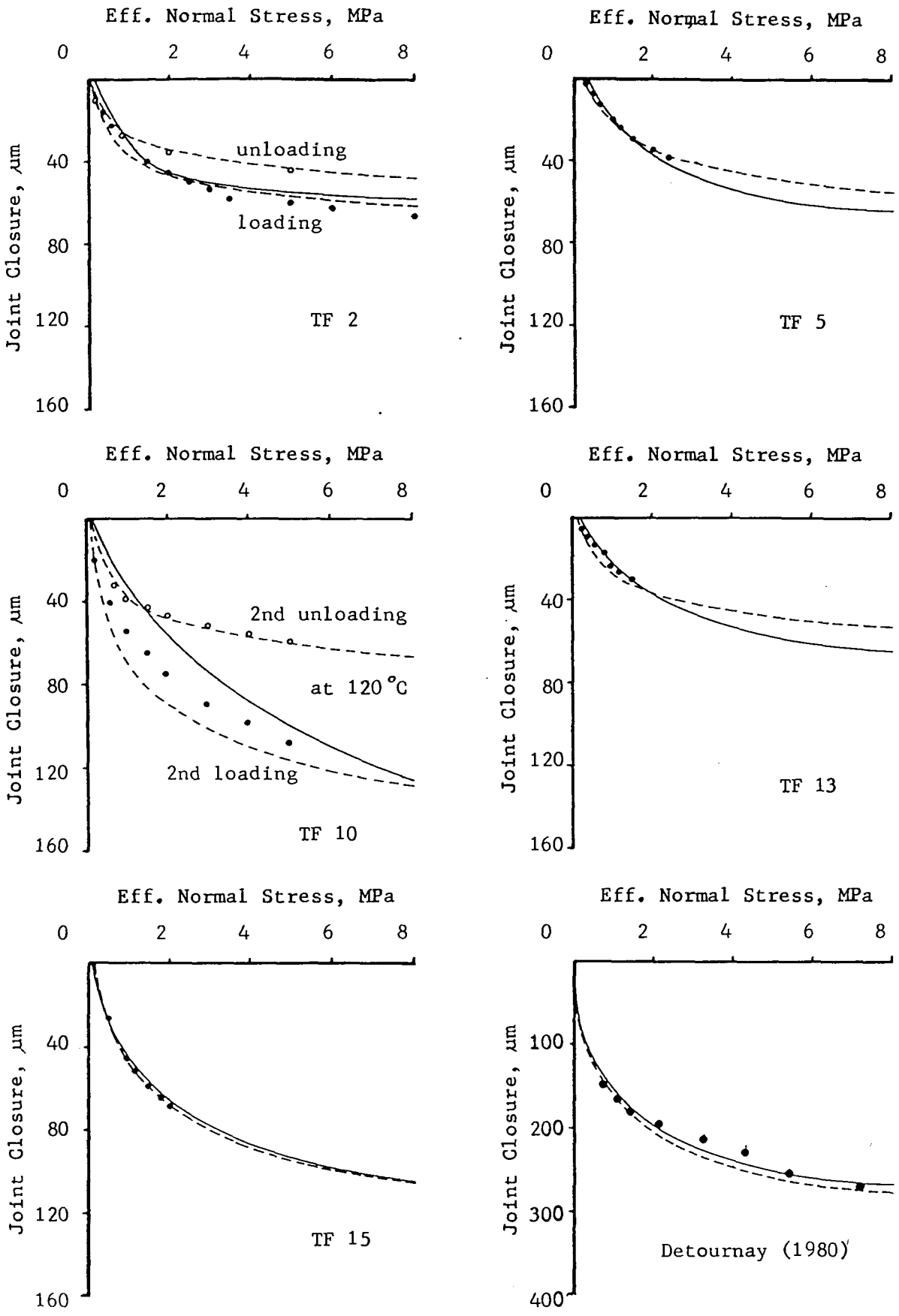


Figure 5.7 (continued). ∘ • Experimental data, ——— Goodman's model, ------- logarithmic relation.

Table 5.3 Joint Stiffness and Parameters in Goodman's Model and Logarithmic Relation

Data Source	Joint Description	Initial Joint Stiffness (MPa/mm)	Stress Level (MPa)	Test Temp. (°C)	Goodman's Model, 1976 $\frac{\sigma' - \zeta}{\zeta} = S\left(\frac{\Delta V}{V_{mc}-\Delta V}\right)^t$ S	t	ζ(MPa)	V_{mc}(μm)	Logarithmic Relation $\frac{E}{E_i} = 1 - B \ln\left(\frac{\sigma'}{\sigma_i'}\right)$ B	E_o(μm)	σ_i'(MPa)	E_i(μm)
NJ1	Natural	28.0			2.90	1.22	0.10	60.2	0.169	60.2	0.10	41.2
NJ3	Joint in	8.9		200	13.46	2.08	0.10	175.2	0.125	175.2	0.10	163.0
NJ3	Granite	25.0		180	28.50	1.34	0.05	90.7	0.126	112.7	0.10	101.2
NJ4		17.2			9.97	0.83	0.12	126.1				
NJ5		29.9			9.02	0.69	0.15	73.2				
NJ6		67.8			12.43	0.74	0.10	34.0				
NJ12		16.7			7.39	0.80	0.15	169.0	0.198	180.0	0.15	180.0
NJ13		24.9			27.94	1.11	0.14	102.0	0.159	102.0	0.30	102.0
NJ14		21.4			17.29	0.65	0.11	168.0	0.181	160.0	0.20	157.7
NJ15		14.8			13.20	1.30	0.10	86.0	0.203	86.0	0.20	79.7
TF2		26.3			8.67	0.74	0.10	60.0	0.173	80.0	0.10	76.2
	Induced								0.183	65.0	0.20	54.9
TF5	Extension	42.4			11.14	0.73	0.15	71.7	0.180	86.7	0.30	84.2
TF7	Fracture	21.1			6.05	0.77	0.12	56.1				
TF7	in			100	15.18	0.78	0.12	186.8				
TF7	Granite			180	50.91	0.91	0.12	480.3				
TF9		13.6			8.17	0.80	0.10	118.8				
TF10		18.2			9.97	0.91	0.15	142.2				
TF10	2nd load			120	73.70	1.12	0.10	245.0	0.121	245.0	0.20	225.2
				120					0.118	133.1	0.60	101.5
TF11					5.47	0.70	0.10	30.8				
TF12		33.9			3.32	0.48	0.25	42.4				
TF13		46.1			22.20	0.89	0.10	81.4	0.161	81.4	0.20	76.2
TF15		16.4			16.44	1.16	0.12	137.1	0.209	157.1	0.50	131.0
	Induced Fracture in Granodiorite											
Goodman	Mating-	68.5	1.72		3.00	0.61	0.46	119.0				
[1976]	Surfaces	153.5	3.45		3.00	0.61	0.46	119.0				
	Non-mating	19.7	1.72		6.00	0.61	0.46	386.0				
	Surfaces	30.0	3.45		6.00	0.61	0.46	386.0				
Detour-	Induced											
nay	Fracture	17.1	0.72		35.87	2.29	(0.1)	457.0	0.160	457.0	0.72	308.0
[1980]	in Granite				17.29	2.31	(0.2)	457.0				
Wither-	Extension											
spoon	Fracture	72.5	1.00									
et al	in Granite	406.3	3.50									
[1980]												
Elliott	Natural	18.5			1.18	0.80	0.30	120.0				
et al	Joint in	34.7			12.50	0.60	0.13	80.0				
[1985]	Granite	20.0			22.40	0.71	0.12	230.0				
		15.1			12.80	1.28	0.12	90.0				

higher values of V_{mc} and S were obtained.

A very good fit to the experimental data was found for the full range of joints as shown in Figure 5.7, despite the large variation in the parameters for each case (Table 5.3).

5.3.3 Joint mechanical behaviour - a logarithmic relation

Walsh [1981] proposed a flow model in studying the effect of pore pressure and confining pressure on the fracture permeability

$$\sqrt[3]{\frac{Q}{Q}} = 1 - B \ln\left(\frac{\sigma'}{\sigma_1'}\right) \qquad (5.2)$$

where Q = flow rate at effective normal stress σ',

Q_1 = the flow rate at a reference effective normal stress σ_1',

B = a fracture parameter, depending on the joint surface geometry.

Since the flow rate $Q \propto e^3$, the equation can be rewritten as:

$$\frac{e}{e_1} = 1 - B \ln\left(\frac{\sigma'}{\sigma_1'}\right) \qquad (5.3)$$

where e and e_1 = the joint hydraulic conducting apertures at effective normal stresses σ' and σ_1'.

However, the above equation was originally derived from fluid flow analysis. Hence the aperture e in the equation is the theoretical hydraulic aperture. The

experimental data show that within the compressive range where a reasonable flow rate through the joint can be obtained, the initial mechanical aperture E_o and the change of mechanical aperture ΔE is approximately linearly proportional to the theoretical initial hydraulic aperture e_o and the change of hydraulic aperture Δe, respectively, and with the same proportionality; i.e.

$$E_o/\Delta E = e_o/\Delta e$$

so, $$E/E_1 = e/e_1$$

Hence,

$$\frac{E}{E_1} = 1 - B \ln\left(\frac{\sigma'}{\sigma_1'}\right) \qquad (5.4)$$

or

$$\frac{V_{mc} - \Delta V}{V_{mc} - \Delta V_1} = 1 - B \ln\left(\frac{\sigma'}{\sigma_1'}\right) \qquad (5.5)$$

where E = the fracture mechanical aperture,

E_1 = the fracture mechanical aperture at reference effective normal stress σ_1',

V_{mc} = the maximum fracture mechanical closure,

ΔV = fracture mechanical closure,

ΔV_1 = fracture mechanical closure at reference effective normal stress σ_1'.

With Goodman's approach, the parameters varied significantly. This may be a major obstacle in applying this model to general engineering practice, for which, more unique values of the parameters are obviously

needed.

The logarithmic approach seems to avoid this problem. A more closely unique value for the parameter B is found for the natural joints and artificially induced extension fractures. Calculated values of B are presented in Table 5.3 with joint stiffnesses and the parameters in Goodman's relation. The value of B varies from 0.16 to 0.21 and is little effected by loading history. The approach gives a good fit to the experimental data, as shown in Figure 5.7.

Both Goodman's model and the logarithmic approach rely on at least one effective normal stress - joint mechanical closure test and the value of initial aperture (or the maximum possible closure). The logarithmic approach has, in practice, a significant advantage in finding the effective normal stress - joint mechanical closure behaviour of rough joints by having a parameter of more closely unique value.

5.4 Flow Rate and Hydraulic Aperture

5.4.1 Flow rate - hydraulic gradient relations

For each applied normal stress, the flow rate (flow volume per unit time) were calculated and plotted against the hydraulic head gradient, as shown in the example in Figure 5.8. The plotting was carried out while conducting the tests. This process enabled the operator to observe the change from laminar to transitional flow

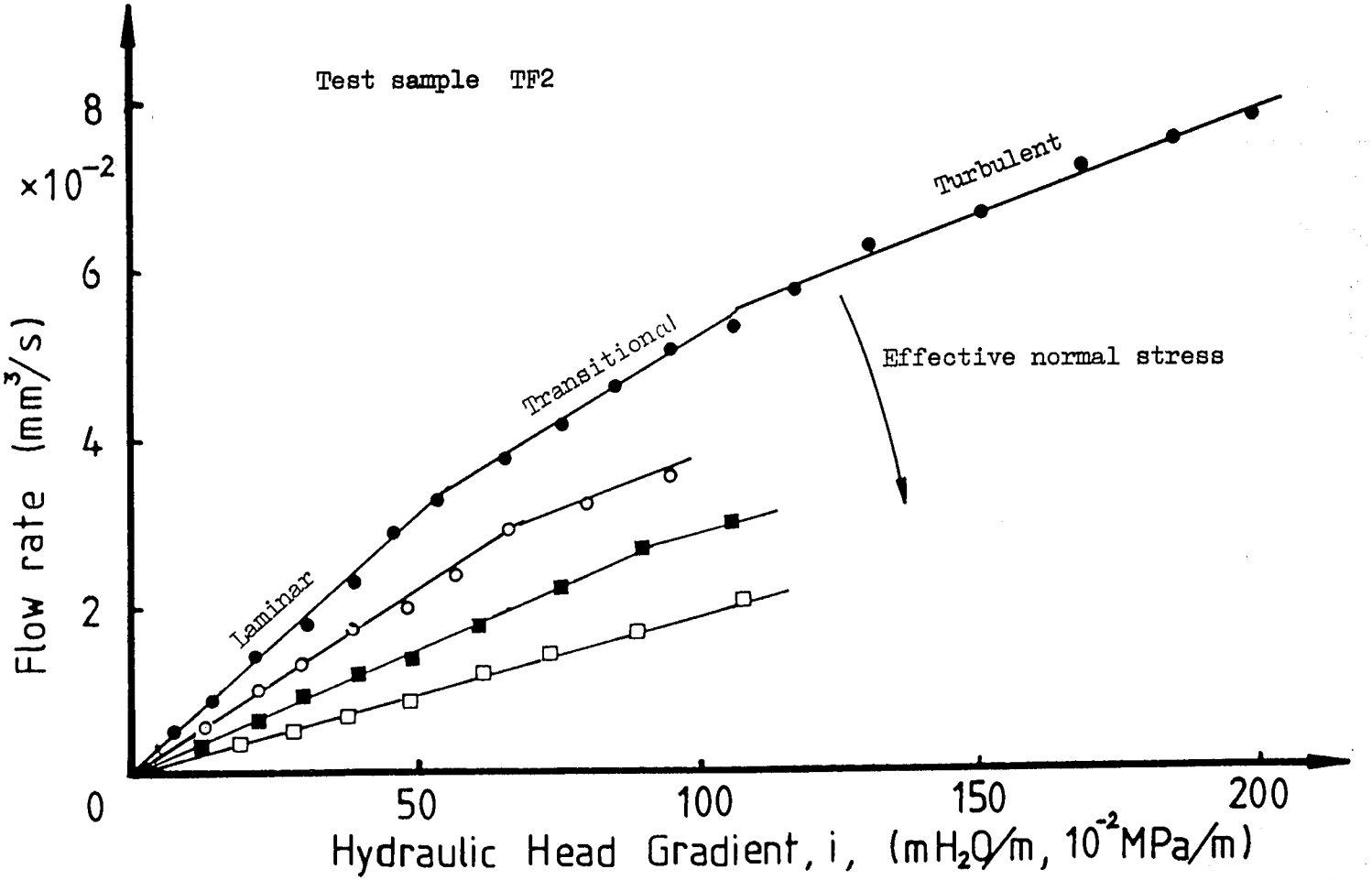


Figure 5.8 Typical Plots of Flow Rate Against Differential Pressure.

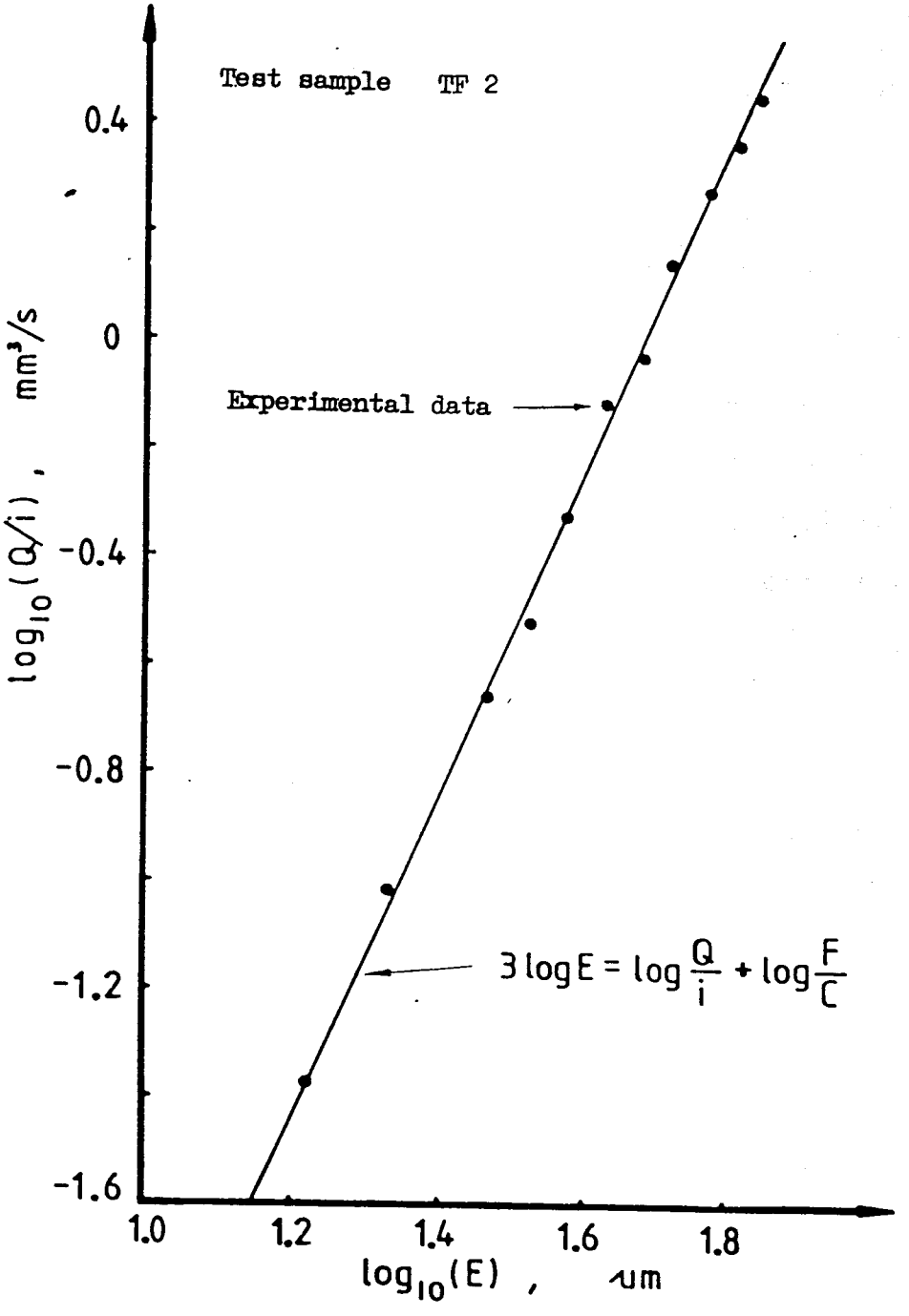


Figure 5.9 Verification of the Cubic Flow Law.

and so to ensure that enough tests were conducted within the laminar flow range. The data describe a curve which for laminar flow would be a straight line through the origin. This example and all other plots showed a distinct curve, concave towards the hydraulic gradient axis at some value of differential pressure. This is generally taken to be a characteristic of the onset of non-laminar flow [Massey 1975, Detournay 1980, Elliott et al 1985]. In those tests in which higher differential pressures were used, laminar, transitional and turbulent phases seemed easily discernible. However, indications of a turbulent phase in these curves were sometimes masked by the influence of high permeating fluid pressures on the joint effective normal stress. This can be seen in Detournay's experimental results [1980]. At low differential pressures, the joint fluid pressure was sufficiently small compared with the applied normal stress; the effect of the joint fluid pressure can be considered negligible. On the other hand, at high differential pressures, the joint fluid pressure in the joint is sufficiently large compared to the applied normal stress. This effect would result in the curve being concave towards the flow rate axis and the delayed appearance of turbulent flow (see Detournay 1980). The curvatures of the flow rate - hydraulic head gradient curves obtained in present study show the onset of non-laminar flow at a hydraulic head gradient of 50 - 100 mm water /mm (0.5 - 1.0 MPa/m length). Since the cubic flow law applies for laminar flow only, the gradient of the

initial part of this curve through the origin is used in the analysis to represent laminar flow properties of the joints and fractures.

5.4.2 Calculation of hydraulic aperture

The validation of the cubic flow law has been carefully examined [Witherspoon et al 1980, Elliott et al 1985]. Elliott et al [1985] showed that the equation provides good predictions of the measured data. As illustrated in Figure 5.9, the flow data were plotted against the joint aperture on log-log axes. The aperture for a given effective normal stress was determined by substracting the measured joint closure from the initial joint aperture determined using the analysis outlined in section 5.2.1. Noting that in Equation (2.16) $Q/i = C/F$ when $E=1$, the modified theoretical cubic flow law was constructed by drawing a straight line with a gradient of 3 through the point (logl, log(C/F)). By comparing the experimental results plotted and the theoretical straight line, Figure 5.8 clearly shows that the cubic flow law is valid in the effective normal stress range used in the tests.

By taking the cubic flow law to be valid, theoretical hydraulic apertures were then calculated directly from measured flow rates using the equation

$$\frac{Q}{i} = C\, e^3 \qquad (2.14)$$

or

$$e = \left(\frac{Q}{C\ i} \right)^{1/3} \qquad (5.6)$$

where Q/i can be obtained directly from Q-i plots and C is a constant parameter for each joint.

5.5 Joint Hydraulic Behaviour Under Normal Stress

5.5.1 Flow rate - effective normal stress relations

The gradients of the curves in Figure 5.8 were calculated for the laminar flow range. These values of Q/i were plotted against effective normal stress as shown in Figure 5.10. The results show the familiar asymptotic reduction in flow with increasing effective normal stress. Similar curves have been obtained by previous researchers [Gale 1975, Iwai 1976, Witherspoon et al 1980, Detournay 1980, Gale 1982, Elliott et al 1985]. Increasing sample temperatures reduced the flow rate in most cases, but did not alter the shapes of the curves. Both the flow rates and the joint closure - effective normal stress relation, both show asymptotic reduction with increase of effective normal stress, but with different asymptotes. As the effective normal stress increases, the joint tends to approach a state of "complete closure", hence the flow rate approaches zero while the the joint deformation approaches the maximum possible closure. Detailed discussion is presented in the next section where a number of models are examined.

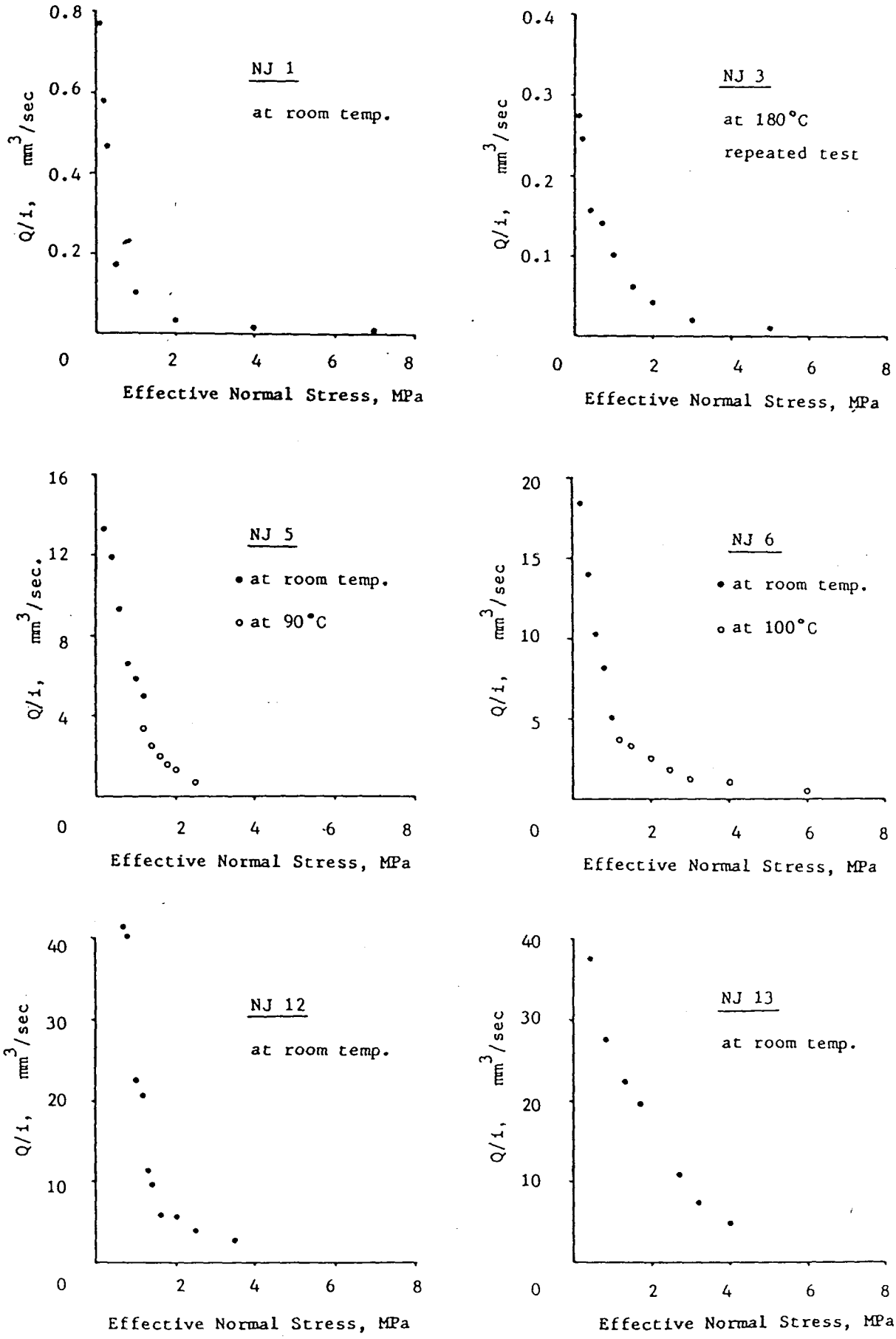
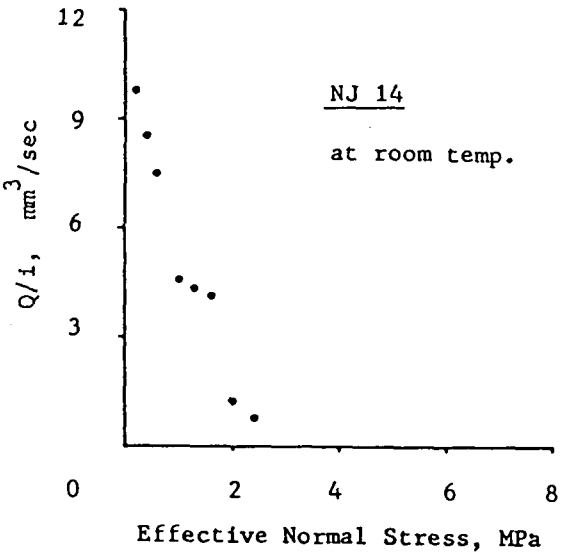
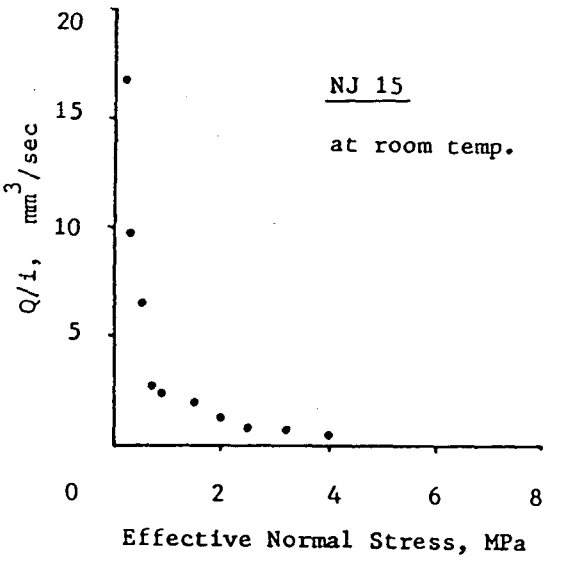
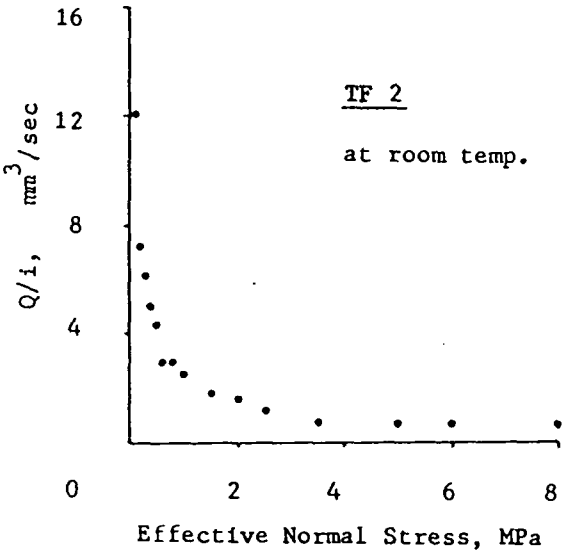
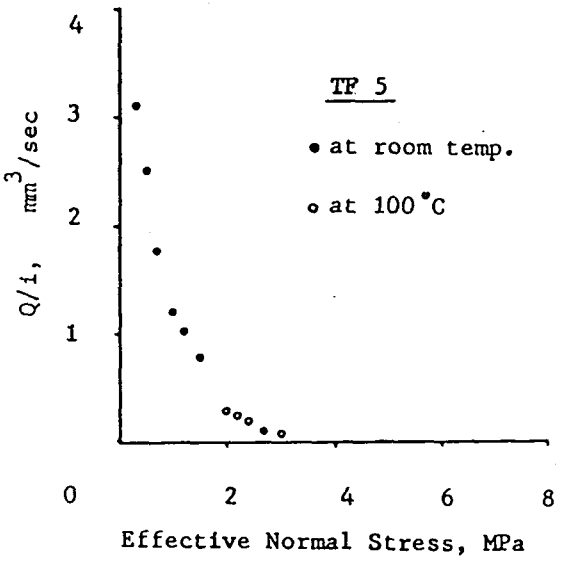


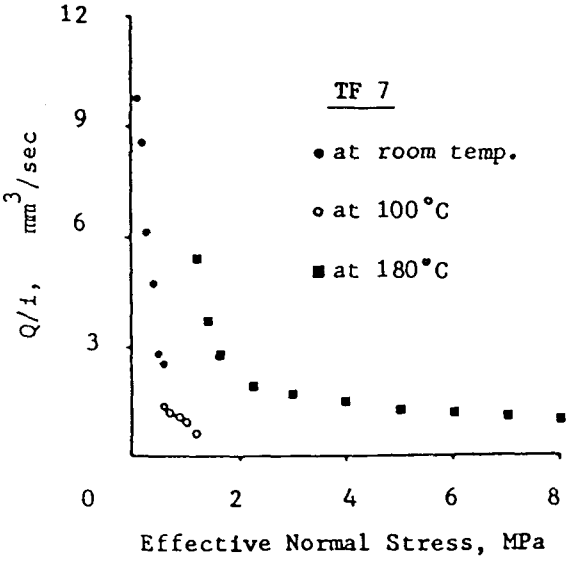
Figure 5.10 Effective Normal Stress - Flow Rate Relation.











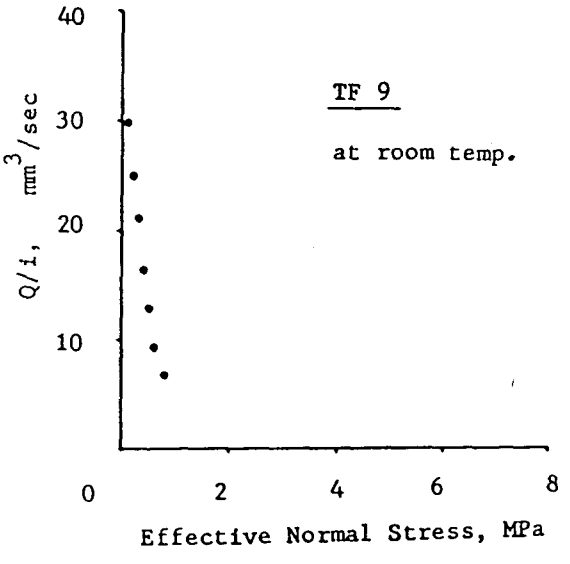
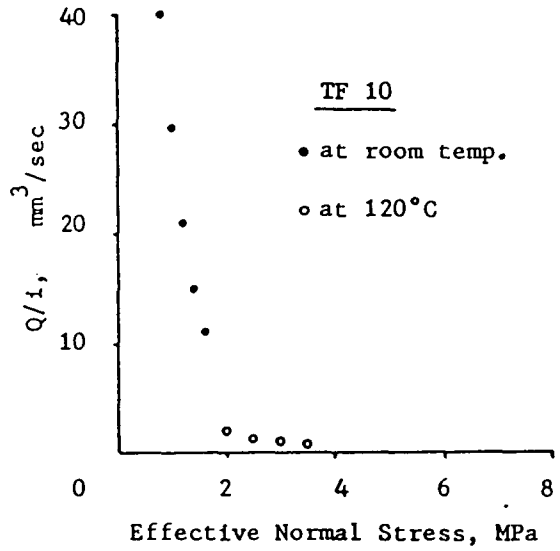
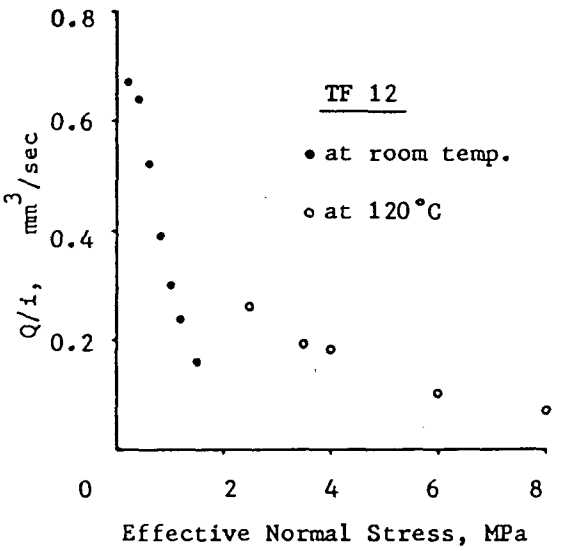
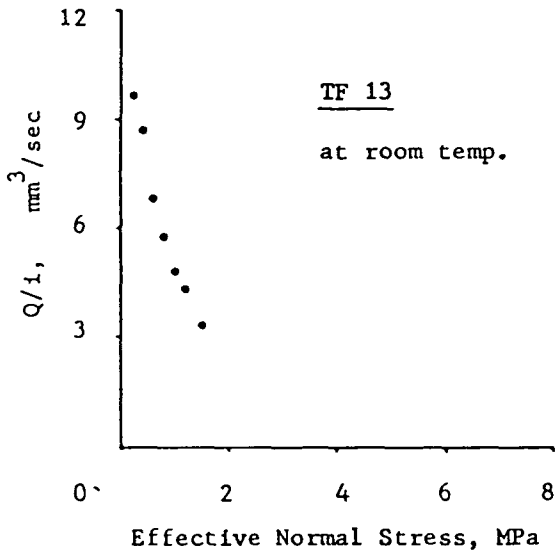


Figure 5.10 (continued).







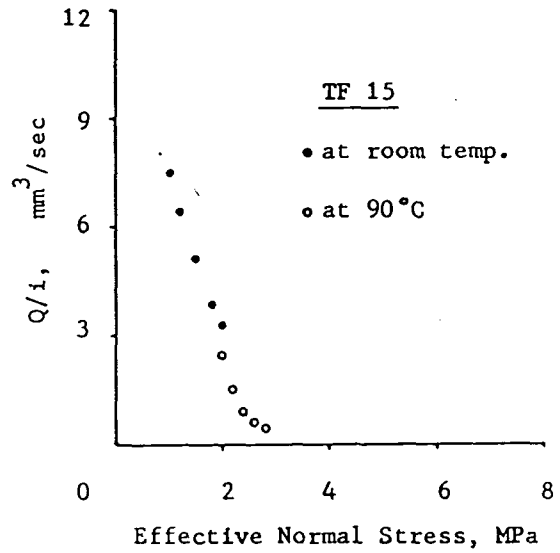


Figure 5.10 (continued).

5.5.2 Joint hydraulic properties and comparison with other models

In Figure 5.11 and Table 5.4, the experimental data are compared with the predictions of the model of Gangi [1975, 1978, 1981], Walsh [1981], Gale [1982] and Swan [1983]. These models relate the hydraulic conductivity of the joint to the effective normal stress, and when coupled with Darcy's law, yield predictions of the flow rate for a given hydraulic gradient in a discontinuity subjected to a certain effective normal stress. Each of these models relies on at least one flow test being carried out on the joint in order to determine the material constants, and to determine the initial equivalent hydraulic aperture. The models are:

$$\text{Gangi} \qquad K = K_o \left[1 - \left(\frac{\sigma'}{D} \right)^{1/n} \right]^3 \qquad (5.7)$$

$$\text{Walsh} \qquad K = K_1 \left[1 - 2 \sqrt{\frac{h}{e_o}} \ln\left(\frac{\sigma'}{\sigma_1'} \right) \right]^2 \qquad (5.8)$$

$$\text{Gale} \qquad K = s\, \sigma'^{a} \qquad (5.9)$$

$$\text{Swan} \qquad K = K_o(c - m \ln \sigma') \qquad (5.10)$$

where K_o = joint permeability at zero effective normal stress,

K_1 = joint permeability at a reference effective normal stress σ_1', with hydraulic aperture e_1,

K = joint permeability at effective normal stress σ',

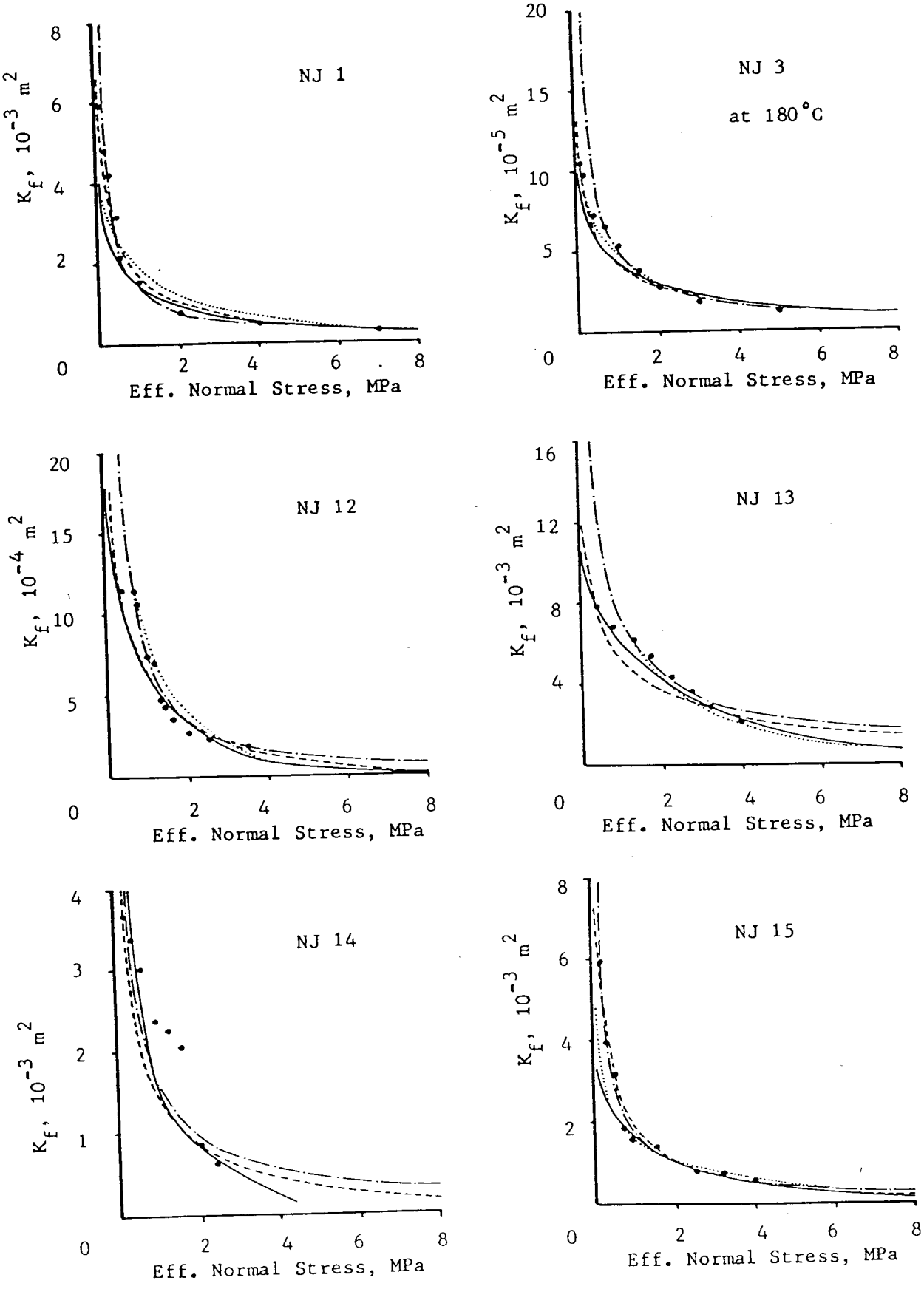
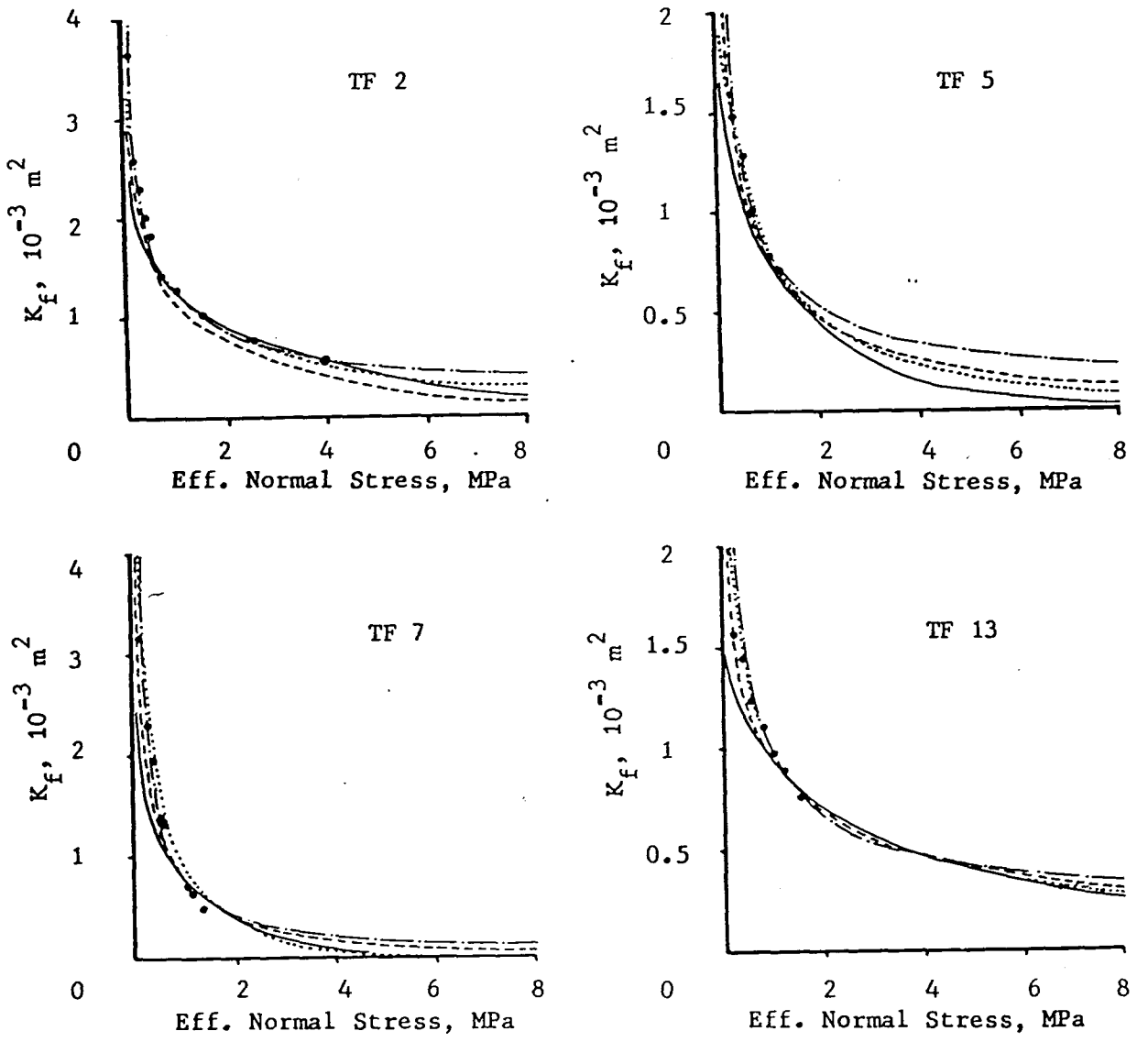


Figure 5.11 Permeability - Stress Data Compared with Various Hydraulic Models.



- Experimental Data

——— Gangi (1978), $K_f = K_o[1 - (\frac{\sigma}{D})^{1/n}]^3$

- - - - - - - Walsh (1981), $K_f = K_i [(1 - 2\sqrt{\frac{h}{e_o}} \ln\frac{\sigma}{\sigma_i})^2]$

——·—— Gale (1982), $K_f = s\ \sigma^{a}$

····· Swan (1983), $K_f = K_o(c - m \ln \sigma)^2$

Figure 5.11 (continued).

Table 5.4 Flow Properties Comparison with Hydraulic Models.

Sample No.	Test Temp. °C	Models											
		Gangi (1978)		Walsh (1981)		Gale (1982)		Swan (1983)		Tsang & Witherspoon (1981)			
		D	n	B	h/e × 10^{-3}	a	s	c	m	β	ω	σ_1' (MPa)	
Natural Joints													
NJ1	Room	52.46	6.00	0.190	9.07	-0.81	1.29	0.39	0.11	1.02	0.70	5.0	
NJ3	180	38.48	3.08	0.150	5.63	-0.78	0.50	0.58	0.15	0.50	0.80	5.0	
NJ12	Room	8.62	1.89	0.287	20.64	-1.11	72.44	0.64	0.31	2.62	0.45	4.0	
NJ13	Room	14.29	1.43	0.176	7.71	-0.67	69.18	0.83	0.28	1.96	0.15	4.0	
NJ14	Room	4.52	0.88	0.213	11.36	-0.72	15.49	--	--	1.63	0.55	3.0	
NJ15	Room	27.94	3.33	0.225	12.66	-0.78	16.22	0.50	0.13	2.20	0.35	4.0	
Extension Fractures													
TF2	Room	39.61	2.92	0.150	5.63	-0.52	12.02	0.61	0.16	1.75	0.45	5.0	
TF5	Room	8.58	1.36	0.213	11.36	-0.62	7.94	0.71	0.24	1.09	0.70	5.0	
TF7	Room	8.17	2.20	0.167	6.98	-0.86	7.24	0.51	0.27	--	--	--	
TF10	Room	--	--	--	--	--	--	--	--	1.43	0.35	4.0	
TF13	Room	54.08	2.50	0.138	4.77	-0.51	19.05	0.74	0.17	1.98	0.35	3.0	
Detournay (1980)	Room	--	--	0.185	8.57	--	--	--	--	--	--	--	
	Room	--	--	(0.229)	(13.14)	--	--	--	--	--	--	--	
Elloitt et al (1985)	Room	--	--	0.210	11.0	-0.85	5.00	--	--	2.17	0.50	3.0	
	Room	--	--	0.228	13.0	-0.92	6.00	--	--	2.50	0.10	5.0	
	Room	--	--	0.167	7.0	-1.40	2.80	--	--	2.20	0.50	5.0	

D = material constant, being the effective modulus of the asperities,

h = r.m.s value of the height distribution of asperities, a constant,

s = constant, being the value of K at a effective normal stress of 1.0 MPa,

n, a, c, m = constants.

All these four models fit the experimental data reasonably well, as shown in Figure 5.11, although Walsh's model apparently gives the best fit. The calculated values of the parameters in Walsh's relation show that $2\sqrt{h/e_o}$ takes a value between 0.14 - 0.23 (Table 5.4). Thus the model can be further simplified for practical engineering purposes to,

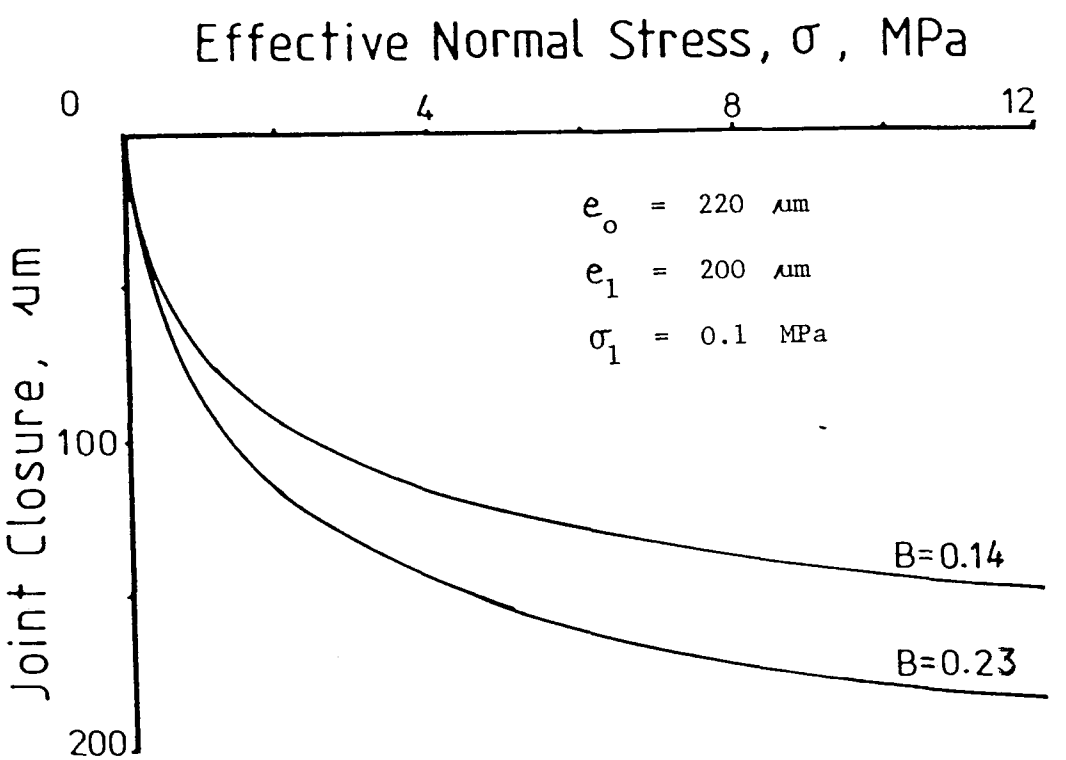


Figure 5.12 Schematics of Walsh's Model with Upper and Lower Boundaries.

$$\frac{K}{K_i} = 1 - (\ 0.14 \text{ to } 0.23\ ) \ln\left(\frac{\sigma'}{\sigma_i'}\right) \qquad (5.11)$$

Using this equation, only one reference hydraulic test is necessary to determine the joint permeability. The values of 0.14 and 0.23 give the upper and lower bound limits which will be restraint of the permeability at each effective normal stress, as shown schematically in Figure 5.12.

In contrast, the statistical model of Tsang and Witherspoon [1981] relies only on effective normal stress - joint mechanical closure data to determine the information, and so obviates the need to undertake any flow tests. However, difficulties arise in establishing the proportion of the joint surface area that is in contact at a particular stress. Despite this difficulty, a reasonably close fit to the experimental flow data was found (Figure 5.13).

In fitting the data obtained from the joints in granite to the models, difficulties were found in finding single values of the material constants that applied to the complete range of data and samples. This may become a major obstacle in obtaining an acceptable correlation using the models (Table 5.4). As already noted, correlation of the data with the model proposed by Walsh [1981] was not conditioned by the same constraints and little difficulty was encountered in fitting this model.

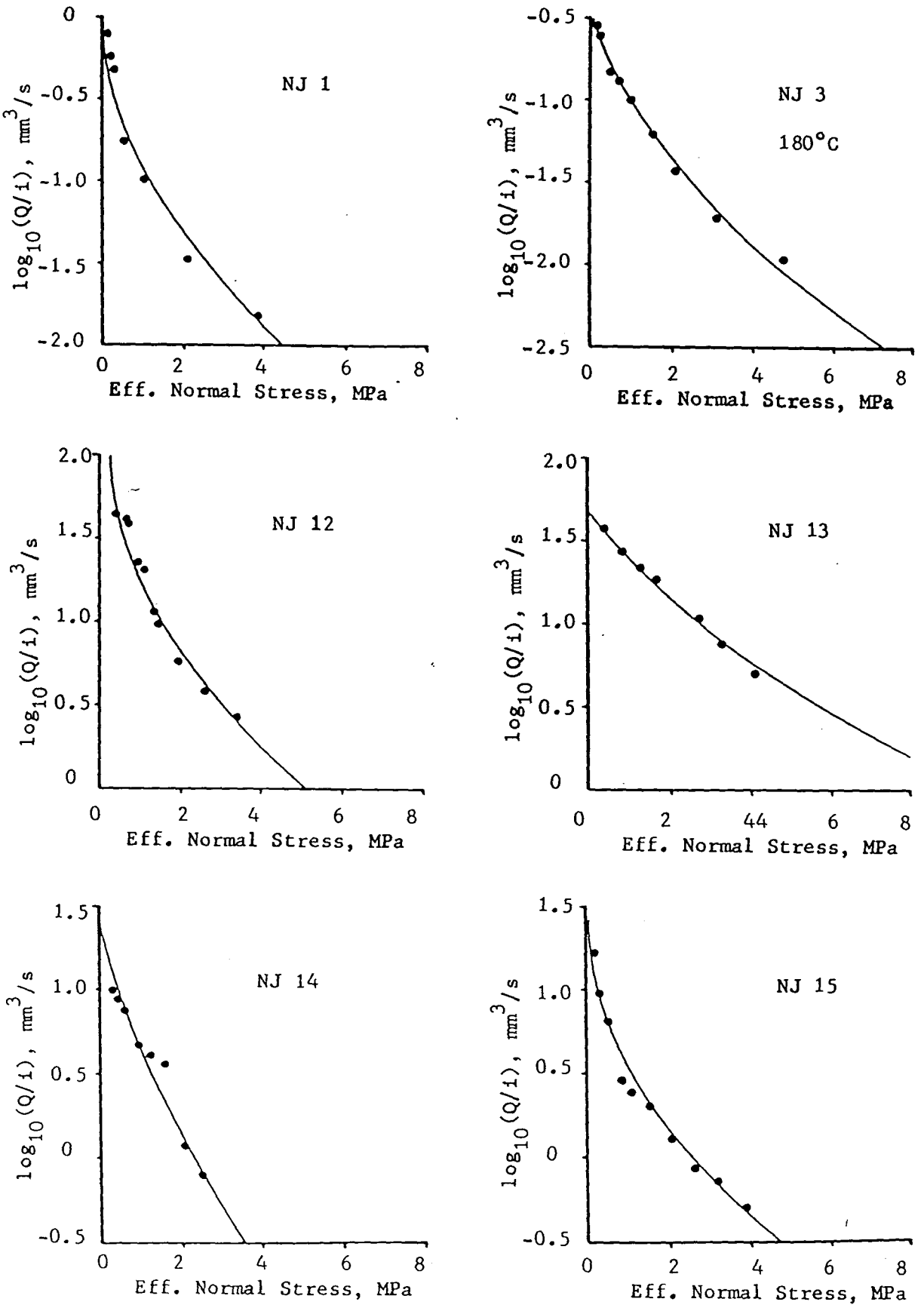
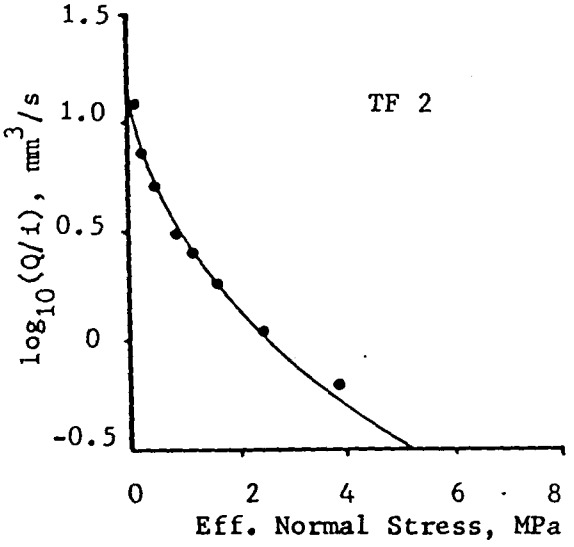
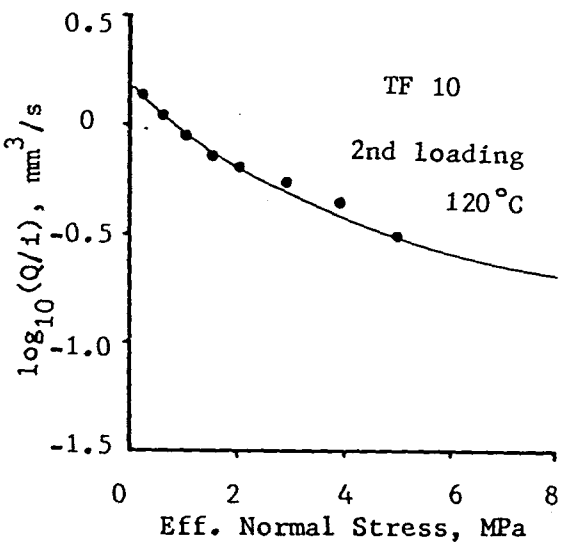
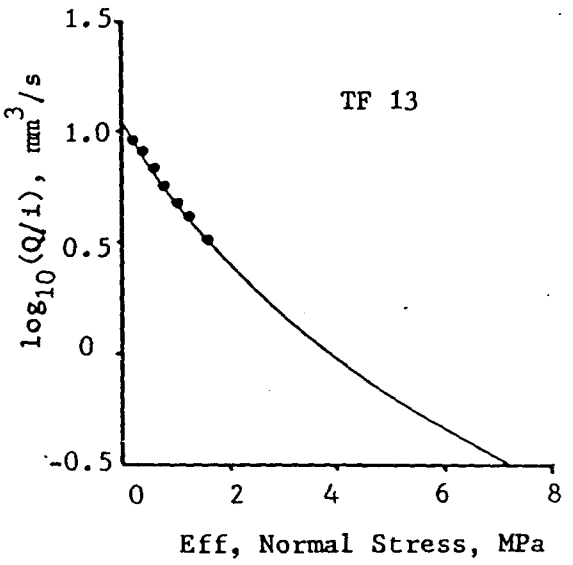


Figure 5.13 Flow Rate Compared with Tsang and Witherspoon's Model.







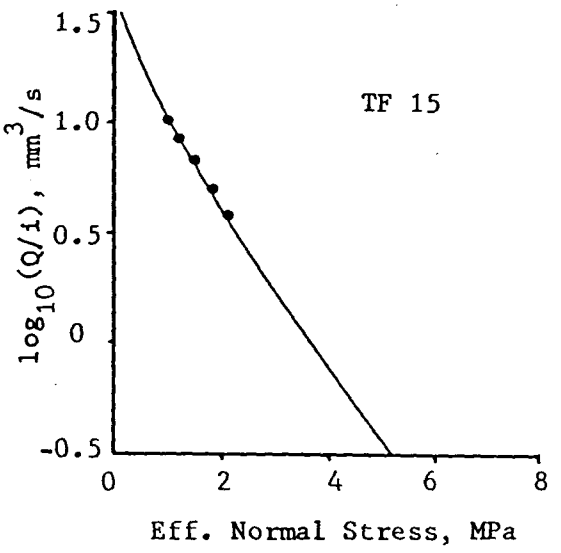
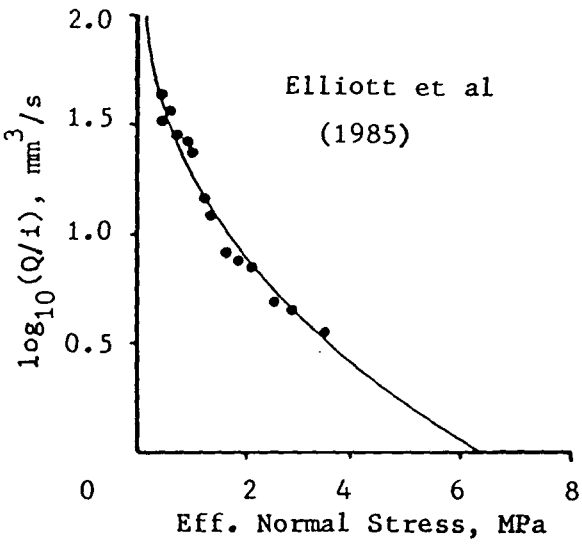
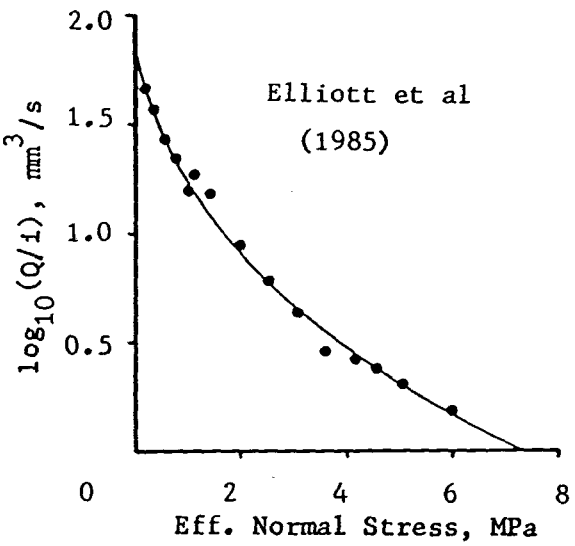


Figure 5.13 (continued).





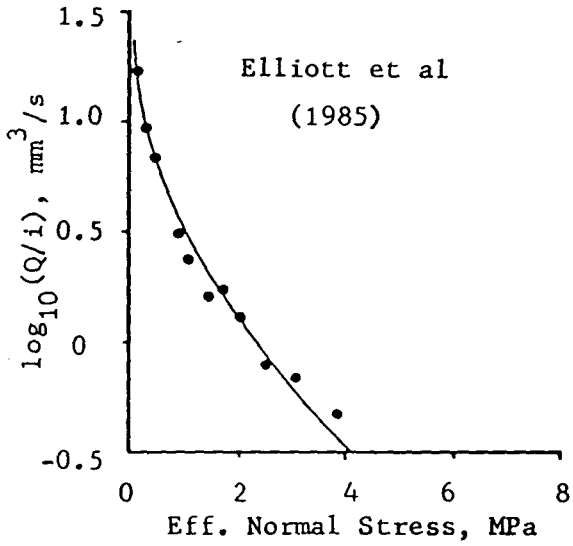


Figure 5.13 (continued).

5.6 Joint Condition Factor, JCF

5.6.1 Calculation of JCF

As noted in section 2.3.4, the equivalent cubic flow law can be written as

$$\frac{Q}{i} = \frac{C}{F} E^3 \qquad (2.16)$$

where F is termed as the Joint Condition Factor [Elliott et al 1985], and

$$F = 1/f^3 \qquad (2.18)$$

and $$f = \Delta e / \Delta E \quad \text{or} \quad f = e/E \qquad (2.20)$$

where e is the theoretical hydraulic aperture, E is the real mechanical aperture, and Δ indicates changes under changing effective normal stress.

The change of the theoretical hydraulic aperture of the joint can be calculated from the measurements of flow rate, as described in section 5.4.2, while the change of the real mechanical aperture can be determined from the measurements of total sample deformation and rock material deformation (section 5.3.1). By plotting Δe against ΔE for each change of effective normal stress, as in the example shown in Figure 5.2 (section 5.2), the points are fitted by a straight line. This is to be expected because of the validation of cubic flow law as demonstrated in section

5.4.2. The gradient of the $\Delta e/\Delta E$ curve is the value of f. This in turn defines the value of the JCF ($JCF = 1/f^3$).

5.6.2 Influences of joint surface properties and of initial aperture

The calculated initial JCF is plotted against Joint Roughness Coefficient and Joint Matching Coefficient, in order to investigate the combined effects. If initial JCF and joint initial aperture E_o at room temperature are also plotted, the dependence of JCF on E_o and JRC is evident as shown in Table 5.5 and Figure 5.14. It is obvious that JCF increases with an increase in JRC and with a decrease in E_o. This suggests that the poorer joint surface properties with small initial apertures generally give higher JCF. That is, for a rough joint, its hydraulic behaviour will approach that given by theoretical smooth parallel plate model only when the aperture is wide enough (hundreds of micrometers) to compare to the dimension of the asperities.

Based on the experimental results, an approximate relationship between JCF, JRC and E is proposed, as,

$$E_o = \frac{JRC^{2.5}}{JCF^{2.2}} \qquad (5.12)$$

This relation is also presented in Figure 5.15. The imprecision of the data presented in Figure 5.14 suggests that the value of JCF depend on more than just JRC; it also depends upon other joint surface properties such as

Table 5.5 Results of Initial Mechanical Aperture E_o, Joint Condition Factor JCF, JRC and JMC.

Sample No.	E_o(μm)	JCF	JRC	JMC
Natural Joints				
NJ1	60.2	3.887	6	5
NJ3	25.1	0.161	11	7
NJ4	126.1	0.173	11	7
NJ5	73.2	1.078	9	8
NJ6	33.9	0.737	10	7
NJ12	160.2	1.269	9	7
NJ13	102.4	0.800	9	7
NJ14	168.1	13.31	8	6
NJ15	86.0	1.031	8	6
Extension Fractures				
TF2	60.0	0.824	8	4
TF3	48.9	0.155	12	6
TF5	71.1	4.538	18	9
TF6	52.5	1.123	12	6
TF7	56.1	0.731	9	4
TF9	118.8	2.044	14	8
TF10	142.2	1.144	13	8
TF11	30.7	9.170	20	10
TF12	40.4	3.781	18	9
TF13	81.4	1.894	16	8
TF15	137.1	3.202	18	9

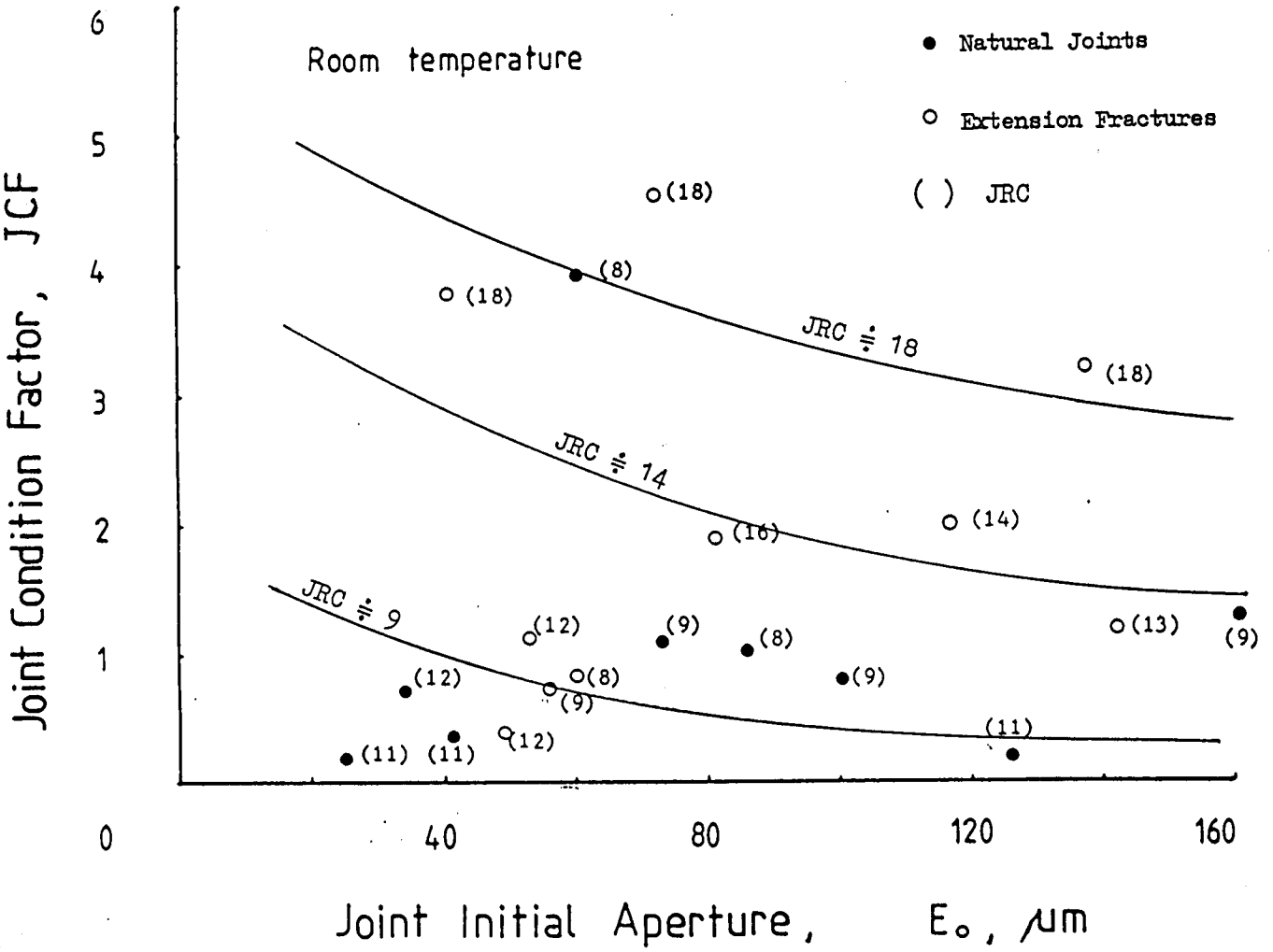


Figure 5.14 Variation of Joint Condition Factor with Joint Initial Aperture and Joint Roughness Coefficient.

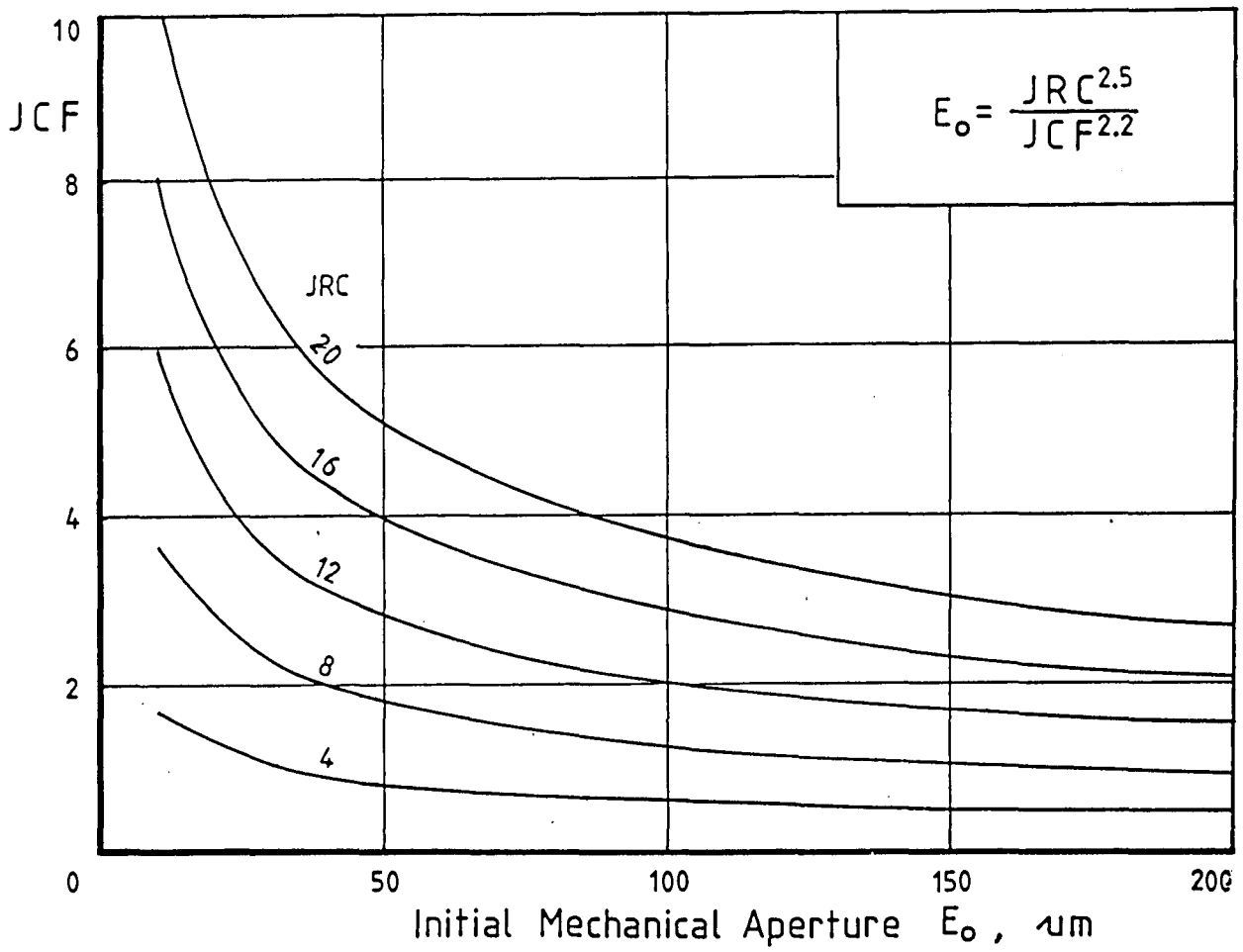


Figure 5.15 Relation Between Joint Condition Factor, Initial Aperture and Joint Roughness Coefficient.

matching, wall strength, previous deformation and alteration. Thus one cannot expect to obtain perfect correlations using the values of JRC alone.

5.6.3 Influence of cyclic loading

The tests were arranged in order to demonstrate the effect of temperature on the JCF. However, the data obtained during the experiments also show an influence of cyclic loading; these data are presented in Table 5.6 for maximum normal stresses of 20 - 30 MPa.

The results demonstrate a clear trend for JCF to increase with cyclic loading. The increase occurs when unloading and reloading the joint. This increase is particularly great at room temperature. The change of JCF will steadily decrease as further continuous loading cycles are applied. The change may become very small after 4 or 5 loading cycles, as the joint deformation is stabilized [Goodman 1976].

Table 5.6 Influence of Cyclic Loading on JCF

Samp. NO.	Temp. (°C)	Loading Cycles			
		First Load/Unload	Second Load/Unload	Third Load/Unload	Fourth Load/Unload
Natural Joints					
NJ5	room	1.77 454.9			
NJ6	100	5.66 6.74			
NJ15	room	1.03 199.0			
Extension Fractures					
TF2	room	0.83 198.5			
TF9	room	7.50 103.8		20.7	0.50 68.19
TF10	120	10.59 12.72	343.0 249.6		
TF12	120	5.13 83.74			
TF12	room		0.44 52.73		
TF13	120	12.58 142.8			
Detournay [1980]					
	room	1.00 6.98			

Chapter 6

RESULTS AND DISCUSSION --EFFECTS OF TEMPERATURE, JOINT HYDRO-THERMO-MECHANICAL RELATIONS AND THERMAL EXPANSION

6.1 Influence of Temperature on Initial Aperture

Initial apertures E_o change with the testing temperature. Calculated values of initial apertures at various temperatures are shown in Table 6.1. In Figure 6.1, the change of temperature ΔT is plotted against $\log(E_o / E_o^*)$, where E_o^* is the joint initial aperture at room temperature. The graph, shows the relationship between temperature and E_o seems to be quite variable. However, the graph points to the major conclusion that the initial aperture E_o increases with the increasing temperature. This change is also dependent on other factors, notably the joint surface properties. In the figure, the JRC values included in brackets show that JRC is one of the critical factors controlling the change of initial apertures. Because the change may be dependent on factors other than JRC alone, perfect results cannot be expected by using JRC only. Other major factors influencing the change of joint initial apertures with temperature are including joint matching, joint material composition and grain sizes. Further research are required to understand the relations in more details.

Table 6.1a Effect of Sample Temperature on Joint Initial Aperture (the values given in the table are E_o with unit of μm).

Sample No.	Sample Temperatures, °C						
	room	90	100	120	140	180	200
Natural Joints							
NJ3	25.1						175.2
NJ3	41.6					90.7	
NJ4	126.1		232.9			303.0	
NJ5	73.2	60.5			277.5		
NJ6	33.9		59.5				
Extension Fractures							
TF3	48.9		56.1				
TF5	71.7		65.6			168.8	
TF6	52.5					182.6	
TF7	56.1		186.8			480.3	
TF9	118.8		107.0		94.8		
TF10	142.2			156.3			
TF11	30.7		71.4				
TF12	40.4			60.4			
TF13	81.4			404.8			
TF15	137.1				185.4		

Table 6.1b Effects of Sample Temperature on Joint Initial Aperture. (values in the table are $\log_{10}(E_o/E_o^*)$

Sample No.	Change in Sample Temperature, (T - T room), °C						
	80	90	100	110	120	160	180
Natural Joints							
NJ3						0.339	0.884
NJ4	0.226					0.381	
NJ5					0.579		
NJ6	0.224						
Extension Fractures							
TF3		0.060					
TF5						0.372	
TF6						0.541	
TF7	0.522					0.933	
TF9	---						
TF10				0.041			
TF11	0.367						
TF12			0.175				
TF13				0.697			
TF15					0.131		

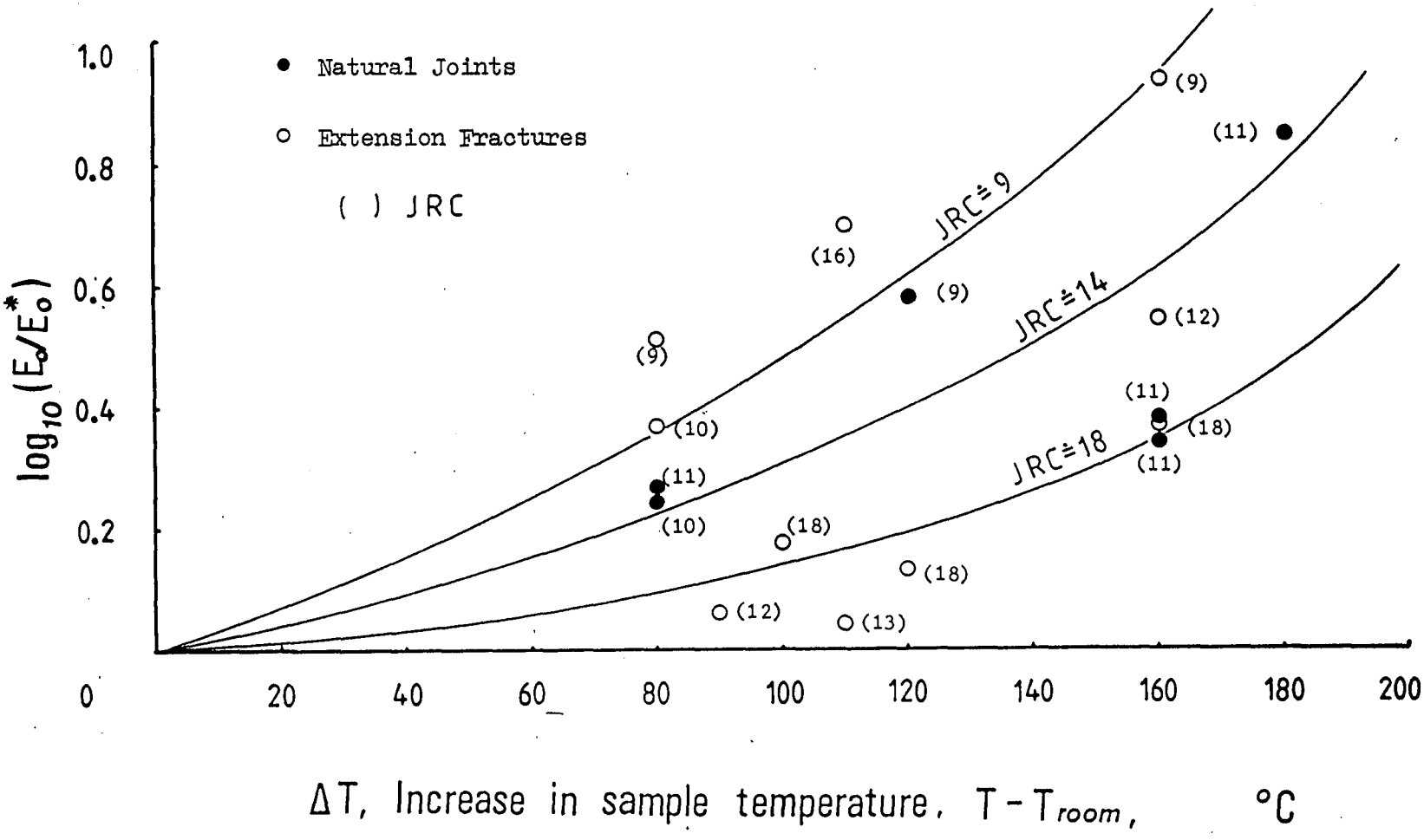


Figure 6.1 Variation of Initial Aperture with Temperature and JRC.

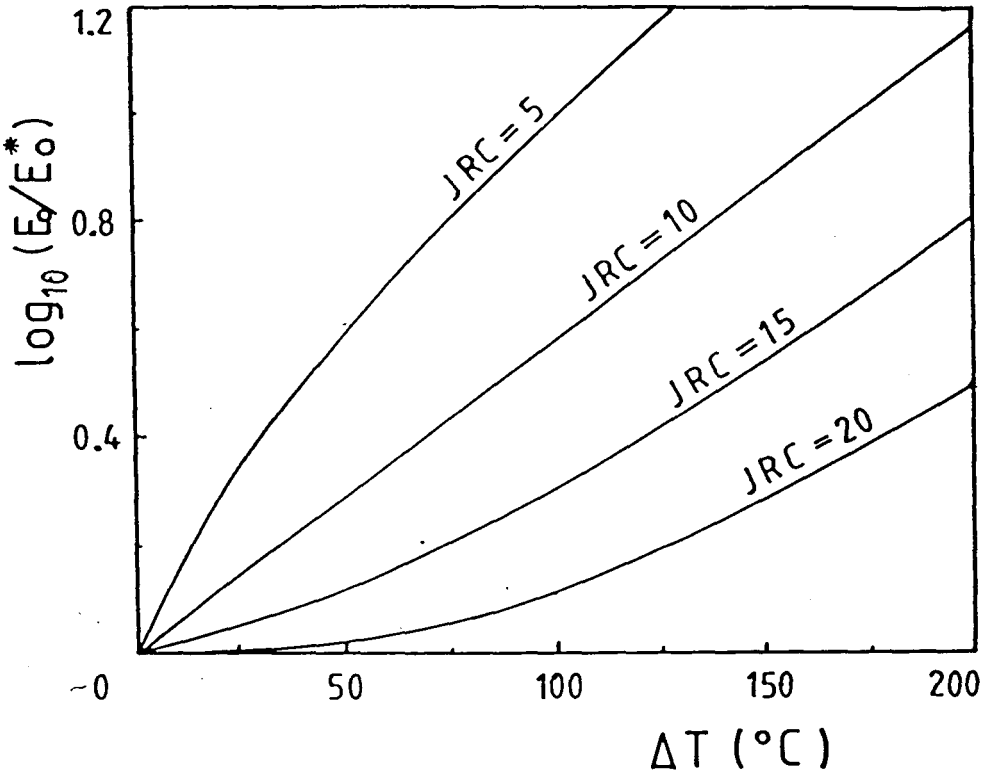


Figure 6.2 Proposed Relation of Initial Aperture, Temperature and JRC.

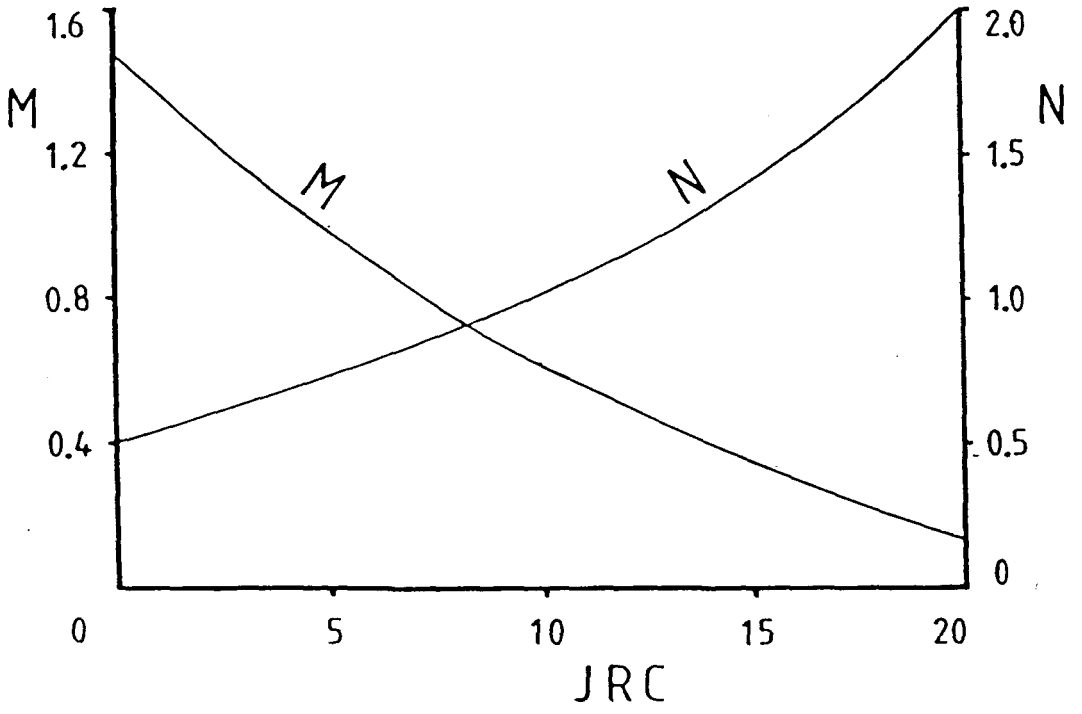


Figure 6.3 Values of Parameters M and N.

An empirical relation between E_o, ΔT and JRC is proposed based on the experimental data. As shown in Figure 6.2, this relation is,

$$\log_{10} \left(\frac{E_o}{E_o^*} \right) = M \left(\frac{\Delta T}{100} \right)^N \qquad (6.1)$$

where M and N are approximate functions of JRC for the joints and fractures tested, such that

when JRC = 5 M = 1.00 N = 0.71

JRC = 10 M = 0.58 N = 1.00

JRC = 15 M = 0.38 N = 1.41

JRC = 20 M = 0.12 N = 2.00

as also shown in Figure 6.3.

6.2 Influence of Temperature on Joint Hydro-mechanical Behaviour

6.2.1 Change of mechanical behaviour

Experimental data for samples tested at elevated temperatures show changes in the parameters in both Goodman's model [Goodman 1976] and the logarithmic relation (section 5.3.3). However, the data can still be well fitted by these models. Samples NJ3, TF7 and TF10 tested at elevated temperatures showed significant increases in the values of maximum closure, V_{mc} and of the parameter S in Goodman's model (Table 5.3). The results obtained in this study may suggest that the

increased values of the parameter S are related to the increases in the maximum joint closure V_{mc} rather than directly to the effect of test temperature. This may also imply that an increase in temperature causes more mismatching in the joint as a result of joint thermal expansion (see section 6.5).

Samples NJ3 and TF10 also showed reductions in the values of the parameter B in the logarithmic relation due to temperature increase, as shown in Table 5.3. These reductions, are reflected in the effective normal stress - joint closure plots by much lowered stiffnesses initially and at earlier stress stages. This may be induced by:

1) an increase in the initial aperture due to heating up of the joints;
2) a decrease in the deformation modulus of the asperities is due to the possible thermal cracking.

6.2.2 Change of hydraulic behaviour

It is evident that raising of test temperature reduces the flow rate considerably. The asymptotic reduction with increase of effective normal stress at elevated temperatures can also be fitted by the models described earlier in section 2.4 and section 5.5. The parameters in each model were calculated and shown in Table 5.4. In the models by Gangi [1975, 1978, 1981], Gale [1982] and Swan [1983], the changes of parameters

are not consistent, and the values of these parameters generally vary within large ranges. Walsh's model [1981] shows a reduction of parameter B for sample NJ3 tested at a temperature of 180 °C. As noted earlier, B is proportional to $\sqrt{h/e_o}$, where h is the root mean square value of the asperity height distribution and e_o is the initial aperture of the joint; hence the reduction in B implies an actual increase in initial aperture, as is to be expected due to thermal expansion (section 6.5)

The reductions in flow rates at elevated temperatures at same effective normal stress level are partially due to the non-homogeneous thermal expansion of the joint surfaces. The expansion of individual compositional material may reduce the aperture at some critical narrow places, and in the extreme cases may block some of the flow pathways. The increase of contact area is evident from the increase of the ω value of sample NJ3 at elevated temperature in Tsang and Witherspoon's model [1981], where ω represents the percentage of contacting area to the total joint surface area.

6.2.3 Change of Joint Condition Factor JCF

The experimental data show that there is a significant change in JRC with increasing test temperature. The relation between JCF and the test temperature is shown in Table 6.2 and Figure 6.4. From the plot, the relation between JCF and temperature increment appears to

Table 6.2a Effect of Sample Temperature on Joint Condition Factor.
(values in the table are the JCF)

Sample No.	Sample Temperatures, °C						
	room	90	100	120	140	180	200
Natural Joints							
NJ3	0.161	1.116					14396.7
NJ3	0.354					355.4	
NJ4	0.173		4.116			1121.5	
NJ5	1.078				1376.8		
NJ6	0.737		9.280				
Extension Fractures							
TF3	0.155		2.818				
TF5	4.538		9.945			2028.2	
TF6	1.123	4.327				1075.6	
TF7	0.731		132.8			711.8	
TF9	2.044		11.01				
TF10	1.144			22.59			
TF11	9.170		38.57				
TF12	3.781			177.2			
TF13	1.894			26.76			
TF15	3.202				339.3		

Table 6.2b Effect of Sample Temperature on Joint Condition Factor.
(values in the table are $\log_{10}JCF/JCF^{*}$)

Sample No.	Change in Sample Temperature, (T - T room), °C						
	80	90	100	110	120	160	180
Natural Joints							
NJ3	0.841					3.002	4.951
NJ4	1.376					3.812	
NJ5					3.106		
NJ6	1.100						
Extension Fractures							
TF3		1.260					
TF5	0.341					2.650	
TF6						2.375	
TF7	2.259					2.988	
TF9	0.731						
TF10				1.295			
TF11	0.624						
TF12			1.671				
TF13				1.150			
TF15					2.025		

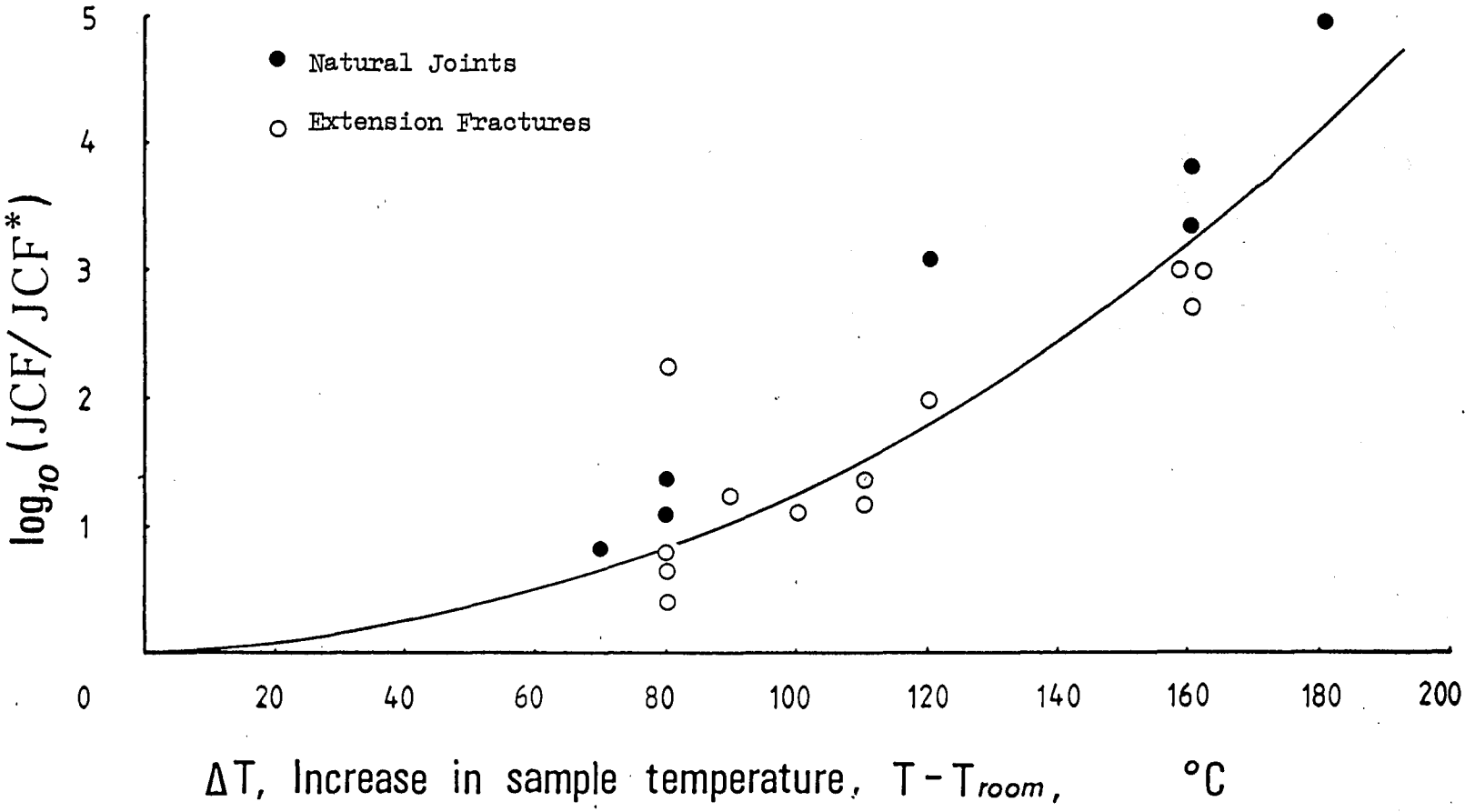


Figure 6.4 Variation of Joint Condition Factor (JCF) with Temperature.

be of the form of

$$\log_{10}\left(\frac{JCF}{JCF^*}\right) = 1.26\left(\frac{\Delta T}{100}\right)^2 \qquad (6.2)$$

where JCF^* = the initial JCF at room temperature;

ΔT = change in temperature, T - T room.

This relation provides a very good fit to the data. However, the change of JCF of natural joints tends to be greater than that of fresh extension fractures, undergoing the same increment in temperature.

Microscopy observations show that thermal cracking occurs as the joint is both heated up and injected with cold water. Thermal cracking may cause a reduction in the joint wall strength, reduce the joint deformation modulus because of thermal cracking of the asperities (see section 6.4), and increase the joint mechanical aperture due to joint thermal expansion (section 6.5). Each mechanism or combined mechanism seems cause a much larger increment in the mechanical closure, ΔE than in the hydraulic aperture closure, Δe, as suggested by the test results. Hence, thermal cracking and expansion cause increases in JCF values as the temperature rises.

6.3 Joint Hydro-thermo-mechanical Properties and a New JCF Approach

Walsh's model [1981] proved to be a consistent and simple approach to determine the hydraulic properties

of a joint. In the simplest case, only one reference hydraulic test is required at a low stress level.

Tsang and Witherspoon's [1981] "asperity or voids" statistical model can deal with both mechanical and hydraulic properties. Using this model, hydraulic properties as represented by the effective normal stress - flow rate relation can be determined from the mechanical properties represented by the effective normal stress - joint mechanical closure relation. It is also possible, in an inverse way, to determine the mechanical properties if flow data are given. In fitting the experimental data to the model, difficulty arises in establishing the proportion of the joint surface area that is in contact at a certain stress level. In the present case, difficulty was found in finding a reasonable single values of the proportion of the joint surface area in contact and of the material constants that applied to the complete range of data.

Based on the experimental data, an empirical joint hydro-thermo-mechanical relation is proposed. The model is derived from the smooth parallel plate theory for laminar flow, i.e., the "cubic flow law". The results presented by Witherspoon et al [1980] and Elliott et al [1985] and the experimental results presented here, suggest that an "equivalent cubic flow law" relating flow rate to aperture cubed is valid for rough joints and fractures with apertures varying from 250 μm down to essentially closed features with apertures as small as 4

μm. By introducing a Joint Condition Factor (JCF), at any state, the hydraulic flow rate, Q, and real aperture, E, can be related by

$$\frac{Q}{i} = \frac{C}{F} E^3 \qquad (2.16)$$

where $C = w\, g / 12\nu$,

F = JCF,

i = hydraulic differential head gradient,

w = width of the aperture,

g = acceleration due to gravity,

ν = fluid kinematic viscosity.

If JCF^* refers as the JCF value at room temperature, it is found that JCF^* can be related with Joint Roughness Coefficient (JRC) and the initial real aperture, E_o by

$$(JCF^*)^{2.2} = \frac{JRC^{2.5}}{E_o^*} \qquad (6.3)$$

In most cases, for normal stress loading on extension fractured joints, when dilation is restricted, the initial aperture E_o can be approximated as the maximum possible joint closure, V_{mc}. Hence

$$E = V_{mc} - \Delta V \qquad (6.4)$$

where ΔV is the mechanical joint closure which is measured directly during the tests.

Experimental data also showed that the initial apertures can be estimated from the joint surface

properties. An empirical relation is proposed as the chart shown in Figure 5.4.

At elevated temperature, T, the results showed that the value of JCF varied significantly following the relation:

$$\log_{10}\left(\frac{JCF}{JCF^{*}}\right) = 1.26\left(\frac{\Delta T}{100}\right)^{2} \qquad (6.2)$$

where $\Delta T = T - T_{room}$.

The initial aperture (or the maximum possible closure) of a rough joint also increases with increase in temperature. A relationship was proposed in section 6.1,

$$\log_{10}\left(\frac{E_o}{E_o^{*}}\right) = M\left(\frac{\Delta T}{100}\right)^{N} \qquad (6.1)$$

where M and N are approximate functions of JRC. A chart was shown in Figure 6.3.

By combining equations (2.16, 6.1, 6.2, 6.3 and 6.4), if one has effective normal stress - joint closure data at normal room temperature, the flow properties of same joint can be estimated easily at any state of temperature and stress. Furthermore, if the initial aperture is estimated from the chart in Figure 5.4, only a few data of effective normal stress - joint closure data points at low stress levels are necessary to determine the whole hydro-thermo-mechanical properties of the rough joints in granite.

Equation (2.16) may provide a new approach to determine the hydro-mechanical properties of all joints in all types of igneous rocks; but further research of evaluating the values of Joint Condition Factor are necessary. Equations (6.1, 6.2, 6.3, 6.4) and Figure 5.4 are applicable to the joints and fractures in Carnmenellis granite. However, the range of applicability of above Equations and Figure may be extended to the joints and fractures in other types of granites with small variations in the parameters.

However, vital roles are played by the joint surface geometrical property parameters. The values of JRC and JMC which can be determined simply by inspection of the joint surface. Therefore, accuracy is essential when assessing the values of JRC and JMC to yield an empirical value of JCF. Accurate values of JCF can be determined by conducting hydro-mechanical tests on the joints. However, the simple method of determining JCF by JMC and JRC will provide good judgement and approximation given that JMC and JRC are empirical and subjective values.

6.4 Effects of Thermal Cracking on the Hydro-thermo-mechanical Behaviour of Rock Joints

6.4.1 Scanning electron microscopy

Thin sections were prepared from extension fracture samples showing the cross section perpendicular

to the fracture surface along the fracture for examination in a Scanning Electron Microscope (SEM). These samples were denoted X, Y and Z. Sample X was a fresh untested extension fracture, and Y and Z were tested samples under permeability tests with effective normal stress up to 30 MPa but heated up to 100°C and 180°C, respectively.

The standard SEM thin sections containing fractures and cracks were cut, hand or machine lapped down to about 30 μm thick using 600 grid Silicon Carbide with smoothness ± 1.0 μm. The thin section were protected by a cover slip with Balsam. Although the thin sections were not ion-milled, their polished surfaces provided satisfactory SEM images. The prepared thin crack sections were examined in the SEM equipped with an energy dispersive X-ray detector in the Department of Geology, Imperial College, London.

6.4.2 Observations

Fresh sample

The fresh sample of granite marked X was examined in order to help distinguish between features that were initially present in the rock and those that were formed as a result of the experiment. These observations also permitted a qualitative comparison of the fresh material with Westerly granite samples studied by others [Sprunt and Brace 1974, Hadley 1976, Vaughan et

al 1986]. As shown in Figure 6.5, the untested fresh fracture and rock material are composed of compact crystalline grains. The hair-like outcrop on the joint surface (Figure 6.5a) was probably a result of the fracturing mechanism which pulls the two surfaces apart suddenly. On the whole, the joint surface and rock material are very dense with very a low number of cracks and pores.

However, there are a few transgranular cracks present in the original material. Transgranular cracks are those intragranular cracks which meet two grain boundaries (Figure 6.5c). Such cracks are present in some of the smaller grains, especially quartz. Cracks which pass from one grain into another, called intergranular cracks, are very scarce. Intragranular cracks in the fresh material are open (Figure 6.5f), that is, the crack faces are separated and the cracks do not contain any filling material.

The grain boundaries between the feldspars are almost always uncracked. However, a small number of the grain boundaries between quartz grains and between two different compositions are cracked (Figures 6.5d and 6.5f).

Pores are present most abundantly in feldspars, and least commonly in quartz. In places where intragranular cracks run through the pores the crack surfaces are rough (Figure 6.5e), but generally, the intragranular crack surfaces are smooth.

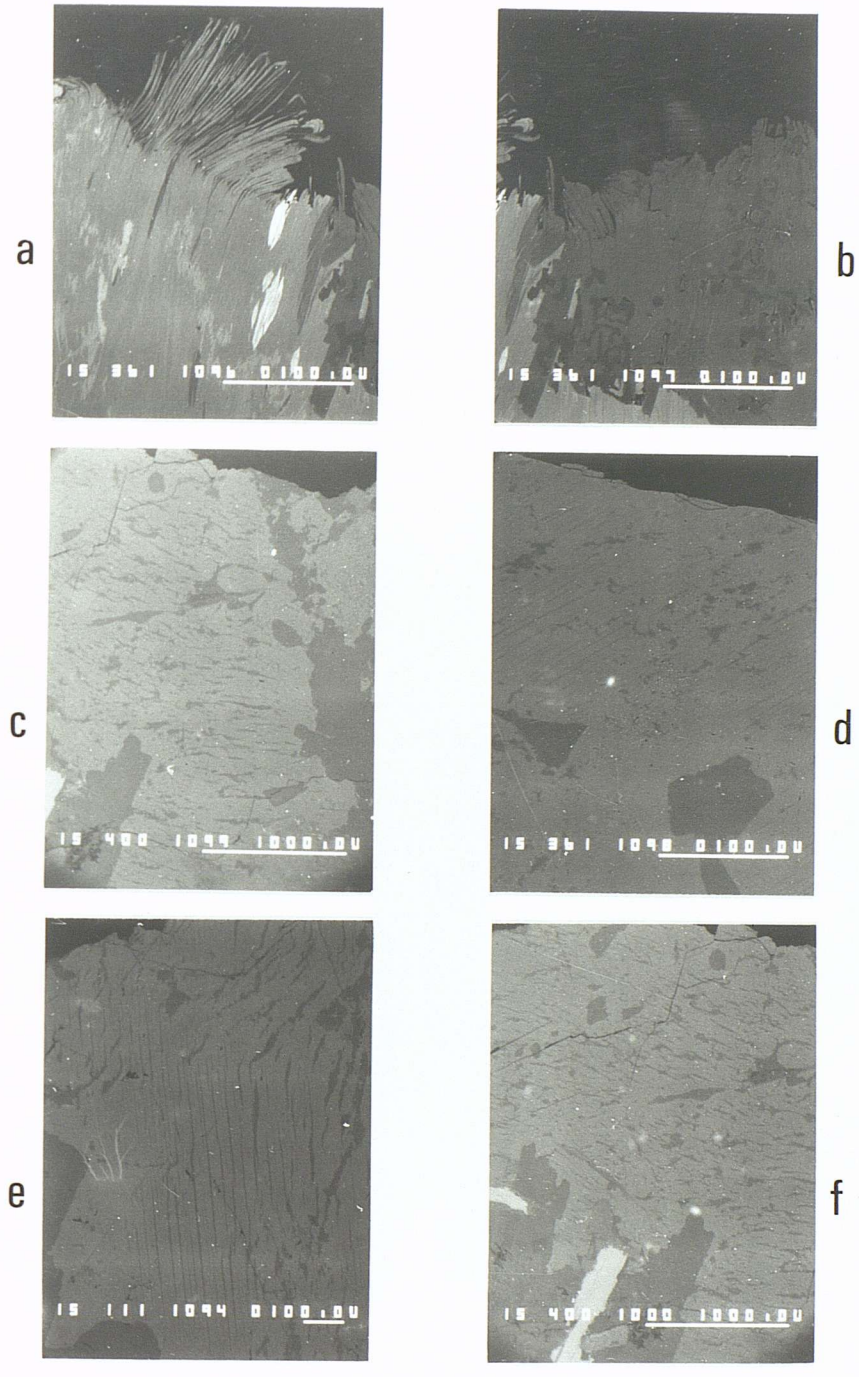


Figure 6.5 Fresh Fractured Granite Sample Under SEM.

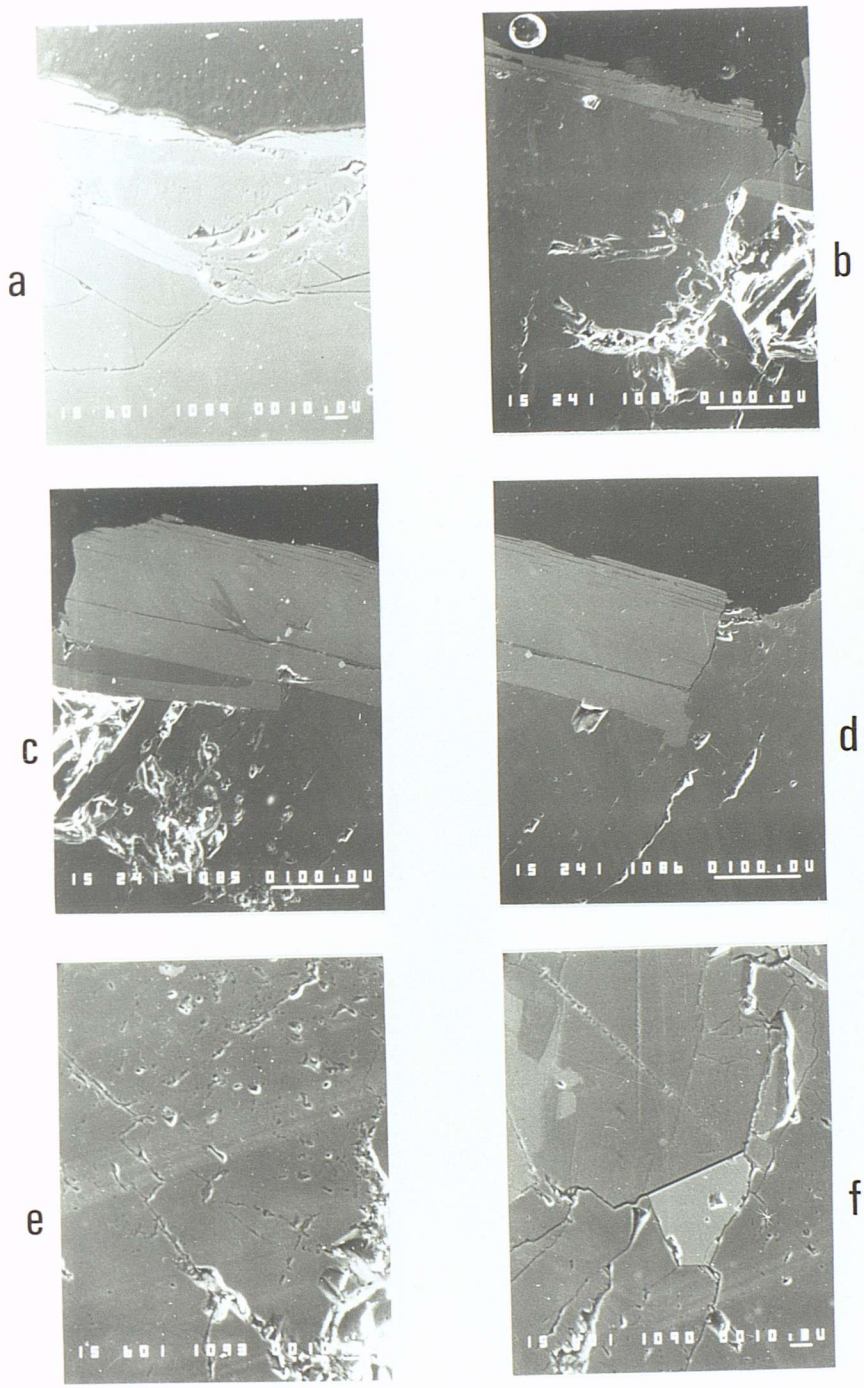


Figure 6.6 Tested Fractured Granite Sample (up to 100°C) Under SEM.

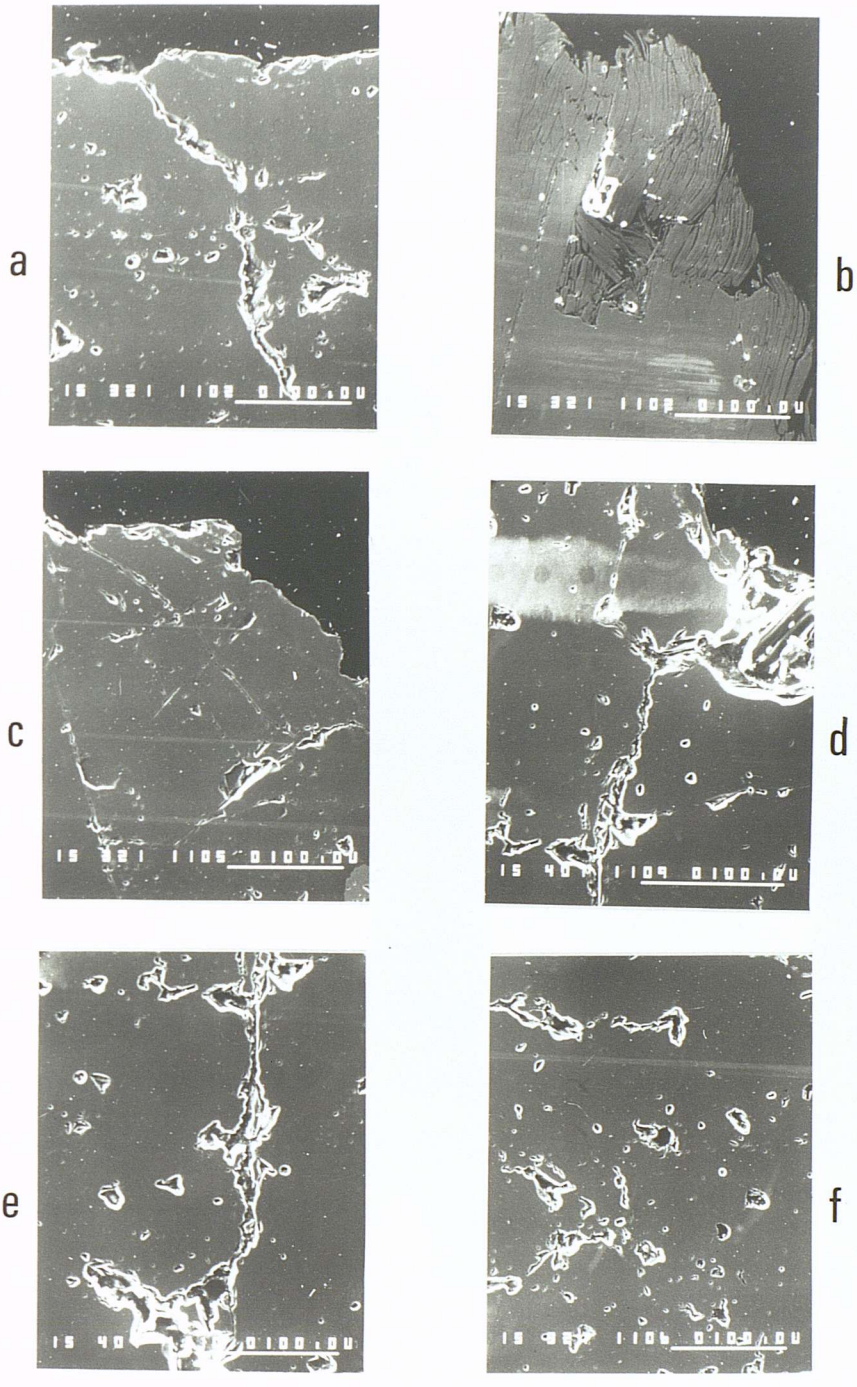


Figure 6.7 Tested Fractured Granite Sample (up to 180°C) Under SEM.

After hydro-thermo-mechanical tests

The crack densities in the tested samples are much greater than those in the fresh samples, as shown in Figure 6.6 and Figure 6.7. In addition to intragranular cracks and grain boundary crack propagation and widening (Figure 6.6f), there are also intergranular cracks which pass through grain boundaries (Figure 6.6f).

The quartz grains in altered samples contain the highest density of intragranular cracks (Figures 6.6c and 6.6d). As quartz grains tend to occur in clusters, the intragranular cracks are intimately associated with grain boundary cracks (Figures 6.6c and 6.6d). Large intragranular cracks in the feldspars are generally similar to those in quartz, although they are somewhat less numerous and have widths of as much as a few microns (Figure 6.6a). In places where the intragranular cracks intersect pores, the crack surfaces are scalloped (Figures 6.6c, 6.7a and 6.7e). The surface roughness of the cracks appears to be increased as a result of the experiment because pores occur more frequently along intragranular cracks in the tested samples than in the fresh materials, particularly when the testing temperature is higher (Figure 6.7).

Simmons and Richter [1976] classified grain boundary cracks as coincident, that is, following the grain boundary, or non-coincident, occurring within a single grain and intersecting a grain boundary. The

altered samples contain arrays of intersecting, transgranular cracks which form networks by meeting cracked grain boundaries. Such transgranular cracks are especially prevalent in quartz. Because these intragranular cracks meet grain boundaries, they may be classified as non-coincident grain boundary cracks. Most of the grain boundaries between feldspars in the fresh sample material were closed and remained closed during the heating and flow experiments. The grain boundaries between quartz and feldspars and those between quartz and the minor minerals in the tested samples are frequently cracked as coincident boundary cracks (Figure 6.6f). The grain boundaries between quartz grains are often cracked in the altered samples and interconnected with intragranular cracks, which sometimes, form a network (Figures 6.6a, 6.6f and 6.7d).

6.4.3 Effect of cracks on the hydro-thermo-mechanical behaviour of joints

The observations made under Scanning Electron Microscope (SEM) showed that the granite material was significantly altered after hydro-thermo-mechanical action. The observations suggested that cracks and pores may play an important role in establishing fluid pathways in addition to the major joint. This network of intragranular cracks provides the interconnected porosity needed to make the rock material more permeable.

Observations on fresh material and altered

samples suggested that some cracks were introduced into the sample probably as a result of pressurization and/or heating. Thermal expansion of the fluid in existing cracks was probably the dominant factor in crack growth with anisotropic thermal expansion of minerals also a likely contributing factor.

The intragranular cracks in quartz grains frequently intersect each other and the cracked grain boundaries. The feldspars exhibit a somewhat lower density of large, intragranular cracks and almost no cracks along grain boundaries with other feldspars. The grain boundaries between feldspars did not crack open after the experiment. Thus, during the experiment the region containing quartz should be substantially more permeable due to the difference in crack distribution. If the quartz forms continuous pathways through the rock, then the permeability is likely to be greater than if it occurs only in isolated clusters. Therefore, the geometrical distribution of the major phases could be an important factor in determining the permeabilities of granitic rocks.

In addition to those cracks, pores with roughly equal dimensions are present. In quartz and K-feldspar, these pores appear to be concentrated along cracks and associated with the cracks (Figures 6.7a, 6.7d and 6.7e). All together, the observation showed that the cracks and pores may provide a new possible fluid flow network additional fluid pathways to the joint.

However, since the flow is concentrated in the joint, the introduction of the additional fluid flow pathways formed by this network has little effect on the overall joint hydraulic behaviour. Simple calculations show that for an additional flow pathway of 5 μm aperture having the same length as the original joint with an aperture of 50 μm, increases the flow rate by about 0.1%; and for the same pathway with one third the length of the joint, the increase in flow rate is less than 0.5%. In contrast, the direct effect of combined hydro-thermo-mechanical alteration under elevated temperature causes major change in the joint hydro-mechanical behaviour [Hudson 1987], changing the values of joint initial aperture, JCF and other parameters.

6.5 Thermal Expansion of Rock Joints

6.5.1 Joint thermal expansion

During the tests, total thermal expansion after heating was recorded by the cantilever device, which measures the total deformation cross the sample containing the joint perpendicular to the measuring device. This measured total thermal expansion is compared with the thermal expansion of the rock material (determined from thermal expansion coefficient of $12\times10^{-6}/°C$, established by previous thermal expansion tests on the same granite [Elliott 1985]). It is found that the total expansion is always greater than the expansion of the

material. This suggests that the joint also expanded due to the heating. By subtracting the rock material expansion from the total expansion, the positive value obtained is taken to be the joint thermal expansion.

By definition, the joint thermal expansion coefficient, α_j , is

$$\alpha_j = \frac{\text{Joint thermal strain, } \varepsilon_j}{\text{Increment in temperature, } \Delta T}$$

where joint thermal strain ,

$$\varepsilon_j = \frac{\text{Joint thermal expansion, } \Delta_j}{\text{Joint initial aperture, } E_o}$$

The experimental data and the calculated results are presented in Table 6.3 and Figure 6.8. From the plots, it is evident that the joint thermal strain increases with temperature. The joint thermal expansion coefficient appears to be dependent on the initial aperture of the joint. However, there are not sufficient data to enable definite conclusions to be drawn. The results do suggest that the joint thermal expansion coefficient, α_j, is lowered as the initial aperture increases. The plot of Figure 6.6 suggests that

$$\alpha_j = 0.44 \; / \; E_o \qquad (6.5)$$

for the "closed" joints in granite. Clearly, this equation is not valid for those joints with their walls separated apart, but may be valid for small cracks.

Table 6.3 Summary of the Results of Joint Thermal Expansion.

Sample No.	Temperature range (°C)	Eff. normal stress (MPa)	Initial aperture (μm)	Joint expan. Δj(μm)	Change of temp. (°C)	Joint therm. strain
Natural Joints						
NJ4	20 - 100	0.9	126.1	23.81	80	0.189
NJ4	100 - 180	1.6	303.0	139.81	80	0.461
NJ5	20 - 90	1.2	73.2	35.62	70	0.487
NJ5	90 - 140	2.5	277.5	21.03	50	0.076
NJ6	20 - 100	1.0	34.0	36.55	80	1.075
Extension Fractures						
TF3	20 - 100	1.2	17.2	20.13	80	1.170
TF5	20 - 100	1.5	71.7	19.79	80	0.276
TF5	100 - 180	3.0	65.6	74.32	80	1.133
TF6	20 - 180	0.6	52.5	55.77	160	1.062
TF9	20 - 100	0.8	118.8	21.82	80	0.184
TF9	100 - 140	2.0	107.0	33.64	40	0.314
TF10	20 - 120	2.0	142.2	43.78	100	0.308
TF12	20 - 120	1.5	94.0	72.35	100	0.770
TF15	20 - 90	2.0	137.1	29.62	70	0.216

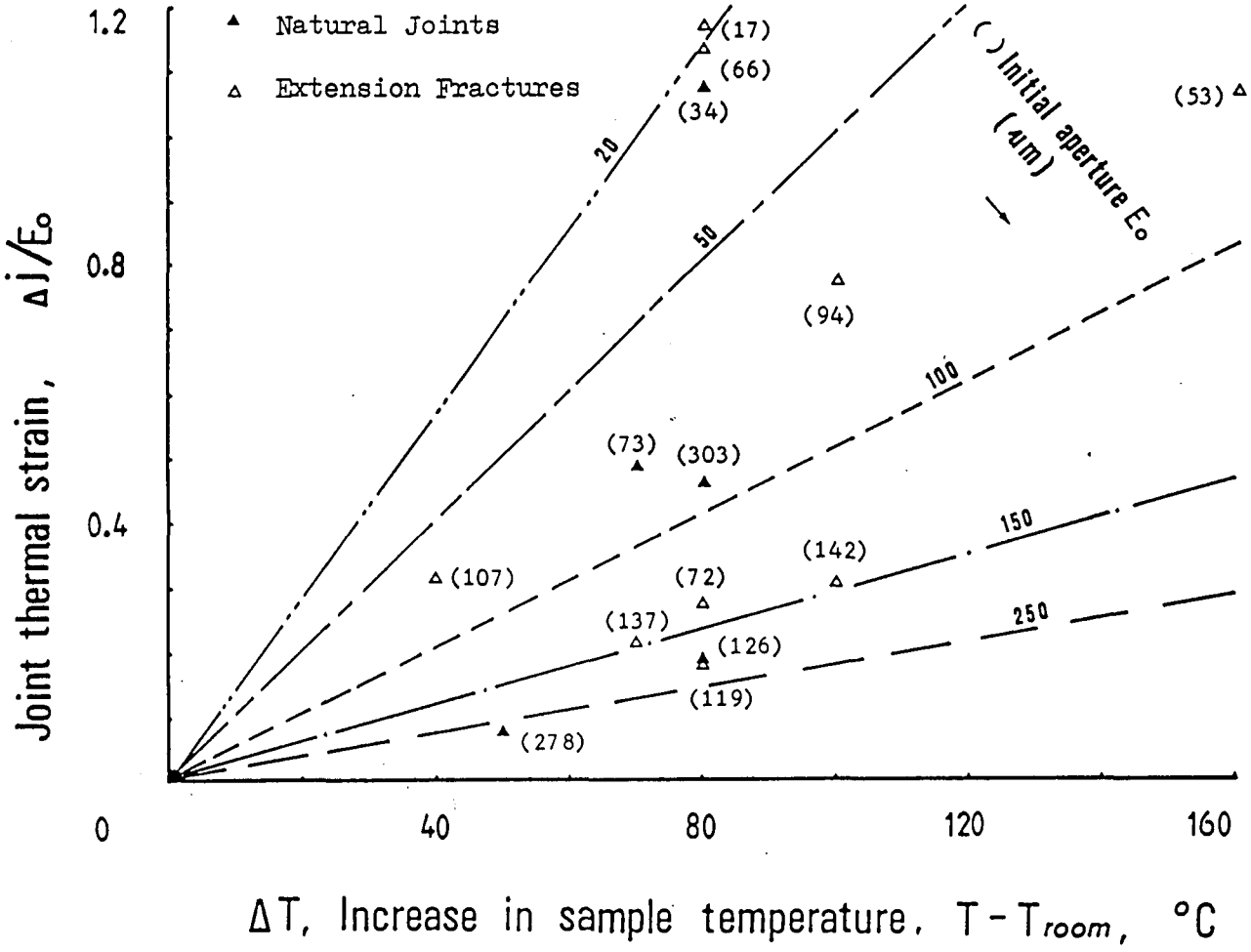


Figure 6.8 Experimental Results for Joint Thermal Expansion.

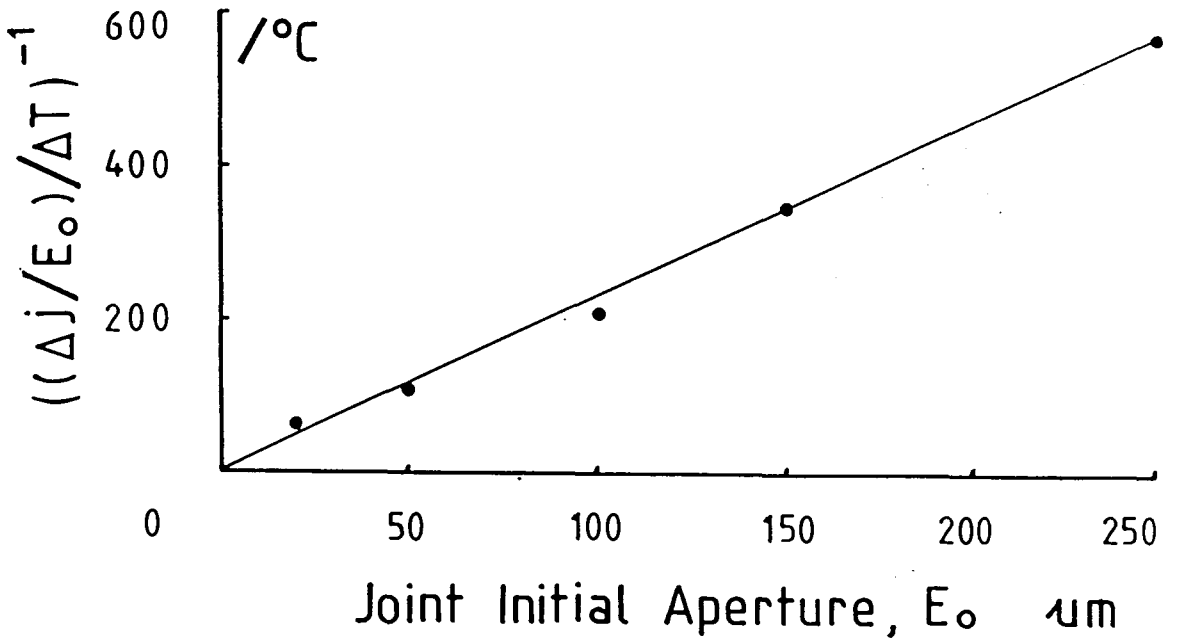


Figure 6.9 Variation of Joint Thermal Expansion Coefficient with Joint Initial Aperture.

6.5.2 Joint thermal expansion mechanism and joint healing mechanism

The experimental results lead to the apparently contradictory conclusions that, in most cases, the joint initial mechanical apertures increased while the joint flow permeability reduced with increasing temperature. This phenomenon can be explained by the joint thermal expansion mechanism and joint healing mechanism.

As noted in section 5.4.3, the joint aperture is the perpendicular distance separating the adjacent rock walls of an open discontinuity, in which the intervening space is air or water filled [Brown 1981]. For a rough joint, the distance between the two rock

walls varies from zero where surfaces are in contact to a maximum value where large voids exist. The aperture then is the mean value of the opening of the joint surfaces. It is determined by the joint wall surface profiles and the positions of contact points and voids. In the general case, the initial mechanical aperture is considered to have a value equivalent to the joint maximum closure. In the case of dilation, they are not equal, and the latter can be greater than the former. When the joint is heated and saturated, the joint wall strength decreases as the result of thermal cracking and chemical alteration. The measured joint maximum closure may be greater than that at room temperature. Hence increasing the temperature may increase the measurement of the initial mechanical aperture. At present, this effect is not able to be eliminated. From the geometrical point of view, this measured aperture is not the true aperture. The initial apertures at elevated temperatures used later in this section and in previous sections include this effect.

When the rock is subjected to slow, uniform heating, it undergoes non-homogeneous thermal expansion due to the different thermal expansion coefficients of the different materials present, particularly feldspar which has large grain sizes and greater thermal expansion coefficient than other materials present in the rock [Kaye and Lamb 1966]. It may result that some areas are more closely contacted and the overall joint walls are push apart by a few contact points of feldspar as shown in Figure 6.10. It in turn, results in a larger

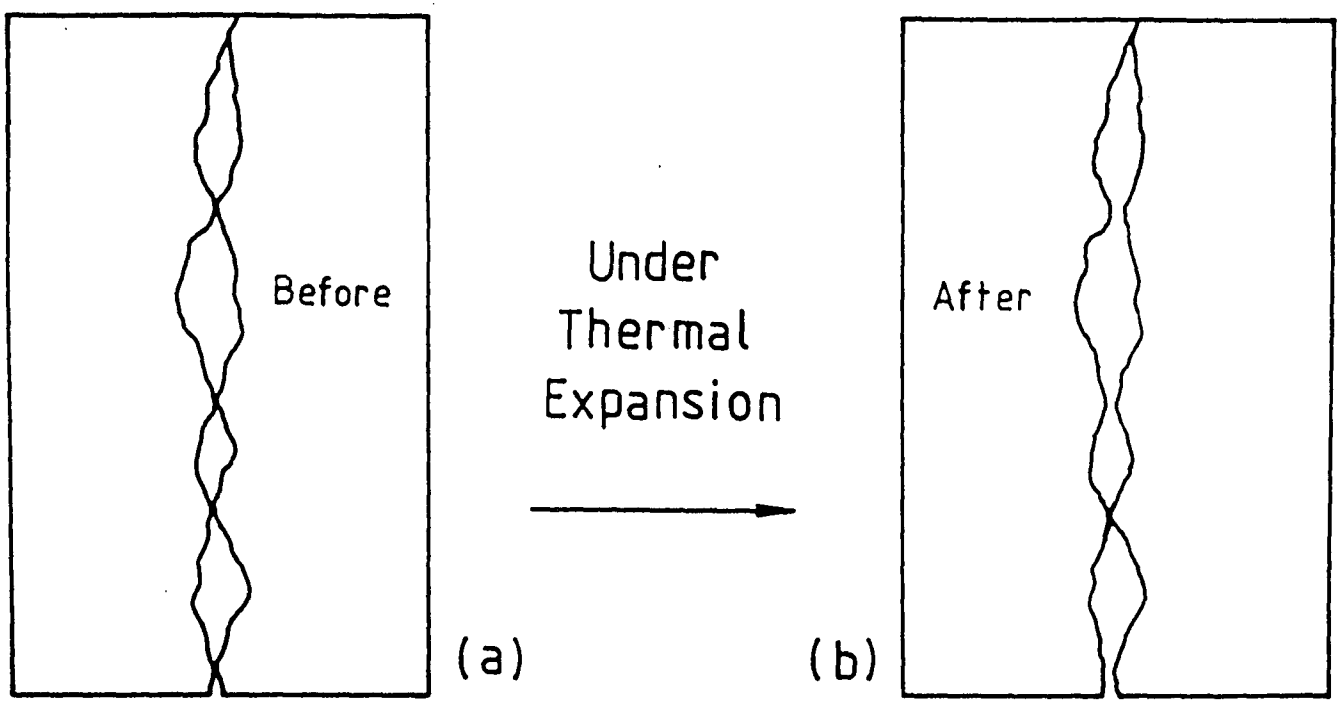


Figure 6.10 Mechanism of Joint Thermal Expansion.

mechanical aperture. This "expansion" of the joint due to the thermal mechanism is termed as the joint thermal expansion.

The joint thermal expansion may be significant at zero normal stress. When the joint is subject to an effective normal stress, the outwards expansion is resisted by the stress. This stress may be exceed the thermal stress pushing the joint walls apart and so the net result is joint closure.

Cook [1983] measured the thermally induced displacement (closure) in the rock mass at Stripa, Sweden, in a quartz monzonite at a depth of 340 meters below surface. Cook found that a consistent and pervasive result to emerge from these experiments was that all the measured values for the thermally induced displacements in the rock were only about half of the corresponding values calculated from the theory of linear thermo-elasticity. This puzzling phenomenon may easily be explained by the effect of joint thermal expansion mechanism, since the rock masses were under a stress of about 10 MPa (estimated value by knowing the site to be 340 m below surface), which was large enough to overcome the thermal stress; however, the closure was resisted by the effect of the tendency for joint expansion which therefore, reduced the overall thermal displacement.

However, the measured fluid permeabilities through the joints at elevated temperatures were reduced in most cases (except TF3, TF7 and TF11). The

permeability is dependent upon the equivalent hydraulic aperture of a joint. The equivalent hydraulic aperture of a joint differs from the mechanical aperture; it is not the mean of the distance apart of the overall joint walls, but rather depends on the critical narrow places in the joint. It is very easy to see in 2-dimensions that although the joint in Figure 6.11b has a much larger mechanical aperture than the joint in Figure 6.11a, it has a much smaller hydraulic conductivity. The following processes may be the possible mechanisms for the reducing of the fluid conductivity:

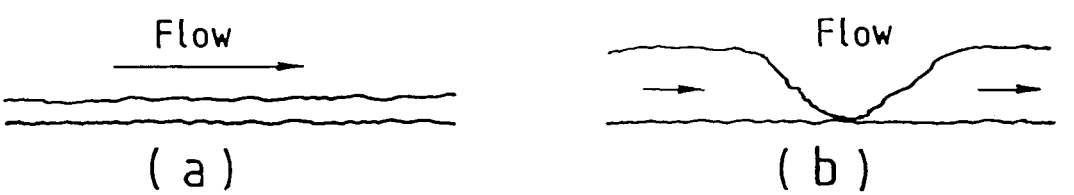


Figure 6.11 Schematics of Flow Through Joints.

1) non-homogeneous thermal expansion, particularly at some contacting area. The expansion of individual constituent material may reduce the aperture of some critical narrow places, and in some cases may even block them;

2) non-homogeneous precipitation of different material present in the joint;

3) precipitation in critical narrow places in the joint; the effect maybe to block some of the flow pathways;

4) crack healing at high temperatures and in the

presence of water;

5) appearance of small particles cracked at high temperatures and presence of water; the particles are specially critical if they block the joint at the narrow places.

Chapter 7

THERMAL ENERGY TRANSFER ANALYSIS AND EXPERIMENTAL STUDIES

7.1 Introduction

In a practical sense, the objective of Hot Dry Rock geothermal energy extraction is to mine the heat alone with fluid artificially circulated through the reservoir. Natural geothermal reservoirs may be categorized as either "vapour-dominated" or "liquid-dominated". In each case the name refers to the dominant mobile phase in the reservoir in its undisturbed state. Most reservoirs are liquid dominated. Once a Hot Dry Rock system is artificially saturated and circulated with fluid (water), the system can be treated as a liquid-dominated hot water type [Donaldson and Grant 1981].

The total heat contained in a geothermal reservoir may be computed if the volume of the reservoir is known and the fluid and rock properties and characteristics can be estimated. However, when this reservoir is mined, only a fraction of this heat energy may reach the end point of the operation. This is due to several factors, which may be included into two main categories --the efficiency of the extracting operation,

and the efficiency of the surface engineering procedures. The latter must depend upon the end use of the energy as well as on many local factors. It is thus appropriate here to consider and study only the below ground effects, i.e., the efficiency of the extracting operation.

The rate of removal of heat and fluid and the temperature of any reinjected fluid may be controlled by the end use demands. However, the below ground processes, the actual extraction of the heat energy from the geothermal reservoir, can be studied in general terms as if they were independent of that end use. Each form, or type, of reservoir (warm water, hot water, two phase, or vapour-dominated, general permeable or fracture controlled, HDR etc.) may behave differently. The study presented here is only concerned with the particular type of HDR reservoir with fluid circulated.

As noted earlier, it is assumed that the HDR system becomes a hot water type reservoir when the system is saturated with circulating fluid. It may be also assumed that the system is one involving single phase flow. Although, in some places, the water temperature may well over 100 ^{o}C (the boiling point of water under atomspheric pressure), due to the high pressure below ground, water may be remains as liquid. Variation of water boiling temperature with pressure is presented in Table 7.1. It shows that in a fully saturated geothermal system at the depth of 2000 meters (approximate 20 MPa), water will evaporate at the temperature of 364 ^{o}C.

Table 7.1 Variation of Water Boiling Temperature at Different Pressures [Shen et al 1965].

Pressure (MPa)	Applied pressure (MPa)	Equivalent appl. head (m H_2O)	Water boil. pt. temperature (°C)
0.1	--	--	99.09
0.103	0.0	0	100.00
0.2	0.1	10	119.62
0.3	0.2	20	132.88
0.4	0.3	30	142.92
0.5	0.4	40	151.11
0.6	0.5	50	158.08
1.1	1.0	100	183.20
1.5	1.4	140	197.36
2.0	1.9	190	211.38
3.0	2.9	290	232.76
4.0	3.9	390	249.18
6.0	5.9	590	274.29
8.0	7.9	790	293.62
10.0	9.9	990	309.53
12.0	11.9	1190	323.15
14.0	13.9	1390	335.09
16.0	15.9	1590	345.74
18.0	17.9	1790	355.35
20.0	19.9	1990	364.08
22.0	21.9	2190	372.10

7.2 Fundamentals of Heat Transfer

The problem of thermal energy extraction is actually a problem of mass and heat transfer. Flow mass transfer was discussed in the earlier chapters. Heat transfer includes the heat transfer from one point to another within the rock mass, and the heat transfer from rock to the circulating water. The two basic types or modes of heat transfer process relevant to a geothermal reservoir are conduction and convection. The third mode of heat transfer, which is assumed not to occur in the system, is radiation. In order to study thermal energy extraction in detail, it is important to understand the fundamental concepts of heat transfer by conduction and convection.

7.2.1 Thermal conduction

Heat conduction is the term applied to the mechanism of internal energy exchange from one body to another, or from one part of a body to another part, by the exchange of the kinetic energy of motion of the molecules by direct communication or by the drift of free electrons in the case of heat conduction in metals. This flow of energy or heat passes from higher energy molecules to the lower energy ones (i.e., from a high temperature region to a lower temperature region). The distinguishing feature of conduction is that it takes place within the boundary of a body, or across the boundary of a body into another placed in contact with

the first, without an appreciable displacement of the matter comprising the body.

The basic law governing heat conduction may best be illustrated by considering the simple, idealized situation shown in Figure 7.1. Consider a small plate section of material having a surface area A and a thickness Δx. Let one side be maintained at a temperature t_1, uniformly over the surface, and other side at temperature t_2. Let q denote the rate of heat flow (i.e., energy per unit time) through the plate, neglecting any edge effects. Experiments have shown that the rate of heat flow is directly proportional to the area A and the temperature difference $(t_1 - t_2)$ but inversely proportional to the thickness Δx [McAdams 1933]. This proportionality is made an equality by the definition of a proportionality k. Thus

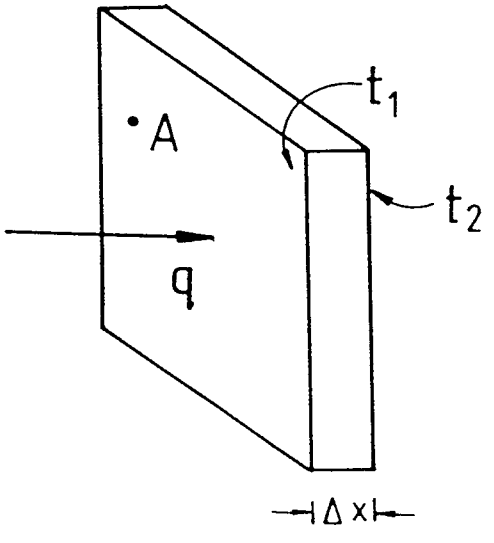


Figure 7.1 Thermal conduction.

$$q = k\,A\,\frac{(t_1 - t_2)}{\Delta x} \qquad (7.1)$$

The constant of proportionality, k, is called the thermal conductivity of the material of which the plate is composed. It is a property dependent only on the composition of the material, not on its geometrical configuration.

The general heat conduction equation which represents the volumetric heat balance, describing in differential form, the dependence of the temperature in the solid on the spartial coordinates and on time can be found in major textbooks on heat transfer, e.g., McAdams [1933] and Holman [1986]. It is expressed as

$$\frac{\partial t}{\partial \tau} = \frac{k}{\rho c_p}\left(\frac{\partial^2 t}{\partial x^2} + \frac{\partial^2 t}{\partial y^2} + \frac{\partial^2 t}{\partial z^2}\right) + \frac{q'}{\rho c_p}$$

$$= \alpha(\nabla^2 t) + \frac{q'}{\rho c_p} \qquad (7.2)$$

where t = temperature,

τ = time,

k = thermal conductivity,

ρ = density,

c_p = specific heat,

q' = internal heat generation rate per unit volume,

x, y, z = perpendicular coordinate directions.

The quantity

$$\alpha = \frac{k}{\rho c_p} \tag{7.3}$$

is called the thermal diffusivity and is seen to be a physical property of the material of which the solid is composed.

For any problem of steady condition, $\partial t/\partial \tau = 0$, since there is no variation of temperature with time. In the absence of internal heat generation, Laplace's equation is obtained

$$\frac{\partial^2 t}{\partial x^2} + \frac{\partial^2 t}{\partial y^2} + \frac{\partial^2 t}{\partial z^2} = 0$$

or $$\nabla^2 t = 0 \tag{7.4}$$

7.2.2 Fluid motion and heat convection

Convection is the term applied to the heat transfer mechanism which occurs in a fluid by the mixing of one portion of the fluid with another portion due to gross movement of the mass of fluid. The actual process of energy transfer from one fluid particle or molecule to another is still one of conduction, but the energy may be transported from one point in space to another by the displacement of the fluid itself.

The fluid motion may be caused by external means (e.g., by a fan, pump, etc.), in which case the process is called forced convection. If the fluid motion

is caused by density differences which are created by the temperature differences existing in the fluid mass, the process is termed free convection or natural convection.

It is virtually impossible to observe pure heat conduction in a fluid because as soon as a temperature difference is imposed on a fluid, natural convection currents will occur as a result of density differences.

The basic laws of heat conduction must be coupled with those of fluid motion in order to describe, mathematically, the process of heat convection. The mathematical analysis of the resulting system of differential equations is perhaps one of the most complex fields of applied mathematics. Thus, for engineering application, convection analysis will seen to be a subtle combination of powerful mathematical techniques and the intelligent use of empiricism and experience.

Later sections will consider analytical solutions to forced convection of heat transfer relating with fluid motion in some detail. The analytical solutions are based on the boundary layer concept. As should be apparent from the discussion, the prediction of the rates at which heat is convected away from a solid surface by an ambient fluid involves a through understanding of the principles of heat conduction, fluid dynamics and boundary layer theory. All the complexities involved in such an analytical approach may be lumped together in terms of a single parameter by introduction of Newton's law of cooling:

$$\frac{q}{A} = h\ (\ t_1 - t_2) \qquad (7.5)$$

The quantity h in this equation is generally known as heat transfer coefficient. It is seen to be a unit conductance, not a material property as is thermal conductivity. It is a complex function of the composition of the fluid, the geometry of the solid surface and the hydrodynamics of the fluid motion past the surface. The typical range of values one might expect to encounter for h varies tremendously which indicates the complexity of the convective process and the difficulty in determining h. Section 7.4 will present detailed analyses of the determination of the heat transfer coefficient for parallel plate flow.

7.3 Experimental Results of Thermal Conductivity of Granite

7.3.1 Testing theory

Measurements of thermal conductivity were made using the transient line heat source method [Woodside and Messmer 1961, Enniss 1979b]. This method uses a line heat source, i.e., a straight wire through which is passed a constant electric current, and a temperature sensitive device (e.g., thermocouple or resistance thermometer). The two elements are embedded alongside each other in the sample under test. When the assembly is at a uniform and

constant temperature, constant power is supplied to the heater and the rise of temperature is recorded during the short heating interval. the rate of rise of temperature is determined by the ability of the test sample to conduct the heat generated away from the line heat source. The thermal conductivity of the sample may be calculated from the temperature - time record and the power input. The theory on which the method is based is developed by Carslaw and Jaeger [1959].

Theory

The equation governing the temperature, T, at a point in an infinite mass containing an uniform linear heater can be determined as [Carslaw and Jaeger 1959]:

$$T(r,\tau) = \frac{P}{2\pi k}\left[\frac{r}{2(\alpha\tau)^{1/2}}\right] \qquad (7.6)$$

where P = power input per unit length of heat source,

k = thermal conductivity of the mass,

α = thermal diffusivity of the mass,

r = radial distance from heat source,

τ = time from start of energy input, and

I is the function

$$I(x) = C - \ln x + \frac{x}{2} - \frac{x^2}{8} + \cdots \qquad (7.7)$$

where C is Euler's constant, 0.5772.

Considering the case where the radial distance

become very small ($r \rightarrow 0$), the term $x = [\, r / 2(\alpha\tau)^{1/2}]$ also becomes very small. Assuming that this situation occurs in the experimental set up, the terms in the expansion of $I(x)$ of order x^2 and higher can be regarded as negligible. This assumption appears to be good for the present experimental system as the thermocouple is attached directly to the line heater.

Therefore, Equation (7.6) may be written

$$T(r,\tau) = \frac{P}{2\pi k}\left[\, C - \ln \frac{r}{2(\alpha\tau)^{1/2}}\right] \qquad (7.8)$$

The temperature rise, T, between times and can be described

$$\Delta T = T(r, \tau_2) - T(r, \tau_1) \qquad (7.9)$$

Using Equation (7.8), this expression with some algebraic manipulation gives:

$$T = \frac{P}{4\pi k} \ln \frac{\tau_2}{\tau_1} \qquad (7.10)$$

From Equation (7.10) it can be seen that term ($P / 4\pi k$) represents the slope of T versus ln (τ) curve. With carefully monitored voltages and current applied to the line heat source, the power dissipated per unit length, P, can be determined allowing the calculation of the thermal conductivity, k.

Several major sources of error are possible in this method. The first is due to the elimination of the higher order of the I(x) function. Direct attachment of

the thermocouple eliminates this error. Secondly, the contact resistance of the probe to the sample can influence the time-temperature curve. This error is eliminated by the use of a standardized, highly conductive potting compound and disregarding the initial portion of the curve. Finally, the power input to the probe can vary due to the change of resistance of the probe with temperature. This effect can be minimized by the use of a constant current power supply and careful monitoring of the probe voltage. Probes showing a voltage variation greater than 1% are not used.

7.3.2 Testing methods and results

A section through the sample stack assembly that was used to implement this method in the Terra Tek System is shown in Figure 7.2. The sample preparation procedures have already been described in Chapter 3. In addition, a 6.5mm diameter hole was drilled along the central axis of each sample. The outside wall of the sample acted as a constant temperature heat sink. Axial heat losses were minimized by using ceramic sample end caps, so that the only flow of heat was radially from the heat source to the sample walls.

During each test the sample was located within the triaxial cell of the Geothermal Rock Test Facility described in Chapter 3. At the start of each test the sample was in an air dried state. The pore space was then evacuated of air before being saturated with the desired

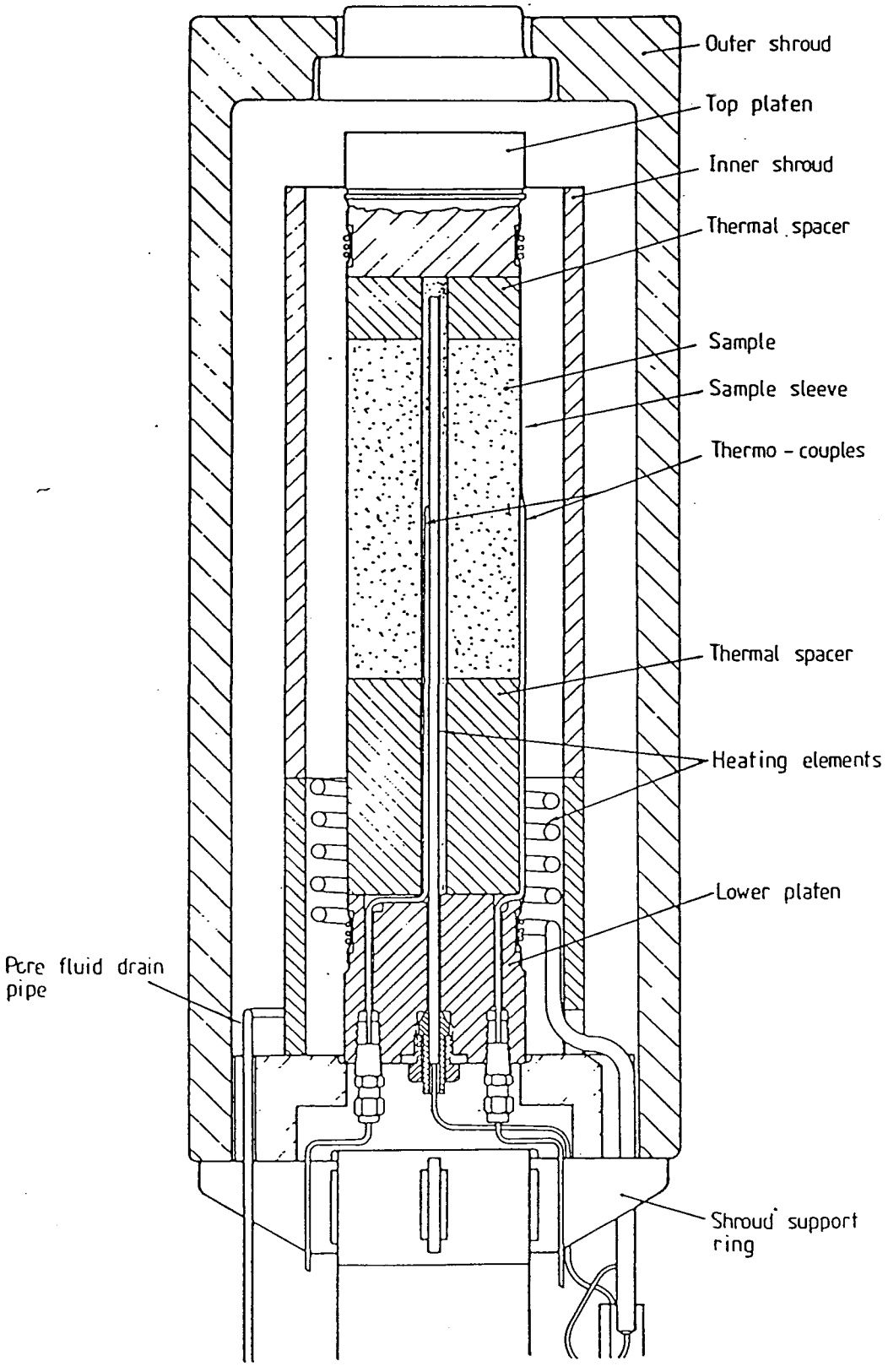


Figure 7.2 Stack Assembly for Thermal Conductivity Test.

fluid. The pressure of the oil filling the cell provided hydrostatic loading to the sleeved sample, and the elevated oil temperature was generated by an immersed heating coil. A Watt meter (1% accuracy) was used to measure the power supply. The rise in temperature recorded by the thermocouple located alongside the line heater was timed in 1°C increments over a 10°C rise. The power was regulated to achieve a total heating interval of about 60 seconds (approximately 8 Watts). Each measurement was repeated twice before incrementing the confining stress, pore pressure or sample temperature. Sufficient time was given between measurements to allow a return to uniform temperature and stress condition.

A typical example of the temperature - time profiles obtained for each heating cycle is shown in Figure 7.3. The thermal conductivity measurement can be determined from the gradient of this line using,

$$\text{Gradient} = \frac{P}{4 \pi k}$$

where P is the electrical power per unit length supplied to the heater and k is the thermal conductivity of the sample. The theory which this method is based was described in previous section.

The reliability and repeatability of this method was checked using a Duran glass calibration specimen. The measured conductivity agreed with that quoted by the sample manufacturers to an accuracy of 8.5% for the optimal power supply. It was found that very low

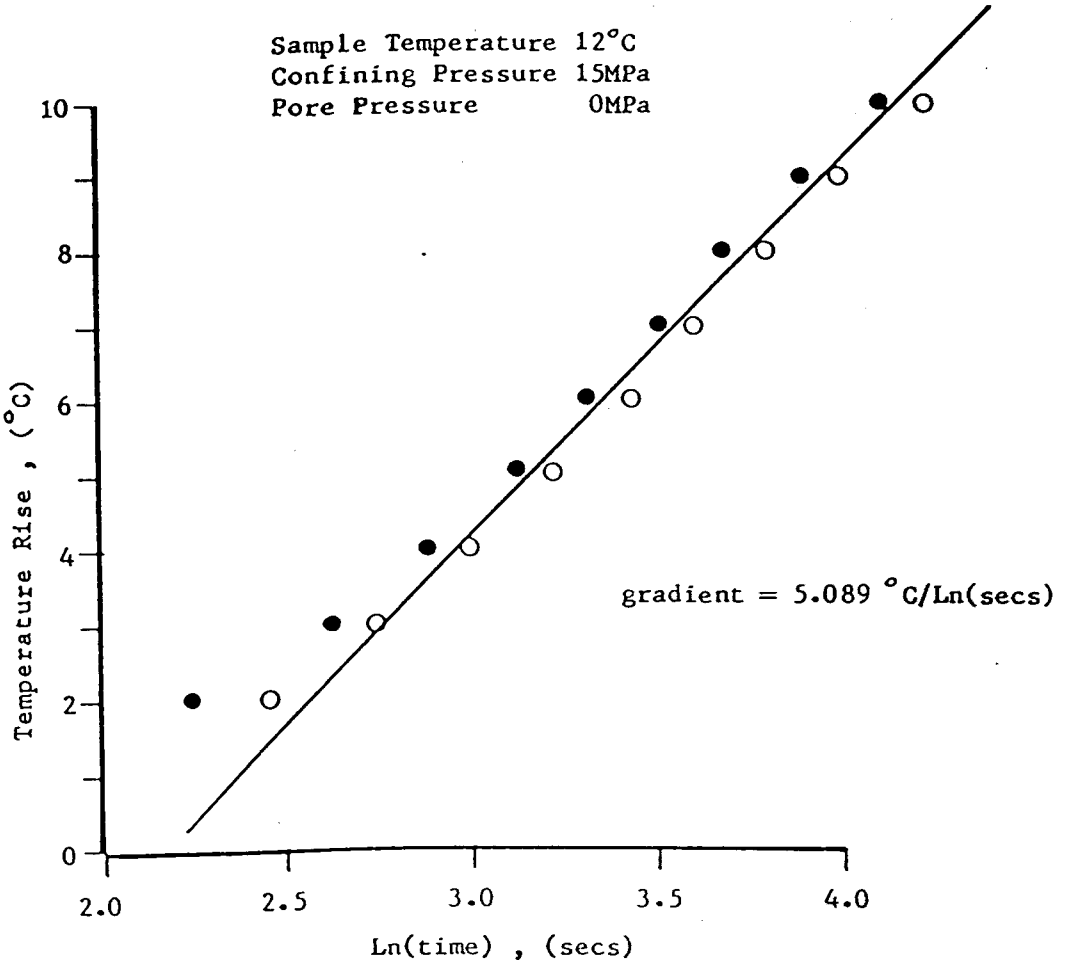


Figure 7.3 Typical Temperature - Time Plot for a Thermal Conductivity Measurement (After Elliott 1985).

or very high power supply rates resulted in temperature - time profiles to which it was difficult to fit unique straight lines. This may have been an indication of the quality of thermal contact between the heater and the specimen. Nevertheless, this optimal power supply was used in tests on the granite.

The results of a series of thermal conductivity measurements made at different stresses, temperatures and pore fluid pressures are shown in Figure 7.4. The results indicate that effective stress, and the presence of a pore fluid have little influence on the measured conductivity. They also suggest that thermal conductivity is influenced slightly by sample temperature and pore pressure, but no particular trend emerges. However, these influences are sufficiently small that, here too, it may be more convenient to concluded that no appreciable influence is detected above that of normal experimental variation.

This response is not altogether unexpected in view of the very low porosity of the rock and the crystalline nature of its constituents. If one considers rock to be a two-phase medium for the purpose of heat flow, it is reasonable to expect that the measured conductivity should be a function of the individual conductivities and volumetric proportions of the solid phase (that forms the rock structure) and the fluid phase (which is contained within the voids formed by the rock structure). The conductivity of the solid phase may be

influenced by effective stress and temperature, and the conductivity of the fluid phase may be influenced by pore pressure and temperature. In a rock where the porosity is so low as to be assumed negligible under normal circumstances, it follows that the contribution of the fluid phase conductivity will be negligible, and hence the influence of the pore pressure will also be very small. Low porosity also implies a very dense structure with high bulk modulus and good grain to grain contact, hence the influence of effective stress might be small over a finite stress range.

7.4 Analytical Solutions for Forced Convection Between Parallel Plates

7.4.1 General considerations

In section 7.2.2, heat convection and the surface heat transfer coefficient, h, were defined. In general applications, h, defined by Newton's law of cooling in Equation (7.5) is presumed known. However, the actual value of h is dependent not only on material properties, but also on the individual geometry of the solid surface and on the hydrodynamics of the fluid. Thus, the purpose of this section is to discuss and develop methods of predicting the values of the heat transfer coefficient of forced convection between parallel plates.

In the case of convection, the analytical

approach to the determination of the heat transfer coefficient would involve the finding of the temperature distribution in the fluid flow passing the solid body surface. If, as is usually the case, the fluid motion in the region immediately adjacent to the surface is laminar, then the heat flux from the surface may be evaluated in terms of the fluid temperature gradient at the surface as illustrated in Figure 7.5. Then the definition of the heat transfer coefficient as the ratio of the heat flux to the difference between the surface temperature and the fluid temperature enables one to write

$$h = \frac{-k_f \, (dt/dn)}{t_s - t_f} \tag{7.11}$$

where k_f = thermal conductivity of the fluid,

t_s = temperature of the solid surface,

t_f = temperature of fluid far removed from surface,

dt/dn = fluid temperature gradient, measured at the surface in a direction normal to the surface.

In order to find the temperature distribution in the fluid so that the above formulation can be used to determine h, it is then necessary to solve the complete fluid mechanics problem in the region near the surface. For the general case of the motion of a convecting fluid in three dimensions a complete description of the fluid motion requires the determination of the three velocity components, the fluid pressure, the fluid temperature,

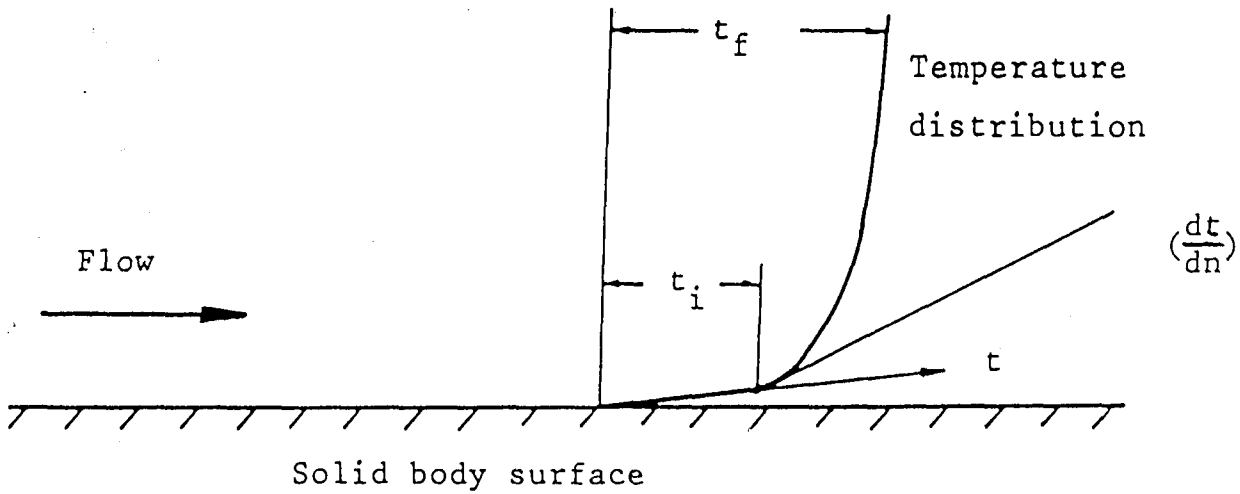


Figure 7.5 Temperature Distribution of Flow between Parallel Plates.

and fluid density --all as functions of position and time. Six equations are required to find these six dependent variables. Newton's law of motion in each of the three coordinate directions yields three partial differential equations, and two additional partial differential equations are obtained from applying the principles of conservation of mass and conservation of energy. The equation of state of the fluid furnishes the sixth algebraic equation.

The general problem requires the simultaneous solution of these six equations, under the appropriate boundary conditions, so that the fluid temperature gradient at the wall may be found to yield h. Such general solutions have been obtained in only a few cases of practical significance. Thus, certain approximate methods of solution must be sought. Most textbooks give detailed methods of solving the above mentioned equations. The related analytical solutions presented in the following section are those given by Chapman [1984].

7.4.2 Working formulae

Four groups of physical parameters are the sought for similarity parameters for the general case of the flow of a viscous fluid past a heated surface. They are:

$$Re = \frac{U\,l}{\nu} = \text{the Reynolds number,} \qquad (7.12)$$

$$Gr = \frac{g\,l^3 \alpha\,\Delta t}{\nu^2} = \text{the Grashof number,} \qquad (7.13)$$

$$Ec = \frac{U^2}{c_p \Delta t} = \text{the Eckert number,} \qquad (7.14)$$

$$Pr = \frac{\mu c_p}{k} = \frac{\nu}{\alpha} = \text{the Prandtl number.} \qquad (7.15)$$

where l = characteristic length,

U = characteristic velocity,

$\Delta t = t_1 - t_2$ = characteristic temperature difference,

$pU/2$ = characteristic pressure,

ν = kinematic viscosity,

g = acceleration due to gravity,

c_p = specific heat,

μ = dynamic viscosity,

k = thermal conductivity,

α = thermal diffusivity.

The Reynolds number, Re, represents a measure of the magnitude of the inertia forces in the fluid to the viscous forces. The Grashof number, Gr, is a measure of the ratio of the buoyant forces to the viscous forces and is absent if buoyancy is neglected. The Eckert number, Ec, is a measure of the thermal equivalent of the kinetic energy of the flow to the imposed temperature difference and arises from the inclusion of the viscous dissipation term in the energy equation. Hence, Ec, is absent when dissipation is neglected. The Prandtl number, Pr, unlike the others, is composed only of physical fluid properties and represents one of the most significant heat transfer parameters. It is a measure of the relative magnitude of the diffusion of momentum, through velocity,

and the diffusion of heat, through conduction, in the fluid.

The ultimate result desired is the heat transfer coefficient, h, defined earlier as

$$h = \frac{-k_f \, (dt/dn)}{t_s - t_f} \tag{7.11}$$

where (dt/dn) represents the fluid temperature gradient at the solid body surface measured in a direction that normal to the surface. If the dimensionless variables $\varphi = (t - t_s)/\Delta t$ and $\bar{n} = n/l$ are introduced, the above definition of h becomes

$$Nu = \frac{h\, l}{k} = -\left(\frac{\partial \varphi}{\partial \bar{n}}\right) \tag{7.16}$$

Thus, a dimensionless heat transfer coefficient has been defined:

$$Nu = \frac{h\, l}{k} = \text{the Nusselt number} \tag{7.17}$$

The dimensionless variables may be represented by the functional relation

$$= f\,(\xi, \eta, Re, Gr, Ec, Pr) \tag{7.18}$$

By use of the definition, Equations (7.16) and (7.18) yield

$$Nu = f\,(\xi, \eta, Re, Gr, Ec, Pr) \tag{7.19}$$

Thus, one expects that the local Nusselt number (i.e., the local heat transfer coefficient) will depend on the position on the solid body surface and Re, Gr, Ec and Pr. Often it will be desirable to evaluate an average h, or an average Nu, by appropriately integrating over the body surface. The resultant average Nusselt will have the following functional dependence:

$$Nu = f\ (Re,\ Gr,\ Ec,\ Pr) \tag{7.20}$$

In pure forced convection, one often neglects any effect of buoyant forces so that

$$Nu = f\ (Re,\ Ec,\ Pr) \tag{7.21}$$

When viscous dissipation is neglected, and

$$Nu = f\ (Re,\ Pr) \tag{7.22}$$

For laminar flow past parallel flat plates, the analytical expressions of Equation (7.22) for the local and average Nusselts number have been verified experimentally and are recommended [Chapman 1984] for use as

$$Nu_x = 0.332\ Re_x^{1/2}\ Pr^{1/3} \tag{7.23}$$

$$Nu_\ell = 0.664\ Re_\ell^{1/2}\ Pr^{1/3} \tag{7.24}$$

$$\left\{\begin{array}{l} 0.6 < Pr < 50 \\ Re < Re_{} = 5\times10^5 \\ \text{properties at } t_m \end{array}\right\}$$

where t_m is the mean film temperature

$$t_m = (t_1 + t_2)/2 \qquad (7.25)$$

Churchill and Ozoe [1973] recommend the following semi-empirical relations:

$$Nu_x = \frac{0.3387\ Re_x^{1/2}\ Pr^{1/3}}{[\ 1 + (0.0468/Pr)^{2/3}]^{1/4}} \qquad (7.26)$$

$$Nu_\ell = \frac{0.06674\ Re_\ell^{1/2}\ Pr^{1/3}}{[\ 1 + (0.0468/Pr)^{2/3}]^{1/4}} \qquad (7.27)$$

$$\left\{\begin{array}{l} Re\ Pr > 100 \\ \text{properties at } t_m \end{array}\right\}$$

At a given condition, the mean film temperature, t_m, can be estimated by using Equation (7.26). At this temperature, the physical properties of the fluid (water in the case presented) are to be found in handbooks and textbooks (e.g., Kaye and Lamb [1966], Eckert and Drake [1959], Rohsenow and Choi [1961], and Chapman [1984]), including the Prandtl number, Pr. However, in the experiments conducted and presented in this report, the flow temperatures were only measured at the inlet and outlet. Hence, the analytical solution should give the results on the average heat transfer coefficient over the plate length. By using given physical properties (α, ν, k) of fluid, the velocity of the flow, v, and the plate length l, the plate length Reynolds number can be calculated using Equation (7.12).

The plate length Nusselt number therefore, can be estimated from Equations (7.24) or (7.27). By rewritting Equation (7.17), the average heat transfer

coefficient h over the plate length l is given by,

$$h = Nu \frac{k}{l} \tag{7.28}$$

It must be noted that the above analytical solutions are used for laminar flow, pure forced convection heat transfer (i.e., buoyancy neglected) and with the dissipation of mechanical energy through viscous friction neglected. To calculate the local Nusselt number for turbulent flow, on the basis of experimental evidence Colburn [1933] recommends:

$$Nu_x = 0.0296\ Re_x^{0.8}\ Pr^{1/3} \tag{7.29}$$

$$5\times10^5 < Re < 10^7$$

$$Nu_\ell = 0.185\ Re_\ell (\log_{10} Re_\ell)^{-2.584}\ Pr^{1/3} \tag{7.30}$$

$$Re > 10^7$$

$$\left\{ \begin{array}{l} 0.6 < Pr < 60 \\ \text{properties at } t_m \end{array} \right\}$$

However, for turbulent flow past flat plates, the average values of Nusselt number must account for an initial laminar section. Cases for such average, mixed flow are treated. The average Nusselt number then becomes:

$$Nu_\ell = (0.037\ Re_\ell^{0.8} - 872) Pr^{1/3} \tag{7.31}$$

$$5\times10^5 < Re < 10^7$$

$$Nu_\ell = [0.228\ Re_\ell (\log_{10} Re_\ell)^{-2.584} - 872) Pr^{1/3} \tag{7.32}$$

$$10^7 < Re < 10^9$$

$$\left\{ \begin{array}{c} 0.6 < Pr < 60 \\ Re_x = 5 \times 10^5 \\ \text{properties at } t_m \end{array} \right\}$$

Thus, to calculated the heat transfer coefficient, h, for turbulent flow, the calculation procedure will follow that discussed earlier for laminar flow, but using Equations (7.31) or (7.32) instead of Equations (7.24) or (7.27).

7.5 Total Heat Transfer Coefficient

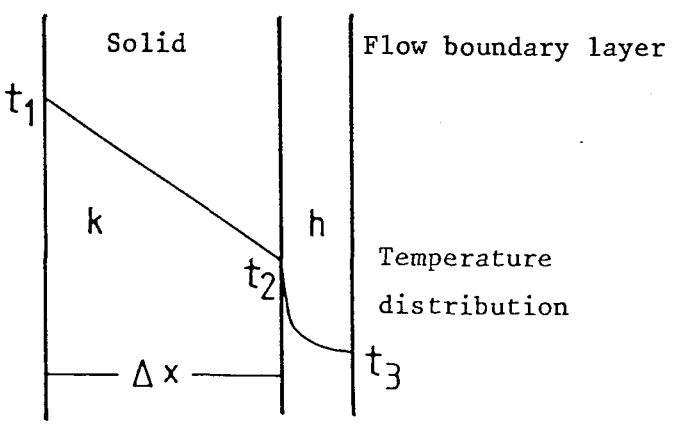


Figure 7.6 Combined Effect of Conduction and Convection.

For general engineering purposes, in cases such as Hot Dry Rock geothermal energy extraction, it might be more practical to define a total heat transfer coefficient accounting for both thermal conduction and heat convection. As shown in Figure 7.6, the heat flow per unit wall area may be written for each "layer" as:

$$\frac{q}{A} = \frac{k}{\Delta x}(t_1 - t_2)$$

$$\frac{q}{A} = h\,(t_2 - t_3)$$

For overall effect is, thus,

$$q = \frac{t_1 - t_3}{\Delta x/kA + 1/hA} \qquad (7.33)$$

where $\Delta x/kA$ and $1/hA$ are usually termed the thermal conduction resistance and convective thermal resistance.

Equation (7.33) may be re-written

$$q = A\left(\frac{1}{\Delta x/k + 1/h}\right)(t_1 - t_3) \qquad (7.31)$$

The value

$$M = \left(\frac{1}{\Delta x/k + 1/h}\right) \qquad (7.32)$$

can be considered as equivalent to the total heat transfer coefficient with the same units as h. Its value and significance will be discussed later in sections 7.6 and 7.7.

7.6 Analysis and Results of Heat Transfer Measurement

The measurements on flow and rock temperatures were collected as described in section 3.3.2. The

situation described in the experiment is clearly a 3-dimensional one, since the temperature varies across the joint and the flow. For reasons of simplicity and practical feasibility, the system is simplified into a 2-dimensional one, as shown in Figure 7.7.

During the tests, the measurements of temperatures T , t_1, t_2 were made, while water was injected at one end with inlet temperature of t_1 . The hydraulic aperture of joint and the flow velocity is calculated from measured flow rate. By balancing the total heat conduction within the rock from oil surrounding surface to interface with water, and the total thermal energy received by the water, the average temperature at rock-fluid interface t_s, is calculated. By finding the mean film temperature t_m , as stated in section 7.4.2, the heat transfer coefficient can be found.

However, several assumptions are made to simplify the analysis; they are as follows

1) The system is 2-dimensional, and the two semi-cylindrical rock bodies are treated as two rectangular parallelpiped bodies with the same width. The height of the rectangular parallelpiped bodies is assumed to be that giving cross-sectional area equal to that of the cylindrical body.

2) The system is symmetrical and heat sources are only applied on the outer surface of the bodies

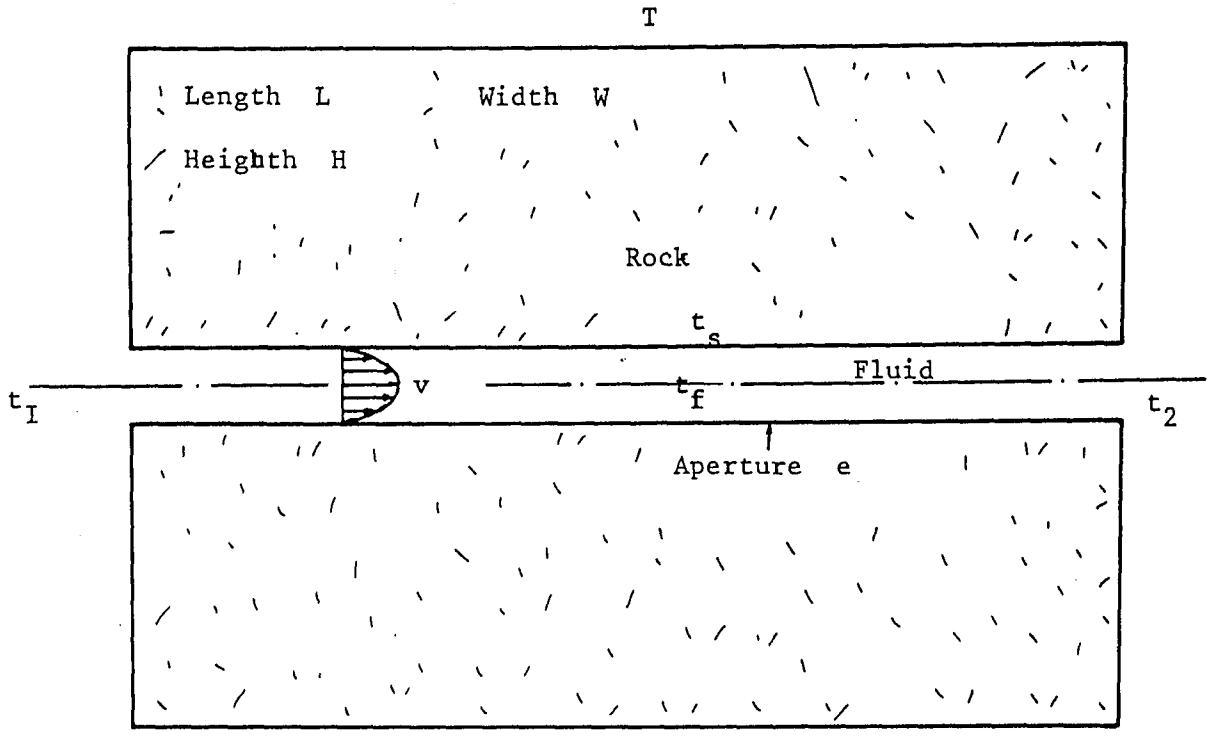


Figure 7.7 2-dimensional Representation of Heat Transfer System.

Table 7.2a Results of Heat Transfer Coefficient Calculations.

Sample Temperature 90°C

Flow velocity mm/S	Inlet temp. °C	Outlet temp. °C	Heat Transfer coefficient $W/m^2-°C$	Total Heat trans. coeff. $W/m^2-°C$
Joint Aperture = 19.17 μm				
10.63	42	87	307.8	113.0
15.31	42	87	372.1	120.7
20.52	41	87	429.1	126.1
25.54	40	87	477.5	130.0
30.08	39	87	518.3	132.8
50.26	37	87	662.2	140.7
76.46	34	87	813.7	146.4
97.75	31	86	924.6	149.7
Joint Aperture = 24.66 μm				
23.06	41	88	453.8	128.1
28.22	40	88	502.0	131.7
35.21	38	88	561.5	135.5
49.21	36	88	659.0	140.5
Joint Aperture = 26.56 μm				
7.18	44	88	257.9	105.5
10.41	43	88	301.0	112.1
12.10	42	88	325.0	115.3
14.43	41	88	355.4	118.9
18.59	40	88	404.0	123.8
Joint Aperture = 30.52 μm				
4.44	44	88	202.2	94.8
6.25	44	88	237.6	102.0
8.20	43	88	268.7	107.3
9.41	43	88	287.8	110.2
10.93	42	88	310.2	113.3
11.74	41	88	321.5	114.8

Table 7.2b Results of Heat Transfer Coefficient Calculations.

Sample Temperature 100°C

Flow velocity mm/S	Inlet temp. °C	Outlet temp. °C	Heat Transfer coefficient $W/m^2-°C$	Total Heat trans. coeff. $W/m^2-°C$
Joint Aperture = 15.85 μm				
42.25	65	96	630.3	139.2
60.86	64	96	757.4	144.5
82.30	62	96	885.0	148.6
102.57	60	96	987.9	151.2
128.20	59	95	1104.5	153.7
Joint Aperture = 16.44 μm				
40.30	62	95	616.3	138.5
60.02	59	95	755.7	144.4
66.09	59	95	793.0	145.8
78.60	58	95	864.8	149.1
Joint Aperture = 16.98 μm				
25.88	61	97	493.9	131.2
53.73	57	96	715.0	142.9
59.46	57	96	752.2	144.4
70.24	56	96	817.5	148.0
78.62	55	96	901.5	149.0
Joint Aperture = 21.16 μm				
22.40	54	94	461.7	128.8
32.79	54	94	558.6	135.3
42.03	53	94	632.4	139.3
63.50	50	94	771.9	145.0
77.45	46	93	852.5	147.7

Table 7.2c Results of Heat Transfer Coefficient Calculations.

Sample Temperature 120°C

Flow velocity mm/S	Inlet temp. °C	Outlet temp. °C	Heat Transfer coefficient $W/m^2-°C$	Total Heat trans. coeff. $W/m^2-°C$
Joint Aperture = 11.95 μm				
63.38	71	117	820.2	146.6
83.00	67	117	938.6	150.6
106.21	64	117	1061.7	152.9
129.64	62	117	1173.0	155.0
155.20	59	117	1283.5	156.8
Joint Aperture = 13.45 μm				
71.11	66	118	853.7	147.7
102.42	62	118	1042.6	152.5
140.80	58	117	1183.4	155.2
167.60	56	117	1291.1	156.9
203.72	55	117	1423.5	158.7
Joint Aperture = 16.72 μm				
63.80	61	118	808.6	146.3
84.17	57	118	928.7	149.8
119.71	54	117	1091.2	153.5

Table 7.2d Results of Heat Transfer Coefficient Calculations.

Sample Temperature 140°C

Flow velocity mm/S	Inlet temp. °C	Outlet temp. °C	Heat Transfer coefficient $W/m^2-°C$	Total Heat trans. coeff. $W/m^2-°C$
Joint Aperture = 14.50 μm				
51.25	84	131	728.6	143.4
71.17	81	131	860.3	147.9
95.48	80	131	996.4	151.4
118.95	79	131	1098.1	153.6
Joint Aperture = 15.50 μm				
69.42	78	130	838.9	147.2
93.92	74	130	975.8	151.0
114.37	73	129	1070.8	153.1
135.77	71	128	1184.23	155.2
Joint Aperture = 16.45 μm				
8.47	78	137	296.8	111.5
14.53	75	134	388.7	122.4
23.83	72	131	497.8	131.4
36.10	69	126	606.3	137.9
45.75	67	124	682.6	141.5
Joint Aperture = 18.09 μm				
32.11	81	128	577.9	136.4
44.12	79	128	677.4	141.3
55.29	75	128	758.3	144.5
72.14	72	128	857.1	147.8
85.11	70	128	930.9	149.8
Joint Aperture = 19.72 μm				
24.54	79	131	505.2	131.9
36.80	75	131	618.6	138.6
44.40	72	128	684.2	141.5
75.71	66	127	884.3	148.6
89.09	63	127	957.3	150.6

parallel to the joint. Heat applied on other sides is neglected.

3) Edge effects are neglected.

4) During the calculations, to enable estimates to be made of the temperature at the rock-fluid interface, the energy extracted and transferred by flow is assumed to be equal to the heat transferred by conduction in rock, without any effects of energy dissipation and losses.

The calculated results for heat transfer h and total heat transfer coefficient M are shown in Table 7.2. The heat transfer coefficient h, varies from 200 to 1400 W/m^2-^oC, and is a function of flow velocity, temperatures, and joint geometry. The relations will be described in later sections.

7.7 Discussion

As noted in the previous section, the heat transfer coefficient is related to and influenced by flow velocity, temperature and joint geometry; the relations are discussed in following text.

7.7.1 Flow velocity - heat transfer coefficient

Theoretically, the analytical Equation (7.28) gives

$$h = Nu \frac{k}{l} \qquad (7.28)$$

and $$Nu_l = 0.664\ Re_l^{1/2} Pr^{1/3} \qquad (7.24)$$

where $$Re = \frac{U\ l}{\nu} \qquad (7.12)$$

By combining the above equations (7.12, 7.24, 7.28), we obtain

$$h = 0.664\ Pr^{1/3} \frac{k}{l} \left(\frac{l}{\nu}\right)^{1/2} v^{1/2}$$

or $$h = \frac{0.664\ k\ Pr^{1/3}}{(l\nu)^{1/2}} v^{1/2} \qquad (7.36)$$

i.e., $$k \propto v^{1/2}$$

But $Pr = \nu/2$ and $\alpha = k/\rho c_p$, so

$$h = \frac{0.664\ (k^2 \rho\ c_p)^{1/3}}{(l^2 \nu)^{1/6}} v^{1/2} \qquad (7.37)$$

Because k, ρ, c_p and ν are affected by temperature, Equation (7.37) indicates that the value of h is only influenced by the temperature condition and the flow velocity. Fig 7.8 shows plots of h against $\sqrt{v}$ for different apertures and inlet water temperatures. The figures clearly indicate that h is directly proportional to $\sqrt{v}$ despite the effects of inlet water temperature or joint aperture.

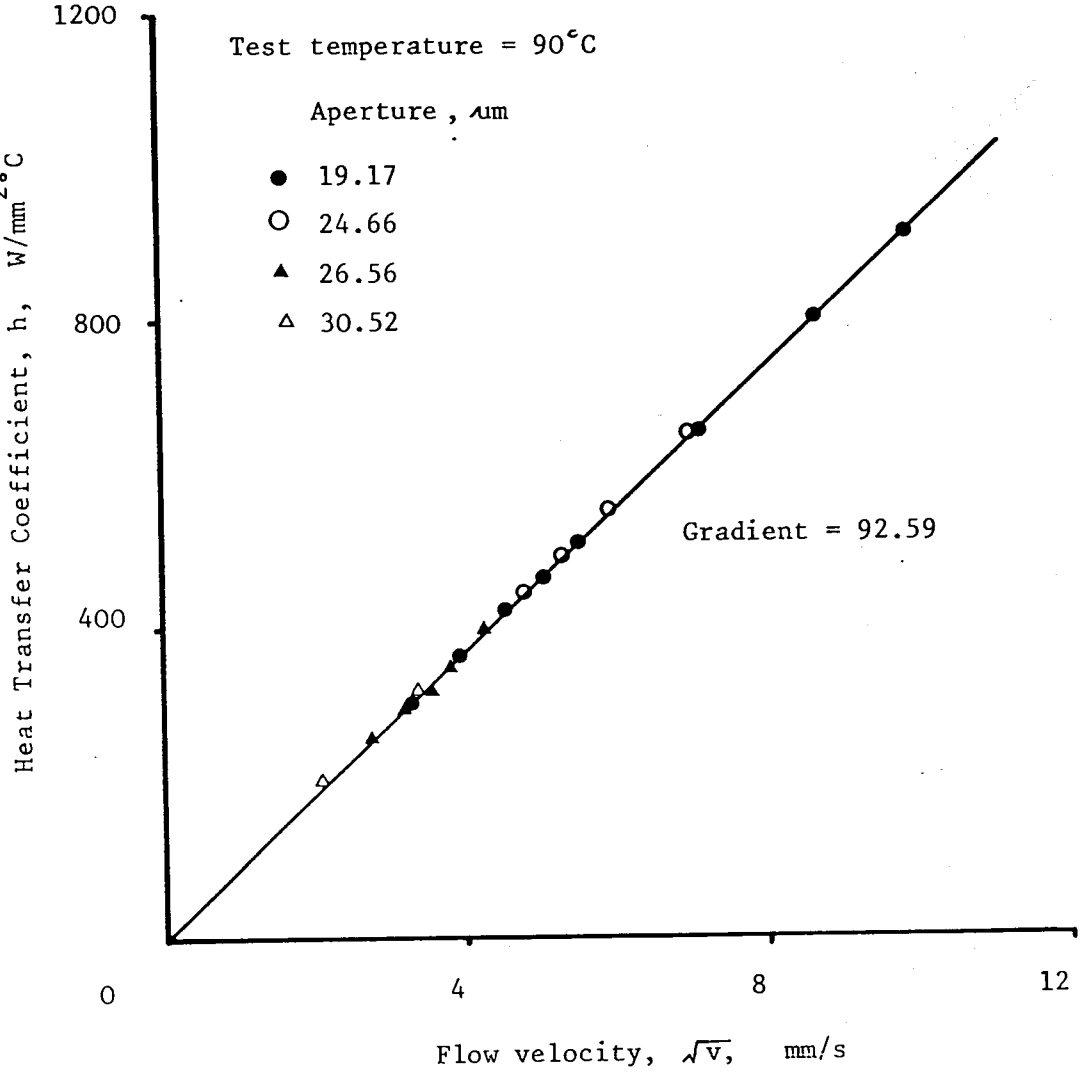


Figure 7.8 Variation of Heat Transfer Coefficient with Flow Velocity.

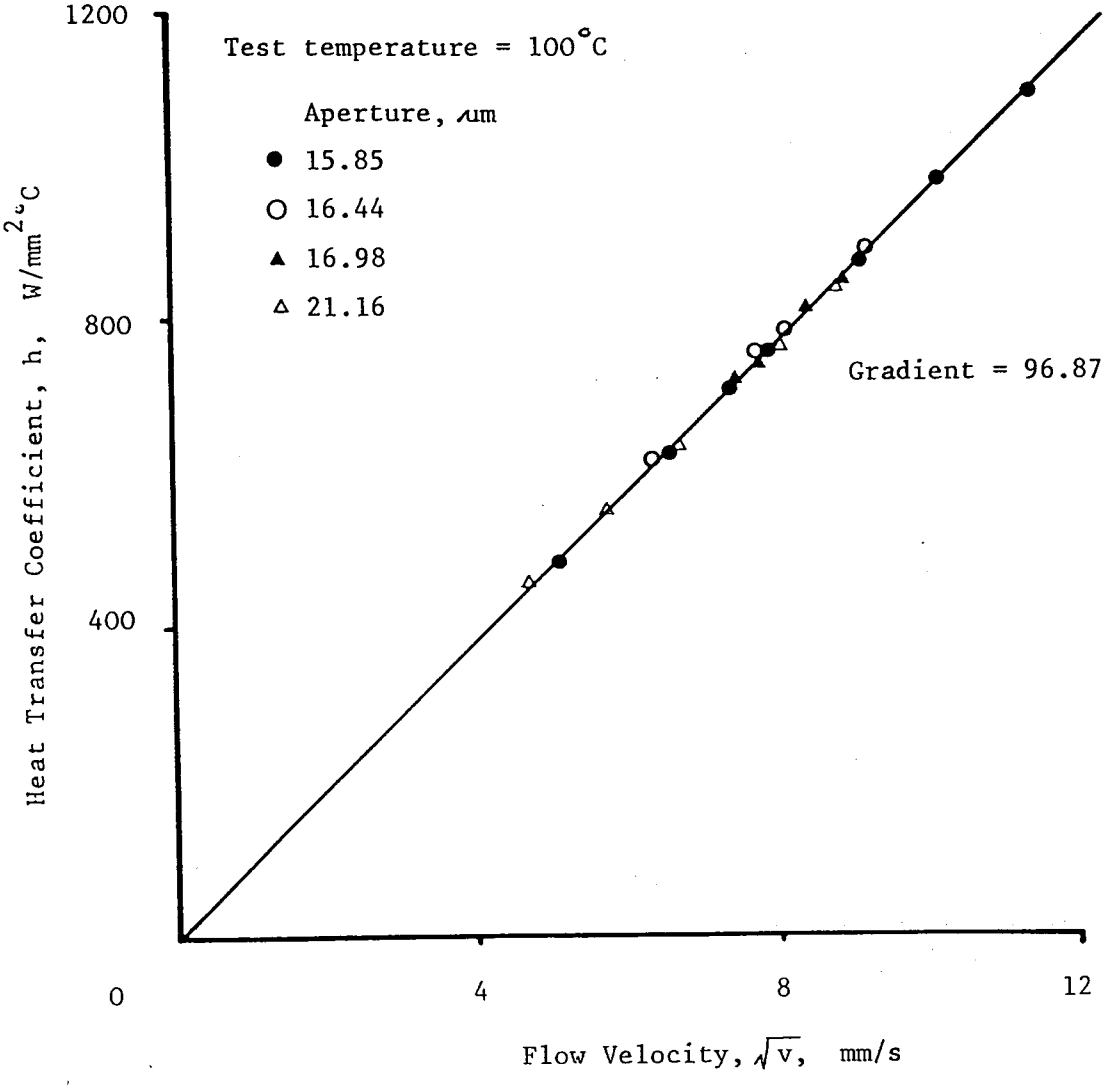


Figure 7.8 (continued)

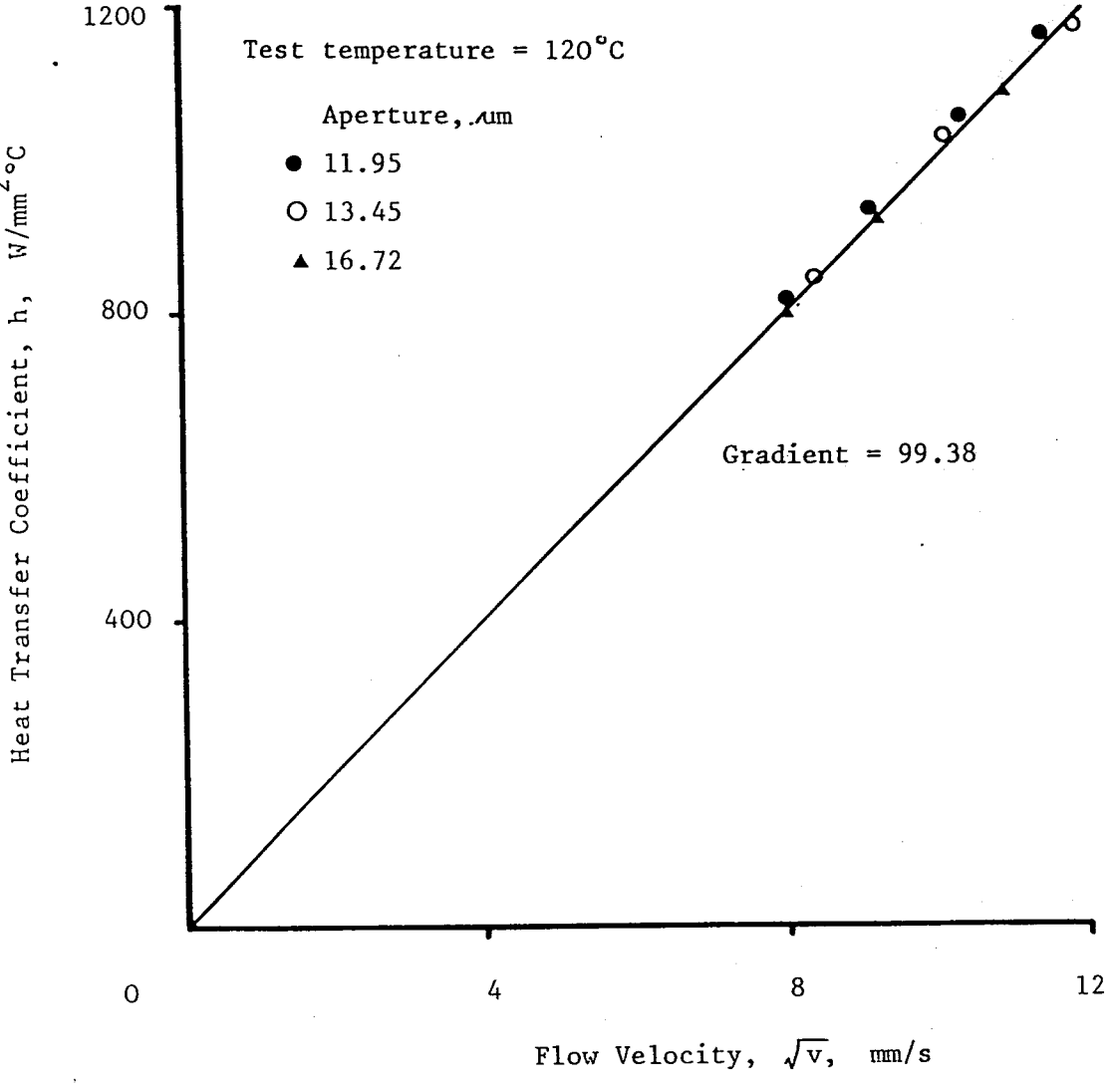


Figure 7.8 (continued)

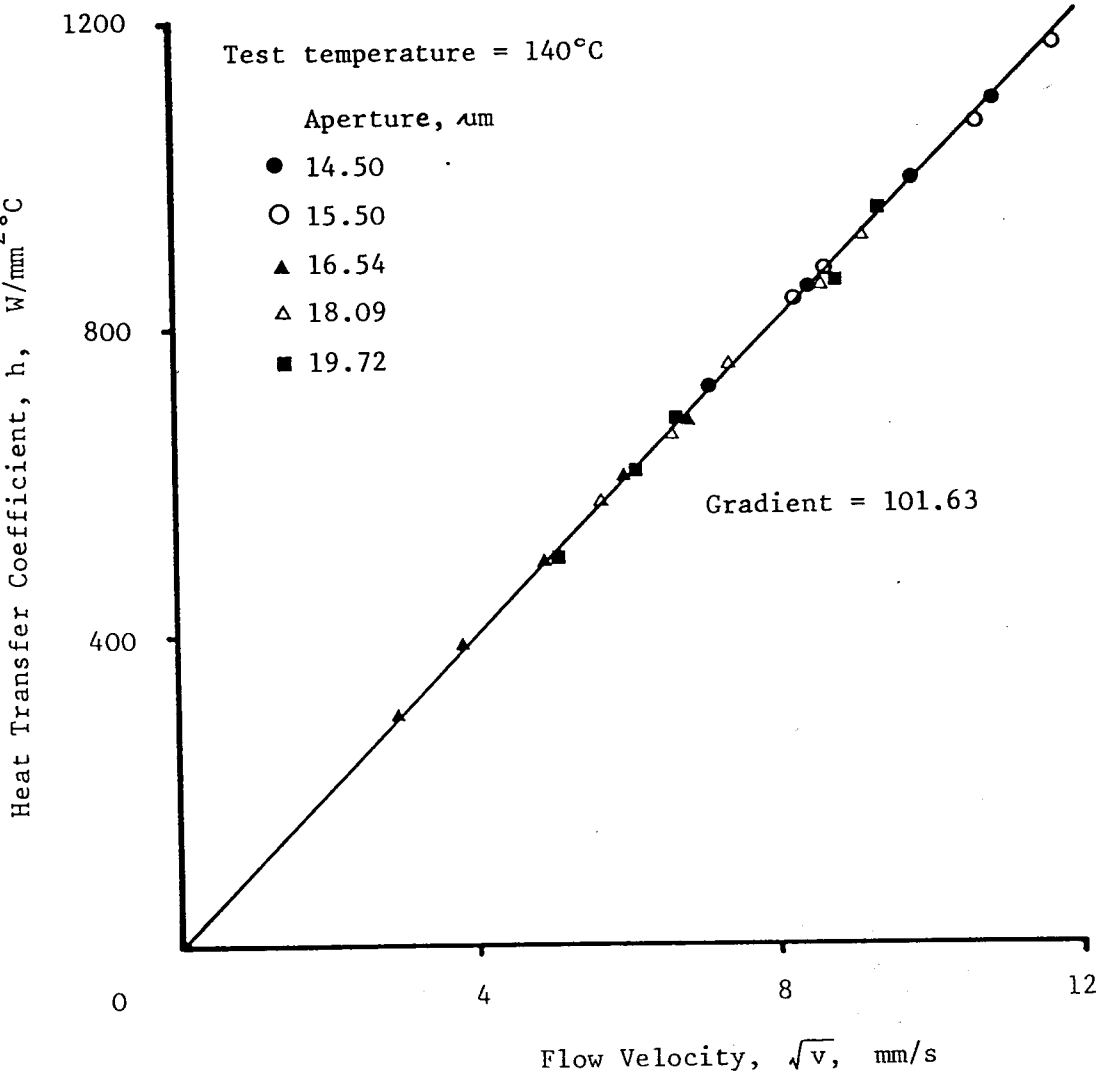


Figure 7.8 (continued)

7.7.2 Temperature -heat transfer coefficient relation

As soon as the heat transport steady state has reached in the joint, the rock-fluid interface temperature is determined by the rock temperature and the flow temperature. These temperatures affect the mean temperature which in the analysis, affect the physical properties (ρ, ν, k and Pr) of the working fluid. However, the effect of inlet water temperature on these physical properties is small and inconsistent. This can be seen from the plots of the experimental results in Figure 7.8. The plots show that h is not affected by a change of joint aperture. By comparing the curves, the results indicate that an increase in rock temperatures leads to an increase in h values. It is practically apparent that a high rock temperature will transfer its heat energy faster; and a high rock-water mean temperature will convect fluid heat energy and flow mass faster.

7.7.3 Joint aperture - energy transport relation

The experimental results and the theory show that the heat transfer coefficient, h, is not affected by the joint flow aperture. However, the total energy transported by the flow does not just depend upon flow velocity, but also upon flow rate, which is partially governed by the cross sectional area perpendicular to the flow direction (i.e., aperture x width). By comparing three equations

$$\text{energy} = c_p \, Q \, \Delta t \tag{7.38}$$

where Q is the fluid flow rate,

$$Q = vA \tag{7.39}$$

and $$\Delta t \propto v \tag{7.40}$$

It is clear that if the flow rate is fixed by boundary conditions, a larger flow velocity and relatively smaller aperture will lead to larger amount of heat energy transfer.

7.8 Methods of Numerical Analysis of Heat Energy Transfer

Numerical analysis of two-dimensional heat convective transfer (Figure 7.7) involves 3 differential equations: the equations of motion in the x, y directions, and an energy equation. The equations for laminar, imcompressible fluid flow neglecting body forces are [Eckert and Drake 1959, Rohsenow and Choi 1961, Chapman 1984]:

$$v_x \frac{\partial v_x}{\partial x} + v_y \frac{\partial v_y}{\partial y} = -\frac{1}{\rho}\frac{\partial P}{\partial x} + \nu \frac{\partial^2 v_x}{\partial y^2} \tag{7.41}$$

$$v_x \frac{\partial v_y}{\partial x} + v_y \frac{\partial v_y}{\partial y} = -\frac{1}{\rho}\frac{\partial P}{\partial y} + \nu \frac{\partial^2 v_y}{\partial x^2} \tag{7.42}$$

$$k_f \left(\frac{\partial^2 t}{\partial x^2} + \frac{\partial^2 t}{\partial y^2}\right) + \mu \left(2 \left(\frac{\partial v_x}{\partial x}\right)^2 + 2 \left(\frac{\partial v_y}{\partial y}\right)^2 + \left(\frac{\partial v_x}{\partial y} + \frac{\partial v_y}{\partial x}\right)^2 \right) + Q$$

$$= c_p \rho \left(v_x \frac{\partial t}{\partial x} + v_y \frac{\partial t}{\partial y} + \frac{\partial t}{\partial \tau} \right) \qquad (7.43)$$

The first two equations are generally known as the Navier-Stocks equations of motion, and the third is the energy equation, where

v_x = flow velocity in x direction,

v_y = flow velocity in y direction,

ρ = fluid density,

P = static flow pressure,

ν = dynamic viscosity,

k = heat conductivity of fluid,

t = fluid temperature,

μ = kinematic viscosity,

c_p = fluid specific heat, and

Q = heat energy input from other source.

Balancing the heat energy transported by convection and conduction yields

$$Q = h \, (t_s - t_f) \, \partial x = k_s \frac{\partial t}{\partial y} \, \partial x$$

Hence,

$$Q = \frac{k_s h}{k_s + w h} (T - t_f) \partial x \qquad (7.44)$$

By putting Equation (7.44) into Equation (7.43), it is clear that there are 3 equations available to solve 3 variables, v_x , v_y and t.

Further simplification can be made by analysing the system in one-dimension. The above 3 equations will thus be reduced to be two, i.e.,

$$v_x \frac{\partial v_x}{\partial x} = - \frac{1}{\rho} \frac{\partial P}{\partial x} + \nu \frac{\partial^2 v_x}{\partial y^2} \qquad (7.45)$$

$$k_f \left(\frac{\partial^2 t}{\partial x^2} + \frac{\partial^2 t}{\partial y^2}\right) + \mu \left(\left(\frac{\partial v_x}{\partial x}\right)^2 + \left(\frac{\partial v_y}{\partial y}\right)^2 \right) + Q$$

$$= c_p \rho \left(v_x \frac{\partial t}{\partial x} + \frac{\partial t}{\partial \tau}\right) \qquad (7.46)$$

Using the above equations, with suitable boundary conditions, the water temperatures and the rate of heat energy transfer can be calculated for a single joint for any given conditions. The calculated heat transfer coefficients and the above equations can be used in some physical models describing geothermal systems, such as the Pipe model [Einarsson 1942, Bodvarsson 1961, White 1962, Elder 1966, Donaldson 1968, 1970] (see Donaldson [1968, 1970]).

Chapter 8

CONCLUSIONS AND APPLICATION

8.1 Summary and Conclusions

1) Hydro-thermo-mechanical tests on joints in the Carnmenellis granite from Cornwall, S.W. England, were carried out using the Terra Tek Geothermal Rock Mechanics Test System of Mineral Resources Engineering Department, Royal School of Mines, Imperial College, London. Both natural joints and artificially induced extension fractures were tested at effective normal stresses up to 40 MPa, differential pore pressures to 6 MPa and temperatures to 200°C.

2) All the joints in the granite tested were rough. However, the roughness of natural joints was lower than that of artificially induced extension fractures because the former had suffered a small degree of weathering and hydro-thermal alteration. The granite samples containing natural joints and those containing extension fractures had the same grain size, so the medium scale (in centimeters) profiles were similar. However, the roughness obtained on the small scale (in millimeters) was greater for the fresh extension

fractures.

3) Apart from joint roughness, and joint wall strength, another parameter describing joint surface geometrical properties was found to have a controlling influence over the joint mechanical behaviour and hydraulic properties. This parameter is joint matching (or mating). Hence a Joint Matching Coefficient (JMC) was developed and coupled with the existing Joint Roughness Coefficient (JRC) to provided a suitable parameter for correlating joint surface properties and to predict joint initial apertures and joint hydro-mechanical properties. The experimental results showed that the joint initial apertures may be related to JRC and JMC.

4) Experimental effective normal stress - joint closure data were fitted by hyperbolic curves and by logarithmic curves. However, significant variation in the parameters in Goodman's hyperbolic model was found for different samples. This provide a major obstacle to obtain acceptable correlations using the hyperbolic model. Hence, a logarithmic relation was proposed which appeared to avoid this problem. More closely unique values of the parameters were found for the natural joints and for the artificially induced extension fractures.

5) Data from flow tests on joints and fractures validated the equivalent cubic flow law derived from the smooth parallel plate theory for laminar flow. The tests also showed a linear relation between flow rate and

differential pressure head for laminar flow at constant effective normal stress.

6) The joint hydraulic models proposed by previous investigators fit the test results closely. However, difficulties were found in finding single values of the material and geometrical constants that applied to the complete range of the data and samples. Tsang and Witherspoon's "asperity and void" statistical model relies only on effective normal stress - joint mechanical closure data to determine the hydraulic behaviour, and so obviates the need to undertake any flow test. However, difficulties arose in establishing the proportion of the joint surface area that was in contact at a particular stress for the statistical model. The calculated values of the parameter in Walsh's model showed it to be a robust unique constant, and was not conditioned by the same constraints which appeared in the other models.

7) Joint Condition Factor (JCF) is a factor that accounts for deviations from the ideal conditions assumed in the smooth parallel plate theory. JCF reflects the effects of joint roughness, joint matching, joint stiffness, deposits of detritus, loading history, sample disturbance, sample size and temperature environment. Based on the experimental results, the initial values of JCF were related to the values of JRC and joint initial apertures. Cyclic loading increased the value of JCF, and the change steadily decreased as further continuous loading cycles were applied. The change may become very small after 4 or 5 loading cycles.

8) A Joint Condition Factor (JCF) approach for correlating the joint hydro-thermo-mechanical properties was developed. The empirical relations developed enable estimates to be made of the joint mechanical and hydraulic behaviours at any given stress and temperature conditions. JCF varied with temperature according to a logarithmic law. For the simplest case, by inspecting the joint (or fracture) surface geometrical properties (JRC and JMC), the joint (or fracture) hydro-thermo-mechanical behaviour can be estimated by coupling the logarithmic relation and the JCF approach.

9) Observations made under the Scanning Electron Microscope (SEM) showed that the granite material was significantly altered after hydro-thermo-mechanical action. The observations suggested that cracks and pores initiated and expanded by the hydro-thermal alteration may play an important role in establishing fluid pathways in addition to the joint. This network of intragranular cracks provides the interconnected porosity needed to make the rock more permeable. However, since the flow is concentrated in the joint, the introduction of the additional fluid flow pathways formed by this network has little effect on the overall joint hydraulic behaviour. In contrast, the direct effect of combined hydro-thermo-mechanical alteration under elevated temperature causes major changes in the joint hydro-thermo-mechanical properties.

10) Initial apertures increased with increasing

sample temperature. This change was also dependent on the joint surface geometrical properties. An empirical logarithmic relation between initial aperture, change of temperature and JRC was proposed based on the experimental data.

11) The experimental results also showed that joint hydraulic conductivity decreased with increasing sample temperature. These apparently contradictory conclusions may be explained in term of a joint thermal expansion mechanism and joint healing mechanism. A joint thermal expansion coefficient was developed for the "closed" joint (and possibly small cracks) in granite; it is inversely proportional to the joint initial aperture.

12) Data on rock-fluid heat transfer were collected during the flow experiments. The results showed that the heat transfer coefficient varies from 200 to 1400 W/m- C, and was a function of flow velocity, joint geometry, the temperature of rock and the temperature of fluid. This extremely important fundamental parameter can be used in numerical analysis of hot dry rock geothermal energy systems and in other fields such as radioactive waste repository design and heavy oil recovery.

8.2 Applications to Hot Dry Rock Geothermal Energy Extraction

Practically all geothermal energy which has been tapped for commercial power production to date is of

the hydrothermal variety. In hydrothermal systems, near surface water seeps through permeable channels in the rock to depths at which it encounters hot rock. The heated fluid (water and/or steam) is then driven upward by buoyancy. Convection cells are created in which leakage to the surface or out of the formation is replenished by inflow of meteoric groundwater. These systems are thus essentially different from Hot Dry Rock systems (prior to exploitation) in which liquid water is transported through artificially induced or stimulated fractures and conduction is also one of the dominant mechanisms of heat transfer [Garg and Kassoy 1981]. The success or otherwise of a hot dry rock venture will depend on the quality of the inter-well fracturing and stimulation. A few dominant connectors may short-circuit the rock mass so that only a limited volume of hot rock will be accessed. In contrast, a high density fracture structure should access a wealth of heat.

The current hot dry rock geothermal energy researches being carried out by the Los Alamos National Laboratory, USA, and in Cornwall suggest that the following fundamental analytical and experimental studies are required for the further reservoir circulation and development [Los Alamos National Laboratory 1981, 1982, 1983, 1984; Camborne School of Mines Geothermal Energy Project 1984a, 1984b, 1985, 1986a, 1986b; Parker and Hendron 1987]:

1) modelling of thermal, tracer, chemical, radon,

active seismics and hydraulic measurements, with a view to drawing these together in composite, or linked models;

2) temperature-dependent properties, and the effects of thermal interference, particularly thermal contraction and thermal cracking;

3) effects of long-term stress relaxation and chemical deposition/leaching as a result of circulation;

4) the effect on heat transfer modelling of heat transport by fluid diffusion to and from the rock mass;

5) the influence of pressure and flow oscillations on reservoir structure and performance;

6) possible dynamic and thermally induced improvements to the reservoir which may take place during circulation;

7) methods of overcoming short-circuits, once they have been identified.

Aspects of (1), (2), (4), (5) and (6) have been studied for joints in the Carmenellis granite and reported on in this thesis.

As noted in earlier chapters, the mass and heat are transported through the hydrofractured or stimulated joints (joints were hydraulic fractured at the Los Alamos project and were explosive stimulated at the Camborne School of Mines project). It is therefore of primary

importance to define (1) the geometry of the fracture system, and (2) its response under a hydrodynamic gradient and stresses. The first part of the studies presented in this thesis (Chapters 1 to 6) were intended to further investigate and define the responses of rock discontinuities (joints and fractures) under varying hydraulic gradients, effective normal stresses and temperatures, and hence to lead to the development of the capability to predict the responses of fracture systems in rock. The relations between joint (or fracture) surface geometrical properties, joint (or fracture) hydro-mechanical behaviour under stress and temperatures were investigated in the laboratory studies. This information can be applied to the further understanding of mass transport in geothermal systems. By using the new JCF approach coupled with joint (or fracture) surface geometrical properties, hydro-mechanical behaviour of joints (or fractures) in geothermal systems may be linked and estimated. The results also provide information on joint response under various effective normal stresses and hydrodynamic gradients and the influence of normal stress oscillations on the joint hydro-mechanical performance.

Temperature-dependent properties of joints in granite were well investigated. Scanning Electron Microscopy suggested that thermal cracking occurs when water is injected into the joints in heated rock. The induced thermal cracks may form new pathways for fluid flow by connecting the cracks and expanded pores and

hence increase the rock mass permeability. This effect could also lower reservoir impedance (defined as the pressure drop across the reservoir divided by the production flow rate).

The second part of the laboratory investigation (Chapter 7) provides data that are essential for the assessment of heat energy transfer in geothermal systems. The values of rock thermal conductivity and coefficient of heat transfer calculated from the experimental results may be used in analyses of geothermal energy extraction using physical models such as the pipe model (Section 7.8), the porous media model [Brownell et al 1977, Garg and Pritchett 1977] and the distinct element FRIP model [Pine and Cundall 1985].

8.3 Aspects Requiring Further Research

1) Some major improvements can be made to the testing system described in Chapter 3 in order to obtain more consistent test results.

(a) At present, the permeating fluid pressures are controlled manually. A servo-controller or intensifier can be adopted to reduce operational errors. Experience indicates that exceeding the desired joint fluid pressure can influence the joint hydro-mechanical behaviour significantly.

(b) A small variation in the test temperature affects

the joint hydro-mechanical behaviour. This variation must be minimized.

2) Throughout this thesis, objective and empirical joint roughness coefficient (JRC) and Joint Matching Coefficient (JMC) are adopted. Accurate monitoring methods should be developed to assess the values of JRC and JMC in order to yield a reliable Joint Condition Factor and to predict joint hydro-mechanical behaviour. An indirect method of estimating the JRC is described by Barton and Choubey (1977). A similar indirect method of estimating the JMC may be developed by performing shearing tests on a joint. Together with values of each peak shear strength, residual shear strength, dilation and JRC the JMC value may be estimated. As emphasized earlier, accurate values of JRC and JMC are necessary and must be determined either by direct profiling or by indirect methods.

3) The proposed relations between joint and fracture hydro-thermo-mechanical properties are based on the experimental results for the Carnmenellis granite. The applicability of these relations to other types of rock joints and fractures must be examined. The relations are expected to be valid for rough joints and fractures in granites and other types of igneous rocks.

4) The importance of secondary thermal cracking and its effects on the joint hydro-mechanical behaviour requires further study, particularly on the microscopic scale. The initiation and propagation of thermal cracks

may be detected by means of wave velocity and acoustic emission measurements. Further research should also be carried out to study the relation between thermal cracking and the rock material mechanical and hydraulic properties.

5) The phenomenon of joint thermal expansion was observed in the experimental study. Further data are necessary to confirm the existence of this effect. A joint thermal expansion mechanism and a joint healing mechanism were postulated to explain the effect of temperature on the joint hydro-mechanical behaviour. However, further study may lead to the development of realistic physical or numerical models.

6) Heat transfer analysis form a major part of the study of hot dry rock geothermal energy systems. Further understanding of mass and heat transport in geothermal systems requires extensive numerical and laboratory studies. At present, very few data on rock-fluid heat transfer are available. The relations between the heat transfer phenomenon and joint surface properties will form a large and interesting research area.

7) A general lack of comparability between the results of laboratory studies and in situ studies of joint hydro-thermo-mechanical properties is evident. Reconciling the test results with in situ studies is necessary.

REFERENCES

ATKINSON, B.K., D. MACDONALD and P.G. MEREDITH (1981). Acoustic response and fracture mechanics of granite subjected to thermal stress cycling experiments. Proc. 3rd Conf. on Acoustic Emission/Microseismic Activity in Geological Structures and Materials, H.R. Hardy and F.W. Leighton (eds), Pennsylvania State Univ., pp.5-18.

ATTEWELL, P.B. and I.W. FARMER (1976). Principles of engineering geology. Chapman and Hall, London, 1045pp.

BAKER, W.J. (1955). Flow in fissured formations. Proc. 4th World Petrol. Congr., Carlo Colombo, Rome, Sect.II/E, pp.379-393.

BALLOU, L.B. (1979). Geological disposal investigations in granite at the Nevada test site. Lawrence Livermore National Laboratory, UCRL-82284.

BANDIS, S. (1980). Experimental studies of scale effects on shear strength and deformation of rock joints. Ph.D. thesis, Univ. of Leeds, 385pp.

BANDIS, S., A.C. LUMSDEN and N.R. BARTON (1983). Fundamentals of rock joint deformation. Int. J. Rock Mech. Min. Sci. Geomech. Abstr., Vol.20, pp.249-268.

BARTON, N.R. (1971). A relationship between joint roughness and joint shear strength. Rock Fracture - Proc. Int. Symp. on Rock Mechanics, Nancy, France, Paper 1-8.

BARTON, N.R. (1972). A model study of rock joint deformation. Int. J. Rock Mech., Vol.9, pp.579-602.

BARTON, N.R. (1973). Review of a new shear strength criterion for rock joints. Engng. Geol., Vol.7, pp.287-332.

BARTON, N.R. (1976). The shear strength of rock and rock joints. Int. J. Rock Mech. Min. Sci. Geomech. Abstr., Vol.13, pp.255-279.

BARTON, N.R. (1986). Deformation phenomena in jointed rock. Geotechnique, Vol.36, pp.147-167.

BARTON, N.R. and V. CHOUBEY (1977). The shear strength of rock joints in theory and practice. Rock Mechanics,

Vol.10, pp.1-54.

BARTON, N.R. and R. LINGLE (1982). Rock mass characterization methods for nuclear waste repositories in jointed rock. **Proc. ISRM Symp. on Rock Mechanics: Caverns and Pressure Shafts**, W. Wittke (ed). Aachen, A.A. Balkema, Rotterdam, pp.3-18.

BARTON, N.R. and K. BAKHTAR (1983). **Rock joint description and modelling for the hydro-thermo-mechanical design of nuclear waste repositories.** Contract Report, Submitted to CANMET, Mining research Laboratories, Ottawa, Part 1-4, 270pp; Part 5, 108pp.

BARTON, N.R., S. BANDIS and K. BAKHTAR (1985). Strength, deformation and conductivity coupling of rock joints. **Int. J. Rock Mech. Min. Sci. Geomech. Abstr.**, Vol.22, pp.121-140.

BATCHLOR, A.S. (1982). **Hot Dry Rock reservoir stimulation in the U.K. --an extended summary.** Camborne School of Mines Geothermal Energy Project Report, 49pp.

BAUER, S.J. and B. JOHNSON (1979). Effects of slow uniform heating on the physical properties of the Westerly and Charcoal granites. **Proc. 20th US Symp. on Rock Mech.**, Austin, Texas, pp.7-18.

BAUER, S.J., M. FRIEDMAN and J. HANDIN (1981). Effects of water saturation on strength and ductility of three igneous rocks at effective pressures to 50MPa and temperatures to partial melting. **Proc. 22nd US Symp. on Rock Mech.**, MIT, Cambridge, MA, pp.73-78.

BERMAN, R.E. (1975). Geothermal energy. Energy Technology Review No.4, Noyes Data Corporation, 336pp.

BESWICK, A.J. (1982). The drilling of two geothermal wells in the Carnmenellis Granite. **J. Camborne School of Mines**, Vol.82, pp.31-39.

BLYTH, F.G.H. and M.H. DE FREITAS (1984). **A geology for engineers**, 7th edn. Edward Arnold, London, 325pp.

BODVARSSON, G (1961). Physical characteristics of natural heat resources in Iceland. **Proc. U.N. Conf. on New Sources of Energy**, Rome, Vol.2, pp.82-89.

BOODT, P.I. and E.T. BROWN (1985). **Some rock mass assessment procedures for discontinuous crystalline rock.** Report No. DOE/RW/85.133 on Contract PECD/7/9/102 submitted to the Department of the Environment, 158pp.

BORG, I. and J. HANDIN (1966). Experimental deformation of crystalline rock. **Tectonophysics**, Vol.68, pp.131-146.

BOWDEN, F.P. and D. TABOR (1950). The friction and lubrication of solids. Vol.1. Clarendon Press, Oxford.

BRACE, W.F. (1980). Permeability of crystalline and argillaceous rocks. Int. J. Rock Mech. Min. Sci. Geomech. Abstr., Vol.17, pp.241-251.

BRADY, B.H.G and E.T. BROWN (1985). Rock mechanics for underground mining. George Allen and Unwin, London, 527pp.

BROWN, E.T. (ed) (1981). Rock characterization, testing and monitoring, ISRM suggested methods. Pergamon Press, Oxford, 211pp.

BROWN, E.T., P.I. BOODT and J.O. WATSON (1982). Estimation of water flow into underground mines. Final Report Prepared for the Commission of the European Communities R & D Programme on Raw Material. Imperial College, Univ. of London, 135pp.

BROWNELL, D.H. Jr., S.K. GARG and J.W. PRITCHETT (1977). Governing equations for geothermal reservoirs. Water Resources Res., Vol.13, pp.929-934.

CAMBORNE SCHOOL OF MINES GEOTHERMAL ENERGY PROJECT (1984a). Hydraulic results. Phase 2 report, 1984, 193pp. (Report No.2-49).

CAMBORNE SCHOOL OF MINES GEOTHERMAL ENERGY PROJECT (1984b). Low flow rate hydraulic tests (RT2019-2041). Phase 2 report, 110pp. (Report No.2-52).

CAMBORNE SCHOOL OF MINES GEOTHERMAL ENERGY PROJECT (1985). Preliminary report on the construction of a deep prototype Hot Dry Rock geothermal system in Cornwall: Vol.1 - Drilling and casing. Phase 2 report, 183pp. (Report No.2B-22).

CAMBORNE SCHOOL OF MINES GEOTHERMAL ENERGY PROJECT (1986a). Circulation results phase 2B 1983-1986. Phase 2 report, 111pp. (Report No.2B-32)

CAMBORNE SCHOOL OF MINES GEOTHERMAL ENERGY PROJECT (1986b). Preliminary report on the construction of a deep prototype Hot Dry Rock geothermal system in Cornwall: Vol.2. Phase 2 report, 81pp. (Report No.2B-36).

CARSLAW, H.S. and J.C. JAEGER (1959). Conduction of heat in solid. Clevedon Press, Oxford.

CHAPMAN, A.J. (1984). Heat transfer, 4th edn. Macmillan, London, 608pp.

CHURCHILL, S.W. and H. OZOE (1973). Correlations for laminar forced convection in flow over an isothermal flat plate and in developing and fully developed flows

in an isothermal tube. J. Heat Transfer, Trans. ASME, Vol.95, pp.416-421.

COLBURN, A.P. (1933). A method of correlating forced convection heat transfer data and a comparison with liquid friction. Trans. AIChE, Vol.29, pp.174-181.

COOLING, C.M., L.W. TUNBRIDGE and J.A. HUDSON (1984). Some studies of rock mass structure and in situ stress. Proc. ISRM Symp., Design and Performance of Underground Excavation, E.T. Brown and J.A. Hudson (eds). Cambridge, British Geotech. Soc., pp.199-206.

COOK, N.G.W. (1983). Effects of joints on thermally induced displacements and stresses. Proc. 24 US Symp. on Rock Mechanics, Texas, pp.303-307.

COOPER, W. and G. SIMMONS (1977). The effects of cracks on thermal expansion of rocks. Earth planet. Sci. Lett., Vol.36, pp.404-411.

DASH, Z.V., H.D. MURPHY, R.L. AAMODT, R.G. AGUILAR, D.W. BROWN, D.A. COUNCE, H.N. FISHER, C.O. GRIGSBY, H.KEPPLER, A.W. LAUGHLIN, R.M. POTTER, J.W. TESTER, P.E. TRUJILLO, Jr. and G. ZYVOLOSKI (1983). Hot Dry Rock geothermal reservoir testing: 1978-1980. In Geothermal energy from Hot Dry Rock. G. Heiken and F. Goff (eds). J. Volcanol. Geothermal Res., Vol.15, pp.59-99.

DAVISON, C.C., W.S. KEYS and F.L. PAILLET (1982). Use of borehole geophysical logs and hydraulic tests to characterize crystalline rock for nuclear waste storage. ONWI-418, 103pp.

DENNESS, B. (1969). Fissure and related studies in selected Cretaceous Rocks of S.E. England. Ph.D thesis, Imperial College, London Univ..

DETOURNAY, E. (1980). Hydraulic conductivity of closed rock fractures: an experimental and analytical study. 13th Canadian Rock Mech. Symp. on Underground Rock Engineering, pp.168-173.

DMITRIYEV,A.P., L.S. KUZYAYEV, Y.I. PROTASOV and V.S. YAMSHCHIKOV (1972). Physical properties of rocks at high temperatures. NASA Technical Translation, N72-7074.

DONALDSON, I.G. (1968). A possible model for hydrothermal systems and methods of studying such a model. Proc. 3rd Australasian Conf. on Hydraulics and Fluid Mech., pp.200-204.

DONALDSON, I.G. (1970). The simulation of geothermal systems with a simple convective model. U.N. Symp. on the Development and Utilization of Geothermal

Resources, Pisa, Geothermics, Special issue, Vol.2, Part I, pp.649-654.

DONALDSON, I.G. and M.A. GRANT (1981). Heat extraction from geothermal reservoirs. In Geothermal systems: principles and case histories. L. Rybach and L.J.P. Muffler (eds), Wiley, New York, pp.145-180.

DURHAM, W.B and A.E. ABEY (1981a). The effect of pressure on the thermal properties of a salt and a quartz monzinite. Proc. 22nd US Symp. on Rock Mech., Cambridge, MA., pp.79-84.

DURHAM, W.B. and A.E. ABEY (1981b). Thermal conductivity and diffusivity of Climax stock quartz monzonite at high pressure and temperature. Lawrence Livermore National Laboratory, UCRL-86619.

ECKERT, E.R.G. and R.M. DRAKE Jr. (1959). Heat and mass transfer. Tata McGraw-Hill, New Delhi, 530pp.

EINARSSON, T. (1942). The nature of springs of Iceland, (in German). Rit. Visind. Isl., Vol.26, pp.1-92.

ELDER, J.W. (1966). Heat and mass transfer in the Earth: hydrothermal systems. New Zealand Dept. of Scientific and Industrial Res. Bulletin, No.169.

ELLIOTT, G.M. (1983). Personal communication.

ELLIOTT, G.M. (1984). An investigation of the mechanical and thermal properties of a Cornish granite (Part A). Rock Mech. Res. Report, Imperial College, Univ. of London, 34pp.

Elliott, G.M. (1985). An investigation of the mechanical and thermal properties of a Cornish granite (Part B). Rock Mech. Res. Report, Imperial College, Univ. of London, 10pp.

ELLIOTT, G.M and E.T. BROWN (1985). Laboratory measurement of the thermo-hydro-mechanical properties of rock. Rock Mech. Res. Report, Imperial College, London, 36pp.

ELLIOTT, G.M., E.T. BROWN, P.I. BOODT and J.A. HUDSON (1985). Hydromechanical behaviour of joints in the Carnmenellis granite, S.W. England. Proc. Int. Symp. on Fundamentals of Rock Joints, O. Stephansson (ed), Lulea Univ., Centek, Sweden, pp.249-258.

ENNISS, D.O., S.W. BUTTERS, C.B. MCFARLAND and A.H. JONES (1979a). Capacities to determine rock properties at simulated geothermal conditions. J. Energy Resources Technol., Trans. ASME, Vol.10, pp.117-123.

ENNISS, D.O., S.W. BUTTERS, R. LINGLE, R.G. VAN BUSKIRK

and F.R. PRATER (1979b). Capacities to measure geothermal material properties at simulated in situ conditions. Terra Tek Report TR79-49, Terra Tek Inc., Salt Lake City, Utah. Report Submitted to Department of Energy, Idaho Falls, Idaho under contract DOE/ET/28031-1.

FRIEDMAN, M., J. HANDIN, N.G. HIGGS and J.R. LANTZ, (1979). Strength and ductility of four dry igneous rocks at low pressures, and temperatures to partial melting. Proc. 20th US Symp. on Rock Mech., Austin, Texas, pp.35-50.

GALE, J.E. (1975). A numerical, field and laboratory study of flow in rocks with deformable fractures. Ph.D. thesis, Univ. of California Berkeley, 255pp.

GALE, J.E. (1982). The effects of fracture type (induced versus natural) on the stress-fracture closure-fracture permeability relationships. Issues in Rock Mechanics, Proc. 23rd US Symp. on Rock Mech., Berkeley, California, pp.290-298.

GANGI, A.F. (1975). Variation of whole- and fractured-porous-rock permeability with confining pressure. Proc. 1st Int. Symp. on Induced Seismicity, Banff, Albert, Canada, pp.15-19.

GANGI, A.F. (1978). Variation of whole- and fractured-porous-rock permeability with confining pressure. Int. J. Rock Mech. Min. Sci. Geomech. Abstr., Vol.15, pp.249-257.

GANGI, A.F. (1981). The variation of mechanical and transport properties of cracked rock with pressure. Proc. 22nd US Symp. on Rock Mech., Cambridge, MA, pp.91-95.

GARG, S.K. and D.R. KASSOY (1981). Convective heat and mass transfer in hydrothermal systems. Geothermal systems: principles and case histories. L. Rybach and L.J.P. Muffler (eds), Wiley, New York, pp.145-180.

GARG, S.K and J.W. PRITCHETT (1977). On pressure-work, viscous dissipation and the energy balance relation for geothermal reservoirs. Advances in Water Resources, Vol.1, pp.41-47.

GOODMAN, R.E. (1976). Methods of geological engineering in discontinuous rock. West, New York, 449pp.

GREENWOOD, J.A. and J.B.P. WILLIAMSON (1966). Contact of nominally flat surfaces. Proc. Royal Soc. London, Ser.A, Vol.295, pp.300-307.

GREENWOOD, J.A. and J.H. TRIPP (1971). The contact of two

nominally flat rough surfaces. Proc. Inst. Mech. Engrs., Vol.185, pp.625-633.

HADLEY, K. (1976). Comparison of calculated and observed crack densities and seismic velocities in Westerly Granite. J. Geophys. Res., Vol.81, pp.3484-3494.

HANLEY, E.J., D.P. DEWITT and R.F. ROY (1978). The thermal diffusivity of eight well-characterized rocks for the temperature range 300-1000 K. Engng. Geol., Vol.12, pp.31-47.

HARDIN, E.L., N.R. BARTON, R. LINGLE, M.P. BOARD and M.D. VOEGELE (1982). A heated flatjack test series to measure the thermo-mechanical and transport properties of in situ rock masses. Office of Nuclear Waste Isolation, Columbus, Ohio, ONWI-260, 193pp.

HEARD, H.C. (1980). Thermal expansion and infra-red permeability of Climax quartz monzonite to 300°C and 27.6 MPa. Int. J. Rock Mech. Min. Sci. Geomech. Abstr., Vol.17, pp.289-296.

HEIKEN, G. and F. GOFF (1983). Hot Dry Rock geothermal energy in the Jemez volcanic field, New Mexico. In Geothermal energy from Hot Dry Rock. G. Heiken and F. Goff (eds), J. Volcanol. Geothermal Res., Vol.15, pp.223-246.

HEIMILI, P. (1972). Water and air leakage through joints in rock specimens (in Norwegian). Fjellsprengning-steknikk, Bergmekanikk, Annual Rock Mechanics Meeting, Oslo, Norway, pp.137-142.

HEUZE, F.E. (1983). High-temperature mechanical, physical and thermal properties of granitic rock --a review. Int. J. Rock Mech. Min. Sci. Geomech. Abstr., Vol.22, pp.251-261.

HILL, J.B and D.A. MACALISTER (1906). The geology of Falmouth and Truro and the mining district of Camborne and Redruth. Memoirs of the Geological Survey of England and Wales, H.M.O.S., London.

HOEK, E. and E.T. BROWN (1980). Underground excavations in rock. The Inst. of Mining and Metall., London, 527pp.

HOEK, E. and J.W. BRAY (1981). Rock slope engineering, 3rd edn. The Inst. of Mining and Metall., London, 358pp.

HOLMAN, J.P. (1986). Heat transfer, 6th edn. McGraw-Hill, New York, 676pp.

HUDSON, J.A. (1983). UK rock mechanics research for radioactive waste disposal. Proc. 5th ISRM Congr.,

Melbourn, 1983, Vol.II, E161-167.

HUDSON, J.A. (1987). The understanding of measured changes in rock structure, in situ stress and water flow caused by underground excavation. **2nd Int. Symp. on Field Measurements in Geomech.**, April, 1987, Kobe, Japan, pp.467-474.

HUDSON, J.A. and J.B. BODEN (1982). Geotechnical and tunnelling aspects of radioactive waste disposal. **Tunnelling 82**, the Inst. of Mining and Metall., London, pp.271-281.

HUITT, J.L. (1956). Fluid flow in simulated fractures. **J. AIChE**, Vol.2, pp.259-264.

IWAI, K. (1976). **Fundamental studies of fluid flow through a single fracture.** Ph.D. thesis, Univ. of California, Berkeley, 208pp.

JAEGER, J.C. (1959). The frictional properties of joints in rocks. Geofis. Pura Appl., Vol.43, pp.148-158.

JAEGER, J.C. and N.G.W. COOK (1979). **Fundamentals of rock mechanics**, 3rd edn. Chapman and Hall, London, 593pp.

JEFFRY, J.A. et al. (1979). **Determination of in-situ thermal properties of Stripa granite, methods and preliminary results.** Lawrence Berkeley Laboratory, LBL-8423.

JOHNSON, B. (1983). Permeability of a simulated fracture as a function of normal stress. **Proc. 24th US Symp. on Rock Mech.**, Texas, pp.519-523.

KAYE, G.W.C and T.H. LAMB (1966). **Tables of physical and chemical constants**, 13th edn. Longmans, London, 249pp.

KLETT, R.D. (1974). Deep rock nuclear waste disposal test: design and operation. Sandia National Laboratories, Albuquerque, SAND-74-0042.

KRANZ, R.L., A.D. FRANKEL, T. ENGELDER and C.H. SCHOLZ (1979). The permeability of whole and jointed Barre granite. **Int. J. Rock Mech. Min. Sci. Geomech. Abstr.**, Vol.16, pp.225-234.

LAGHINA SERAFIM, J. (1968). Influence of interstitial water on the behaviour of rock masses. In **Rock mechanics in engineering practice.** K.G. Stagg and O.C. Zienkiewicz (eds), Wiley, London, pp.55-98.

LAMB, H. (1932). **Hydrodynamics**, 6th ed. Cambridge Univer-

ROHSENOW, W.M. and H.Y. CHOI (1961). **Heat, mass and momentum transfer.** Prentice Hall International, London, 537pp.

RYBACH, L. (1981). Geothermal systems, conductive heat flow, geothermal anomalies. In **Geothermal systems: principles and case histories.** L. Rybach and L.J.P. Muffler (eds), Wiley, New York, pp.3-36.

SCHRAUF, T.W. (1984). **Relationship between the gas conductivity and geometry of a natural fracture.** M.Sc. thesis, Dept. of Hydrology and Water Resources, Univ. of Arizona, 156pp.

SHARP, J.C. (1970). **Fluid flow through fissured media.** Ph.D. thesis, Imperial College, Univ. of London, 181pp.

SHARP, J.C. and Y.N. MAINI (1972). Fundamental considerations on the hydraulic characteristics of joints in rocks. **Proc. Symp. on Percolation Through Fissured Rock, ISRM, IAEG,** Stuttgart, pap.T1-F.

SHARP, J.C, Y.N. MAINI and T.R. HARPER (1972). Influence of groundwater on the stability of rock masses, part 1, hydraulic with rock masses. **Inst. of Mining and Metall. Trans., Sect.A,** Vol.81, No.82, pp.A13-A20.

SHARP, J.C., Y.N. MAINI and T.L. BREKKE (1973). Evaluation of hydraulic properties of rock masses. **Proc. 14th. US Symp. on Rock Mech.,** ASCE, New York, pp.481-500.

SHEN, V.D., P.Z. ZHEN and D.A. JIANG (1965). **Engineering thermodynamics,** (in Chinese). Education Publications, Beijing, 383pp.

SIMMONS, G. and D. RICHTER (1976). Microcracks in rocks. In **The physics and chemistry of minerals and rocks.** R. Strens (ed), Wiley-Interscience, New York, pp.105-137.

SMITH, M.C. (1983). A history of Hot Dry Rock geothermal system. In Geothermal energy from Hot Dry Rock, G. Heiken and F. Goff (eds), **J. Volcanol. Geothermal Res.,** Vol.15, pp.1-20.

SNOW, D.T. (1968). Rock fracture spacings, openings and porosities. **Proc. ASCE,** Vol.96 (SM 1), pp.73-91.

SPRUNT, E. and W.F. BRACE (1974). Direct observations of microcavities in crystalline rocks. **Int. J. Rock Mech. Min. Sci. Geomech. Abstr.,** Vol.11, pp.139-150.

SUMMERS, R., K. WINKLER and J. BYERLEE (1978). Permeability changes during the flow of water through Westerly granite, at temperatures of 100-400 C. J. Geophys.

MAINI, Y.N. (1971a). In-situ hydraulic parameters in jointed rock; their measurement and interpretation. Ph.D. thesis, Imperial College, Univ. of London, 312pp.

MAINI, Y.N. (1971b). Drainage of rock masses. Proc. Symp. on Rock Fracture, Nancy, France, pap.III-11.

MAINI, Y.N. (1973). A numerical simulation of the coupled stress flow phenomenon in fractured systems. Colloquium Abstract, Int. Colloquium, Seismic Effects of Reservoir Impounding, Roy. Soc. London, March 1973.

MAINI, Y.N., J. NOORISHAD and J.C. SHARP (1972). Theoretical and field considerations on the determination of in situ hydraulic parameters in fractured rock. Percolation through fissured rock, Proc. Symp. ISRM, IAEG, Stuttgart, pap.T1-E.

MASSEY, B.S. (1975). Mechanics of fluids, 3rd edn. Nostrand Reinhold Company, London, 132pp.

MAVKO, G. and A. NUR (1978). Effect of non-elliptical cracks on the compressibility of rocks. J. Geophys. Res., Vol.83, pp.4459-4468.

MCADAMS, W.H. (1933). Heat Transmission. McGraw-Hill, New York, 383pp.

MCLAREN, J.R. and I. TITCHELL (1981). Physical properties of granite relevant to near field conditions in nuclear waste depository. AERE, Harwell, Report AERE-R-10046.

MOREY, G.M. and J.M. HESSELGESSER (1951). The stability of some minerals in superheated steam at high pressures. Ecom. Geol., Vol.46, pp.821-835.

NELSON, R. (1975). Fracture permeability in porous reservoirs: experimental and field approach. Ph.D. thesis, Texas A&M Univ., College Station.

NEUZIL, C.E. and J.V. TRACY (1981). Flow through fractures. Water Resources Res., Vol.17, pp.191-199.

O'CONNELL, R.S. and B. BUDIANSKY (1974). Seismic velocities in dry and saturated cracked solids. J. Geophys. Res., Vol.79, pp.5412-5420.

PAGE, L. and H.C. HEARD (1981). Elastic moduli, thermal expansion, and inferred permeability of Climax quartz monzonite and Sudbury Gabbro to 500 C and 55 MPa. Proc. 22nd US Symp. on Rock Mech., Cambridge, MA, pp.103-110.

PARKER, R.H. and R.H. HENDRON (1987). The hot dry rock geothermal energy projects at Fenton Hill, New Mexico and Rosemanowes, Cornwall. In Inst. of Electrical Engrs. 5th Int. Conf. on Energy Options: the role of alternatives in the world energy scene, Univ. of Reading.

PATTON, F.D. (1966). Multiple modes of shear failure in rock. Proc. 1st ISRM Congr., Lisbon, Vol.1, pp.509-513.

PINE, R.J. and A.S. BATCHELOR (1982). In situ stress and jointing in the Carnmenellis granite and the implication for hydraulic behaviour. J. Camborne School of Mines, Vol.82, pp.40-48.

PINE, R.J. and P.A. CUNDALL (1985). Application of the fluid-rock interaction program (FRIP) to the modelling of hot dry rock geothermal energy system. Proc. Int. Symp. on Fundamentals of Rock Joints, O. Stephansson (ed), Lulea Univ., Centek, Sweden, pp.293-302.

PINE, R.J. and P. LEDINGHAM (1983). In situ hydraulic parameters for the Carnmenellis granite Hot Dry Rock geothermal energy reservoir. Proc. 58th Annual Technical Conf., San Francisco Soc. of Petrol. Engrs. of AIME.

PRATT, H., T. SCHRAUF, W. HUSTRULID and E. SIMMONS (1979). A large scale in-situ study of determine temperature, deformation, and stress field associated with heater experiments in crystalline rocks. Proc. 4th ISRM Congr., Montreux, Vol.2, pp.539-544.

RAVEN, K.G. and J.E. GALE (1985). Water flow in a natural rock fracture as a function of stress and sample size. Int. J. Rock Mech. Min. Sci. Geomech. Abstr., Vol.22, pp.251-261.

RICE, J.R. and D.A. SIMONS (1976). The stabilization of spreading shear faults by coupled deformation - diffusion effects in fluid-infiltrated porous materials. J. Geophys. Res., Vol.81, pp.4322-4334.

RICHTER, D. and G. SIMMONS (1974). Thermal expansion behaviour of igneous rocks. Int. J. Rock Mech. Min. Sci. Geomech. Abstr., Vol.11, pp.403-411.

ROBERTS, A. (1977). Geotechnology. Pergamon Press, Oxford, 347pp.

ROBINSON, E.S., R.M. POTTER, B.B. MCINTEER, J.C. ROWLEY, D.E. ARMSTRONG and R.L. MILLS (1971). A preliminary study of the nuclear subteerene. Appendix F, Geothermal Energy, Los Alamos Scientific Laboratory Report, LA-4547, 62pp.

sity Press, New York, 738pp.

LINDROTH, D.P. (1974). Thermal diffusivity of six igneous rocks at elevated temperatures and reduced pressures. US Bureau of Mines Report of Investigations, RI-7954.

LINDROTH, D.P. and W.G. KRAWZA (1971). Heat content and specific heat of six rock types at temperatures to 1000 C. US Bureau of mines Report of Investigations, RI-7503.

LO, K.Y and R.S.C. WAI (1982). Thermal expansion, diffusivity and cracking of rock cores from Darlington, Ontario. Canadian Geotech. J., Vol.19, pp.154-166.

LOMIZE, G.M. (1951). Water flow in jointed rock (in Russian). Gosenergoizdat, Moscow.

LOS ALAMOS NATIONAL LABORATORY (1981). Hot dry rock geothermal energy development program: annual report 1981. Los Alamos, New Mexico, 140pp. (LA-9287-HDR).

LOS ALAMOS NATIONAL LABORATORY (1982). Hot dry rock geothermal energy development program: annual report 1982. Los Alamos, New Mexico, 127pp. (LA-9780-HDR).

LOS ALAMOS NATIONAL LABORATORY (1983). Hot dry rock geothermal energy development program: annual report 1983. Los Alamos, New Mexico, 91pp. (LA-10347-HDR).

LOS ALAMOS NATIONAL LABORATORY (1984). Hot dry rock geothermal energy development program: annual report 1984. Los Alamos, New Mexico, 31pp. (LA-10661-HDR).

LOUIS, C. (1969). A study of groundwater flow in jointed rock and its influence on the stability of rock masses. Rock Mech. Res. Report No.10, Imperial College, Univ. of London, 90pp.

LOUIS, C. (1973). Rock hydraulics. In Rock Mechanics, L. Muller (ed), Int. Centre for Mechanical Sci., Courses and Lectures No.165, Udine, Italy, pp.299-387.

LOUIS, C. and Y.N. MAINI (1970). Determination of in situ hydraulic parameters in jointed rock. Proc. 2nd ISRM Conf., Belgrade, Vol.1, pap.1-32.

LOUIS, C., J.L. DESSENNE and B. FEUGA (1976). Interaction between water flow phenomena and the mechanical behaviour of soil or rock masses. French Bureau de Recherches Geologiques et Minieres, Report 76 SGN 322 AME, 30pp.

LUNDSTROM, L. and H. STILLE (1978). Large scale permeability tests in the granite of Stripa Mine (Sweden). Lawrence Berkeley Laboratory, LBL-7052.

Res., Vol.83, pp.339-344.

SWAN, G. (1978). The mechanical properties of stripa granite. Lawrence Berkeley Laboratory, LBL-7074.

SWAN, G. (1983). Determination of stiffness and other joint properties from roughness measurements. Rock Mech. and Rock Engng., Vol.16, pp.19-38.

TERZAGHI, K. VAN (1943). Theoretical soil mechanics. Wiley, New York, 510pp.

TERZAGHI, K. VAN and R.B. PECK (1967). Soil mechanics in engineering practice, 2nd edn. Wiley, New York, 729pp.

TODD, D.K. (1959). Groundwater hydrology. Wiley, New York, 336pp.

TSANG, Y.W. and P.A. WITHERSPOON (1981). Hydro-mechanical behaviour of a deformable rock fracture subject to normal stress. J. Geophys. Res., Vol.86, pp.9287-9298.

TSANG, Y.W. and P.A. WITHERSPOON, (1982). Correlations between fracture roughness characteristics and fracture mechanical and fluid flow properties. Proc. 23rd US Symp. on Rock Mech., pp.560-567.

TULLIS, J. and R.A. YUND (1977). Experimental deformation of dry Westerly granite. J. Geophys. Res., Vol.82, pp.5705-5718.

TUNBRIDGE, L.W. and L.R. RICHARDS (1983). Geotechanical site assessment methodology. Report DOE/RW/83.063.

VAN DER MOLEN, I. (1981). The shift of α-β transition temperature of quartz associated with the thermal expansion of granite at high pressures. Tectonophysics, Vol.73, pp.323-342.

VAUGHAN, P.J., D.E. MOORE, C.A. MORROW and J.D. BYERLEE (1986). Role of cracks in progressive permeability reduction during flow of heated aqueous fluids through granite. J. Geophys. Res., Vol.91, pp.7517-7530.

VERRUIJT, A. (1970). Theory of groundwater flow. Macmillan, London, 190pp.

VOEGELE, M., E. HARDIN, D. LINGLE, M. BOARD and N.R. BARTON (1981). Site characterization of joint permeability using the heated block test. Proc. 22nd US Symp. on Rock Mech., Cambridge, MA, pp.120-127.

WALSH, J.B. (1965). The effect of cracks on the

compressibility of rocks. J. Geophys. Res., Vol.70, pp.381-389.

WALSH, J.B. (1981). Effect of Pore Pressure on Fracture Permeability. Int. J. Rock Mech. Min. Sci. Geomech. Abstr., Vol.18, pp.429-435.

WALSH, J.B. and E.R. DECKER (1966). Effects of pressure and saturating fluids on the thermal conductivity of compact rock. J. Geophys. Res., Vol.71, pp.3053-3061.

WALSH, J.B. and M.A. GROSENBAUGH (1979). A new model for analysing the effect of fractures on compressibility. J. Geophys. Res., Vol.84, pp.3532-3536.

WHITE, R.D. (1961). Premliminary evaluation of geothermal areas by geochemistry, geology and shallow drilling. Proc. U.N. Conf. on New Sources of Energy, Rome, Vol.2, pp.402-408.

WITHERSPOON, P.A., J.S.Y. WANG, K. IWAI and J.E. GALE (1980). Validity of the cubic law for fluid flow in a deformable rock fracture. Water Resources Res., Vol.16(6), pp.1016-1034.

WITTKE, W. (1973). General report on the Symposium Percolation through fissured rock. Bulletin of the Int. Assoc. of Engng Geol., Krefeld, No.7, pp.3-28.

WONG, T.F. and W.F. BRACE (1979). Thermal expansion of rocks: some measurements at high pressure. Tectonophysics, Vol.57, pp.95-117.

WOODSIDE, W. and J.H. MESSMER (1961): Thermal conductivity of porous media. J. Appl. Physics, Vol.32, No.9, pp.1688-1706.

YONG, C. and C.Y. WANG (1980). Thermally induced acoustic emission in Westerly granite. Geophys. Res. Letters, Vol.7, pp.1089-1092.